Galaxy evolution in a large sample of X-ray clusters

by

Sheona Anne Urquhart
MPhys., University of Edinburgh, 2006

A Dissertation Submitted in Partial Fulfillment of the
Requirements for the Degree of

DOCTOR OF PHILOSOPHY

in the Department of Physics and Astronomy

Galaxy evolution in a large sample of X-ray clusters

by

Sheona Anne Urquhart
MPhys., University of Edinburgh, 2006

Supervisory Committee

Dr. J.P. Willis, Supervisor
(Department of Physics and Astronomy)

Dr. L. Simard, Member, Departmental Member
(Department of Physics and Astronomy; Herzberg Institute of Astrophysics)

Dr. L. Ferrarese, Member, Departmental Member
(Department of Physics and Astronomy; Herzberg Institute of Astrophysics)

Dr. A. Monahan, Outside Member
(School of Earth and Ocean Sciences)

Supervisory Committee

Dr. J.P. Willis, Supervisor
(Department of Physics and Astronomy)

Dr. L. Simard, Member, Departmental Member
(Department of Physics and Astronomy; Herzberg Institute of Astrophysics)

Dr. L. Ferrarese, Member, Departmental Member
(Department of Physics and Astronomy; Herzberg Institute of Astrophysics)

Dr. A. Monahan, Outside Member
(School of Earth and Ocean Sciences)

ABSTRACT

It is long established that the evolution of populations of galaxies is dependent upon the environment in which they are located, from low mass galaxy groups to rich galaxy clusters. However, what is not so clear is which physical process(es) dominate this evolution. There are a number of different mechanisms which have been proposed and these can be broadly divided into two categories. There are those caused by interactions with the cluster environment itself (including ram-pressure stripping) and those caused by galaxy-galaxy interactions (including merging events). Disentangling these is a non-trivial task.

In this thesis, we use a number of parameters to do so all based upon our uniform CFHT Megacam photometry for X-ray selected galaxy clusters drawn from the X-Ray Multi-Mirror (XMM) Large Scale Structure (LSS) survey and the Canadian Cluster Comparison Project (CCCP). These clusters possess well determined X-ray temperatures spanning the range $1 < \mathrm{kT(keV)} < 12$ and occupy a relatively narrow redshift

interval ($0.15 < z < 0.41$) in order to minimise any redshift dependent photometric effects.

We investigate the colour bimodality of cluster galaxy populations and compute blue fractions using the criteria of Butcher and Oemler (1984) and identify a trend of observing increasing blue fractions versus redshift in common with numerous previous studies. However, we also identify an environmental dependence of cluster blue fraction in that cool (low mass) clusters display higher blue fractions than hotter (higher mass) clusters.

Introducing the local galaxy density parameter, Σ_5, we find that there is a greater variation in blue fraction as a function of Σ_5 in the low mass groups compared to the high mass clusters, but all of our samples (cool, mid and hot temperatures) show a decrease in blue fraction with an increase in local galaxy density, consistent with galaxy-galaxy interactions. We also show that the global cluster environment is playing a role since we observe that, at similar local galaxy densities, there is a greater decrease in the blue fraction as the cluster temperature increases. A further, important consideration is that of the timescales required for environmental effects to become effective. Through simple modelling, we find that our mid and hot samples have had sufficient halo mass for sufficient lengths of time for environmental mechanisms to act. We also observe that the value of f_B does not depend strongly on the current state of the X-ray gas.

Our studies of the red-sequence luminosity functions and the related dwarf-to-giant ratios (DGR) add further support to an emerging picture of galaxy-cluster and galaxy-galaxy interactions where we find that the dwarf population is produced via ram-pressure stripping and passive reddening before being converted into giants via the effects of merging.

As one would expect, galaxy interactions (whether with other galaxies or the cluster environment) should have some impact upon the morphology. Using the `GIM2D` modelling package to determine morphological parameters, we observe an increase in the fraction of bulge-dominated galaxies with increasing local galaxy density but that the morphological mix responds less strongly to variations in global environment than does the colour mix. We also find that our bulge-to-total distributions show, in the cool sample, passively reddening disk galaxies prior to their disruption via merging with our distributions of disk scale lengths suggesting that the destruction of disks in the mid and hot samples must be a rapidly occurring process.

Contents

List of Tables

List of Figures

ACKNOWLEDGEMENTS

I would love to say that this was all down to me and me alone, but in all honesty, there are many people I need to thank for the parts they played (however small) in this thesis.

Firstly, I would like to thank my supervisor, Dr. Jon Willis. He has shown me unwavering support, patience and enthusiasm throughout my time here, even when I made things as difficult as possible....! I would also like to thank him for caring about me.

For useful and interesting science chat and advice, I want to acknowledge Dr. Henk Hoekstra and Dr. Graham Smith (even if we do disagree on what environment means) and my CCCP buddy, Dr. Chris Bildfell.

There are two individuals who deserve as much credit for this work as I do (if not more), they are the two most important people in my life, my Mum and Dad. Their unquestioning faith in my abilities, their support (good ol' bank of Mum and Dad!) and the fact that they were ALWAYS there for me, no matter what time of the day and night was what got me through this. I could not have done it without them.

My sister Katie also deserves a mention here! Whenever I needed a laugh or some light hearted banter, she was there. And even though I moaned about it, her teasing about nerds was pretty good at keeping me down to earth (just don't tell her I said that).

Continuing the theme of thanking family members, I need to say a massive thanks to Jackie. You happily let me impose myself in your home, gave great "normal" chat and are doing a grand job of keeping my Dad on the straight and narrow! Ian, thanks, for everything. You exude calmness and patience. And last, but by no means least, Gran and Grandma-you guys rock, you are amazing role models.

My friends. Where to start? I have met the best friends of my life through doing my PhD. Three people are now firmly part of my family. Niko, Ryan and Kaushi. You are the best friends anyone could ask for, and I know that no matter where our paths take us, we will always be close. And sleeping on each others couches. And sponging off each others families!

I also want to thank some other fellow grads over the years. Greg, you know you're my dear buddy. Chris B, Jillian, Charli and Sarah. You guys listened to me moan, made me leave my desk for coffee and lunch and generally made life a lot more pleasant round here.

And last, but by no means least, I really need to thank the office staff here over the years. Monica, Michelle, Amanda, Susan, Jolene, Rosemary, you are all worth your weight in gold. I can't thank you enough for all the help you have given me, this department would fall apart without you guys.

If I have forgotten anyone, I can assure you that it's unintentional. What can I say? My brain has turned to mush.

I won't slave for beggar's pay, likewise gold and jewels, but I would slave to learn the ways to sink your ship of fools.

Robert Hunter and Jerry Garcia

DEDICATION

Mum and Dad, this one is for you.

Chapter 1

Introduction

The properties of galaxies depend strongly upon the environment in which they are located. This environment can be classified on a global scale (e.g. via the mass of the cluster or group in which a galaxy resides) or on a local scale (through measurements of the local galaxy density). This manifests itself in a number of observational trends, including the *morphology-density relation* (Dressler 1980) and the related *star-formation rate-density relation* (Gómez et al. 2003) whereby the fraction of star-forming galaxies is suppressed and the fraction of early type galaxies is increased in areas of higher density (e.g. clusters) over the lower density field. In addition to this, the fraction of "blue" galaxies (i.e. star forming galaxies) in clusters has been observed to increase with increasing redshift. This is the so called "Butcher-Oemler Effect" (Butcher and Oemler 1984).

What is not so clear however are the underlying physical mechanisms giving rise to these observations. Many processes have been suggested, including ram-pressure stripping (e.g. Gunn and Gott 1972) and galaxy-galaxy interactions (e.g. Mihos and Hernquist 1996). It is expected that these different effects will dominate on different physical and time scales, with galaxy-galaxy interactions being more effective in smaller, lower velocity dispersion group environments and ram-pressure stripping being more effective in higher mass, higher velocity dispersion clusters. However, distinguishing between the various effects is observationally challenging largely due to the fact that they leave similar photometric signatures.

With a large, uniform photometric dataset covering many different environments, such as that presented in this thesis, it is increasingly possible to study the impact of environment upon galaxies both on a local and global scale with improved statistics and a consistent analysis.

1.1 Galaxy Formation

Originally, it was believed that galaxies were formed through the Monolithic Collapse (Eggen et al. 1962) scenario. In this model, it was the gravitational collapse of a cloud of primordial gas in the early stages of the universe which formed all parts of a galaxy concurrently. In this collapse of a large proto-galactic nebula, the oldest stars formed early on almost radial trajectories and with low metallicities. Following this, the disk formed as a result of conservation of angular momentum (disk stars are therefore younger and more metal rich) with galaxy formation occuring on a free-fall timescale of the order of 1 Gyr. However, there are a number of observed features of the Milky Way that cannot be explained by this simple model. Very high initial star-formation rates are required (100-1000$M_\odot$/yr) whereas now, we see only $\sim M_\odot$/yr, along with observations of some halo stars showing retrograde motion (we would expect most stars to move in approximately the same direction due to the initial rotation of the proto-galactic cloud) and age differences (2-3 Gyr) in some Globular Clusters (we expect <1 Gyr spread, on order of the free-fall time). Clearly, an alternative model is required to explain the formation process(es) and one such model is that of a "bottom-up" scenario (Searle and Zinn 1978).

1.1.1 Λ Cold Dark Matter

Hierarchical or "bottom-up" models of galaxy formation are based on the idea that small overdensities collapse first at early cosmic times with subsequent merging occuring to form larger structures, continuing until the present day. Detailed observations of the Cosmic Microwave Background (CMB) show that, following the Big Bang, the universe was almost homogeneous, but that the small anisotropies which were present (changes in density dominated by dark matter) began to grow and condense as the universe cooled due to expansion forming haloes of dark matter. Alongside this, hydrogen and helium also condensed forming the first stars and ultimately forming the first proto-galaxies. These structures continued to grow to form the objects we see today, including galaxies and clusters of galaxies. A schematic diagram of this hierarchical model of galaxy formation is shown in Figure 1.1. This is the currently favoured model of structure formation in the universe, the Λ Cold Dark Matter (ΛCDM) model.

This model has had great success between observations and the simulations of dark matter, as can be seen in Figure 1.2. This Figure shows the predicted distribution of

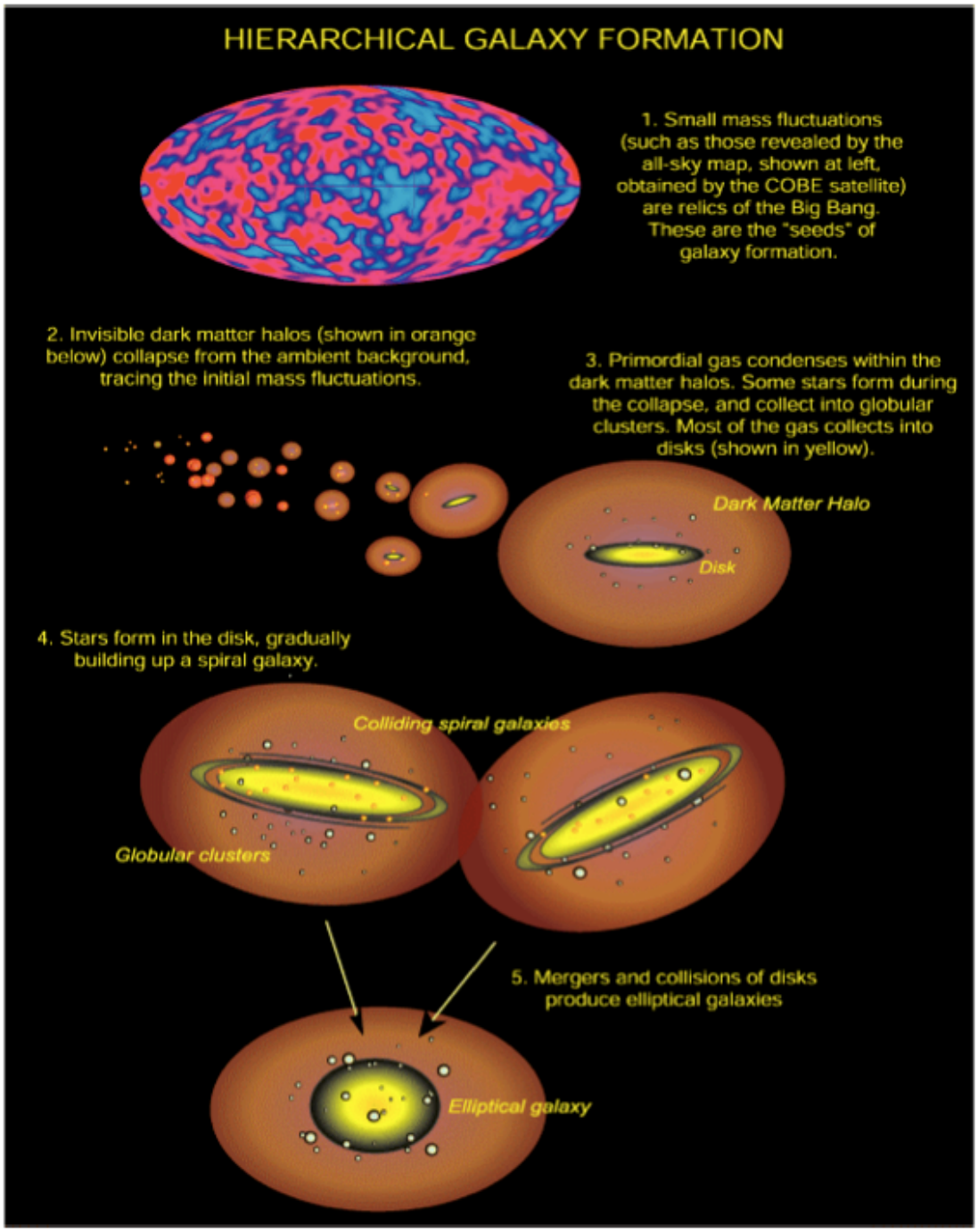

Figure 1.1: Schematic diagrm of hierarchical galaxy formation, timescales for the various phases depend on cosmological parameters. In an accelerating Universe most ellipticals form at redshifts >1. Abraham and van den Bergh (2001).

dark matter from simulations (shown in red) alongside observed galaxy distributions (shown in blue and purple) with remarkable agreement between the two. Further evidence to support the hierarchical formation model can be seen in the observations of galaxy merging events, whereby it is possible for the disks of spiral galaxies to be destroyed, leaving behind an elliptical galaxy (Barnes and Hernquist 1992) along with accretion events such as the discovery of stellar streams in our Galaxy and M31 (e.g. Ibata et al. 1994).

1.2 Clusters of Galaxies

Galaxy clusters play a vital role in the understanding of large scale structure in the universe. In this hierarchical CDM model of structure formation, galaxy groups and clusters are the largest gravitationally bound objects in the present day universe.

When referring to these dense regions, the terms "cluster" and "group" are often interchanged, the distinction between these being somewhat arbitrary. Typically, groups contain up to 50 galaxies or less and have velocity dispersions on the order of 150kms^{-1}. Clusters on the other hand can display a wider range in sizes and properties. They can be roughly divided into "poor" clusters, containing ∼50 members to "rich" clusters which can contain thousands of galaxies, have velocity dispersions of approximately 800kms^{-1} and can have 10-20% of their mass in the form of very hot (10^{7-8}K) intracluster gas observable as X-rays.

As an illustrative example of the differences between these classifications, an image of a group is shown in Figure 1.3. This is an optical image of XLSSC044 taken in the $u'r'z'$ bands using the Canada France Hawaii Telescope (CFHT) to create the composite image. Overplotted are the X-ray contours from the X-ray Multi Mirror (XMM) telescope. This group lies at a redshift of 0.26 and has X-ray temperature, T_X=1.27keV [1] (Pacaud et al. 2007).

As a comparison, Figure 1.4 is a composite g′r′ image of the considerably richer cluster Abell 1914. This clusters is found at z=0.17 and has T_X=9.48keV.

1.2.1 Detecting Clusters of Galaxies

Detecting clusters and groups of galaxies is a non-trivial observational challenge and there exist a number of techniques which can be used. Irrespective of which technique

[1] T(K)=1.16x10^{7}T(keV)

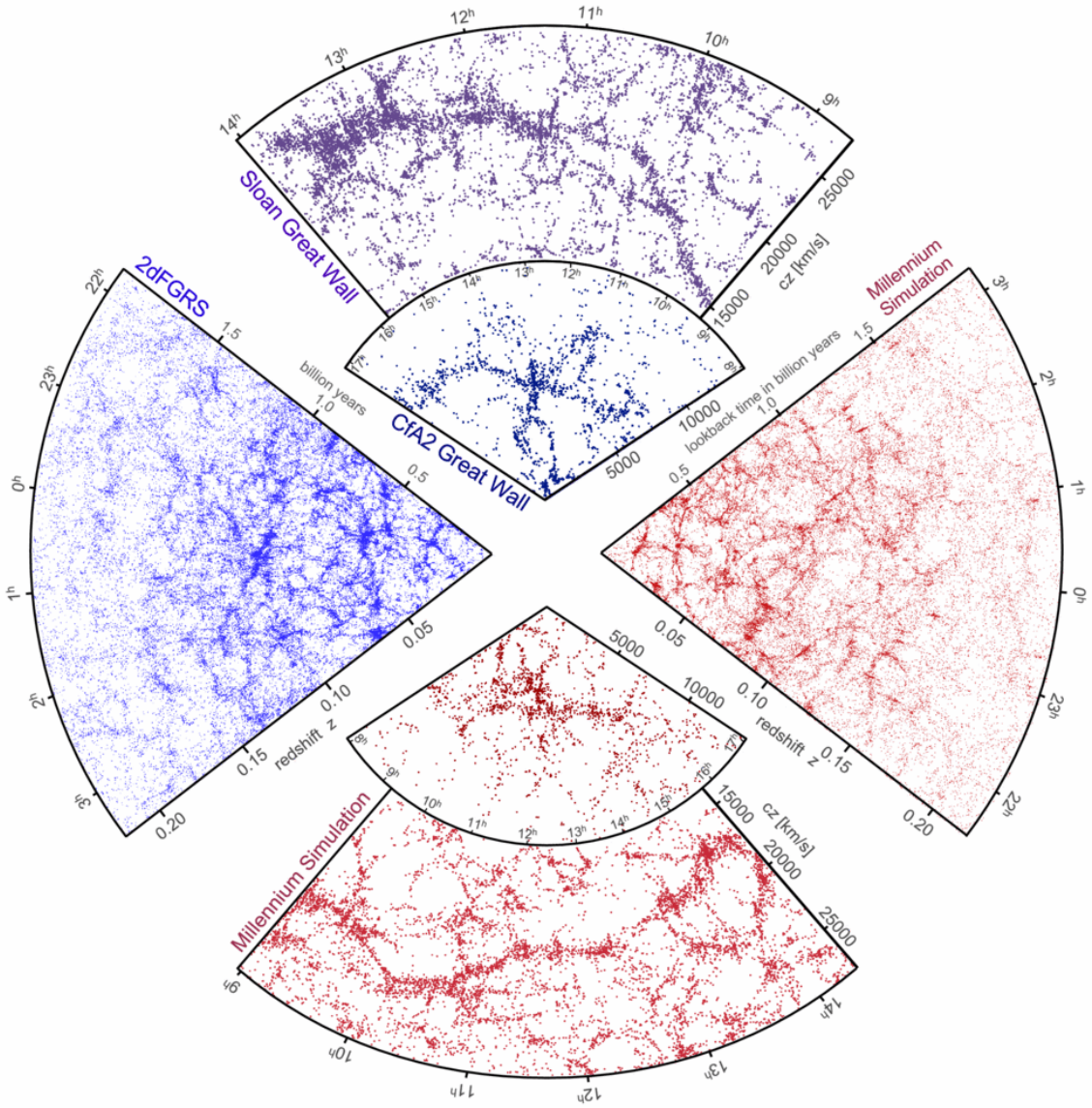

Figure 1.2: Galaxy distribution obtained from spectroscopic redshift surveys and from mock catalogues constructed from cosmological simulations. The blue and purple slices show galaxies as seen from the SDSS (York et al. 2000) and 2dFGRS(Colless et al. 2001) surveys. The red slices show the mock galaxy survey results using semi-analytic methods to model galaxy formation and evolution within the evolving dark matter distribution of the 'Millennium" simulation (selected with matching survey geometries and magnitude limits). Springel et al. (2006).

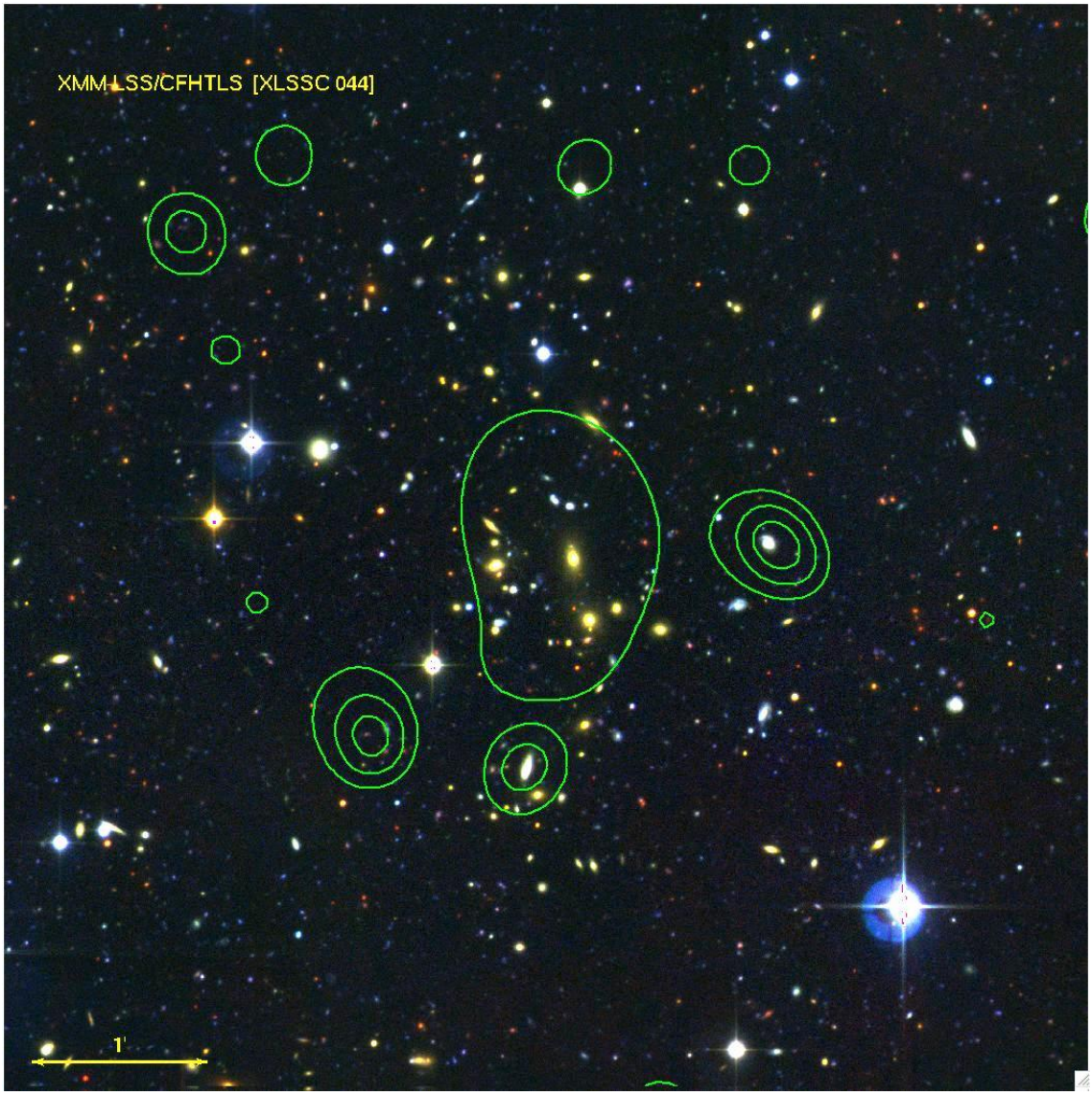

Figure 1.3: $u'r'z'$ band CFHTLS composite image of the XLSSC044 group. The X-ray contours are overplotted in green, the proper size of the image is 1.5Mpc at the cluster redshift (z=0.26). Pacaud et al. 2007.

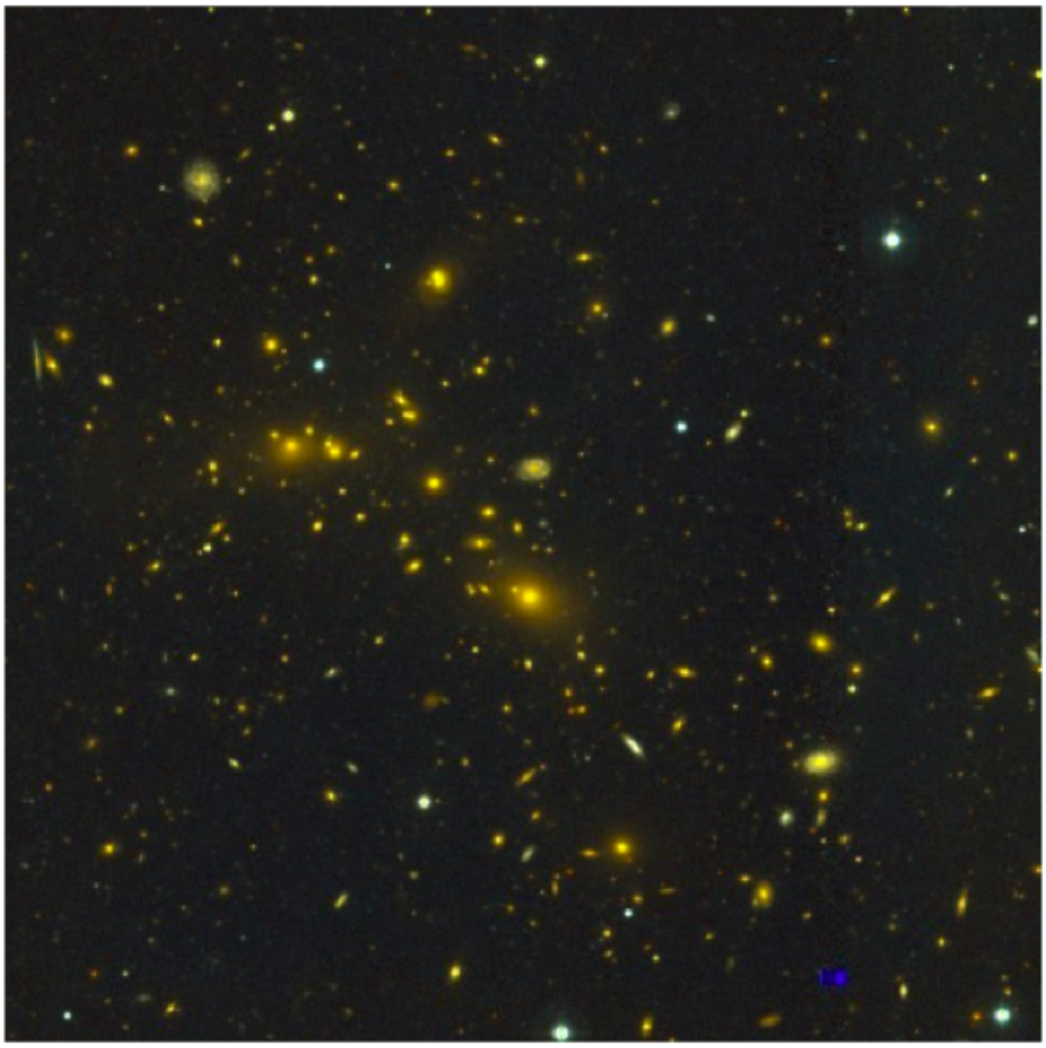

Figure 1.4: Composite g′r′ image of the cluster Abell 1914 using the `MEGACAM` camera on the Canada France Hawaii Telescope. The field is 6.2x6.2 arcmins. *Image credit*: Hoekstra, CCCP Collaboration.

is employed, they are all required to be quantitative and repeatable with the clusters being uniformly selected and well understood (Melin et al. 2005) with parameters (e.g. cluster mass) that can be derived from the observed cluster properties.

Optical detection

For many years, clusters have been selected using optical observations. This was first attempted in a systematic manner by Abell (1958) using data from the Palomar Sky Survey to detect ∼2000 clusters by applying two selection criteria. To ensure that a cluster contained a sufficient number of members, a richness criterion was applied whereby each cluster must contain at least 50 members with apparent magnitudes of $< m_3+2$ (where m_3 is the apparent magnitude of the third brightest member). Alongside this, a compactness cut was applied whereby only galaxies within $1.5h^{-1}$Mpc from the cluster centre were deemed to be members. This Abell catalogue was originally constructed through a visual inspection of photographic plates which introduces a bias towards centrally-concentrated clusters, suffers from a relatively low redshift cutoff (although at the time, selecting clusters at z∼0.2 was pioneering work), no redshift interlopers and strong plate to plate variations along with photometric errors and other inhomogeneities. However, it represented the first large, quantitively selected cluster sample and it remains remarkably useful.

More recent examples of optical detection techniques include the Cluster Red Sequence (CRS; Gladders and Yee 2000) method. This exploits the fact that all clusters exhibit a tight locus of early-type galaxies in colour-magnitude space known as the red sequence, the colour of which depends on the redshift of the cluster. By creating colour slices and searching for overdensities in these slices it is possible to determine the most likely redshift of potential cluster candidates. However, like all optical detection techniques, this too suffers from potential bias and problems. For example, by nature these methods can select systems as being clusters when they are simply chance alignments on the sky. Even when used in conjunction with infra-red (IR) observations, the effects of cluster and field galaxy evolution can cause problems, being poorly determined at $z > 1$ (Yee et al. 2000). There are also advantages to optical surveys; they are based upon relatively inexpensive observations which can cover a large area, are sensitive to lower mass structures (modulo an increasing contamination rate) and, in the absence of spectroscopic information, redshifts can still be determined using the colours of the observed red-sequences.

When spectroscopic information is available, it is possible to use this information to detect galaxy clusters by means of a friends-of-friends algorithm (e.g. Farrens et al. 2011). This technique uses a galaxy's right ascension, declination and redshift to detect clusters by searching for galaxies that are separated by less than some distance threshold and having a velocity difference less than some threshold (e.g. Huchra and Geller 1982). By detecting clusters in this way, it removes the problems associated with subtracting the background population of galaxies which is vital in any cluster analysis.

X-Ray detection

Both clusters and groups contain significant amounts of extended X-ray emission (e.g. Mulchaey et al. 2003; Ponman and Bertram 1993) on scales reaching hundreds of kiloparsecs. It was in 1966 that a study of the galaxy M87, at the centre of the Virgo cluster, revealed the presence of this X-ray emission (e.g. Byram et al. 1966). Five years later, X-rays had also been detected in the Coma and Perseus clusters (e.g. Meekins et al. 1971), and it was this same year that Cavaliere et al. (1971) proposed that extragalactic X-ray sources were generally associated with groups and clusters of galaxies. With the launch of the Uhuru X-ray satellite and the subsequenct survey of the entire sky for X-ray emission (Giacconi et al. 1972), this assertion was confirmed. These X-ray bright sources were found to have X-ray luminosities of 10^{43-45}ergs^{-1} and were spatially extended with sizes comparable to the size of the underlying galaxy distributions (e.g. Kellogg et al. 1972). The X-rays emission is consistent with production via thermal bremsstrahlung (free-free) emission from hot gas (Felten et al. 1966) which would have to exist in the intra-cluster medium (ICM) and have very high temperatures ($\sim 10^8$K) corresponding to typical photon energies of 1-10keV (therefore the gas is fully ionised) and having low densities ($\sim 10^{-3}$atom cm^{-3}).

Bremsstrahlung radiation occurs when free electrons interact with an ion and continue to remain free after the interaction has occurred. The electron subsequently loses energy in the interaction through the emission of a photon (Figure 1.5). The emissivity of thermal bremsstrahlung (emission power per unit frequency per unit volume) is related to the density and temperature as

$$\epsilon_{ff}(\nu) \propto n^2 T^{-1/2} exp\left(\frac{-h_p \nu}{k_B T}\right) \tag{1.1}$$

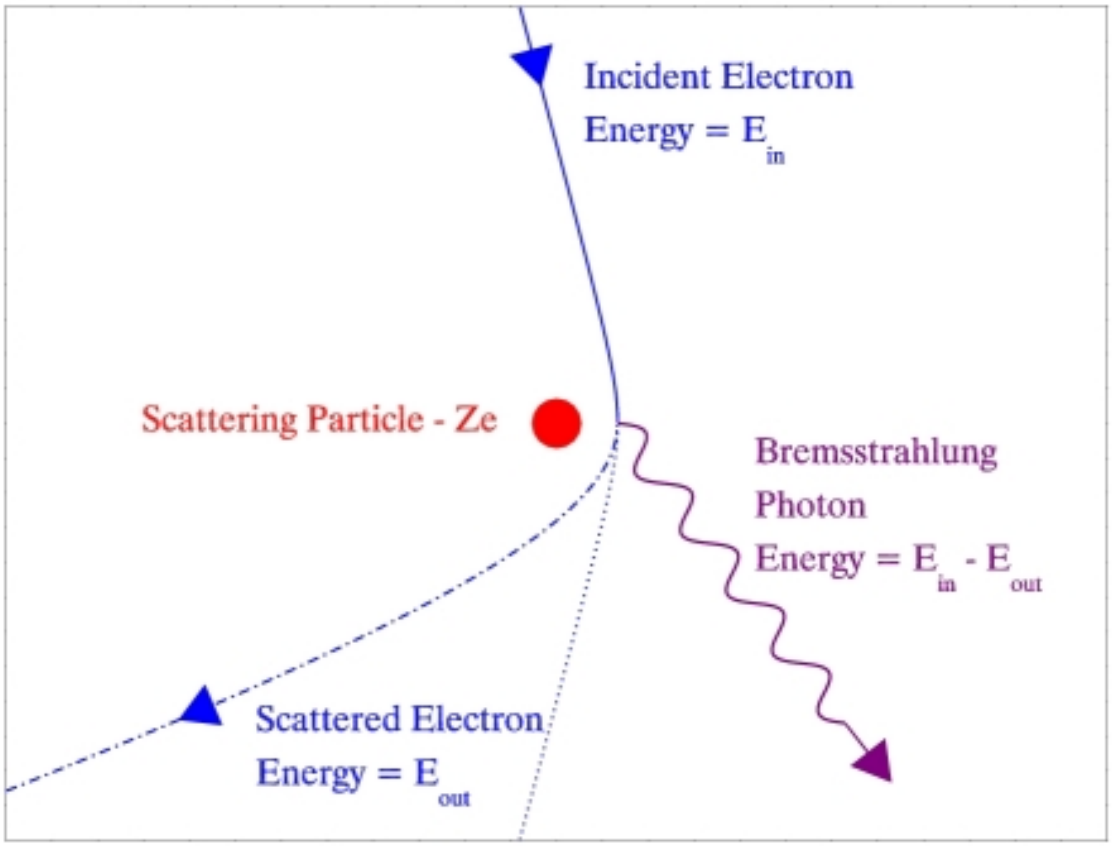

Figure 1.5: Free-free interaction in which an electron approaches an ion with charge Ze.

In practice, it is the X-ray surface brightness (S_ν) which is observed. This is the emissivity along the line-of-sight (ignoring the effects of surface brightness dimming due to the expansion of the universe) and is given by

$$S_\nu(x, y) \propto \int \epsilon_{ff}(\nu; x, y, z) dz \tag{1.2}$$

Therefore, by measuring S_ν as a function of ν (photon energy), it is possible to estimate the temperature at a given projected position from the shape of the spectrum. This temperature can subsequently be used to, for example, determine a characteristic radius (see Equation 2.1) of the cluster or as a proxy for the cluster mass (via the $M - T_X$ relation).

Such scaling relations in the observable properties of clusters arise from the CDM model (see Section 1.1.1) which provides predictions for the structure of clusters of

galaxies (e.g. Kaiser 1986), including the existence of a universal density profile (e.g. Dubinski and Carlberg 1991). Using X-ray telescopes, it is possible to directly map the ICM (the distribution of dark matter and the dominant baryonic component). In relaxed clusters, this ICM is close to hydrostatic equilibrium and therefore spatially resolved X-ray spectra can be used to derive the total mass as a function of radius (e.g. Sarazin 1988).

The advantages of selecting objects using X-rays are that it will limit potential biases due to the optical properties of the component galaxies, the presence of X-ray emission suggests a bound system that is virialised (i.e. merging processes and the collapse of matter have finished, the system is now in dynamic equilibrium), removing the problem of identifying systems that are simply chance alignments on the sky but would otherwise have appeared clustered if they were optically selected. However, like all other techniques, this too suffers from bias. These include being biased against, for example, clusters with compact gas distributions or clusters which are very extended (having low S_ν).

The sample of galaxies used in this thesis were all selected based upon X-ray observations, the details of which are given in Chapter 2.

Sunyaev-Zeldovich detection

One of the recently developed ways of detecting galaxy clusters is through the use of the Sunyaev-Zeldovich (SZ) effect. This describes the inverse-Compton scattering of cosmic microwave background (CMB) photons with energetic electrons in the cluster ICM. The low energy photons collide with high energy electrons in the cluster, receiving an energy boost which in turn creates a distortion in the blackbody spectrum of the CMB (Sunyaev and Zeldovich 1970, Sunyaev and Zeldovich 1972).

The SZ method, being a distortion in the CMB spectrum, does not depend on cluster distance and therefore the detection of clusters in this way has a selection function that is nearly redshift-independent (Carlstrom et al. 2002). In addition to this, the relationship between the integrated SZ flux and cluster mass is expected to have low scatter (e.g. Shaw et al. 2008) giving a near constant mass detection limit with redshift (Holder et al. 2000).

1.3 Galaxy Populations

1.3.1 Galaxy Morphological Classification

The first comprehensive system to classify galaxies was introduced by Edwin Hubble, known as the "Hubble Tuning Fork", and remains relevant today. This scheme divides galaxies into two broad categories: elliptical and spiral galaxies, referred to as "early" and "late"-type galaxies respectively. These categories are then subdivided based upon their observed properties. Ellipticals are assigned a number based upon their ellipticity, ranging from E0 (circular) to E7 (flat) where the value of the ellipticity is computed as $10(a-b)/a$ with a being the projected length of the major axis and b being the projected length of the minor axis. Spirals are initially divided into those with and without bars. The non-bar spirals are then classified based on how tightly the spiral arms are wound, with Sa being the tightest and Sd being the most loosely wound. Barred spirals are classified in a similar way, with SBa having tightly wound spiral arms and SBc having loosely bound arms. The galaxies classed as S0 are known as lenticulars and are a type of galaxy which appears to be intermediate between an elliptical and a spiral, consisting of a central bulge and disk but no spiral arms. This scheme is illustrated in Figure 1.6.

In addition to these galaxies, there exists another class known as the cD galaxy. This is an elliptical galaxy with an extended stellar halo (Matthews et al. 1964) that is usually found at the centre of a galaxy cluster with as many as 20% of all rich clusters containing such a galaxy (e.g. Bautz and Morgan 1970). They are believed to have been formed from the merger of smaller galaxies with the central brightest cluster galaxy and as such are important components of the cluster environment.

1.3.2 Galaxy Colour and Spectral Classification

As well as classifying galaxies based upon their morphology, it is also possible to classify populations using their colour. This can be done using the colour-magnitude plane where a well established bimodality has been observed (e.g. Baldry et al. 2004; Balogh et al. 2004). This bimodality takes the form of red galaxies (more gas poor, lower specific star-formation rates, preferentially found in denser environments) forming a tight locus in colour-magnitude space (Figure 1.7) known as the "red sequence" (which has been observed to already be established $z\sim1$ Bell et al. 2004) and blue galaxies with active star-formation and a late-type morphology and exists to at least

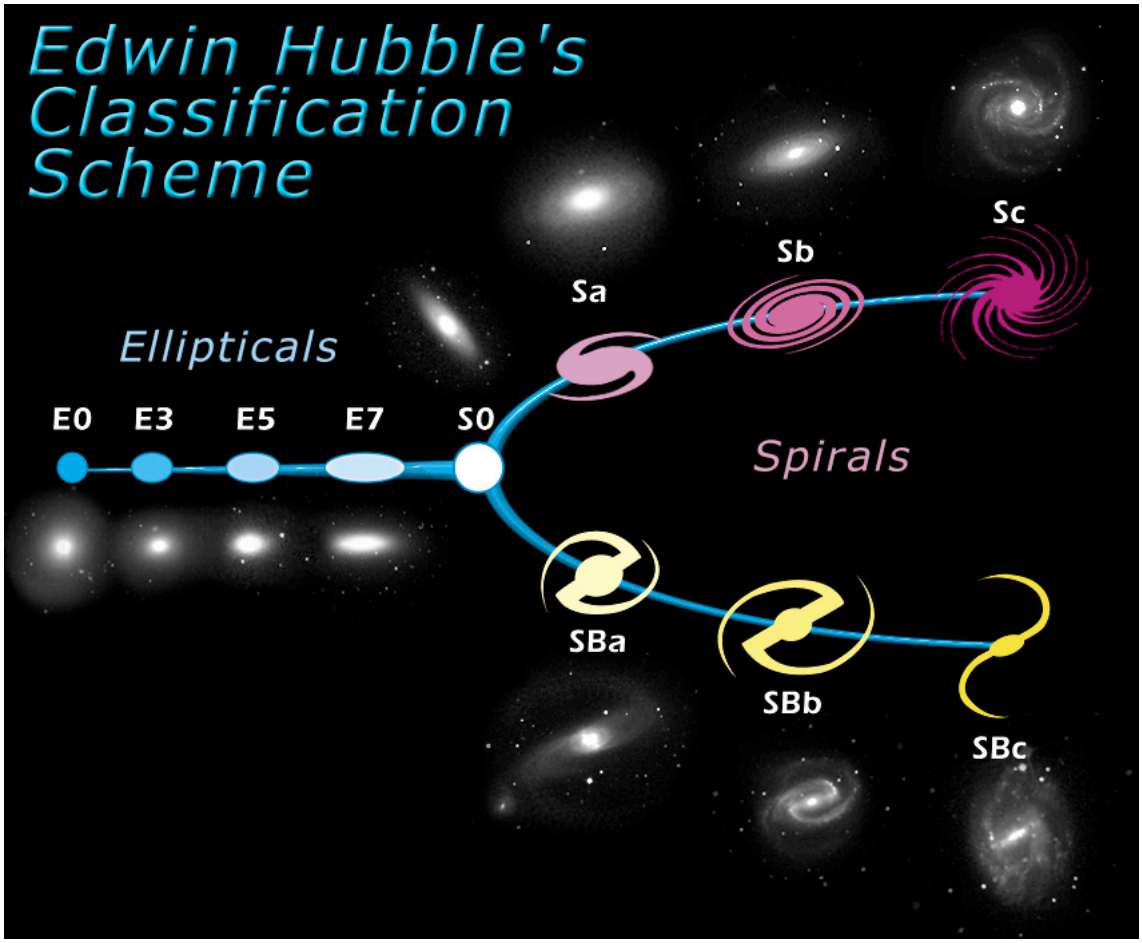

Figure 1.6: Diagram of the Hubble Tuning Fork (Credit: *SDSS/SkyServer*).

$\simeq$1 (e.g. Tanaka et al. 2005). Weinmann et al. (2006) divide galaxies further by introducing an intermediate class of red and active galaxies. These galaxies occupy the region of the colour-specific star-formation rate plane where early and late type galaxies overlap and so the authors suggest that they comprise a mix of dusty late types and early types. The colour-magnitude diagram and colour distribution of of their galaxies, selected from the Sloan Digital Sky Survey (SDSS) are shown in Figures 1.8 and 1.9 respectively.

1.3.3 Galaxy populations in different environments

Galaxy morphology depends upon environment (e.g. Dressler et al. 1997, Treu et al. 2003), an effect characterised via the morphology-density relation, an observationally determined relationship between the morphological type of a galaxy and the local environment in which it is located. Specifically, early-type galaxies (those classified as elliptical and S0) are found in high density environments (e.g. rich cluster cores) and late-type galaxies are generally found in lower density environments. Related to this is the morphology-radius relation whereby the fraction of late-type galaxies increases with increasing cluster-centric radius due to the decrease in galaxy density when travelling outwards from the cluster core. Much work has been done on these relations, for example, Treu et al. (2003), looked at a Hubble Space Telescope (HST) survey of the z$\sim$0.4 cluster CL 0024+16. This HST data was combined with spectroscopy taken from the literature and was studied to a cluster radius of $\sim$ 5Mpc. Morphological types for 2181 galaxies were visually assigned and the morphology-radius (T-R) and morphology-density (T-Σ) relations were calculated. They found that the fraction of early-type galaxies declines steeply from the cluster centre (densest regions) to a radius of 1Mpc and more gradually thereafter (towards less dense regions), asymptoting to the field value at the edges of the cluster. This morphology-density relation is shown in Figure 1.10, confirming previous work (e.g. Dressler et al. 1997) and clearly showing that the fraction of early-type galaxies is increasing with increasing projected surface density.

It has also been observed that galaxy populations, as well as depending on environment, also evolve with redshift. Recent work studying the evolution of the morphology-density relation since z$\sim$ 1 has shown the the fraction of early-type galaxies in cluster cores and groups have increased with time (e.g. Postman et al. 2005; Desai et al. 2007; Treu et al. 2003; Smith et al. 2005) as illustrated in Figure 1.11. For

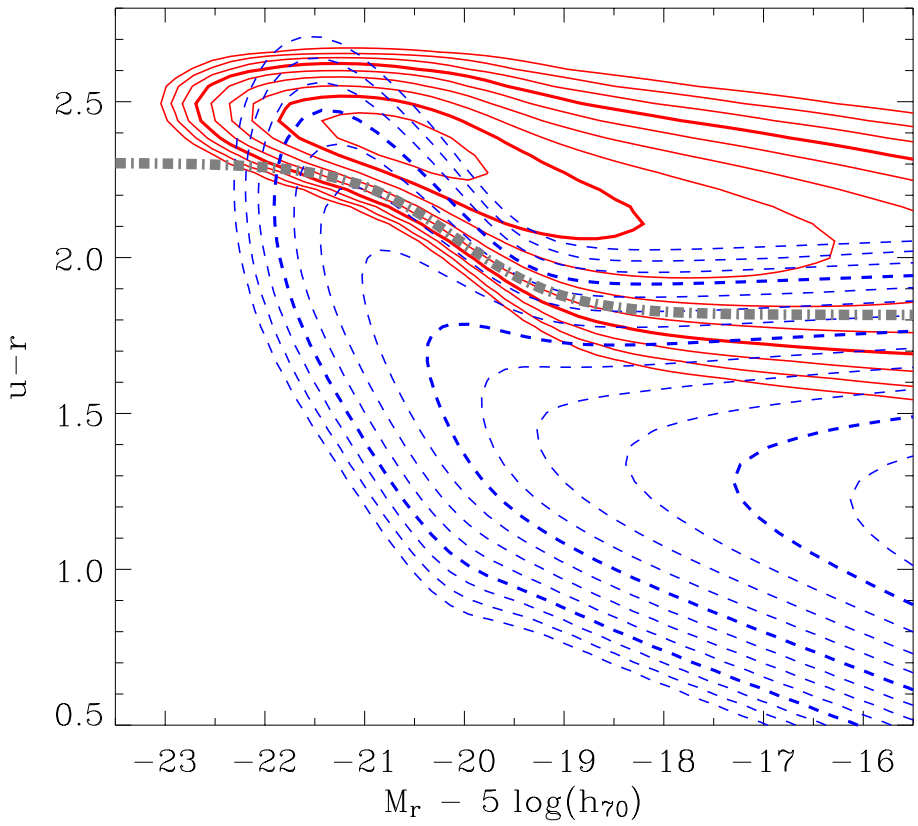

Figure 1.7: Colour-luminosity plane showing a two-Gaussian model for the colour distibution at each absolute magnitude separating the red sequence from the blue cloud (Baldry et al. 2004).

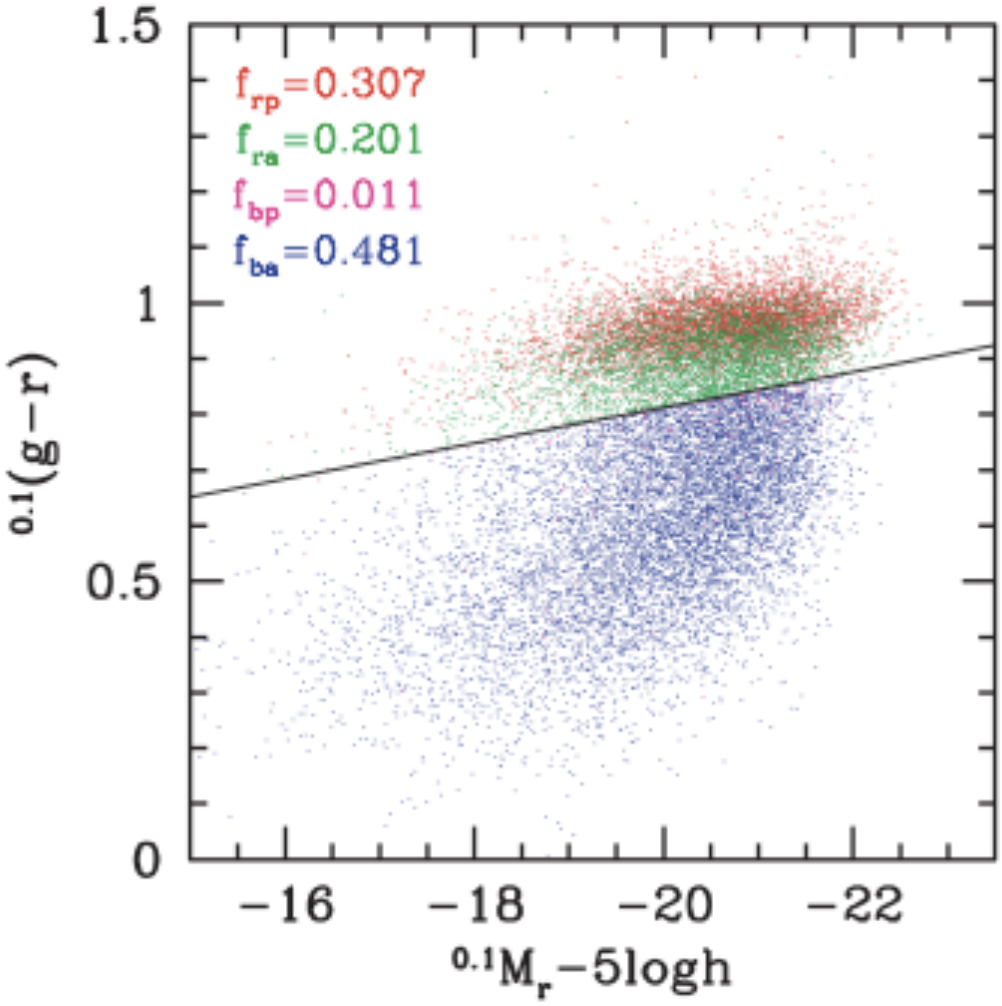

Figure 1.8: Colour-magnitude relation for the SDSS galaxies analysed in Weinmann et al. (2006). The solid line marks the split between the "active" and "passive" subsamples. Red dots (30.7% of the population) represent those galaxies defined as red and passive, blue dots (48.1% of the population) represent those galaxies defined as blue and active, green dots (20.1% of the population) represent red and active galaxies and magenta dots (1.1% of the population) are blue and passive galaxies.

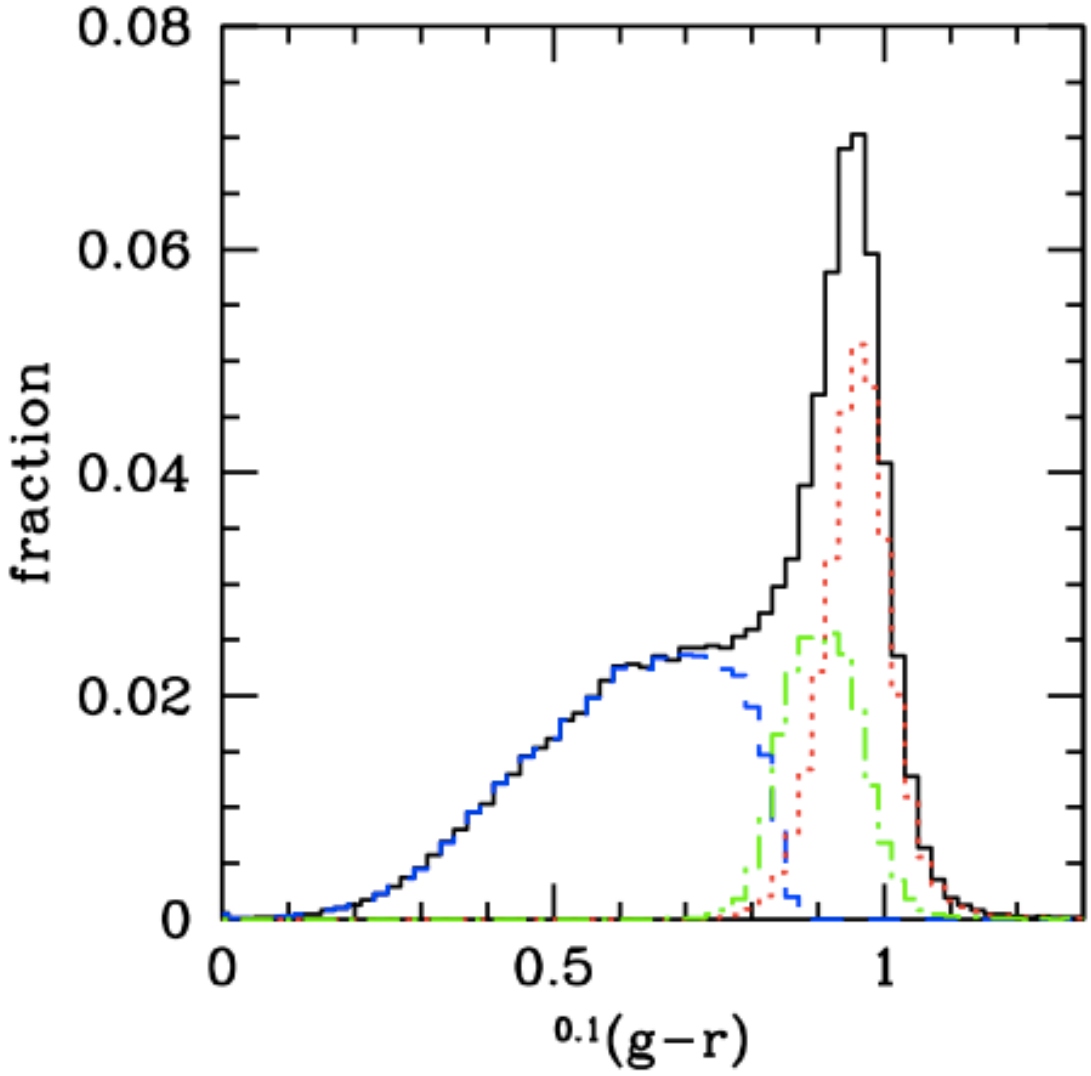

Figure 1.9: Histogram of the distribution of galaxies as a function of $(g-r)$ colour. The black solid line, blue dashed line, red dotted line and green dot-dashed line are the distributions for the full sample, late-types, early-types and intermediate-types respectively. Weinmann et al. (2006).

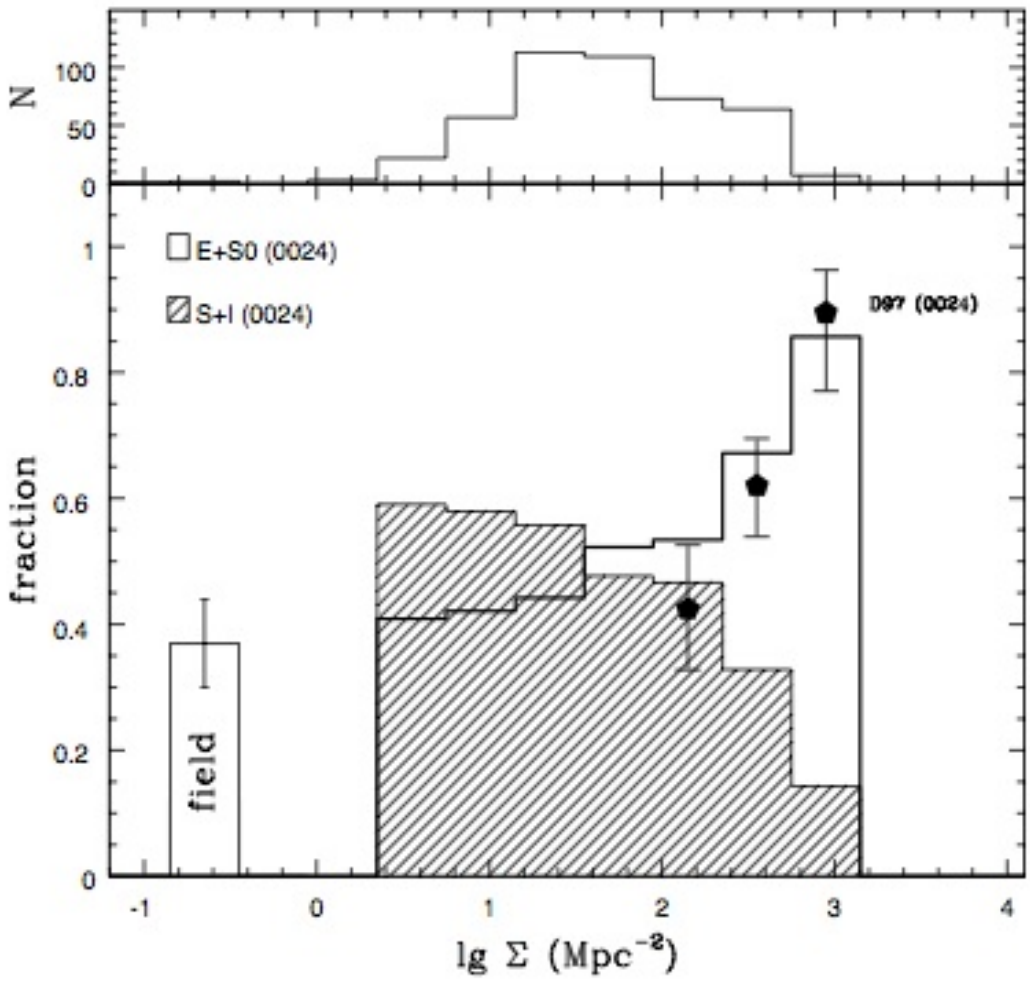

Figure 1.10: Morphology-projected density relation for galaxies in CL 0024+16. For comparison, symbols with error bars show the fraction of E+S0s determined by the Morphs collaboration for the central field of this cluster (Smail et al. 1997, Dressler et al. 1997). The histogram with error bar at low surface densities represents the fraction of E+S0s in the field at z∼0.4. Treu et al. (2003)

the highest density bins, we see an increase in f_{E+S0} from 0.7 to 0.9 between z=1 and today. However, field galaxies do not show this same evolution which would suggest that galaxy evolution depends strongly upon environment. Clearly, the existence of differential evolution between field and cluster environments indicates that there must be some physical process(es) causing a morphological transformation of galaxies in denser environments.

This evolution also manifests itself in the long established Butcher-Oemler effect (Butcher and Oemler 1978). This effect is the observation that high redshift galaxy clusters have an excess of blue galaxies compared to low redshift clusters (e.g. Margoniner et al. 2001; Poggianti et al. 2006). This increase in the blue fraction of galaxies with increasing lookback time is important in constraining models of galaxy formation since, for example, it is not reproduced by primordial collapse models which predict uniformly red galaxies to redshifts of $\sim$2 and so some other process must be occurring in galaxy formation (e.g. secular evolution [2], merger events). It has also been known, since its discovery, that the blue fraction of galaxy clusters depends on many things including cluster richness (higher in richer clusters; e.g. Margoniner et al. 2001), clustercentric radius (e.g. Ellingson et al. 2001) and galaxy magnitude limit and so measuring this effect requires great care and uniform data.

Further evidence of this environmental dependence, observed as early-type galaxies (generally redder, more gas poor and having lower specific star formation rates) being preferentially located in denser environments is presented in comparisons of current star formation rates in galaxy populations drawn from low density (the field) and high density (rich galaxy clusters) environments. For example, Balogh et al (1999) demonstrated this through measurements of the spectral indices for 1823 galaxies selected from the Canadian Network for Observational Cosmology 1 (CNOC1) sample. This sample consists of 15 X-ray luminous clusters spanning the redshift range $0.18 < z < 0.55$. They measured 3 spectral indices in this analysis. The first of these was the break strength at 4000Å (D4000), defined as the ratio of the flux in the red continuum to that in the blue continuum, tracing old stellar populations. The other two indices used were the rest-frame equivalent widths of the Hδ Balmer absorption line, W_0(Hδ), indicating the presence of A-type stars and sensitive to star formation that took place up to 1Gyr ago and the equivalent width of the [OII]λ3727 emission line, W_0(OII), which acts as an indicator of current star formation. They found that

[2]This is a slow, steady evolution, resulting from either long-term galaxy-environment interactions or internal processes due to, for examples, the actions of spiral arms and bars

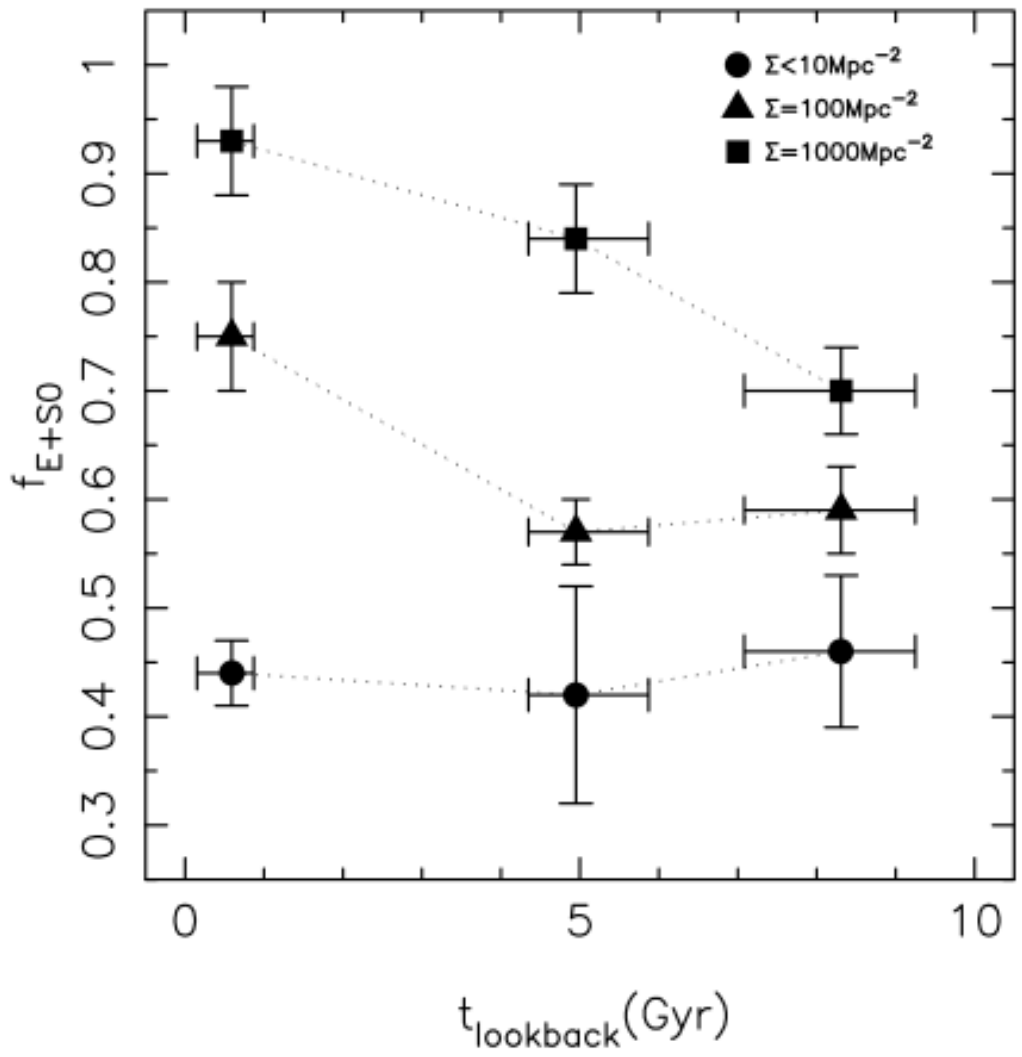

Figure 1.11: Evolution of the early-type fraction f_{E+S0} vs. look-back time for various projected densities (density is defined using the projected area enclosed by a galaxy's 10 nearest neighbours). Smith et al. (2005).

in the cluster environment, there is evidence for older stellar populations over those found in field galaxies and that the radial trends of D4000, $W_0(\mathrm{H}\delta)$ and $W_0(\mathrm{OII})$ are all consistent with an age sequence, i.e. the last episode of star formation occurred more recently in galaxies farthest from the cluster centre, in the least dense regions of the cluster. This would suggest that the densest regions of these clusters were more efficient at quenching star formation in galaxies than the less dense regions.

Lewis et al. (2002) presented further evidence that star formation rates depend on environment. Figure 1.12 shows the results of this study in which galaxies with $0.05 < z < 0.1$ in the 2dF Galaxy Redshift Survey (2dFGRS) lying in the fields of 17 known clusters were selected and the star formation rate, μ^*, (normalised to a characteristic luminosity) was calculated and expressed as a function of local galaxy density. As expected, it can clearly be seen, that as local density decreases, the star formation rate increases.

These results are further supported by Poggianti et al (2006). Here, they use the [OII] emission line as a signature of ongoing star formation to study how the proportion of star-forming galaxies evolves between z=0.8 and z=0 as a function of galaxy environment. This work is based on data from the ESO Distant Cluster Survey (EDisCS), a photometric and spectroscopic survey of galaxies in 20 fields containing galaxy clusters from z=0.4-1 and a local comparison sample taken from the SDSS ($0.04 < z < 0.08$). They found that at both high and low redshifts, the fraction of star forming galaxies depends on the velocity dispersion of the cluster/group. At higher redshifts (z=0.4-0.8), it was generally seen that more massive clusters (higher density) have a lower fraction of star forming galaxies and that the strength of the star formation in star forming galaxies varies systematically with environment.

Further properties, such as the integrated colour of clusters also vary as a function of changing environment. Blanton et al. (2005) studied the local environments of 114,994 galaxies as a function of their colours, luminosities, surface brightnesses and radial profile shapes selected from the Sloan Digital Sky Survey (SDSS) to have $14.5 < r < 17.7$ and $0.05 < z < 0.22$. What was found was that the structural properties of galaxies (i.e. Sérsic index and surface brightness) appeared to be less related to environment than were measurements of the star formation history (colour and luminosity).

Continuing the investigation of galaxy populations in clusters using colours, it was studies of the fraction of blue galaxies which provided some of the first evidence for the physical transformation of galaxies in cluster environments. The landmark

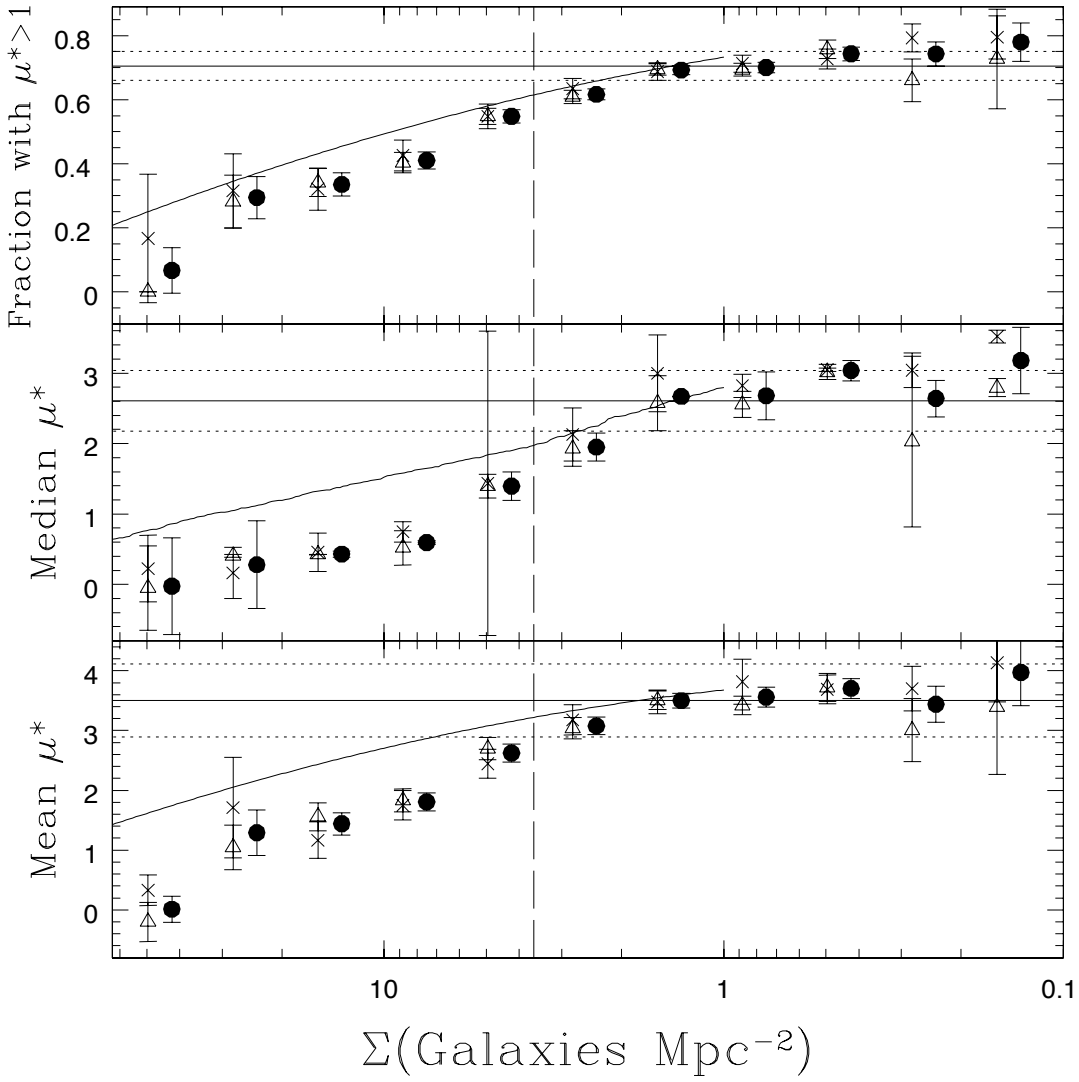

Figure 1.12: The vertical dashed line represents the mean projected density of galaxies within the virial radius of the clusters. The solid curves are the expected trends due to the morphology-density relation of Dressler (1980), assuming the field population is composed of 18% E, 23% S0 and 59% spiral galaxies (Whitmore et al. 1993). Lewis et al. (2002).

work by Butcher & Oemler (1984) looking at 33 rich galaxy clusters at intermediate redshifts ($0.3 < z < 0.5$), found an increase in the fraction of blue galaxies compared to local clusters (Figure 1.13). It is worth commenting on the somewhat discrepant data point at the highest redshift. This is the cluster CL0016+16 with a redshift of z=0.541 and a calculated blue fraction of 0.02±0.7, a particularly low value of f_B. The authors note that in work undertaken at a similar time by Henry & Lea (1984) a strong correlation was found between f_B and T_X (hotter clusters have fewer blue galaxies) and that this is intriguing since CL0016+16 is a hot cluster of T_X=9keV but they were, at that time, unable to comment on the significance of this result. As will be shown in subsequent sections, this dependence of f_B on T_X has also been found for the data presented in this work.

Since 1984, there has been a substantial amount of work undertaken in this area. However, the technique is not as straightforward as it may first appear since the results of any sort of study are only as good as the cluster sample used. Butcher & Oemler (1984) were working with a cluster sample that was decidedly non-uniform. Their data came from a number of different sources; 4 clusters had V and R band photometry taken using the Kitt Peak National Observatory (KPNO), 15 clusters were imaged using the KPNO and Cerro Tololo Inter-American Observatory (CTIO), a further 10 had data from the Palomar 1.2m Schmidt telescope and there were a few clusters (e.g. Virgo) whose data were taken from the literature. Using so many different datasets and filters can only introduce more uncertainties, corrections and biases. They are not alone in this problem, work done subsequent to this has suffered from difficulties in trying to achieve a large enough, yet uniform, data sample (Newberry et al. 1988) although this was successfully overcome by Loh et al. (2008).

One must also consider the discrepancies between different studies when comparing results to those in the literature. When calculating a blue fraction, these clearly include how does one make a colour cut between red and blue galaxies. Although what is often done is to transform the original definitions of Butcher & Oemler (1984) to the appropriate bands, this is not the only option. Another technique would be to allow the data to be the guide and to look at the colour distribution of the data being considered and to make cuts based upon the observations.

As well as considering the appropriate way to quantify the bimodality of the data, which cluster radial cuts to make and characteristic radius to employ has to be decided upon. The reason for requiring a characteristic radius is that when comparing galaxy populations between clusters, if a fixed physical scale was used, it is possible that

this could simply be covering the cores of the most massive clusters and conversely, contain a significant number of field galaxies in the smallest clusters. In the original Butcher & Oemler paper, they utilised the quantity R_{30}, defined as the radius of the circle containing 30% of a cluster projected galaxy distribution. For a typical cluster in their sample at z$\sim$0.3, R_{30} has a value of $\sim$641kpc. Other options include using the virial radius (Wake et al. 2005) given by

$$R_V = 3.80\beta_T^{-1/2}\Delta_z^{-1/2}(1+z)^{-3/2}(\frac{kT}{10keV})^{1/2}h_{50}^{-1} \tag{1.3}$$

with

$$\Delta_z = \frac{\Delta_c(\Omega_z,\Lambda)\Omega_0}{18\Pi^2\Omega_z} \tag{1.4}$$

taken from Arnaud et al. (2002), where $\Delta_c(\Omega_z,\Lambda)$ is the density contrast and β_T is the normalisation of the virial relation $GM_V/2R_V = \beta_T kT$. For a typical cluster at z$\sim$0.3, this gives an R_V of $\sim$1.7Mpc. These are not the only two options, and the choice made throughout this work was to use a characteristic radius based upon r_{500}, defined as the radius at which the enclosed cluster mass density is equal to 500 times the critical density of the universe at the cluster redshift (Pacaud et al. 2007). Converting the relation of Finoguenov et al. (2001) to a ΛCDM cosmology, Willis et al. (2005) define

$$r_{500} = 0.375T^{0.63}h_{73}(z)^{-1}Mpc \tag{1.5}$$

where T is the measured X-ray temperature in keV and h_{73} is the Hubble constant in units of 73kms^{-1}Mpc^{-1}. For a typical poor cluster at $z \sim 0.3$, r_{500} is of the order of 500kpc and for a richer cluster, can be between approximately 1.1Mpc and 1.3Mpc. One has to take these differences in radius into account when comparing results with those from literature for overlapping clusters (e.g. Wake et al, 2005) since the fraction of blue galaxies in a cluster does vary significantly with radius with f_B increasing with increasing clustercentric radius (Ellingson et al. 2001).

Even taking these various factors into consideration when calculating the blue fraction statistic, this technique remains a model independent cut of galaxy populations in the colour-magnitude diagram (CMD) plane and therefore warrants further investigation. This has included looking at Butcher-Oemler type effects as a function of morphology (i.e. increasing spiral fractions in clusters with increasing redshift; Poggianti et al. 1999) and an infra-red Butcher Oemler effect (increasing fraction

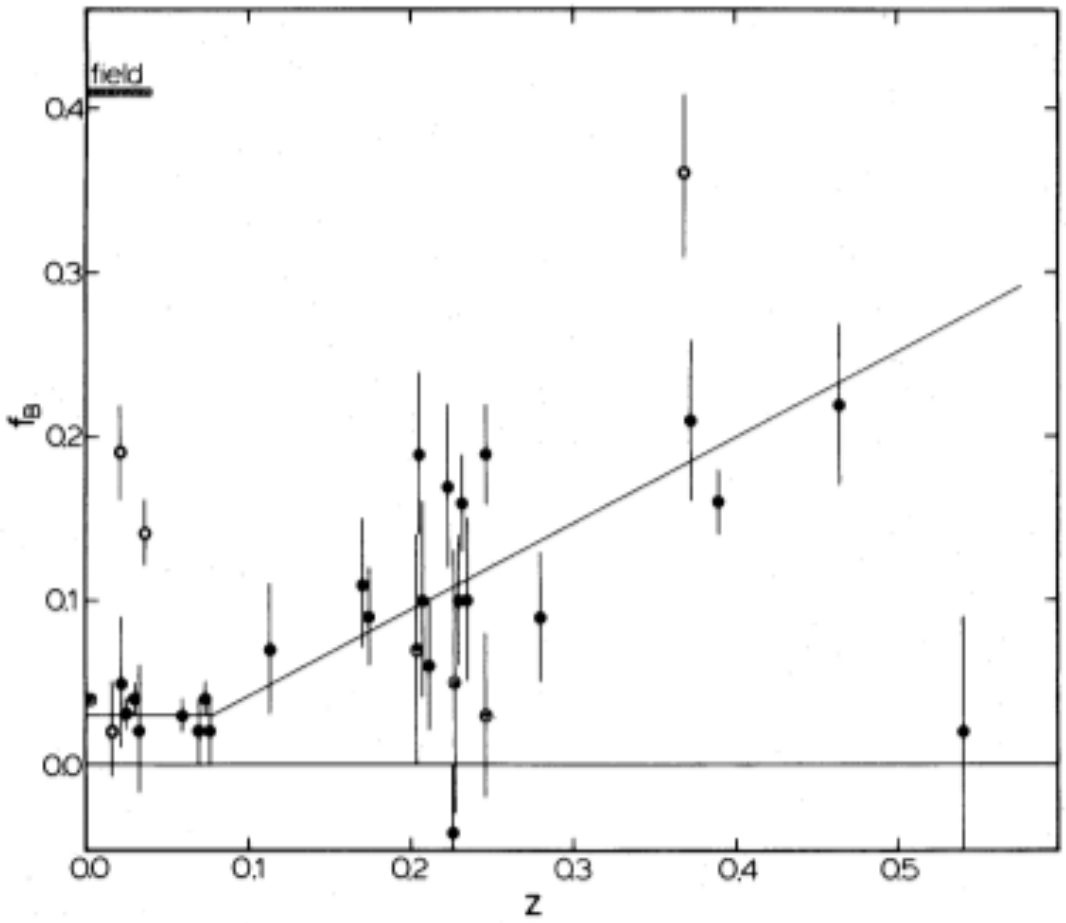

Figure 1.13: Blue galaxy fraction versus redshift (Butcher & Oemler, 1984).

of dusty star forming galaxies in clusters with increasing redshift; e.g. Duc et al. 2002). A somewhat alternative approach is to consider an environmental Butcher-Oemler effect, whereby the redshift interval is minimised to allow the variation of blue fractions to be investigated as a function of varying intrinsic cluster properties, once again, with the aim of determining the physical process(es) at work on a galaxy in a cluster environment.

1.4 Physical Processes acting in Galaxy Clusters

When we consider the physical processes acting on galaxies in different environments, it is useful to divide them into various categories. This has been done by many previous authors, including Treu et al. 2003. They divide these processes into 3 categories;

interactions between the galaxy and the intra-cluster medium (ICM), interactions between the galaxy and the gravitational influence of the cluster and finally galaxy-galaxy interactions. A summary of these key mechanisms and the physical scales on which they are most likely to dominate within a cluster are given in Figure 1.14 and Table 1.1. Determining which of these physical processes are dominating the transformation of a galaxy population (e.g. Spitzer & Baade, 1951; Gun & Gott, 1972) remains unclear.

1.4.1 Galaxy-ICM interactions

Ram-pressure stripping

One suggested mechanism is that of ram pressure stripping of the gas of a galaxy. In 1972, Gunn & Gott created a model describing this ram-pressure stripping, the effective force experienced by the diffuse gas component of the infalling galaxy as it travels through the hot, dense ICM. The ram-pressure is given by

$$P_r \approx \rho_e v^2 \tag{1.6}$$

where ρ_e is the external (to the galaxy, i.e., the intra-cluster) density and v is the velocity of the galaxy. For a typical spiral galaxy, the material is held in the plane by a force per unit area which cannot exceed

$$F = 2\pi G \sigma_s \sigma_g \tag{1.7}$$

where σ_s is the star surface density and σ_g is the gas surface density on the disk of the galaxy. Therefore, it is expected that stripping can occur if [3]

$$\rho_c > \frac{2\pi G \sigma_s \sigma_g}{v^2} \tag{1.8}$$

The ICM contains more than 90% of the baryonic mass in a galaxy cluster (White et al. 1993) and has temperatures of $\sim 10^8$keV and as such, the effect it has on a galaxy falling into the cluster environment can be powerful.

For example, if we consider a disk similar to that of the Milky Way (stellar mass of $5\text{x}10^{10} M_\odot$, ISM mass of $5\text{x}10^9 M_\odot$, disk of radius 10kpc and velocity 1000kms^{-1})

[3]Note that this condition applies to the cold gas component, the hot gas will be less tightly bound.

this gives ρ_c >4.6x10$^{-27}gcm^{-3}$ as the ram pressure condition. The typical density of the ICM in clusters is of the order of $10^{-27}gcm^{-3}$, that which is required for effective ram-pressure stripping.

Additional effects, although not as dramatic as ram-pressure stripping may also be acting on a galaxy due to the ICM. These include the interaction of the high temperature ICM with the cooler gas within a galaxy causing thermal evaporation (Cowie and Songaila 1977) or through gas stripping caused by turbulence (Nulsen 1982).

Further evidence for interactions with the cluster environment were presented by Smith et al. (2010) who used deep UV observations of the Coma cluster to identify 13 star-forming galaxies exhibiting asymmetric morphologies. Combining these observations with broad-band optical and Hα imaging, they interpret their results as being due to gas stripping leaving a wide range of structures including filaments and knots (so-called "jellyfish" galaxies) and extended HI tails.

Strangulation/Starvation

Ram-pressure stripping, as discussed in section 1.4.1, has the potential to strip a galaxy of its cold gas reservoir and thus abruptly quench star formation. However, if only the outer parts of the gas disk of a galaxy are stripped, or if there is no stripping of the tightly bound disk (strangulation can occur without ram pressure stripping), it is possible for star formation to continue until there is no fuel left. As well as being believed to be surrounded by dark matter halos, galaxies are thought to also be surrounded by hot/warm gas composed of gas which is falling into the system for the first time, gas which has fallen in and been shocked to high temperatures but not yet cooled, and gas which has been reheated and expelled by some feedback process. Since the infall and cooling of this material replenishes the interstellar medium as star formation proceeds, the galaxy can form stars over long time scales. However, this gas reservoir is only loosely bound and therefore is easily stripped (via tides or ram pressure) and so one would expect a substantial amount of this gas to be removed as a galaxy is accreted into a cluster environment, causing a slow decrease ($\sim$1Gyr Hernández-Fernández et al. 2012) in the star formation rate, known as strangulation or starvation (Larson et al. 1980). Strangulation, like ram-pressure stripping, in combination with merging (see section 1.4.2) can reproduce many of the observations of star formation and morphology with stellar mass and environment.

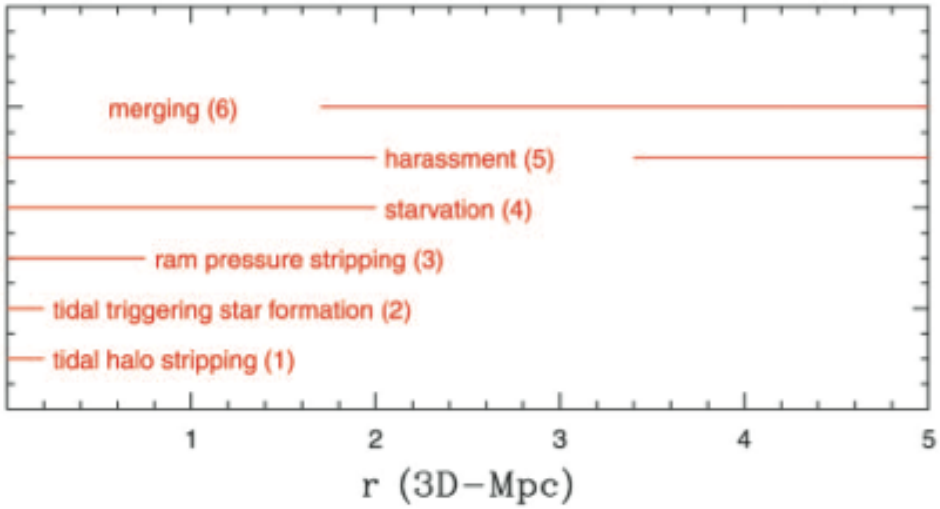

Figure 1.14: Summary of the regions where key physical mechanisms are likely to occur. Horizontal lines indicate the radial regions where the mechansms are most effective. The virial radius, r_V ∼1.7Mpc. Treu et al. (2003).

Table 1.1: Physical mechanisms underlying galaxy processing.

Process	**Timescale**	**Spatial Scales**
Galaxy mergers	$\sim 10^7$yrs (Mihos and Hernquist 1996)	∼Size of galaxy (Hernández-Fernández et al. 2012)
Ram-pressure stripping	$\sim 5\text{x}10^7$ years (Abadi et al. 1999)	∼Across ICM of virial region (Hernández-Fernández et al. 2012)
Strangulation/Starvation	Several Gyr (Treu et al. 2003)	≥Virial radius (Boselli and Gavazzi 2006)
Galaxy-gravitational interactions	$\sim 10^8$yrs (Treu et al. 2003)	
Tidal Truncation	>Cluster crossing time, few Gyrs (Treu et al. 2003)	∼Size of galaxy (Hernández-Fernández et al. 2012)
Harassment	Few Gyrs (Moore et al. 1999)	≥Virial radius (Boselli and Gavazzi 2006)

Both the hot (strangulation, section 1.4.1) and cold (ram-pressure) gas can be stripped from an infalling galaxy, thus exhausting the available gas supply which would otherwise have cooled and formed stars (Abadi et al. 1999; Kawata & Mulchaey 2008; McCarthy et al. 2008). From hydrodynamical simulations (Kawata & Mulchaey 2008; McCarthy et al. 2008), it is possible for group and cluster environments to strip ∼70% and ∼100% respectively of the hot gas from an infalling spiral galaxy over one crossing time [4]. This would cause a rapid decline in star formation rate on a timescale comparable to the rate at which the unstripped cold gas is consumed. This hypothesis is supported by the work of Wolf et al. (2009). Here, they studied the properties of optically passive spirals and dusty red galaxies in the A901/2 cluster complex at z∼0.17 using rest-frame near-ultraviolet-optical spectral energy distributions, 24μm infrared data and HST morphologies from the STAGES data set. They observed red (i.e. passive) spiral galaxies on the red sequence, supporting the view that some fraction of galaxies experience the stripping of disc gas via ram-pressure effects. It is worth noting that all of these gas stripping effects leave the stars unaffected.

1.4.2 Galaxy-galaxy interactions

At a similar time that Gunn and Gott (1972) were studying ram pressure stripping, Toomre and Toomre (1972) were modelling strong tidal interactions between galaxies. Observationally, it was clear that such interactions had a strong effect on the morphologies of the galaxies involved, exhibiting, for example; bridges, tails, stellar bars and sometimes enhanced spiral structures. Prior to this work by Toomre and Toomre (1972), it had been argued that these features were caused by magnetic fields and nuclear jets and could not simply be due to gravitational effects. However, by modelling the interactions of four pairs of galaxies, these authors were able to show that gravity alone was enough to reproduce the observed features.

Toomre (1977) further went on to suggest that the remnants of the mergers of disk galaxies could account for the population of elliptical galaxies in the Universe. This became known as the "merger hypothesis". Following on from this, in 1980, Larson et al. (1980) suggested that the stripping of gas in clusters is able to stop star formation in spiral galaxies turning them into S0s, and Cowie and Songaila (1977) suggested that the hot X-ray gas removed the intergalactic gas in spiral galaxies leaving behind

[4]Where the crossing time is given by; t_{cross}=R/σ with R being the size of the system and σ being the typical velocity.

S0s. There is also recent observational evidence for enhanced galaxy-galaxy interactions in denser environments (compared to the field) provided by observations taken with the Hubble Space Telescope (Dressler et al. 1994; van Dokkum et al. 1999).

When considering galaxy-galaxy interactions, this can refer to a range of encounters. They may be tidal, whereby the halo gas is moved outward to be more readily stripped (Chung et al. 2007), high speed ("harassment" or "threshing"), also resulting in the stripping of halo gas (Moore et al. 1996) or infalling galaxies merging with previously existing cluster members.

In order to try and predict the outcome of a merger, the relative masses of the galaxies involved need to be considered. Large mass ratios enhance star formation in the satellite galaxy but may not do so in the more massive galaxy (Cox et al. 2008). Equal mass ratio mergers can completely destroy the infalling spiral galaxy creating a bulge dominated system along with a central star burst (Di Matteo et al. 2007). These strong interactions can give rise to a short term enhancement in star formation preceding the exhaustion of the cold gas available. When considering the environmental dependence of galaxy evolution, strong galaxy-galaxy interactions are extremely interesting. The merger rate for two equal mass galaxies can be quantified by the relation

$$K = \left[\frac{1}{x} + \frac{2}{x^3} - \frac{2exp(-x^2)}{x^3} - \frac{3\pi^{1/2}}{2}\frac{erfx}{x^2}\right] \tag{1.9}$$

(Mamon 1992). Where $x = \alpha_v v_g / 2v_{cl}$ with v_{cl} being the one-dimensional velocity dispersion of the cluster, α_v being a dimensionless number and v_g being the one-dimensional internal velocity dispersion of the two colliding galaxies. This relation arises from the integration of the merger cross section and the probability that the relative velocities of two merging galaxies falls between v and $v + dv$ at some time t for a cluster that is assumed to be virialised. It is a maximum for $v_{cl} \simeq 0.7 v_g$ and falls off as $(v_{cl}/v_g)^{-3}$ for $v_{cl} \gg v_g$ to values approximately 25 times lower for typical ratios found in clusters. This is shown in Figure 1.15.

Clearly, the merging rate is a strong function of environment, being more likely to occur in lower mass groups where velocity dispersions are generally lower than rich clusters of galaxies.

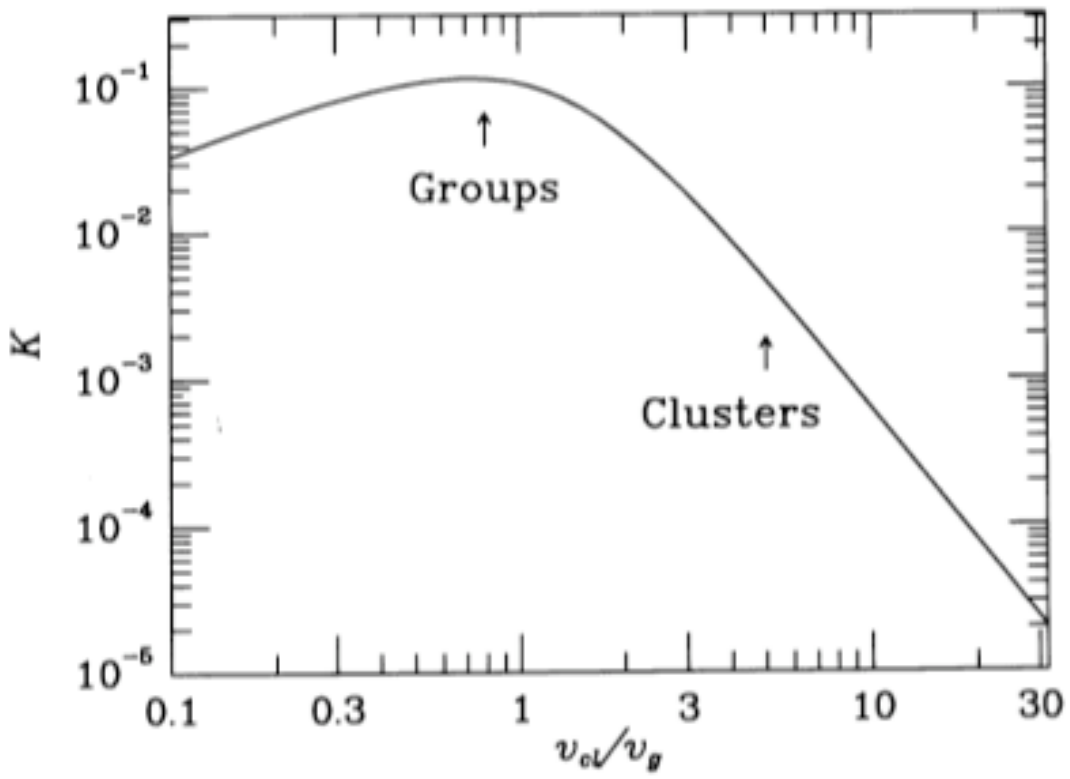

Figure 1.15: Dimensionless merger rate K vs. ratio of cluster to galaxy velocity dispersions. (Mamon, 1992).

1.4.3 Galaxy Preprocessing

In the current model of hierarchical structure formation, it is the infalling of groups of galaxies which build up the rich clusters we can observe today. Therefore, the environmental processes which are occurring and causing the observed morphology-density relations and truncating star formation may be taking place in the longer lived group environment (Zabludoff and Mulchaey 1998). Such an idea is referred to as "galaxy preprocessing".

Support has been given to the importance of preprocessing by a number of authors, including Fujita (2004). In this work, the author considers disk galaxy evolution in clusters using analytical models based on the hierarchical clustering scenario. The results suggest that, for disk galaxies in subclusters surrounding the main cluster, the effects of ram-pressure stripping cannot be neglected despite the subclusters being considerably less massive than the main cluster itself. The preprocessing mechanisms they propose as the most likely are those of "strangulation" (the stripping of warm gas from a galaxy) along with the evaporation of the cold gas by the surrounding intra-cluster medium (ICM). They further propose that the morphological transformation of disk galaxies at z <1 is not primarily due to merging events between galaxies.

Bahé et al. (2013) used high-resolution cosmological hydrodynamic simulations to study galaxies in groups and clusters spanning a wide range in mass, and therefore a wide range in environment ($\log_{10}(M_{host}/M_{\odot})$=[13.0,15.2]). Their results showed a depletion in hot and cold gas along with a decline in the star-forming fraction of galaxies out to a clustercentric radius of $\sim 5r_{200}$ with as many as $\sim$50% of the galaxies around massive clusters being affected by preprocessing (less than 10% around groups).

Cortese et al. (2006) presented further evidence in support of pre-processing in groups in a multiwavelength study of a compact group of galaxies falling (at high speeds) into the cluster Abell 1367. This infalling group is referred to as the Blue Infalling Group (BIG) and provides a unique environment of study. The authors find that the brightest galaxy in the BIG is likely to be an S0 which has recently ($\sim$1.5 Gyr) undergone a minor merger and a consequent burst of star-formation. Thus implying that S0 galaxies can form outside clusters before joining them, that groups are natural sites for gravitational interactions to produce the transformation of normal spirals into these S0s.

McGee et al. (2009) investigated the accretion of galaxies into groups and clusters at different redshift epochs using semi-analytic galaxy catalogues. Their results

indicated that at all redshifts studied (z=0, 0.5, 1.0, 1.5), a significant fraction of clusters have had their galaxies accreted through groups. At z=0, ∼40% of cluster galaxies having $M_{Stellar}$ $>10^{9}h^{-1}M_{\odot}$ were accreted through halos of masses greater than $10^{13}h^{-1}M_{\odot}$. At their highest redshift, this number decreases to ∼25% of galaxies being accreted through $10^{13}h^{-1}$ into $10^{14.5}h^{-1}M_{\odot}$ mass clusters. They also observe that the galaxies which are accreted through the group environment are on average more massive than those accreted from the field with the fraction of galaxies accreted from isolated environments being independent of the final cluster mass. One of their most significant conclusions is the observation that the effects of environment upon galaxies begin in halos of 10^{12}-$10^{13}h^{-1}M_{\odot}$ and act on timescales greater than 2Gyrs, supporting the idea of a long lifetime, gentle process like strangulation.

Further observational support for pre-processing was found by Li et al. (2009) in their study of the environmental influence on the galaxy populations of 16 intermediate redshift ($0.17< z <0.55$) galaxy clusters from the Canadian Network for Observational Cosmology (CNOC) Survey. They use the galaxy red fraction (f_{red}) as a measure of evolutionary status of cluster galaxies and find that cluster galaxies which belong to moderately massive infalling galaxy groups show a much stronger evolution in f_{red} than those classified as non-group galaxies, a clear signature of preproessing.

However, at the same time, Berrier et al. (2009) found that the majority of galaxies in clusters experienced no pre-processing in groups prior to being accreted into the cluster environment in their study of 53 simulated clusters in N-body ΛCDM simulations. It was found that ∼70% of cluster galaxies fell directly in from the field with at most 12% being prior members of group, suggesting that processes such as merging in the group environment is a less important effect to those from the global cluster environment (e.g. Ram-pressure stripping).

The issue of pre-processing is obviously still a contentious one, and so it is with an open mind that we consider the effect in this thesis.

1.5 Luminosity distributions

A basic and fundamental property of a galaxy is the luminosity, which is roughly proportional to the number of stars contained (and so is a measure of the stellar mass). As the stellar content changes with time (the stars evolve), so too does the

luminosity function [5] (LF) and therefore it can provide information on the evolution of the galaxy population. In any given galaxy cluster, there are a wide range of galaxy luminosities and the luminosity function gives the relative number of galaxies in a luminosity bin,

$$dn(L) = \phi(L)dL \tag{1.10}$$

where $dn(L)$ is the comoving number density of galaxies having luminosities in L, $L + dL$. LFs can tell us about such things as primordial density fluctuations and physical processes acting upon galaxies and any galaxy formation/evolution theory must be able to reproduce them.

Galaxy LFs are generally fit using a Schechter (1976) function. This was first done on a sample of Abell clusters as shown in Figure 1.16. This function has the following form

$$\Phi(L)dL = \phi_* \left(\frac{L}{L_*}\right)^{\alpha} exp\left(-\frac{L}{L_*}\right) d\left(\frac{L}{L_*}\right) \tag{1.11}$$

where L_* is a characteristic luminosity separating the low and high luminosity regimes (and can be considered as the mean luminosity of giant galaxies; Bañados et al. 2010), α is the power law slope at low luminosities (measuring the relative abundance of dwarf galaxies; Bañados et al. 2010) and n_* is a normalisation factor.

Since galaxy populations can be divided into red-sequence and blue cloud galaxies, it is possible to study how the galaxy luminosity function depends on colour by studying it for only red sequence galaxies (or similarly, for only blue cloud galaxies). Previous work has found that, on average, red galaxies have a brighter characteristic magnitude (M^*) and a shallower faint end slope (α) than blue galaxies. This would suggest a decreasing number of red galaxies with decreasing luminosity. However, this result is still contentious given that an upturn in the LF of the red galaxies has been observed (Blanton et al. 2005) at the faint ($M_r - 5\log h \gtrsim -17$) end.

The faint end of the LF is especially hard to study given that the detected numbers of faint galaxies decreases with increasing redshift (e.g. De Lucia et al. 2007, Stott et al. 2007). Some authors have detected a decrease in the slope of the faint end with increasing redshift. Liu et al. 2008 observed this trend out to a redshift of 0.5 and Khochfar et al. 2007 saw this in their simulations. However, Andreon 2008 observed no evolution out to a redshift of 1.3.

[5] A true luminosity function contains a volume term, however we do not know the volume of a cluster (since it is a cylinder of uncertain line-of-sight depth), therefore there is no volume term and thus the term "luminosity distribution" rather than "luminosity function" is more accurate.

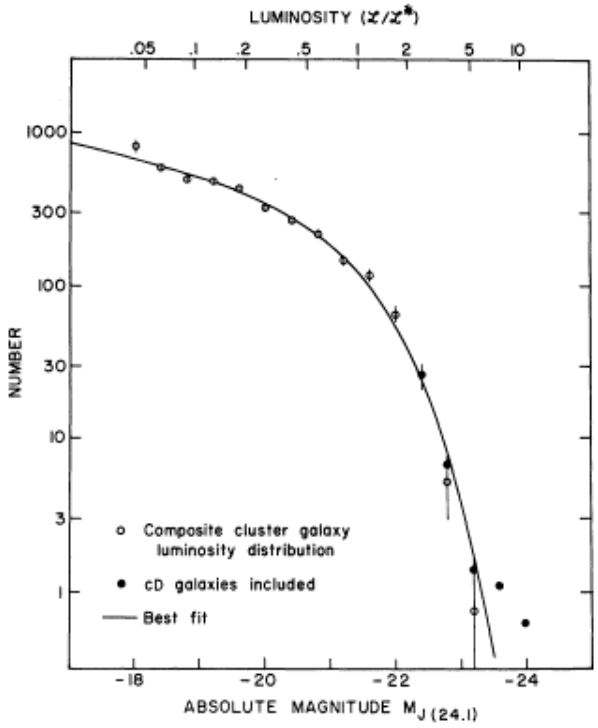

Figure 1.16: Best fit of analytic expression to observed cluster galaxy luminosity distribution. Filled circles show the effect of including cD galaxies in composite (Schechter 1976).

Given the relationship between galaxy colour and galaxy morphology, it follows that there is a relationship between the luminosity function and morphology. Galaxies of different morphological types exhibit different luminosity functions as is shown in Figure 1.17. It is clear that, in clusters, the bright end is dominated by elliptical galaxies (with a Gaussian form) with the faint end being dominated by dwarf ellipticals (with a Schechter form) with spirals dominating in the intermediate luminosity range (also with a Gaussian form). The rising faint end could be explained by the presence of these dwarf elliptical galaxies (and to a lesser extent, by dwarf irregulars).

A natural next step given these colour and morphological dependences is to consider how the luminosity function depends on environment. Observations of cluster and field samples have shown that for cluster galaxies, there is a turnup in the LF at the faint end and an extended tail at the bright end (e.g. Popesso et al. 2006). Referring once again to Figure 1.17, the LFs for different types of galaxies are similar for clusters and the field, the differences seen in the composite LFs are from differences in the amplitudes of the LFs for each morphological type. This is consistent with the morphology-density relation and so is perhaps not a surprising conclusion. Thus we can consider the environmental dependence of the LF as arising from the morphological dependence discussed previously.

However, the shape and slope of the LF is not universally agreed upon. A number of studies have been carried out measuring the LFs of individual clusters (e.g. Goto et al. 2002, Yagi et al. 2002) and measuring the LF of clusters compared to the field. Significant differences between the LFs of individual clusters and between clusters and the field have been observed in a number of studies (e.g. Christlein and Zabludoff 2003) whilst others (e.g. Paolillo et al. 2001, Andreon 2004) have observed a universal LF in all environments.

This "universal LF hypothesis" was introduced by Schechter (1976) in his seminal paper whereby he analysed the LFs of 14 clusters and presented the analytic function now known as the Schechter function. He also proposed that the shape of the cluster LFs was universal with only the normalisation factor varying.

A related question is the origin and build up of the red sequence; which is still causing debate in the literature with a number of conflicting studies appearing. One way to study this problem is through the galaxy luminosity function (LF). For example Bower et al. (2006) demonstrated that the bright end of the LF can be affected by feedback from AGN and Adami et al. (2007) showed that LFs can be used to investigate star-formation in faint galaxies.

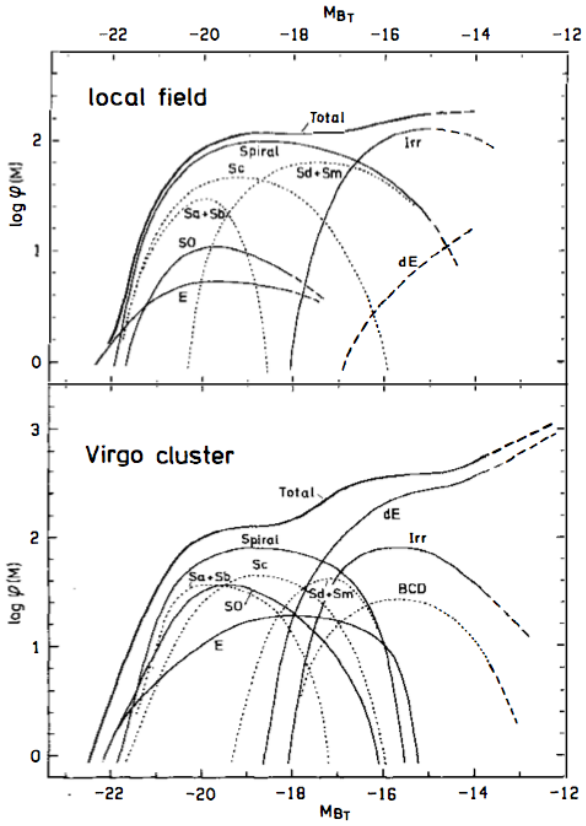

Figure 1.17: Luminosity function of field galaxies (top) and Virgo cluster members (bottom) for individual galaxy types. (Binggeli et al. 1988).

An alternative, but related way to investigate how different galaxy populations evolve in cluster and group environments is to calculate the dwarf-to-giant ratio (DGR) or the reciprocal giant-to-dwarf rate (GDR). The standard model of galaxy formation predicts that giants are more likely to form in high density regions than dwarfs (White et al. 1987), but environmental effects will likely take over as a galaxy evolves, influencing this DGR measurement (Zabludoff and Mulchaey 2000). This non-parametric measurement is also a robust calculation of the fraction of faint-to-bright (or bright-to-faint for GDR) galaxies and has the advantage over the LF of not requiring a functional fit to the data yet still being a probe of galaxy evolution.

The DGR has been extensively studied as a function of a number of different parameters. Driver et al. (1998) found a large variation in the DGR ($0.8 \leq \mathrm{DGR} \leq 3.1$) from cluster to cluster (in a study of seven rich clusters) in the inner regions ($r < 0.56$Mpc) alongside an anticorrelation with mean local projected density out with this radius (i.e. DGR increasing towards lower densities). In work by Dahlén et al. 2004, as well as finding evidence for the universal shape of the LF for different morphological types and no evidence for a universal total LF, they observed a correlation between DGR and surface density whereby dwarf galaxies are not found in high density cluster cores. Goto et al. (2005), in a study of the massive cluster MS 1054-0321 find an increase in the GDR inside of the virial radius (see Figure 1.18), coinciding with an environment where the star-formation rate and morphology density relations take effect. Also observed are strong trends in GDR with morphology and local galaxy density (see Figure 1.20).

1.6 The aim of this thesis

The aim of this thesis is to measure the aforementioned observational trends as a function of varying environment to investigate this influence upon the evolution of galaxy populations. We classify environment on two scales. The first of these is "global" whereby we use the cluster X-ray temperature (a proxy for cluster mass) to provide a measure of the effect of the cluster environment itself upon the constituent galaxies. We would expect this to represent the physical effects of, for example, ram-pressure stripping. Our second measurement is on a "local" scale, using the local galaxy density as a representative measurement of the effects of galaxy-galaxy interactions, for example for merging events. Ultimately, it is the disentangling of these two broad mechanisms that has been the subject of much study and this thesis

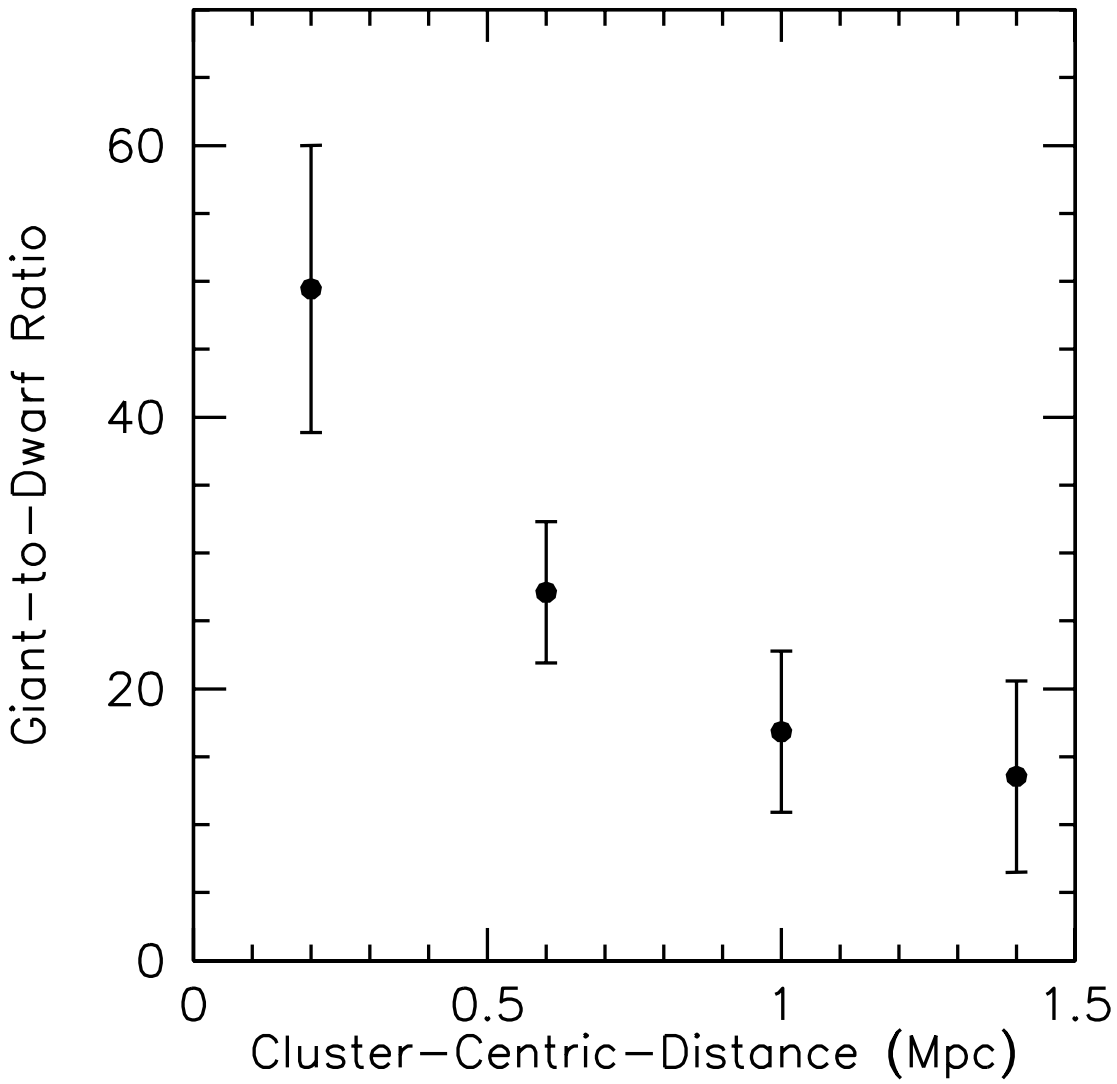

Figure 1.18: Giant-to-dwarf ratio as a function of clustercentric distance. Goto et al. (2005).

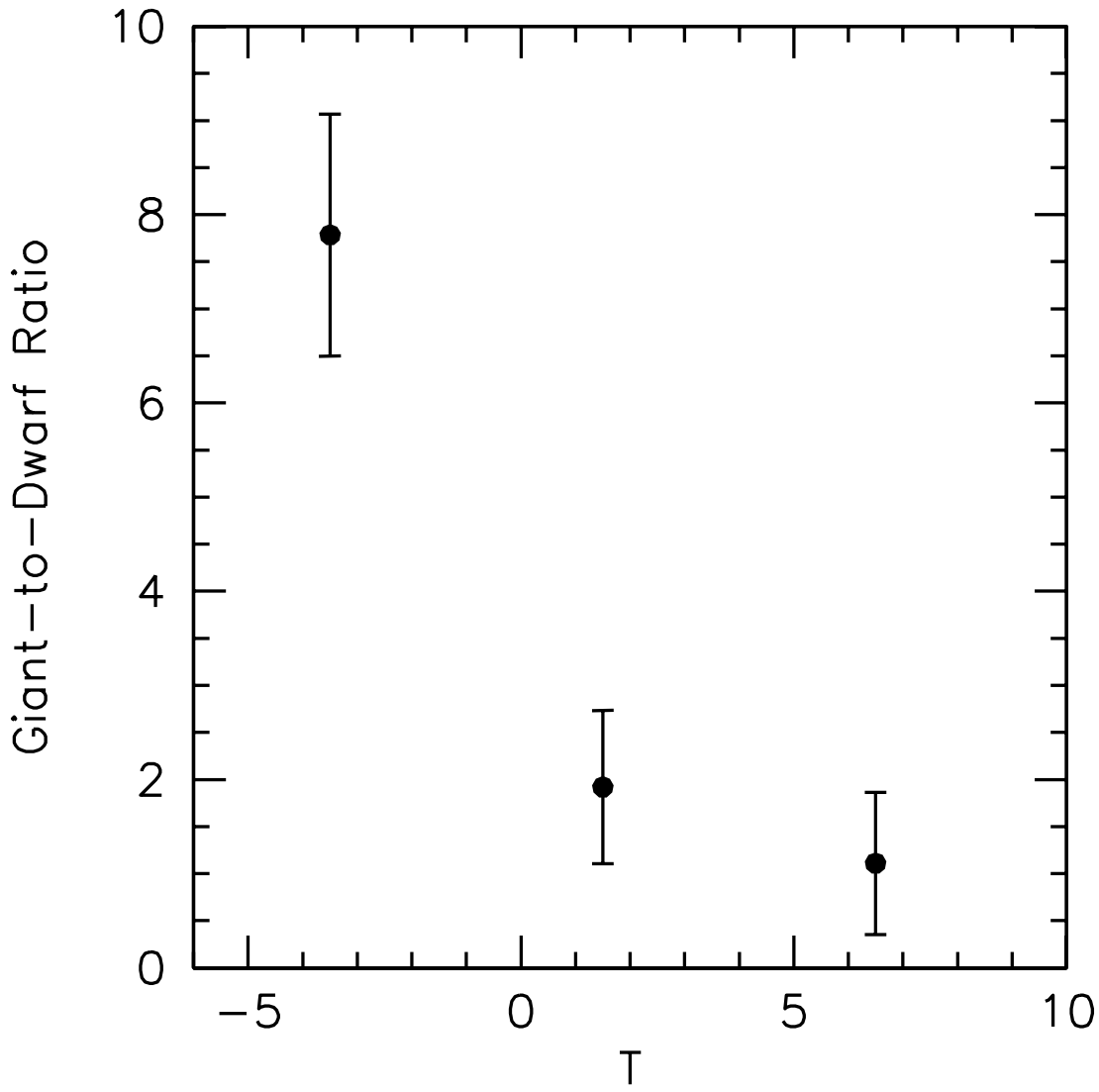

Figure 1.19: Giant-to-dwarf ratio as a function of morphological type. Goto et al. (2005).

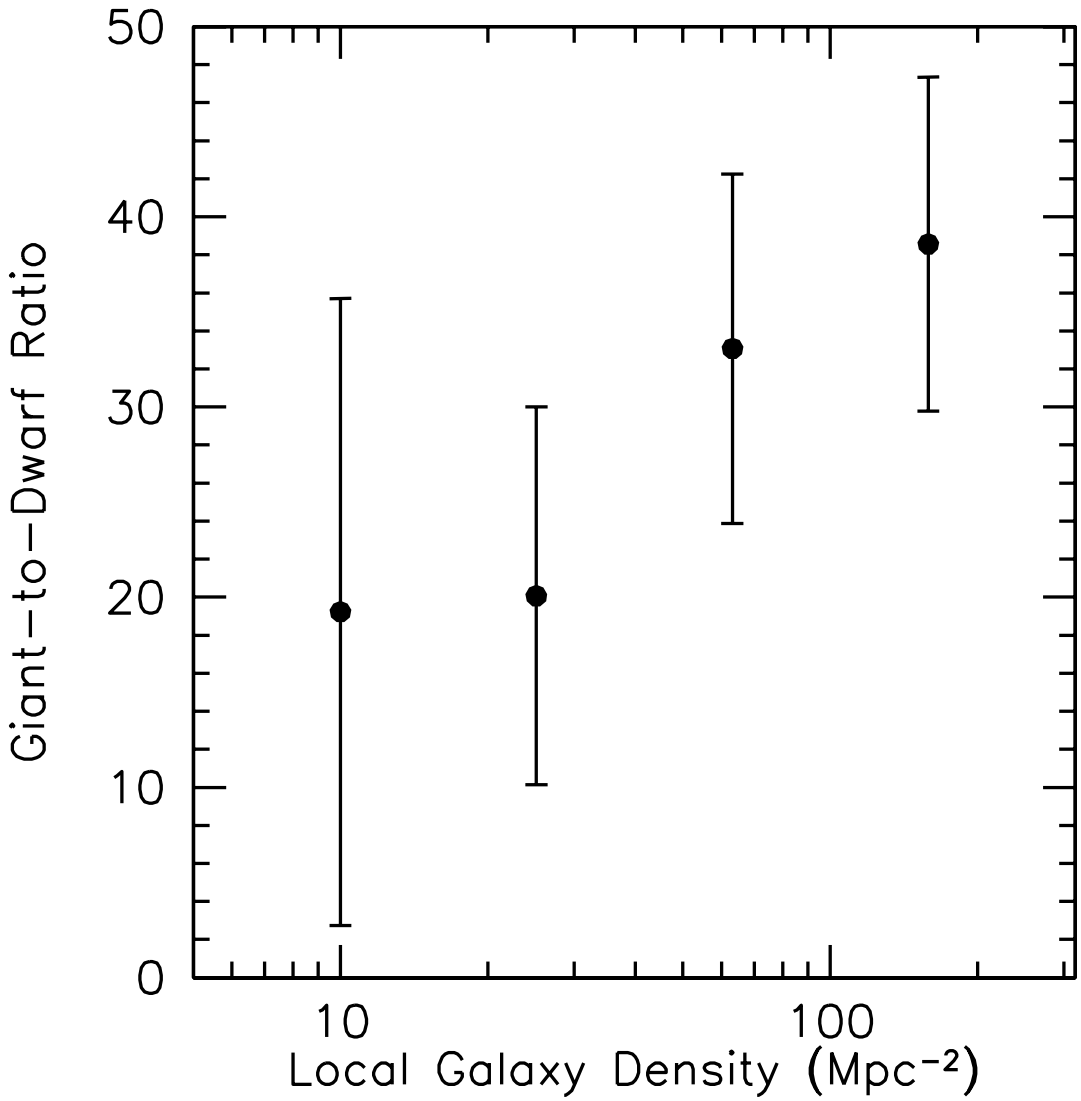

Figure 1.20: Giant-to-dwarf ratio as a function of local galaxy density. Goto et al. (2005).

aims to tackle this problem, utilising the best available dataset to us.

We will be using a large sample of X-ray selected clusters spanning a wide range of environments, from poor groups to rich clusters. However, unlike previous work, all of our clusters and groups possess uniform optical photometry and global properties defined using their X-ray properties therefore we are able to confidently compare our systems.

Chapter 2 is a detailed description of the data sets which the scientific analysis of this thesis are based on. Chapter 3 presents a detailed study of the fraction of blue galaxies for our clusters and groups as a function of environment (in this case X-ray temperature) and is published in Urquhart et al. (2010). This work is then followed in Chapter 4 by a simultaneous analysis of both "local" and "global" environments and we relate our results to the physical processes of merging and ram-pressure stripping. Chapter 5 is an analysis of the luminosity distribution and related dwarf-to-giant ratios for our sample of clusters and groups. The final science chapter, Chapter 6 gives the results of our morphological analysis using the modelling program `GIM2D`. The work of the thesis is then drawn together in Chapter 7 along with a proposal to build upon this work in the future.

Chapter 2

Data Set

This chapter provides a detailed description of the data used throughout the thesis. It includes the X-ray properties of the clusters and the optical photometry for all samples. We require our sample to have a wide X-ray temperature, T_X, baseline since this translates into a wide cluster mass, M_X, baseline. It is preferable to measure T_X over the X-ray luminosity, L_X since there is less scatter on the M_X-T_X relation (with typical scatter of $\pm$0.1dex) than on the M_X-L_X relation (with typical scatter $\pm$0.2dex) as shown in Figures 2.1 and 2.2.

We also require our sample to contain many clusters to provide good statistics, whilst at the same time limiting the redshift interval to reduce the effects of evolution and k-corrections. And finally, we require our sample to have uniform optical photometry in order to provide reliable measures of galaxy stellar populations.

2.1 X-ray selected Galaxy Clusters

2.1.1 XMMLSS Survey

The first sample of data consists of clusters with X-ray temperatures of $T_X < 3$keV spanning the redshift range $0.25 < z < 0.35$ drawn from the X-ray Multi-Mirror (XMM) Large Scale Structure (LSS) survey (Pierre et al. 2004).

The entire XMM-LSS survey covers an area of 11.1deg^2 in the [0.5-2]keV band to a flux limit of $\sim$1x10^{-14}ergs^{-1}cm^2. The survey consists of 91 positions on the sky with a total of 124 pointings being executed (117 observed combined with 7 from Subaru XMM-Newton Deep Survey, SXDS; Ueda et al. 2008). The XMM-LSS survey area is located around 2^h30^m -5° and the layout on the sky is shown in Figure 2.3.

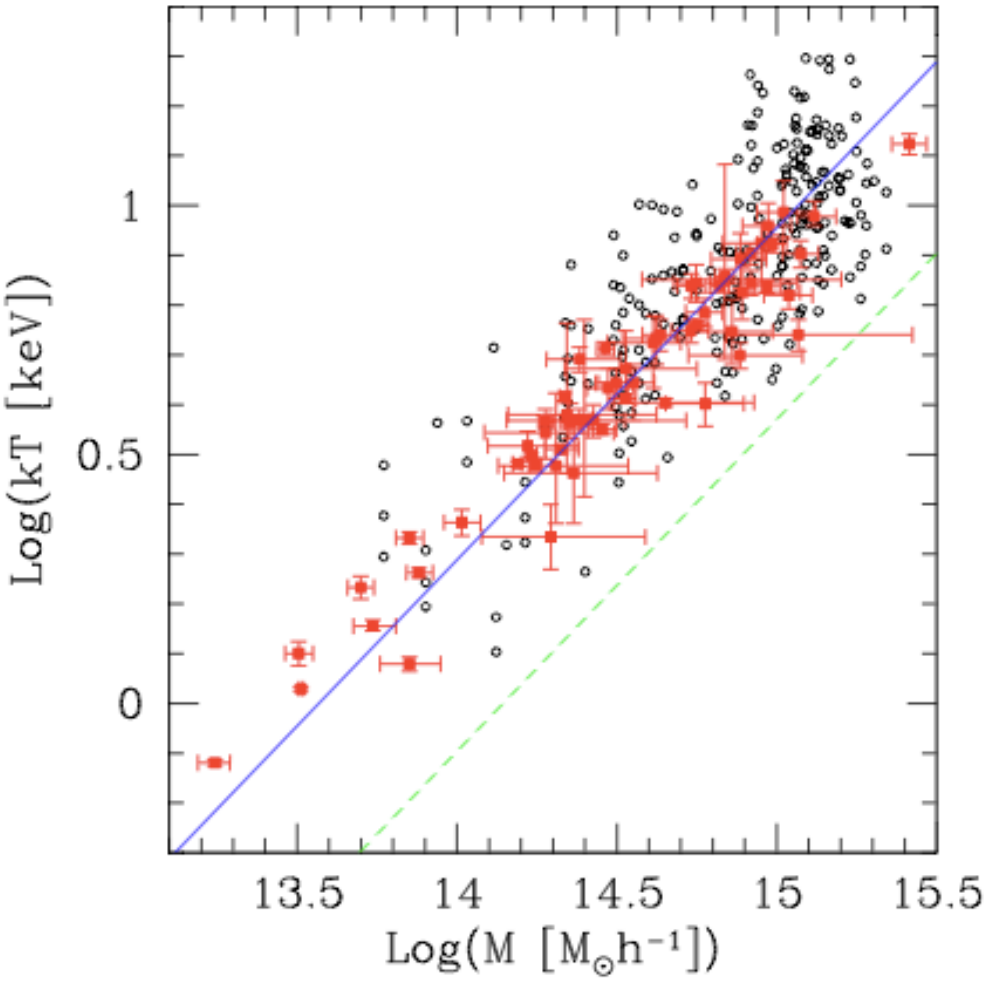

Figure 2.1: Mass-temperature relation for low redshift clusters (Fedeli and Bartelmann 2007).

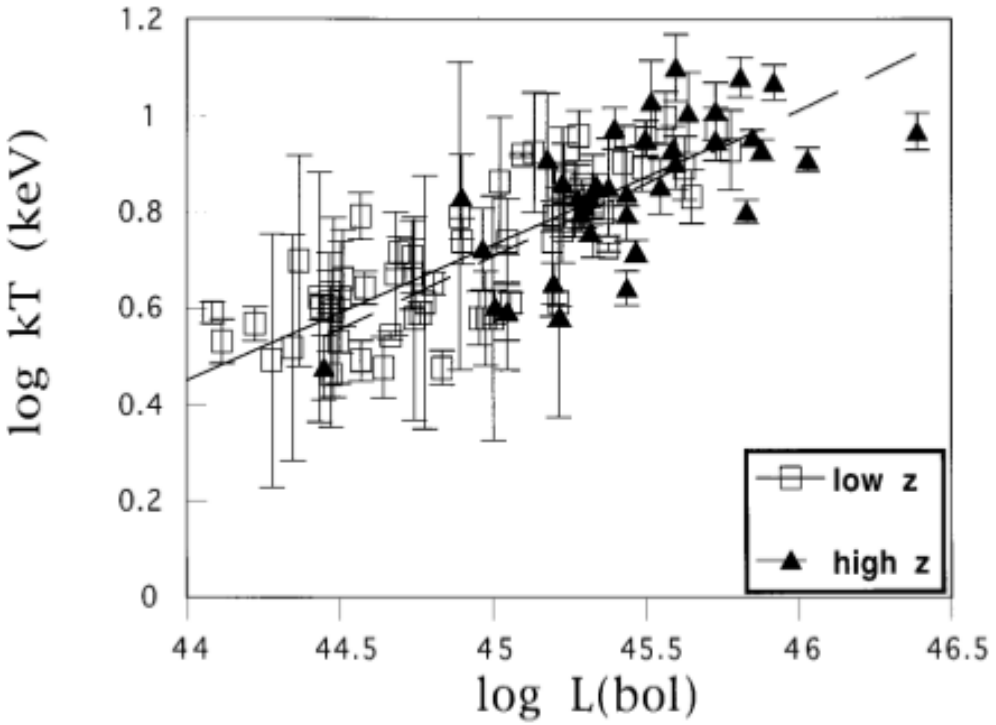

Figure 2.2: Luminosity-temperature relation for a low-redshift ($z < 0.1$, open squares) and a high-redshift ($z > 0.14$, filled triangles) sample of clusters (Mushotzky and Scharf 1997).

There resulted in 6721 objects in the deep full-exposure catalogue and 5572 in the 10ks-limited catalogue.

The clusters used here are taken from the "Class 1 (C1)" sample (Pacaud et al. 2007) containing the largest number of uncontaminated extended sources. The details of these clusters are given in Table 2.1. The clusters are drawn from an area of 5deg^2 out to a redshift of z=1.05. The distribution peaks at z=0.3 and T=1.5keV with half of the detected objects being groups having temperatures less than 2keV. Using optical photometry and spectroscopy from either CTIO/MOSAIC II in the Rz' bands (Andreon et al. 2004) or CFHT/MEGACAM in the $ugriz$ bands, these X-ray sources were confirmed as galaxy clusters based on there being a significant overdensity of galaxies with characteristically red colours within a specified region and spectroscopically determined redshift.

A characteristic projected radius is required in order to define cluster membership in any study of this sort. The radius used throughout this thesis is r_{500}. This is defined as the radius at which the cluster mass density reaches 500 times the critical density of the universe at the cluster redshift (Pacaud et al. 2007). After a conversion to a ΛCDM cosmology and using the mass-temperature relation of Finoguenov et al. 2001, Willis et al. (2005) define the following relation

$$r_{500} = 0.375\mathrm{T_X^{0.63}h_{73}(z)^{-1}Mpc} \tag{2.1}$$

where T_X is the X-ray temperature in keV and h_{73} is the Hubble constant in units of 73kms^{-1}Mpc^{-1}.

2.1.2 Canadian Cluster Comparison Project (CCCP)

In addition to the XMM-LSS data, galaxy clusters were also taken from the Canadian Cluster Comparison Project (CCCP; Bildfell et al. 2008). This was created primarily to study the baryonic tracers of cluster mass, to explore the thermal properties of the hot diffuse gas and to study the dynamical states of the clusters. The entire sample consists of 50 clusters in the redshift range $0.15 < z < 0.55$ observed with either the CFH12k camera or `MEGACAM` on the Canada France Hawaii Telescope (CFHT). This restricts the cluster sample to -15° < dec < 65°. Cluster are also required to have *ASCA* (Advanced Satellite for Cosmology and Astrophysics) $\mathrm{T}_X > 3$keV. The cluster temperatures are taken from a systematically reduced cluster catalogue of Horner 2001 based on archival *ASCA* data.

Table 2.1: Properties of the cluster sample. Clusters are sorted with increasing temperature. Clusters possessing $T(\mathrm{keV}) < 3$ are labelled "Cool", clusters possessing $5 < T(\mathrm{keV}) < 8$ are labelled "Mid" and those possessing $T(\mathrm{keV}) > 8$ are labelled "Hot".

Cluster	R.A. (deg.)	Dec. (deg.)	T_X (keV)	z	r_{500} (kpc)
XLSSC 13	36.858	-4.538	$1.03^{+0.1}_{-0.08}$	0.31	340
XLSSC 51	36.498	-2.826	$1.22^{+0.12}_{-0.13}$	0.28	384
XLSSC 44	36.141	-4.234	$1.27^{+0.09}_{-0.1}$	0.26	399
XLSSC 08	36.337	-3.801	$1.30^{+0.7}_{-0.22}$	0.30	387
XLSSC 40	35.523	-4.546	$1.57^{+1.07}_{-0.25}$	0.32	402
XLSSC 23	35.189	-3.433	$1.67^{+0.29}_{-0.16}$	0.33	497
XLSSC 22	36.916	-4.857	$1.69^{+0.08}_{-0.07}$	0.29	472
XLSSC 25	36.353	-4.679	$2.00^{+0.22}_{-0.17}$	0.26	533
XLSSC 18	36.008	-5.090	$2.04^{+0.65}_{-0.42}$	0.32	615
XLSSC 27	37.014	-4.851	$2.84^{+0.6}_{-0.54}$	0.29	653
XLSSC 10	36.843	-3.362	$2.40^{+0.49}_{-0.36}$	0.34	574
MS0440+02	70.805	2.166	$5.02^{+0.61}_{-0.5}$	0.19	957
A1942	219.600	3.669	$5.12^{+0.71}_{-0.56}$	0.22	957
A0223	24.477	-12.815	$5.28^{+0.63}_{-0.52}$	0.21	964
A2259	260.033	27.668	$5.32^{+0.29}_{-0.27}$	0.16	1007
A1246	170.9972	21.482	$6.04^{+0.42}_{-0.37}$	0.19	1078
A2537	347.092	-2.187	$6.08^{+0.59}_{-0.49}$	0.30	1039
A0959	154.433	59.556	$6.26^{+0.93}_{-0.81}$	0.29	1022
A0586	113.072	31.637	$6.39^{+0.72}_{-0.6}$	0.17	1127
A0115	13.980	26.422	$6.45^{+0.33}_{-0.31}$	0.20	1120
A0611	120.228	36.065	$6.69^{+0.51}_{-0.44}$	0.29	1100
A0521	73.510	-10.244	$6.74^{+0.5}_{-0.45}$	0.25	1106
A2261	260.609	32.139	$6.88^{+0.47}_{-0.41}$	0.22	1153
A2204	248.192	5.574	$6.97^{+0.18}_{-0.18}$	0.15	1247
MS1008-12	152.632	-12.652	$7.47^{+1.56}_{-1.21}$	0.30	1169
CL1938+54	294.555	54.159	$7.52^{+0.38}_{-0.37}$	0.26	1200
A0520	73.554	2.924	$7.81^{+0.74}_{-0.64}$	0.20	1262
A1758	203.205	50.538	$7.95^{+0.74}_{-0.62}$	0.28	1186
A2111	234.914	34.429	$8.02^{+0.95}_{-0.77}$	0.23	1267
A0851	145.746	46.9945	$8.99^{+1.34}_{-1.01}$	0.41	1291
A0697	130.740	36.3662	$9.14^{+0.6}_{-0.54}$	0.28	1343
A2104	235.029	-3.3017	$9.31^{+0.5}_{-0.47}$	0.16	1438
A1914	216.512	37.8244	$9.48^{+0.49}_{-0.45}$	0.17	1444
A2163	243.920	-6.1438	$12.12^{+0.62}_{-0.57}$	0.20	1663

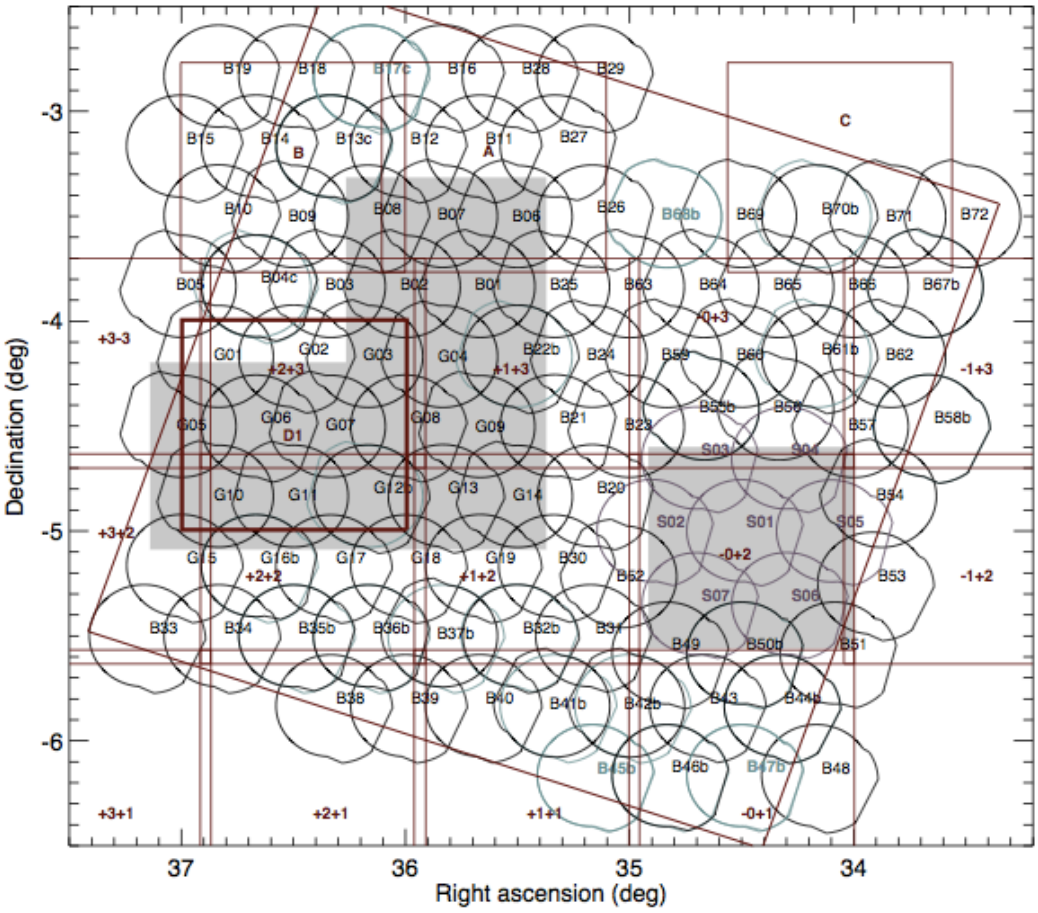

Figure 2.3: Layout of the XMM-LSS pointings and coverage in other wavebands. The dark gray squares indicate the tiles of the CFHTLS W1 survey, supplementary pointings marked as A, B and C and the CFHTLS D1 field (thick black line). Chiappetti et al. 2012.

Table 2.2: Characteristics of the optical data.

Sample	g-band	r-band	
	t_{exp}(s)	t_{exp}(s)	seeing ($''$)
XMM-LSS	2500	2000	0.8
CCCP	1800	4800	0.7

For this thesis, to ensure uniformity across the samples, only those with imaging from the `MEGACAM` imager are included. This created a sample of clusters having $0.15 < z < 0.41$ and $5.02 < \mathrm{T(keV)} < 12.12$.

These CCCP clusters all lie above the nominal X-ray flux limit of the XMM-LSS survey, covering the full range of scatter observed in scaling relations including L_X-T_X. Therefore, the CCCP clusters would all be detected by X-ray images of the same quality as the XMM-LSS survey images (irrespective of how the CCCP clusters were originally selected). However, XMM-LSS has insufficient areal coverage to detect such massive clusters which display low sky surface densities and so combining XMM-LSS with CCCP provides a representative, (largely) unbiased sample of X-ray clusters spanning a relatively narrow redshift range but a broad range in X-ray temperature ($1 < \mathrm{kT(keV)} < 12$) and therefore representing a variety of different environments from low mass groups to high mass clusters.

2.2 Optical Photometry

One of the important aspects of this work is the uniform nature of the sample i.e. all of the clusters are X-ray selected/detected and of uniform optical photometry. The XMM-LSS clusters are drawn from the CFHT Legacy Survey (CFHTLS) 'Wide Survey', W1 area. The data consists of 72 pointings centred at RA(J2000)=02h 18m 00s and DEC(J2000)=07°00′ 00°. Observations were done in the $u'g'r'i'z'$ bands.

Optical photometry for the CCCP clusters were also observed using the CFHT with `MEGACAM` in the g' and r' bands. Characteristics of the optical data are given in Table 2.2.

Approximately 4deg^2 of the XMM-LSS footprint lies beyond the northern declination limit of the CFHTLS W1 field, 3deg^2 of which has been imaged in the $g'r'z'$ bands as part of the XMMLSS follow up campaign. The remaining 1deg^2 was excluded from further analysis due to the presence of the bright star Mira. To ensure consistency, the image exposure times in these additional fields were matched to the

exposures of the CFHTLS wide fields in each filter.

2.2.1 Catalogue Creation

In order to have a uniform catalogue creation between the XMMLSS and CCCP images, rather than use the photometric catalogues produced by `TERAPIX` [1](Traitement Elementaire, Reduction et Analyse des PIXels de megacam), we performed our own catalogue creation. Source extraction and photometry were performed using `SExtractor v2.5.0` (Bertin and Arnouts 1996) in two-image mode with source detection being performed on the r'-band images. For full details of the configuration and parameter files used to generate the catalogues, please see Appendix A. Magnitudes were measured within the Kron radius (defined as the radius that contains approximately 90% of an objects light) as well as in 3″ diameter circular apertures and are quoted in AB magnitudes. We decided to perform the analysis using the fixed 3″ aperture since it gave a lower scatter in the colour-magnitude diagrams. Where images were affected by saturated stars and detector artefacts, these regions were excluded from the analysis by determining the saturation level, replacing all saturated pixels with a constant value and masking these pixels, eventually ending up with a 20,000 x 20,000 pixel mask. These were used to create weight images as part of the `SExtractor` input before performing the source extraction.

In addition to the 19 W1 fields for which catalogues were created, 3 further fields were added to the area (A, B and C as shown in Figure 2.4, the Northern extension).

Magnitude zeropoints for sources detected in CFHTLS W1 were extrapolated from common sources in the Sloan Digital Sky Survey (SDSS) equatorial patch which overlaps the southern edge of the W1 area. Zero point information was also determined for the northern extension using overlaps with the W1 regions (Figure 2.4).

The sources common to the overlapping regions between Fields A, B and C and p1p3, p2p3 and m1p3 respectively (see Figure 2.4) were matched and their magnitudes in the g', z', r' bands were compared. An example of this for the r'-band in the B and p2p3 fields is shown in Figure 2.5.

The zeropoint correction is then given by:

$$m_{new} = m_{old} + (ZeroPoint - 30) \tag{2.2}$$

[1]http://terapix.iap.fr/

where *ZeroPoint* is the value of the y-axis intercept of the fitted line (Figure 2.5), and the value of 30 accounts for the default zeropoint magnitude of the CFHTLS catalogues.

Colour-colour plots were created to compare the location of the stellar locus in the W1 fields with that of the SDSS both before and after applying the zeropoint corrections. This can be seen in Figure 2.6 for the m0p1 field. After applying the correction, the stellar locus more closely matches that of the SDSS.

2.2.2 Star-galaxy separation and source flagging

`MEGACAM` is a wide-field imager which comprises 36 CCDs of 2048 x 4612 pixels, covering a 1x1 degree field of view and having a resolution of 0.187″ per pixel. Limitations in the wide-field optics are the main source of variations in the point spread function (PSF) and the 36 individual CCDs which make up `MEGACAM` exacerbate the variation in the PSF over each of the `MEGACAM` fields. This is an important consideration when performing star-galaxy separation based upon the r'-band half-light radius (HLR; the radius from within which half of the galaxy light is contained).

This PSF variation versus focal plane location has the effect of broadening the stellar locus as observed in the r'-band HLR versus r'-band magnitude distribution, meaning that a single cut in HLR to distinguish between stars and galaxies is reduced in effectiveness. In order to account, and subsequently minimise this effect, the weighted mean HLR of the stellar locus in each of the 36 CCDs per field was determined and used to rescale the HLR for all sources in each CCD such that the stellar values mapped on to a single locus defined in a reference CCD near to the optical centre of the detector. Although a component of the PSF variation over the field is anisotropic, for the purposes of star-galaxy separation, an isotropic scaling factor appears to provide an acceptable correction. The results of this scaling are shown in Figure 2.7.

As well as only retaining those sources which we identify to be galaxies, we also performed a cut in the `SExtractor FLAG` parameter. This parameter identifies objects which have close neighbours, bright neighbours, blended objects, corrupted objects or any combination of these. Objects suffering from these effects were discarded from our analysis (i.e. Only sources with a `FLAG` value = 0 are accepted).

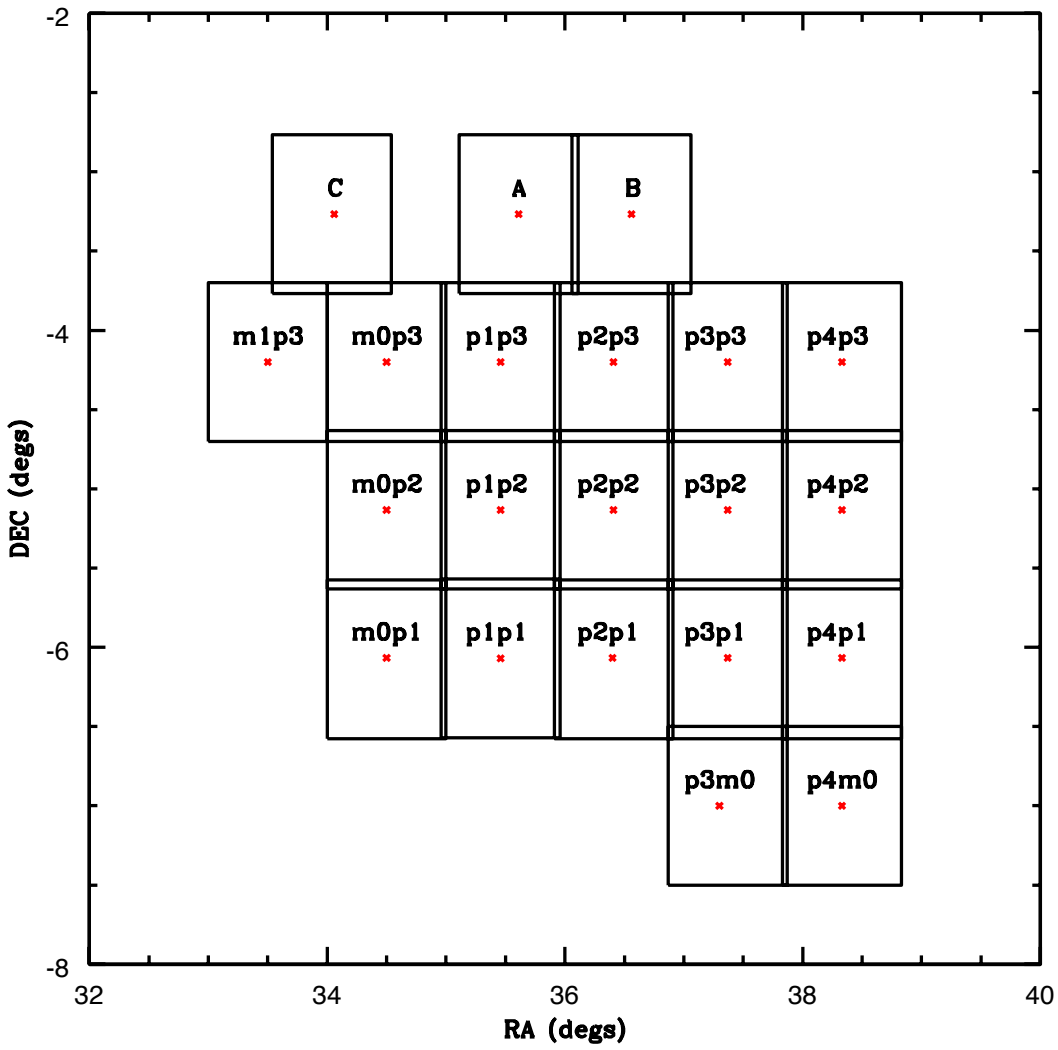

Figure 2.4: Positions of the W1 fields and the northern extension (Fields A, B and C).

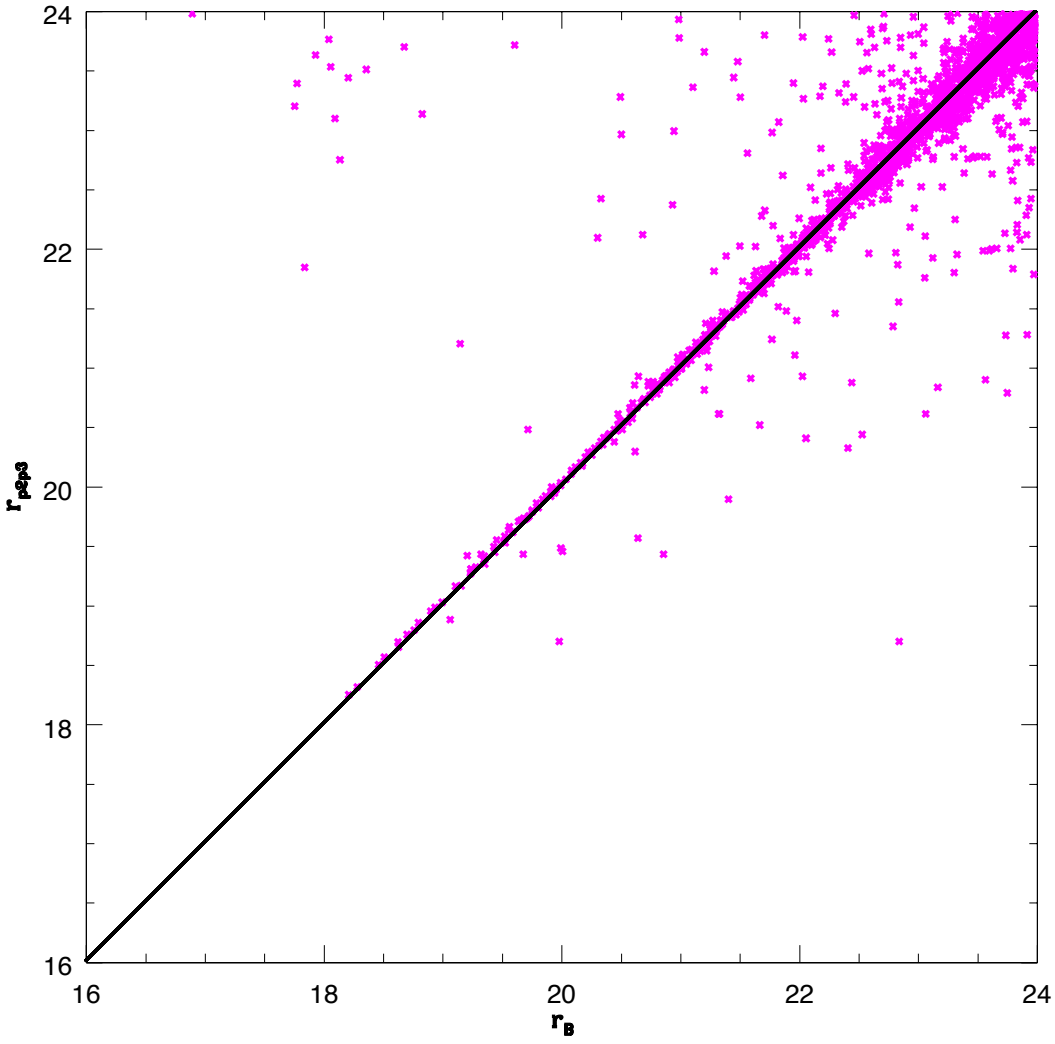

Figure 2.5: Overlapping r' magnitudes for the B and p2p3 fields.

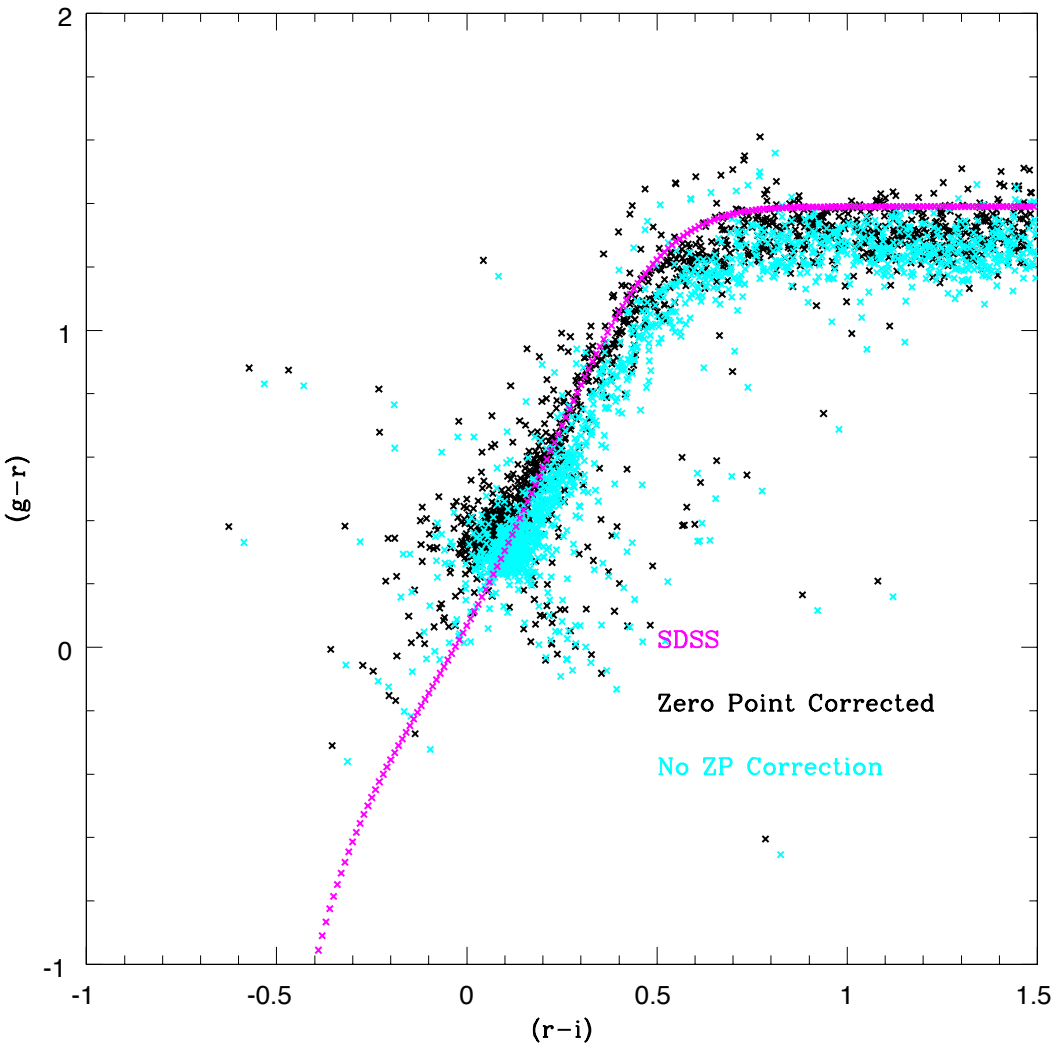

Figure 2.6: Comparison between the stellar locus of the SDSS (magenta points) with that of m0p1 before (cyan points) and after (black points) zeropoint correction.

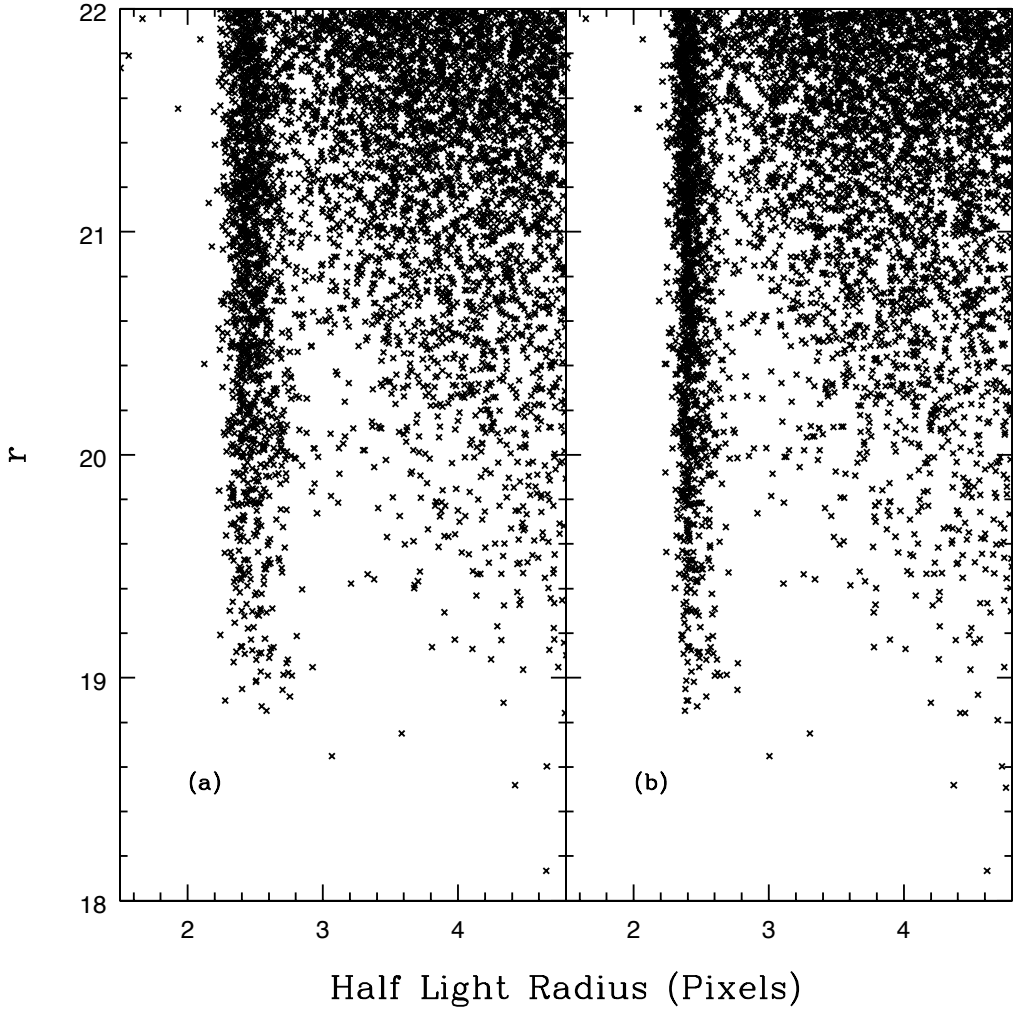

Figure 2.7: Location of the Stellar Locus in a typical CFHTLS Wide Megacam field. (a) Before PSF scaling is applied. (b) After PSF scaling is applied.

2.2.3 Completeness

Completeness of both the XMM-LSS and CCCP samples was determined by calculating number counts as a function of $3''$ diameter r-band magnitudes for representative CCCP and CFHTLS wide megacam fields (figure 2.8). These were also compared to the CFHTLS Deep Megacam fields. A limit of r=23.5 was adopted for this thesis (unless otherwise noted), thus ensuring that the photometric samples drawn from all data sets can be considered as complete.

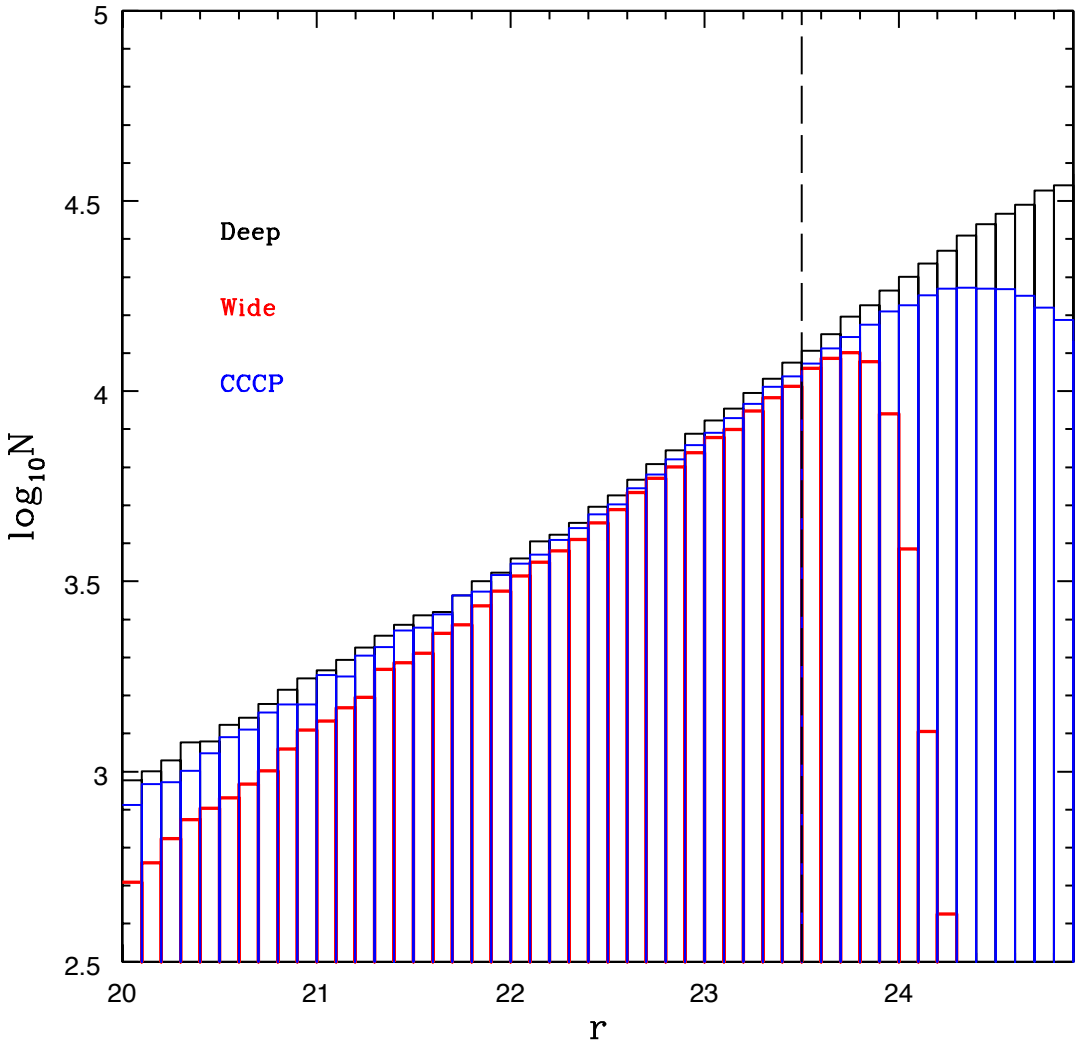

Figure 2.8: Number counts as a function of 3″ r-band magnitudes in representative CCCP and CFHTLS Wide Megacam fields are compared to number counts in representative CFHTLS Deep Megacam fields. The vertical line indicates r=23.5 as the limiting faint magnitude.

Chapter 3

An environmental Butcher-Oemler effect

In this work, an analysis of the fraction of star-forming galaxies (as determined from their colour) was performed as a function of the global cluster environment. These "blue fractions" (f_B) were calculated using the definition of Butcher and Oemler (1984) and the observed trend of increasing f_B with increasing redshift was confirmed. However, a new approach was also applied, identifying an environmental dependence of cluster blue fractions. In the cool (low mass) sample higher blue fractions were observed compared to those of hotter (higher mass) clusters.

3.1 Introduction: Galaxy Populations in Clusters

The observed properties of galaxy populations reflect the environment in which they are located. Comparisons of galaxy populations drawn from low (the field) and high density (rich galaxy clusters) environments indicate that the population distribution described using measures such as current star formation rate (e.g. Balogh et al. 1999, Poggianti et al. 2006), integrated colour (e.g. Blanton et al. 2005) and morphology (e.g. Dressler et al. 1997, Treu et al. 2003) varies as a function of changing environment. From studies such as these it is clear that galaxies located in the cores of rich clusters display lower star formation rates, redder colours and more bulge dominated morphologies compared to galaxies located in the field.

Studies of the fraction of blue galaxies contributing to a galaxy cluster provided some of the first direct evidence for the physical transformation of galaxies in cluster

environments. Butcher and Oemler (1984) reported an increase in the fraction of blue galaxies in 33 rich galaxy clusters out to $z \sim 0.5$ compared to local clusters. However, subsequent studies designed to expand upon this initial discovery highlighted the many complexities associated with this relatively straightforward technique, including varying intrinsic cluster properties with redshift (e.g. X-ray luminosity as discussed by Andreon and Ettori 1999), the use of k-corrections to determine rest frame colour distributions (Andreon, 2005) and the challenge of obtaining large samples with uniform photometry (successfully overcome by Loh et al. 2008).

In addition to the Butcher-Oemler (BO) effect measured employing optical galaxy colours, analogous BO-type effects have been reported as either a morphological BO effect (increasing spiral fraction in clusters with increasing redshift; Poggianti et al. 1999) and an infra-red (IR) BO effect (increasing fraction of dust enshrouded star forming galaxies in clusters with increasing redshift; Duc et al. 2002; Saintonge et al. 2008) to name two examples.

An alternative approach is to consider an environmental Butcher-Oemler effect whereby one attempts to determine the variation of blue fraction as a function of varying intrinsic cluster properties selected over narrow redshift intervals. This has been achieved by comparing blue fractions within clusters at increasing clustercentric radii (e.g. Ellingson et al. 2001; Loh et al. 2008) or by considering blue fractions measured between clusters of differing X-ray luminosities (e.g. Wake et al. 2005). A number of studies report the decrease of the fraction of blue galaxies with decreasing scaled clustercentric radius, e.g. the virial radius determined employing either cluster dynamics (Ellingson et al., 2001), correlation properties (Loh et al., 2008), or extrapolated from X-ray properties (Wake et al., 2005).

The currently favoured explanation for these observed trends is that infalling field galaxies are processed physically as they travel from the field, through the cluster outskirts and virialise in the central cluster region (Berrier et al., 2009). However, the extent to which cluster galaxies were "pre-processed" by physical effects occuring during an earlier residence in a galaxy group[1] remains contested (Li et al., 2009). Numerous physical processes have been suggested as the agents of this apparent transformation of galaxy populations. However, the dominant physical process(es) to which an infalling galaxy is subject remains unclear.

The two principal examples of such processes are ram pressure stripping and

[1]Note that we generally refer to both groups and clusters of galaxies as "clusters" in this paper and quantify our description using the X-ray temperature.

galaxy galaxy interactions. Ram pressure stripping describes the effective force experienced by the diffuse gas component of the infalling galaxy as it travels through the hot, dense intra-cluster medium (ICM; Gunn and Gott 1972). Both hot and cold gas may be stripped from the infalling galaxy leading to the exhaustion of the available gas supply that will otherwise cool and form stars (Abadi et al. 1999; Kawata and Mulchaey 2008; McCarthy et al. 2008). Hydrodynamical simulations have indicated that the ICM associated with galaxy group and cluster environments will strip of order 70% to 100% respectively of hot gas from a typical infalling spiral galaxy within one crossing time (Kawata and Mulchaey 2008; McCarthy et al. 2008). The effect is manifest as a sharp decline in the galaxy star formation rate effective on a timescale comparable to the rate at which the unstripped cold gas supply is consumed. The observations of a population of red (i.e. passive) spiral galaxies contributing to the red sequence would appear to support the view that some fraction of galaxies experience the stripping of disc gas via ram pressure effects (Wolf et al., 2009). The observation of galaxies displaying extended HI tails in the Virgo cluster (Chung et al., 2007) is nominally consistent with the expectations of ram pressure stripping. However, we note that the authors also report the presence of close companions to these galaxies in a number of cases and comment that a combination of ram pressure and tidal stripping provides a more compelling explanation.

When referring to galaxy-galaxy interactions we note that this may indicate one of a wide range of encounters. Interactions may be predominantly tidal between close neighbours resulting in halo gas being moved outward where it is more readily stripped (e.g. Chung et al. 2007). High speed encounters (either referred to as harrassment or threshing in the literature) may also result in tidal stripping of halo gas (Moore et al., 1996). Finally, infalling galaxies may merge with existing cluster members. The products of such merger encounters may be predicted by considering the mass ratio of the merging galaxies: large mass ratios result in enhanced star formation in the satellite galaxy yet may not lead to a star burst in the more massive companion (Cox et al., 2008). Equal mass mergers on the other hand result in the complete disruption of the infalling spiral galaxy (for example) to form a bulge dominated system accompanied by a significant central star burst (Di Matteo et al., 2007). The internal disruption associated with such strong interactions can result in a short term enhancement in star formation followed by a rapid exhaustion of the available cold gas supply. The potential effect of such strong galaxy-galaxy interactions is of interest to studies of the environmental dependence of galaxy evolution as the merging rate

(the product of relative velocity and interaction cross section) is predicted to be a strong function of environment: the cross section for disruptive encounters increases as the cluster velocity dispersion approaches the internal velocity of the infalling galaxy (Makino and Hut, 1997). Compelling evidence for enhanced galaxy-galaxy interactions in rich cluster environments is provided by Hubble Space Telescope (HST) observations indicating a high merger fraction in such environments compared to field comparison samples (Dressler et al. 1994; van Dokkum et al. 1999). However, such observations must be contrasted with mid-infrared selected moderate starburst galaxies located in rich cluster environments whose optical morphologies resemble undisturbed spiral galaxies (Geach et al. 2009; Oemler et al. 2009).

A picture is therefore emerging whereby multiple mechanisms (ICM stripping, merger induced star formation and tidally induced star formation) may participate in the physical processing of infalling galaxies. Currently unanswered questions focus upon whether more than one physical process acts upon a typical galaxy falling into a dense environment (and which might be considered dominant) and whether the relative importance of each of the suggested physical processes changes as a function of the global properties of the group/cluster environment into which the galaxy falls. In this chapter we attempt to answer the related question of whether the effectiveness of galaxy processing can be determined as a function of global cluster environment. Our approach is to compute the blue fraction as defined by Butcher and Oemler (1984) for a sample of X-ray selected galaxy clusters and to determine whether the blue fraction displays a significant trend versus X-ray temperature (here employed as a proxy for the global cluster mass).

Throughout this chapter, values of $\Omega_{\mathrm{M},0} = 0.3$, $\Omega_{\Lambda,0} = 0.7$ and $H_0 = 73\,\mathrm{kms}^{-1}\,\mathrm{Mpc}^{-1}$ are adopted for the present epoch cosmological parameters describing the evolution of a model Friedmann-Robertson-Walker universe. All magnitude information is quoted using AB zero point values.

3.2 Cluster Properties

A detailed description of the data is given in Chapter 2. In order to study the environmental dependence of cluster galaxies, we, unique to this thesis, split our data into 3 samples; cool, mid and hot. The cool sample is defined as clusters having X-ray temperature, T$<$ 3keV and therefore consists of the XMM-LSS sample. The mid sample is defined as clusters displaying 5 $<$ T(keV)$<$ 8 and the hot sample is

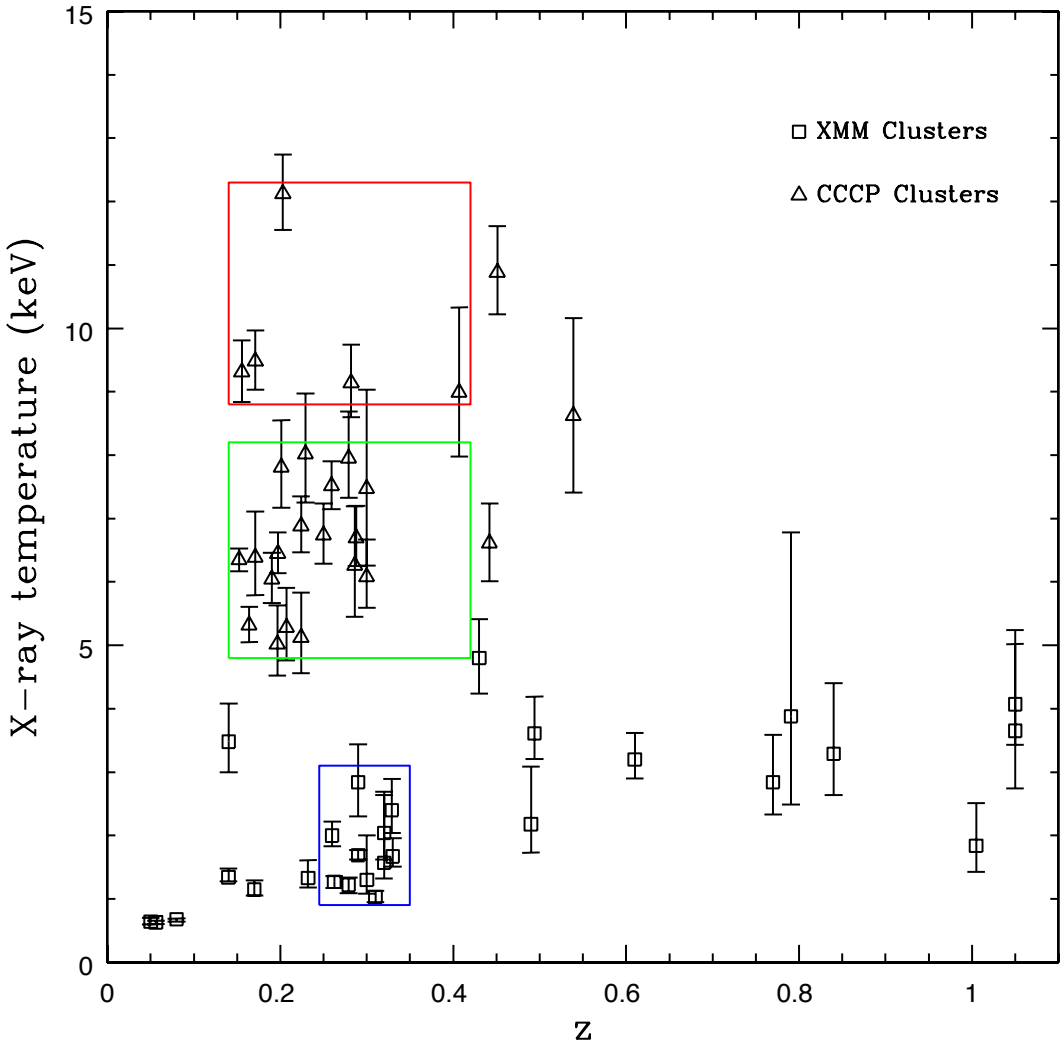

Figure 3.1: Redshift and temperature distribution of the hot, mid and cool clusters samples as defined in the text. Open triangles represent CCCP clusters and open squares represent XMM-LSS clusters.

defined as having T > 8keV. In addition to this, the CCCP samples are limited to a redshift range of $0.15 < z < 0.4$ to maximise the available sample size whilst reducing the redshift interval over which photometric quantities are k-corrected to a common epoch. The properties of the samples are summarised in Table 2.1 and the X-ray temperature and redshift distributions are shown in Figure 3.1. The boxes marked on Figure 3.1 were not chosen to distinguish between known separations of cluster populations (i.e. prior distinction between cool, mid and hot clusters in other work) but as a distinction based upon our data.

The CCCP clusters all lie above the nominal X-ray flux limit of the XMM-LSS survey and cover the full range of scatter observed in scaling relations such as the X-ray $L - T$ relation (see Figure 3.2). In this sense, the CCCP clusters would all be detected by X-ray images of the same quality as the XMM-LSS survey images (irrespective of how the CCCP cluster were originally selected). However, XMM-LSS lacks the areal coverage to detect such massive clusters which display low sky surface densities. Therefore, the combined XMM-LSS/CCCP sample is a representative, (largely) unbiased sample of X-ray clusters with temperatures $1 < kT(\mathrm{keV}) < 12$. We note that the XMM LSS clusters populating the cool sample are moderately biased toward higher X-ray luminosities than the average cluster population at that temperature (see Pacaud et al. 2007, Figure 8). This implies a moderate bias toward gas rich or centrally condensed systems which we will recall at relevent points in the following discussion.

The characteristic cluster scaling radii employed in this work are based upon r_{500} (see Equation 2.1).

3.2.1 Colour Magnitude Diagrams

Colour magnitude diagrams for each hot, mid and cool cluster are shown in figures 3.3, 3.4 and 3.5 respectively, each showing all sources which lie within r_{500} of the measured X-ray centre of each cluster.

Before the computation of a cluster blue fraction could be performed, the location of the red sequence (linear colour sequence followed by cluster early-type galaxies) had to first be determined. Once this has been found, it provides a reference value to which the blue galaxy population in each cluster can be defined.

To determine the location of the red sequence requires a statistical background subtraction technique to be applied to each cluster to highlight the population of

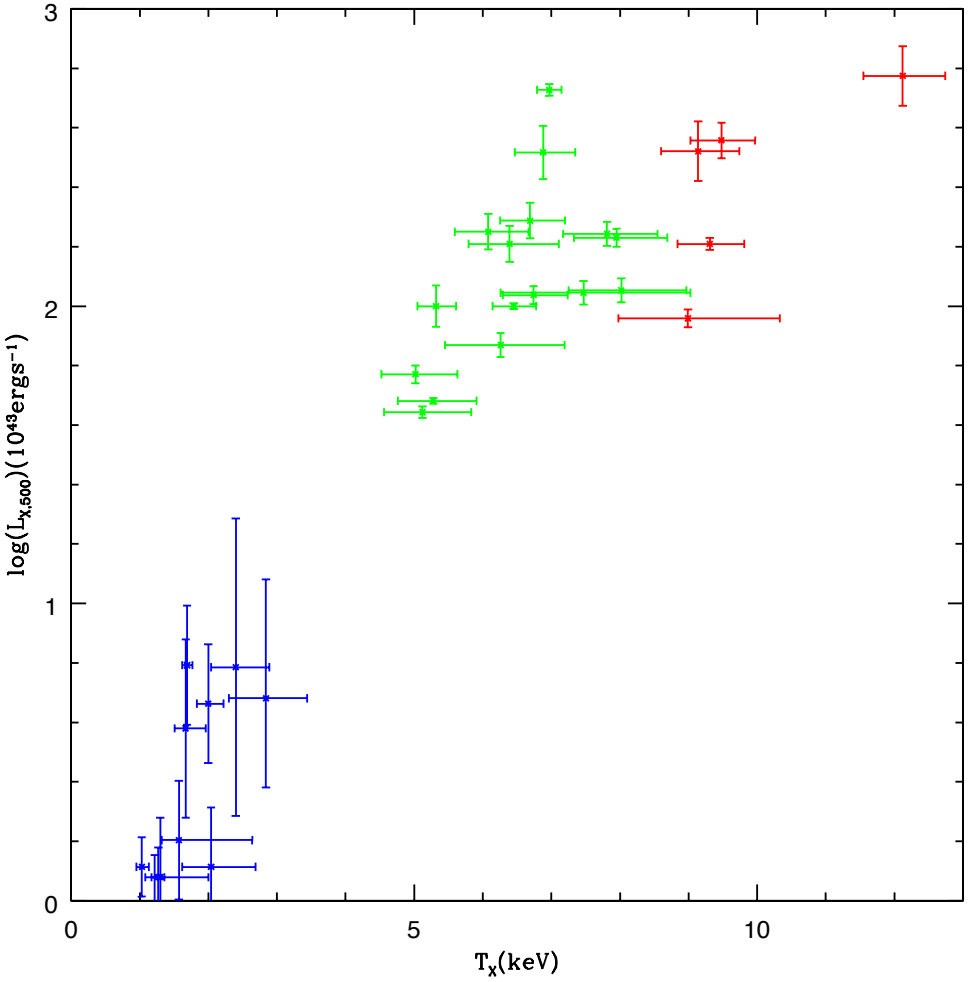

Figure 3.2: Luminosity-Temperature relation for the cluster sample (Mahdavi et al. 2013, Pacaud et al. 2007).

cluster members (in the absence of spectroscopic redshifts). We achieved this through the application of the method of Pimbblet et al. (2002) whereby the field population and the cluster plus field population were each represented on a colour-magnitude grid. The probabilty that a galaxy occupying a particular grid position is a field galaxy is given by

$$P(col, mag)_{Field} = \frac{A \times N(col, mag)_{Field}}{N(col, mag)_{Cluster+Field}}, \tag{3.1}$$

where A is an areal scaling factor required to match the area of the field sample to that of the cluster. The field colour-magnitude distribution was computed using all galaxy sources lying at a radii$>8r_{500}$ from the X-ray cluster centre. For each galaxy within r_{500}, membership was determined by comparing a random number in the interval [0,1] to the calculated field probability value and the whole procedure was repeated 100 times per cluster. An example of this subtraction is shown in Figure B.1 in Appendix B.

For each realisation of the background subtraction technique, the location of the red sequence was found using a weighted, linear least squares fit before calculating the mean slope and zero-point over the distribution of 100 values.

We checked and, if required, refined the location of the mean red sequence for each cluster by considering the "red edge" diagram (an example of which is shown in Figure 3.6 for XLSSC 22). This shows the number of galaxies located at a colour offset $\Delta(g-r)$ at fixed r-magnitude from the red sequence in a particular cluster. The zero-point of the red sequence was subsequently adjusted to set the peak in the red edge distribution at zero colour offset.

This procedure was successful for the mid and hot cluster samples, however, following statistical background subtraction, the cool clusters typically possesed insufficient cluster members to generate a reliable red sequence fit. Therefore, in this case, we applied the red sequence relation that was computed for the stacked mid cluster sample (see Section 3.4) to the cool clusters. This red sequence was then adjusted using the red edge diagram procedure to improve the fit on a cluster by cluster basis.

3.2.2 k-corrections

The k-correction employed to convert absolute V-magnitude to apparent r-magnitude at the redshift of each cluster assumes an early-type galaxy spectral energy distribu-

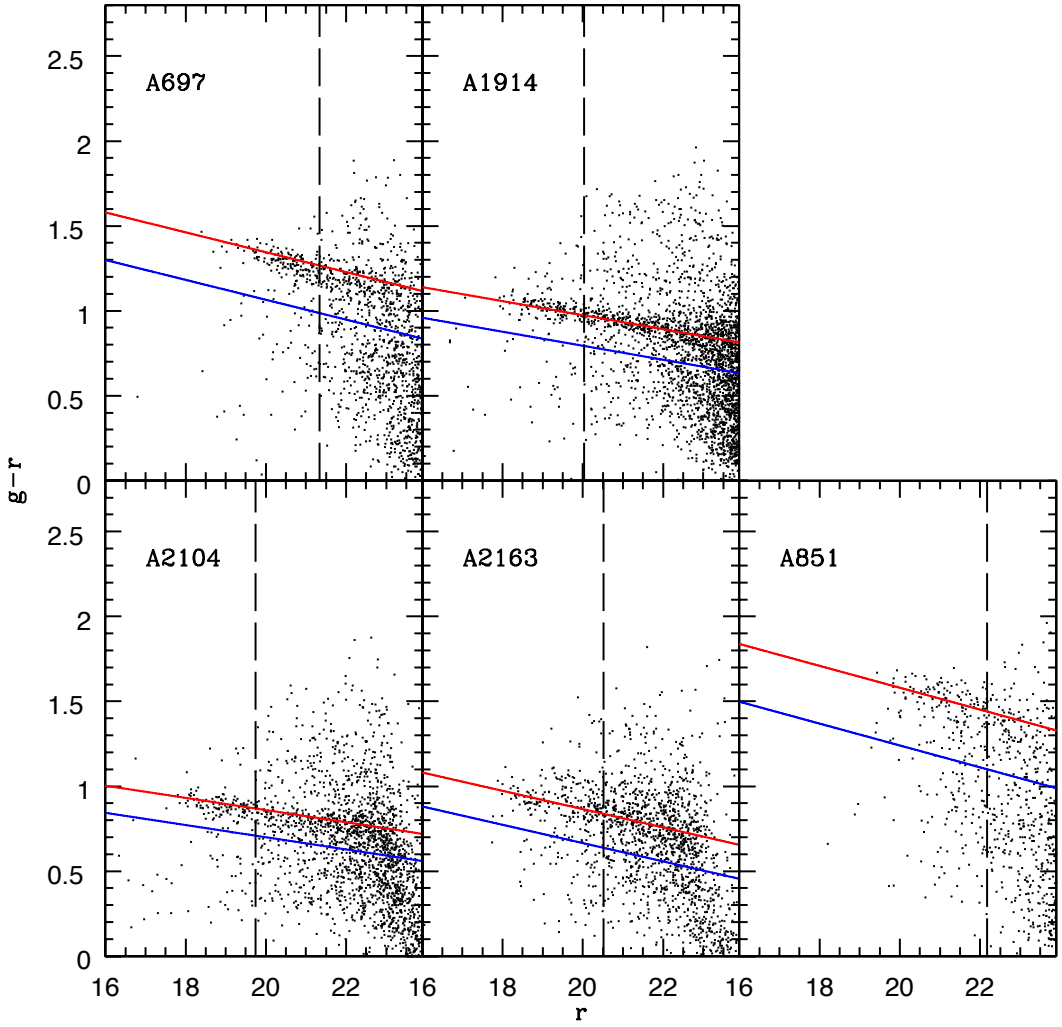

Figure 3.3: Hot sample clusters. All sources within r_{500} of the cluster centre are plotted. The red line marks the location of the red sequence and the blue line marks the Butcher & Oemler (1984) cut as described in the text. The vertical dashed line indicates the r magnitude corresponding to $M_V = -20$ at the cluster redshift.

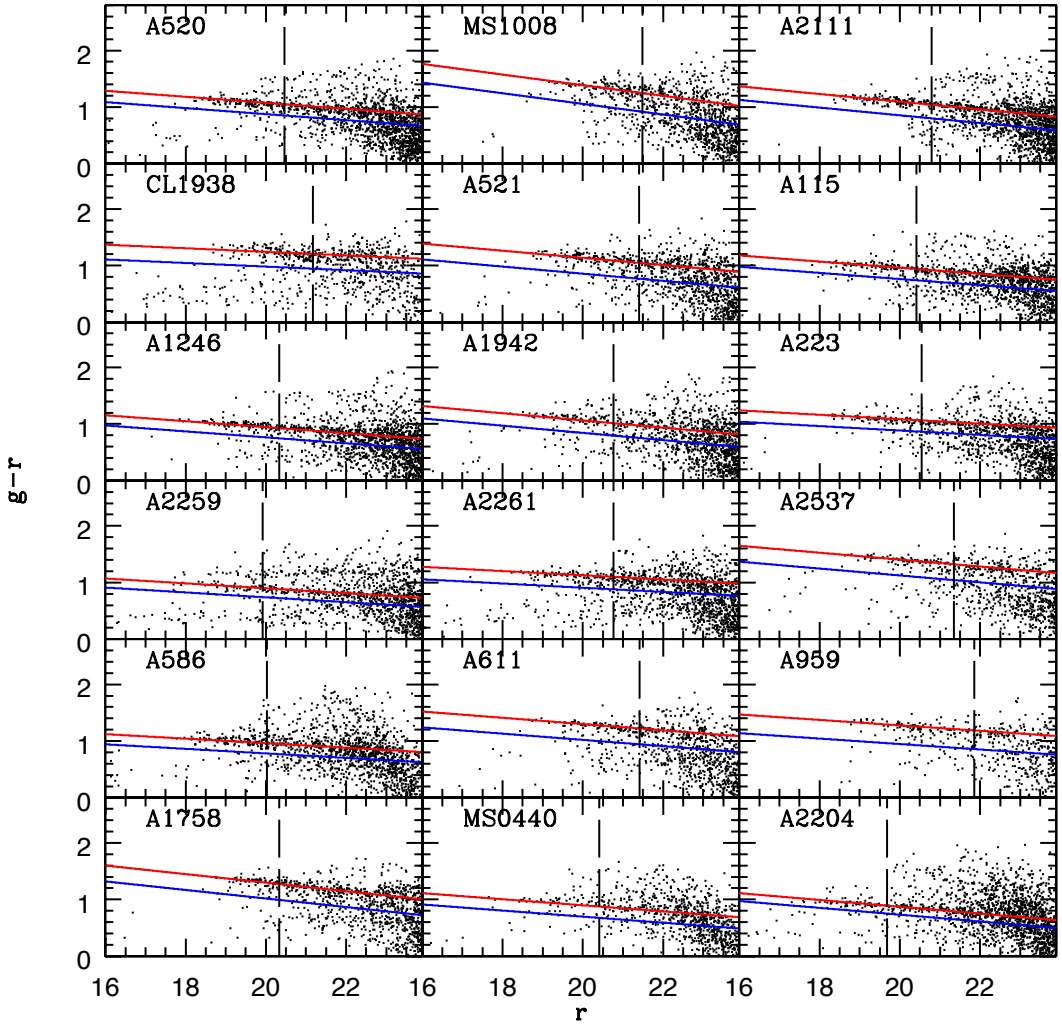

Figure 3.4: Mid sample clusters. All sources within r_{500} of the cluster centre are plotted. The red line marks the location of the red sequence and the blue line marks the Butcher & Oemler (1984) cut as described in the text. The vertical dashed line indicates the r magnitude corresponding to $M_V = -20$ at the cluster redshift.

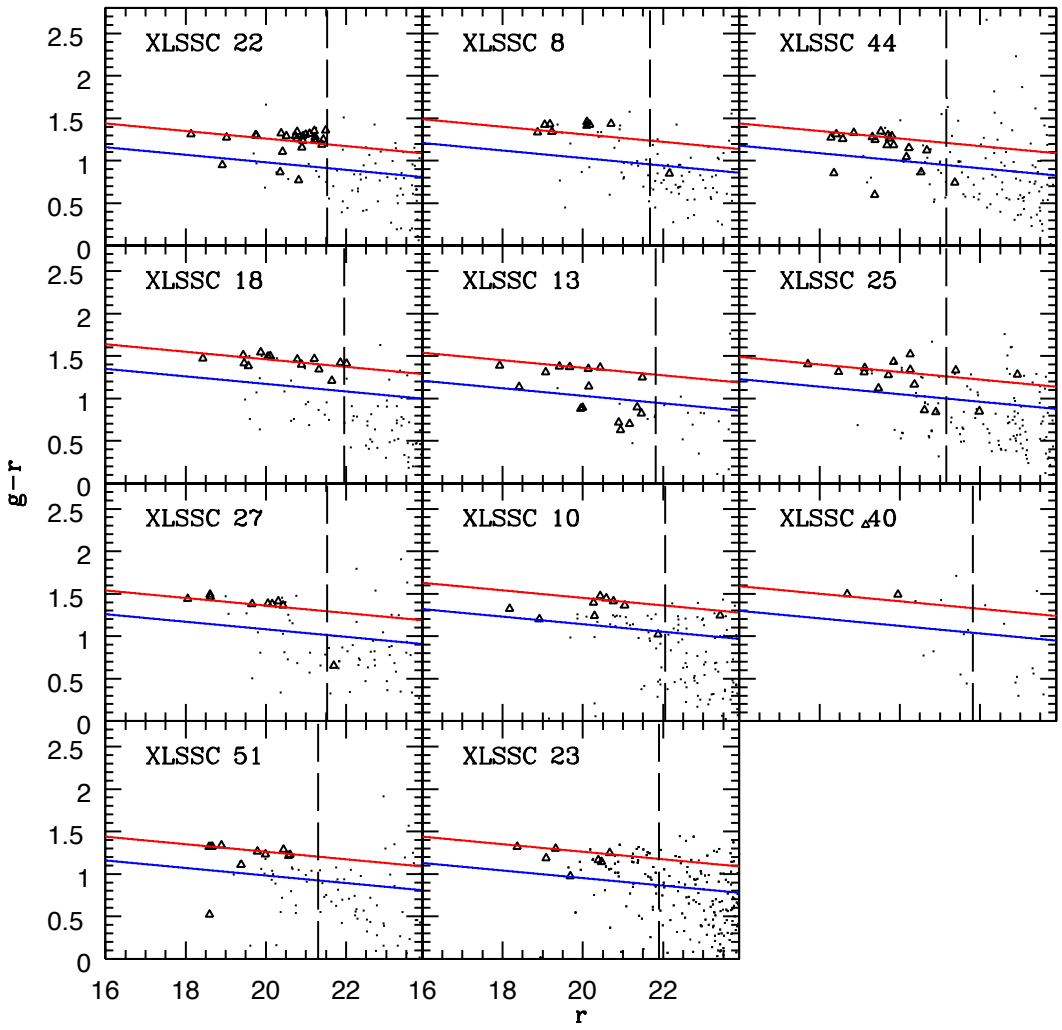

Figure 3.5: Cool sample clusters. All sources within r_{500} of the cluster centre are plotted. The red line marks the location of the red sequence and the blue line marks the Butcher & Oemler (1984) cut as described in the text. The vertical dashed line indicates the r magnitude corresponding to $M_V = -20$ at the cluster redshift. The triangles represent spectroscopically confirmed members.

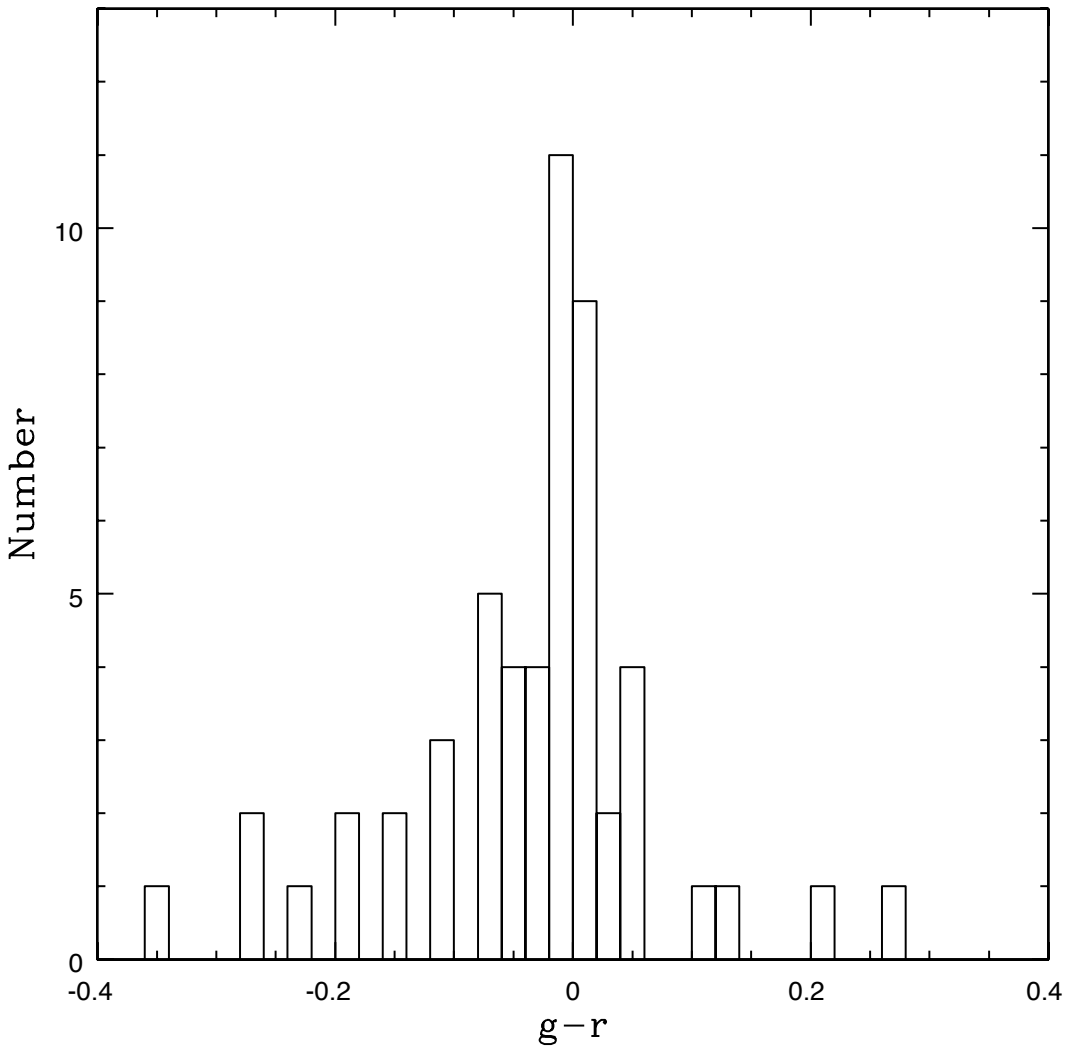

Figure 3.6: Red edge diagram for XLSSC 22. See text for more details.

tion (SED; Kinney et al. 1996). We note however that the exact choice of template is not a significant factor when computing the apparent r-magnitude reference location on the red sequence as the k-correction is dominated by the bandwidth term at $z \sim 0.3$. Furthermore, due to the small slope of the fitted red sequence relation in each case ($\sim$0.05), small systematic magnitude errors result in negligible colour uncertainties.

The best fitting SED describing the observed colour evolution of the mid and hot cluster red sequences (Figure 3.7) is computed employing a linear interpolaiton between an early-type (Ell) and early-type spiral (Sab) SED, e.g.

$$SED(\lambda) = (1 - x)Ell(\lambda) + xSab(\lambda) \tag{3.2}$$

where the parameter x is computed using a χ^2 minimisation procedure. The best fitting SED model was found to be approximately 70% Elliptical and 30% Sab. We employ this template as a reference point from which to determine accurate k-corrections and blue galaxy colour thresholds for all clusters (cool, mid and hot) in the subsequent analyses.

3.3 Blue Fractions

The blue fraction of each cluster was computed following the definition of Butcher and Oemler (1984). Following their approach, all galaxies displaying $M_V \leq -20$ are considered and blue galaxies are defined as those displaying a rest frame colour offset $\Delta(B - V)$=-0.2 measured relative to the red sequence. We add a further criterion that galaxies within r_{500} of the cluster X-ray centre are considered part of the "total", i.e. cluster plus field, populations, and galaxies at clustercentric radii $> 8r_{500}$ and within the same Megacam field are considered as the "field" population. The blue fraction within each cluster is then computed as

$$f_B = \frac{N_{Blue,Total} - AN_{Blue,Field}}{N_{Total} - AN_{Field}} \tag{3.3}$$

where $N_{Blue,Total}$ is the number of blue galaxies in the cluster plus field, $N_{Blue,Field}$ is the number of blue field galaxies, N_{Total} is the total number of galaxies in the cluster plus field and N_{Field} is the total number of field galaxies. The symbol A denotes an areal scaling factor to correct the field population area to that of the cluster area.

The rest frame Butcher and Oemler (1984) magnitude and colour criteria were

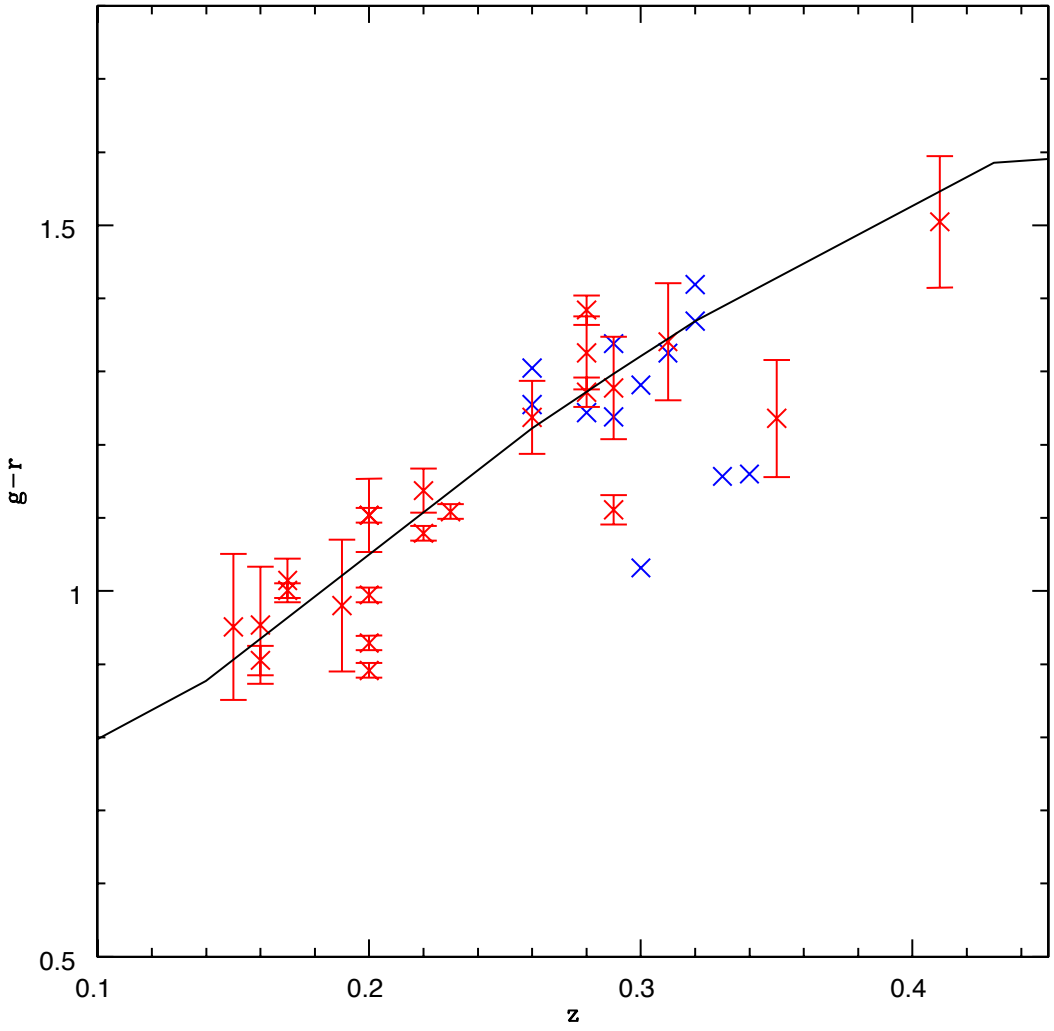

Figure 3.7: The red crosses indicate the $g-r$ colour of the fitted red sequence relation measured at $M_V = -20$ for the mid and hot samples. The solid line shows the best fitting SED model from Equation 3.3. Blue crosses indicate the location of the red sequence in the cool clusters determined using the mid cluster red sequence relation.

expressed as observed frame $r-$magnitude and $\Delta(g-r)$ colour offsets at the redshift of each cluster by considering the galaxy SED implied by the cluster red sequence colour. The colour offset was computed by generating a second SED model according to Equation 3.2 displaying $\Delta(B-V)$=-0.2 compared to the reference SED describing the cluster red sequence relation. This "blue-cut" SED model was found to be 75% Sab and 25% Sbc. Employing this SED model, $\Delta(g-r)$ corresponding to $\Delta(B-V)$=-0.2 was calculated for each cluster at the appropriate redshift.

The blue fraction error is estimated by computing a distribution of blue fraction values for each cluster. Each blue fraction value is computed as follows: circular apertures of radius r_{500} are placed at random locations within the Megacam field of each cluster. The galaxy population within each aperture is employed as the background value for Equation 3.3. The error on the blue fraction for each cluster is then estimated as the interval about the median blue fraction value containing 67% of the distribution. Errors computed using this method are typically 1.7 times larger than those computed assuming Poissonian incertainties alone.

Figure 3.8 displays the blue fraction as a function of redshift for all clusters and shows an apparent trend of increasing blue fraction versus redshift. However, splitting the sample by X-ray temperature reveals that this trend may instead arise from the varying global environment of each cluster modulo the slightly different redshift interval covered by each of the cool, mid and hot samples.

Figure 3.9 displays the blue fraction as a function of cluster X-ray temperature for the cool, mid and hot samples. In addition, blue fraction values and Poisson uncertainties are list in Table 3.1. The data indicate that typical blue fraction in each cluster and the dispersion in blue fraction values within a given temperature sub-sample increase as the temperature of the X-ray cluster decreases.

Clusters of similar properties have been studied by Wake et al. (2005) and we also compare their results to ours as a function of cluster X-ray temperature in Figure 3.9. One immediately notes that the blue fraction values for the current sample are consistently larger than the sample of Wake et al. (2005) though nominally covering a similar range of X-ray temperature. Blue fractions in the Wake et al. (2005) sample are computed within an aperture of radius one-third of the virial radius. This corresponds to a radius of approximately equal to $0.7r_{500}$ and we have corrected the Wake et al. (2005) values to the aperture used in this work using the blue fraction versus radius curve appropriate to each cluster temperature (shown in Figure 3.13). This correction is necessarily approximate and clearly offsets between the two samples re-

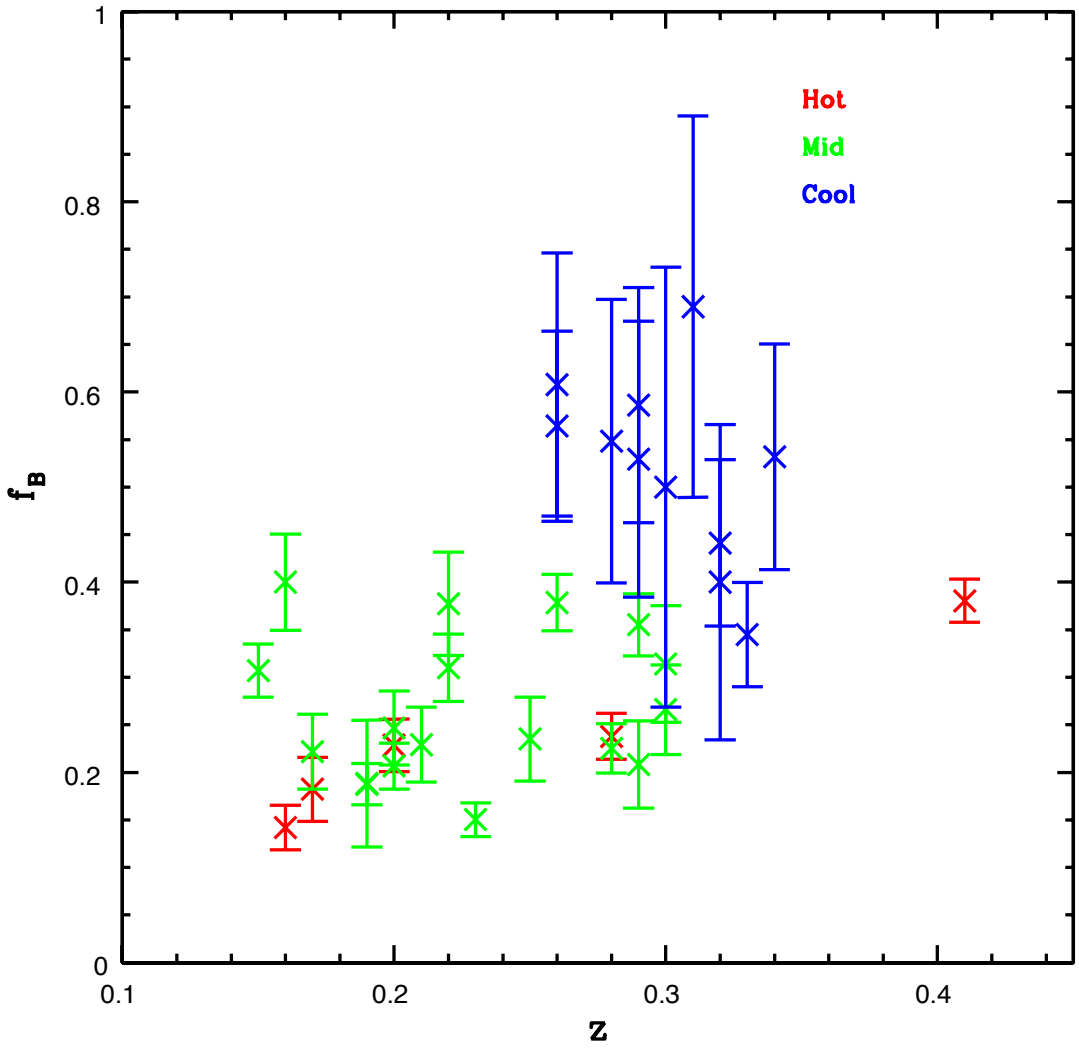

Figure 3.8: Cluster blue fractions as a function of redshift.

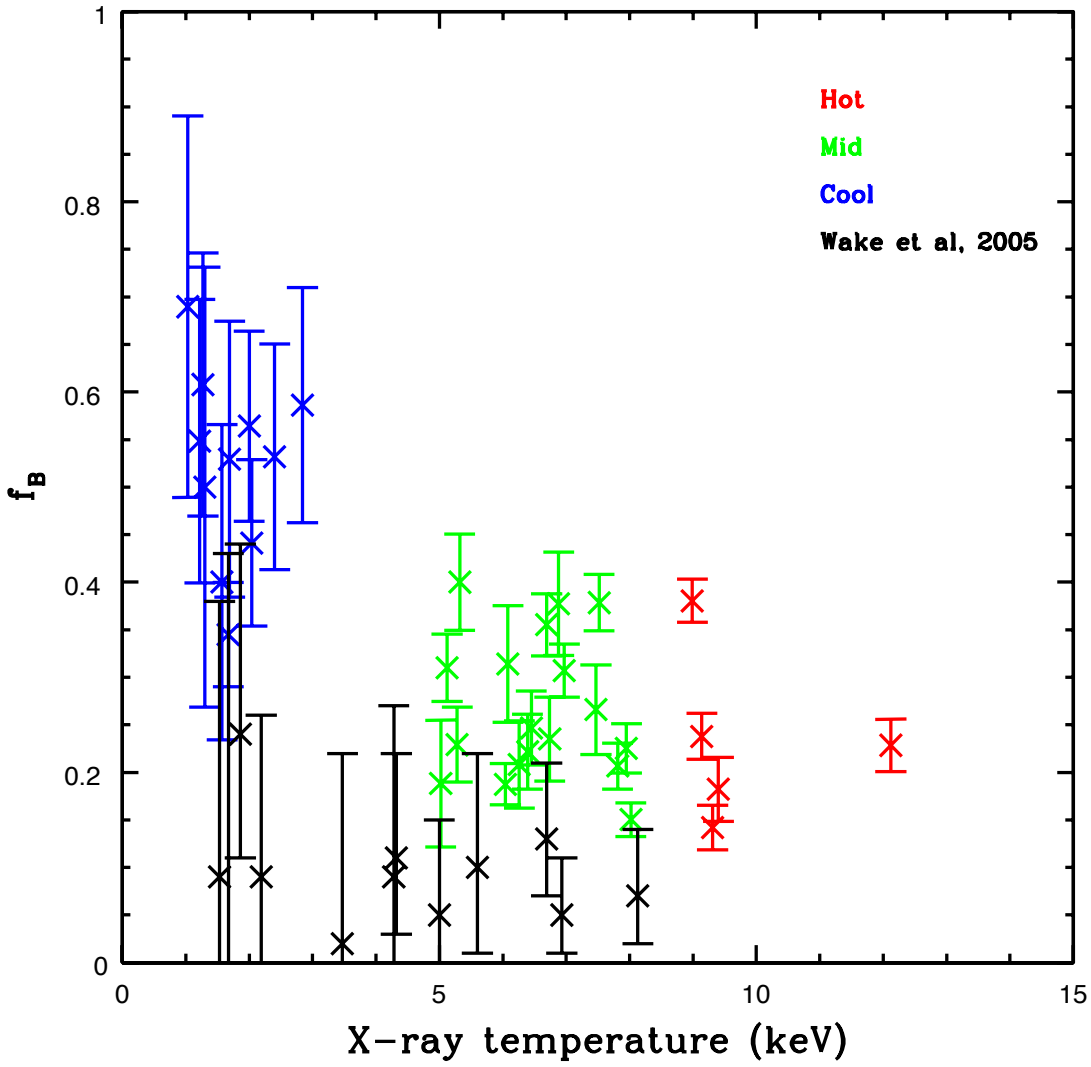

Figure 3.9: Cluster blue fraction as a function of X-Ray temperature.

Table 3.1: Blue Fractions for all clusters employing a limiting magnitude $M_V = -20$ within r_{500} of the cluster centre.

Cluster	f_B	Number of blue galaxies
XLSSC 13	0.69 ± 0.20	11
XLSSC 51	0.55 ± 0.15	11
XLSSC 44	0.61 ± 0.14	13
XLSSC 08	0.50 ± 0.23	14
XLSCC 40	0.40 ± 0.17	5
XLSSC 23	0.35 ± 0.05	16
XLSSC 22	0.53 ± 0.15	10
XLSSC 25	0.56 ± 0.10	17
XLSSC 18	0.44 ± 0.09	14
XLSSC 27	0.59 ± 0.12	12
XLSSC 10	0.53 ± 0.12	20
MS0440+02	0.19 ± 0.07	16
A1942	0.31 ± 0.04	49
A0223	0.23 ± 0.04	30
A2259	0.40 ± 0.05	50
A1246	0.24 ± 0.02	30
A2537	0.31 ± 0.06	54
A0959	0.21 ± 0.05	25
A0586	0.22 ± 0.04	39
A0115	0.25 ± 0.04	38
A0611	0.36 ± 0.03	65
A0521	0.24 ± 0.05	55
A2261	0.38 ± 0.05	80
A2204	0.31 ± 0.03	35
MS1008-12	0.27 ± 0.05	58
CL1938+54	0.38 ± 0.03	95
A0520	0.21 ± 0.02	43
A1758	0.23 ± 0.03	52
A2111	0.15 ± 0.02	26
A0851	0.38 ± 0.02	97
A0697	0.24 ± 0.02	54
A2104	0.14 ± 0.02	24
A1914	0.18 ± 0.03	35
A2163	0.23 ± 0.03	69

main. The remaining differences arise from the different methods used to determine blue fraction values in each sample. Specifically, Wake et al. (2005) assume that the SED representing the cluster colour magnitude relation is a pure elliptial model rather than the composite elliptical plus Sab model adopted here. The use of different spectral models results in different k-corrections versus redshift with the consequence that the observed frame colour offset employed to define the blue cut in each cluster is typically larger in the Wake et al. (2005) sample than that employed here. The application of a bluer cut relative to the CMR in a given cluster results in a smaller blue fraction. We therefore conclude that the remaining offset in blue fraction versus temperature between the Wake et al. (2005) sample and that presented here reults from such methodology differences.

As noted by Margoniner et al. (2001) and Hansen et al. (2009), the observed trends in cluster blue fractions can be explained as a function of both redshift and cluster mass. In order to determine the relative influence of varying redshift and cluster temperature (here used as a proxy for cluster mass) upon the blue fractions we fit the data for the three samples with a simple function of the form

$$f_B(z, T) = \beta_0 + \beta_z z + \beta_T T^{-1} \tag{3.4}$$

where β_0, β_z and β_T are constants to be determined employing a minimum χ^2 algorithm and T is expressed in keV. The best fitting values are $\beta_0 = 0.04 \pm 0.02$, $\beta_z = 0.67 \pm 0.08$ and $\beta_T = 0.42 \pm 0.07$. Confidence intervals of the fitted values of β_T and β_z are shown in Figure 3.10. The minimum value of χ^2 obtained using this procedure is approximately 3 per degree of freedom and, if the blue fraction errors are accurate, may indicate the presence of intrinsic scatter in the distribution of blue fraction values. The current sample of XMM-LSS and CCCP clusters is insufficiently large and does not cover a large enough interval in either redshift or temperature to constrain both the exponents of the the redshift and temperature dependence of Equation 3.4 in addition to the coefficients. We can rule out no redshift evolution but the temperature dependence is relatively unconstrained (and is complicated by the degeneracy with β_0 as the power law exponent of T tends to zero).

An alternative approach is to investigate the trends in the data employing a non-parametric technique. In this case, we apply a partial Spearman rank analysis to the data in order to examine the extent of any correlation between f_B and either temperature or redshift while controlling for the variation of the second variable. The

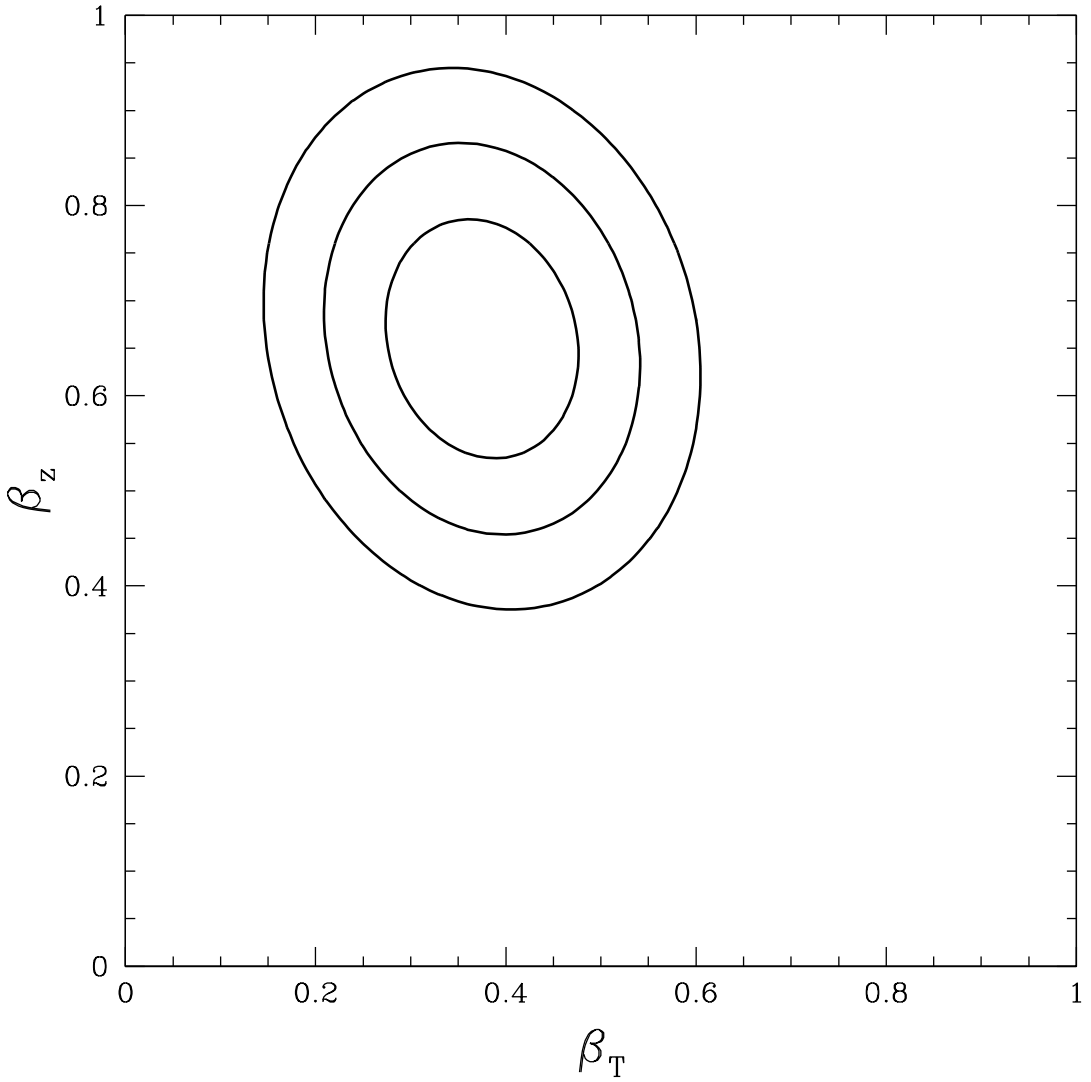

Figure 3.10: Confidence intervals on the fitted values of β_z and β_T (1, 2, and 3-sigma confidence intervals are shown).

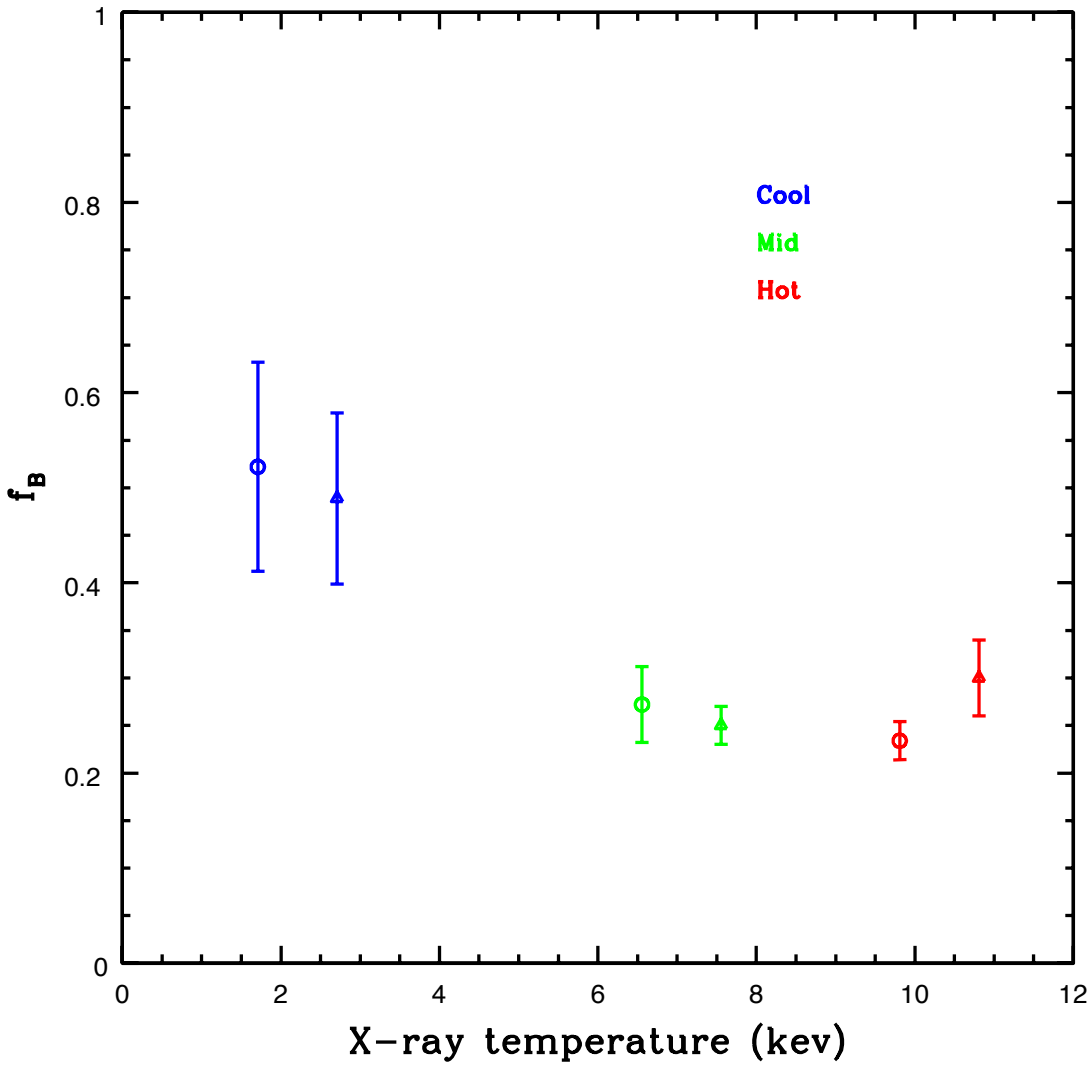

Figure 3.11: A comparison of blue fraction computation methods versus temperature. The circular points indicate the average blue fraction in each of the three temperature sub-samples computed using the BO84 method. The triangles indicate the average blue fraction per temperature sub-sample computed using the definition $f'_B = 1 - f_R$ (see text for details). The triangles have been offset in temperature from the circles for clarity

partial correlation coefficient describing blue fraction and redshift while controlling for temperature is $r(f_B, z, T) = 0.39$ while the corresponding coefficient describing blue fraction versus temperature while controlling for redshift is $r(f_B, T, z) = -0.64$. The probability of obtaining $r = -0.64$ from the sample by chance is approximately 0.2% whereas the corresponding probabiliy for the value $r = 0.39$ is somewhat greater at approximately 1.8%. Overall, both the parametric and non-parametric approach confirm the evolution in the cluster blue fraction with both redshfit and cluster temperature. The significance of the greater blue fraction versus decreasing temperature can also be seen in Figure 3.11 where the average blue fraction for the cool sample is significantly higher than either the blue fraction for the mid and hot samples.

One may further investigate the dependence of blue fraction on cluster temperature by correcting f_B values for individual clusters to a common epoch at z=0.3 using Equation 3.4 and the best fitting coefficients. The corrected f_B values are displayed in Figure 3.12 and confirm the trend to observe greater blue fraction values in cooler clusters. We next consider the effects of the various choices made during the blue fraction analysis on the overall robustness of the blue fraction trends versus redshift and temperature.

3.3.1 Testing the blue fraction computation assumptions

The cluster blue fraction may be computed employing one of a number of criteria to segregate the red and blue cluster galaxy population. We apply the original definition of Butcher and Oemler (1984) in this work but note the work of Andreon (2005) who argue that adopting a fixed rest frame colour offset relative to the red sequence is prone to give misleading blue fraction trends as galaxies of different SEDs drift in and out of the adopted colour interval as a function of redshift. To assess whether this is an important consideration in our analysis, we compare the average blue fraction per cluster sub-sample to a modified blue fraction determined by fitting the red fraction associated with the stacked CMD of clusters by temperature. We follow the method described by Loh et al. (2008) and model the red wing of the red sequence of the CMD of all clusters stacked by temperature once k-corrected to a common redshift z=0.3. The red wing is modelled as a double Gaussian function and the best-fitting function is reflected about the location of the red sequence to determine the number of red galaxies in each distribution. We then compute the red fraction in an analagous manner to the blue fraction and define a modified blue fraction as $f'_B = 1 - f_R$. We

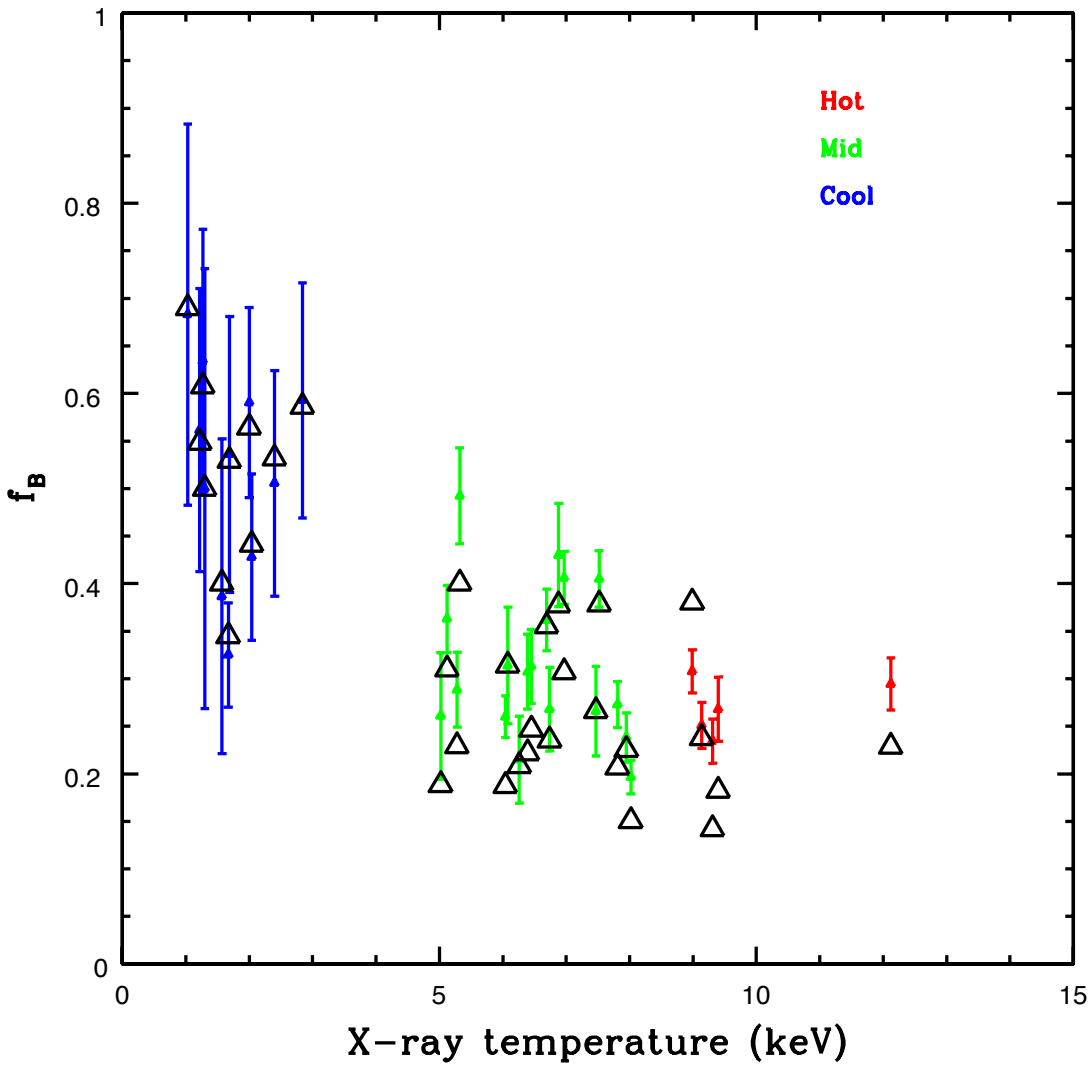

Figure 3.12: Cluster blue fraction as a function of X-Ray temperature. The black points indicate the result of correcting the original blue fraction values to a common epoch at $z = 0.3$.

compare the original and modified blue fraction values for each temperature sub-sample in Figure 3.11 and note that each approach reveals the same trend (and that the points are identical within the errors). We are therefore satisfied that the original Butcher and Oemler (1984) definition produces reliable results and we avoid the requirement to fit double Gaussian features to individual cluster colour distributions which, in the case of the cool clusters, typically result in poorly constrained models.

We next consider the variation of the computed blue fraction with assumed cluster radius to a) investigate whether the choice of radius introduces a bias into the trend of observed blue fraction versus temperature, b) determine the effect of uncertainty in the estimated r_{500} value for each cluster on f_B and c) relate blue fractions computed for the current sample to comparable studies in the literature. Figure 3.13 displays the average blue fraction per temperature sub-sample computed within circular apertures of radius expressed as a fraction of r_{500}. This variation of the blue fraction with characteristic radius has been noted in previous studies and the trends displayed in Figure 3.13 are consistent with those of Fairley et al. (2002), Ellingson et al. (2001) and Wake et al. (2005). This increasing trend of blue fraction with scaled aperture radius is nominally consistent with a blue infalling field population that is processed by ram pressure stripping upon falling into the cluster. The average blue fraction at r_{500} in each temperature sub-sample reflects the trend observed in Figure 3.9. What can be noted at this point is that the exact choice of radius within which the blue fractions are computed does not affect the conclusion that cooler clusters display greater blue fractions than hotter clusters (within the range $0.5r_{500} < r < 2r_{500}$). It is useful to point out that the value of r_{500} in each case is computed employing the observed cluster temperature and an assumed mass-temperature relation. X-ray spectral measurements from which the cluster temperature is computed are typically extracted within an on-sky aperture of size of the order of r_{500} in each cluster. Therefore, employing computed r_{500} values to define aperture sizes up to several times the virial radius would involve a considerable extrapolation beyond the scale on which the X-rays are measured.

Uncertainty in the temperature computed for each cluster propagates to an error in the value of r_{500} computed for each cluster. The typical temperature error for the XMM-LSS clusters contributing to the cool sample are of the order 10-20% (Willis et al. 2005). The gradient of the trend of f_B versus r/r_{500} estimate at r_{500} is approximately 0.15. This indicates that incertainty in cluster X-ray temperature will contribute a fractional f_B error of the order of a few percent, i.e. small compared to

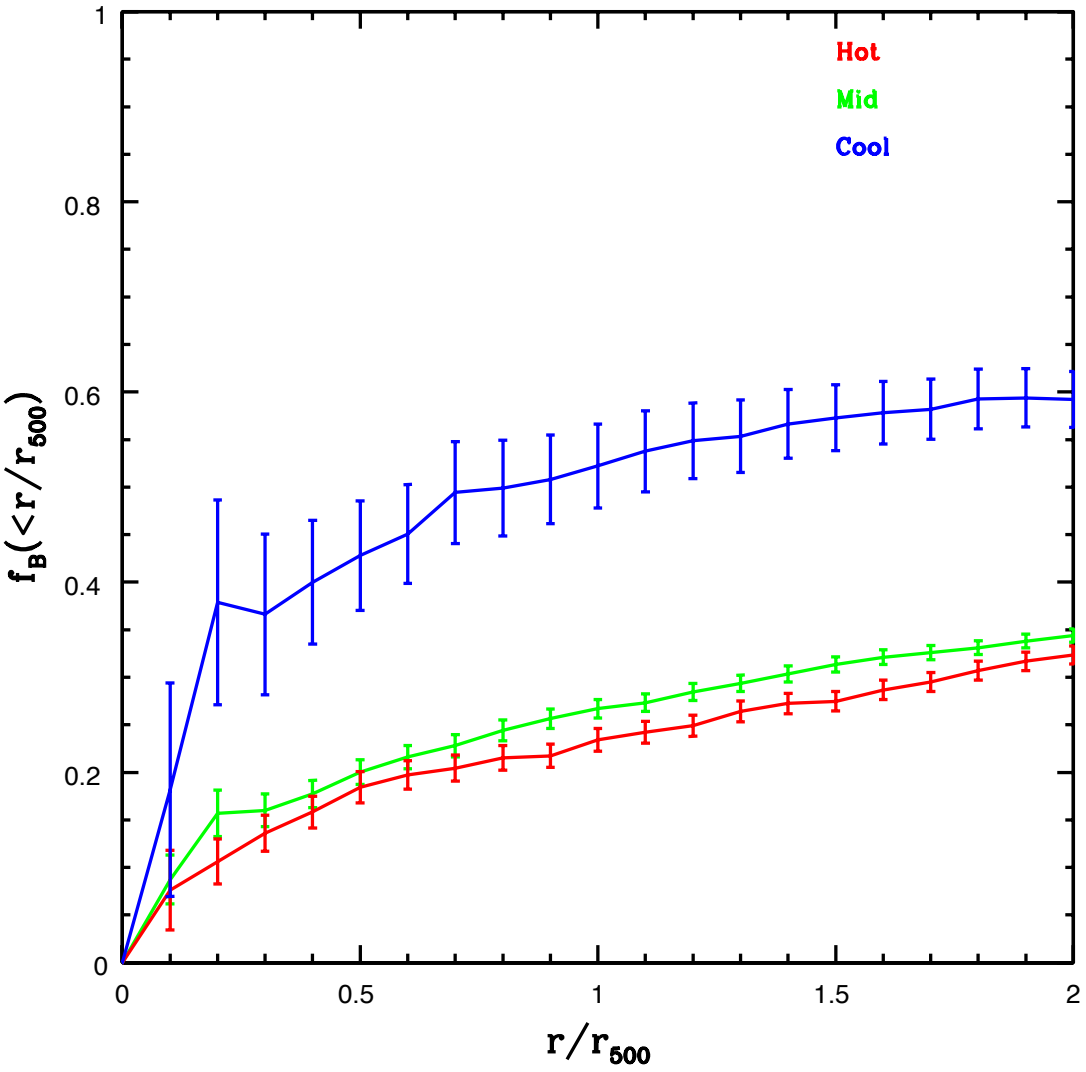

Figure 3.13: Radial variation of the cluster blue fraction

the Poissonian error in f_B computed for an individual cluster.

The mid temperature CCCP cluster MS1008 is common to both this work and that of Kodama and Bower (2001) and provides a useful check upon our results. The value of the blue fraction obtained by these authors was $f_B = 0.161 \pm 0.036$ and was calculated within R_{30} (the radius containing 30% of the total number of galaxies in the cluster) corresponding to an angular radius of $2.82'$. We obtain a value $f_B = 0.27 \pm 0.04$ within r_{500} corresponding to an angular radius of $4.44'$. The radial cut used by Kodama and Bower (2001) corresponds to approximately $0.63r_{500}$ and when the blue fraction was recalculated within this fraction of r_{500}, a value of $f_B = 0.18 \pm 0.04$ was obtained, improving the agreement with Kodama and Bower (2001). The errors quoted here are however purely Poissonian and do not account for the effect that minor differences in the methodology used in each study (e.g. k-correction, computation of the red sequence relation) have upon the computed value of f_B.

We next consider the effect of extending the faint absolute magnitude cut applied when computing the blue fraction. Figure 3.14 displays the average blue fraction per temperature sub-sample computed within a circular aperture of r_{500} as the applied faint magnitude cut is varied from M_V=-22 to -18. The main feature of the diagram is that the excess fraction of blue galaxies observed in cool clusters compared to the mid and hot samples continues to increase as the sample magnitude limit is extended to fainter magnitudes.

When considered together, the variation of blue fraction with both radius and magnitude indicate that the excess blue galaxy fraction observed in cool clusters is dominated by the contribution of faint galaxies at large radius.

3.4 Stacked Colour Magnitude Diagrams

The previous analyses have identified a relative excess in the fraction of blue galaxies in cool X-ray clusters compared to the mid and hot samples. While the blue fraction is a useful quantity to investigate, it may prove informative to consider the average CMD for each temperature sample for which blue fractions are computed. The statistical background subtraction method described in Section 3.2.1 was applied 100 times to each cluster and the average CMD was computed by stacking the individual CMDs on a binned colour magnitude plane in intervals of 1 mag. in magnitude and 0.5 mag. in colour. The average background subtracted CMD for each cluster was then

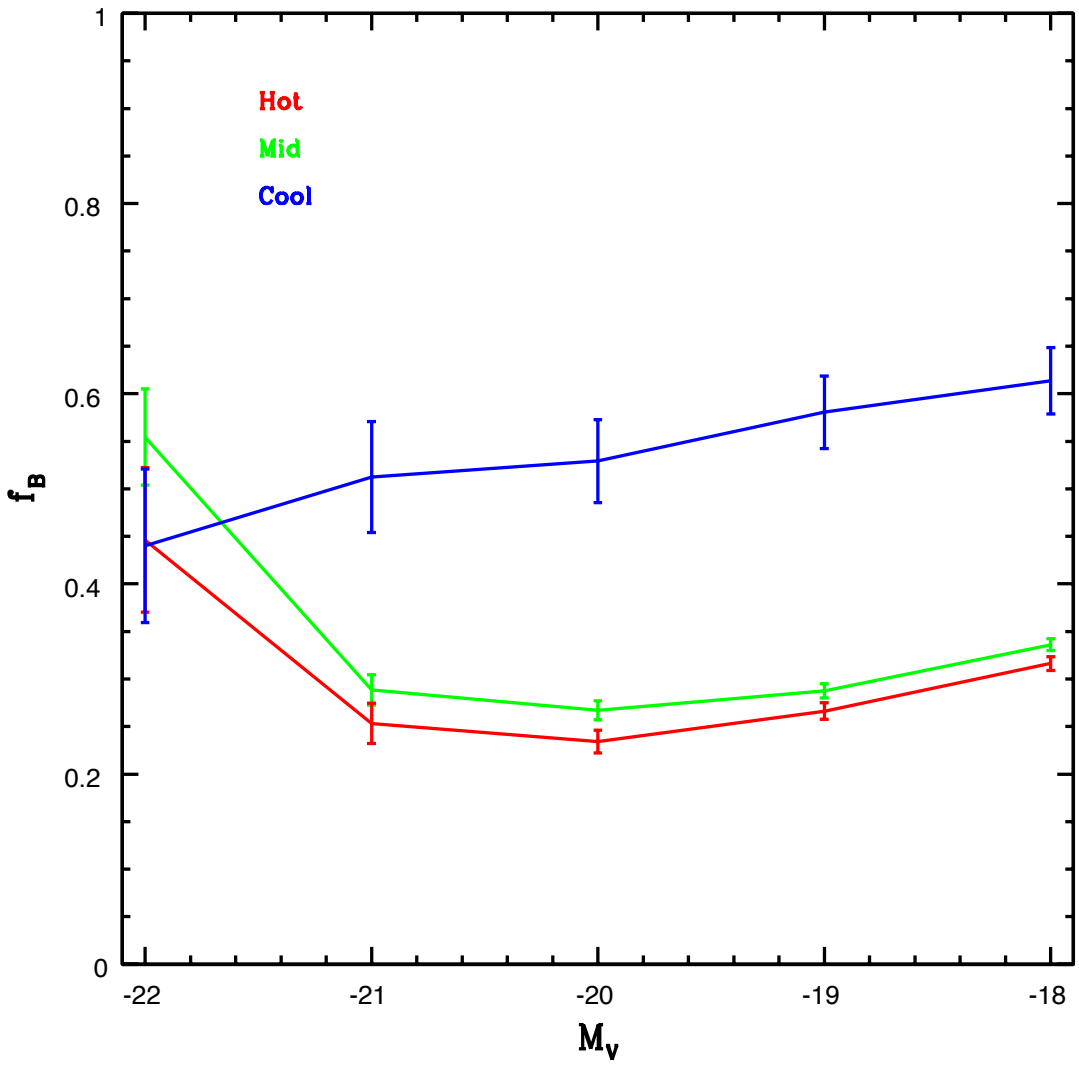

Figure 3.14: Variation of the cluster blue fraction for each cluster sample with faint magnitude cut.

transformed to a common redshift $z = 0.3$. The transformation described the effects of distance dimming and the k-correction. The k-correction for each colour pixel on the CMD plane was computed using the best-fitting interpolated spectral template required to reproduce the observed colour value at the cluster redshift. Individual cluster CMDs within each temperature sub-sample were then stacked on the $z = 0.3$ CMD plane. Each cluster CMD was assigned equal weight in the stacking process by normalising all transformed CMDs to a total contribution of unity summed withing the region $21 < r < 22$ and $1 < g - r < 1.5$. The stacked colour magnitude diagrams for each sample are shown in Figure 3.15. In addition, the fourth panel in Figure 3.15 indicates the result of subtracting the mid cluster stacked CMD from the corresponding cool cluster sample to highlight the location on the CMD of the excess fraction of blue galaxies found in the cool sample. As indicated in the plots, the relative excess appears uniform across a range of colours bluer than the red sequence. There is some evidence for an excess of faint ($r > 23$) blue ($g - r \sim 0.2$) galaxies in the cool sample. However, the CFHTLS optical data used to construct the cool CMD begins to be incomplete at these magnitudes and the purely visual impression may be flawed.

An alternative approach is to consider the colour distribution of all galaxies brighter than some limit. The colour distributions derived from the unweighted sum of all clusters in each temperature sample (corrected to $z = 0.3$) are shown in the upper three panels of Figure 3.16. The limiting magnitude is $r = 21.5$, approximately equal to $M_V = -20$ at this redshift. In order to investigate the distribution of blue galaxies in each sample the red sequence was modelled and removed in each case. Following Loh et al. (2008) the red wing of the red sequence was fitted using a double Gaussian model with the mean of each Gaussian set to the location of the red sequence and the best fitting full-width at half-maximum (FWHM) and normalisation of each profile determined using a minimum χ^2 algorithm. The resulting model is then reflected about the location of the red sequence and subtracted from the corresponding colour distribution.

The mean $g - r$ colour of all galaxies bluer than the location of red sequence for each sample was calculated and found to be 0.70, 0.675 and 0.675 for the cool, mid and hot samples respectively. We hesitate to place too much emphasis on the trend to observe redder mean colours in the blue cloud for lower temperature X-ray systems. This is principally due to potential limitations such as a) the obvious subtraction artefact in the mid sample red sequence subtracted distribution and b) the broad

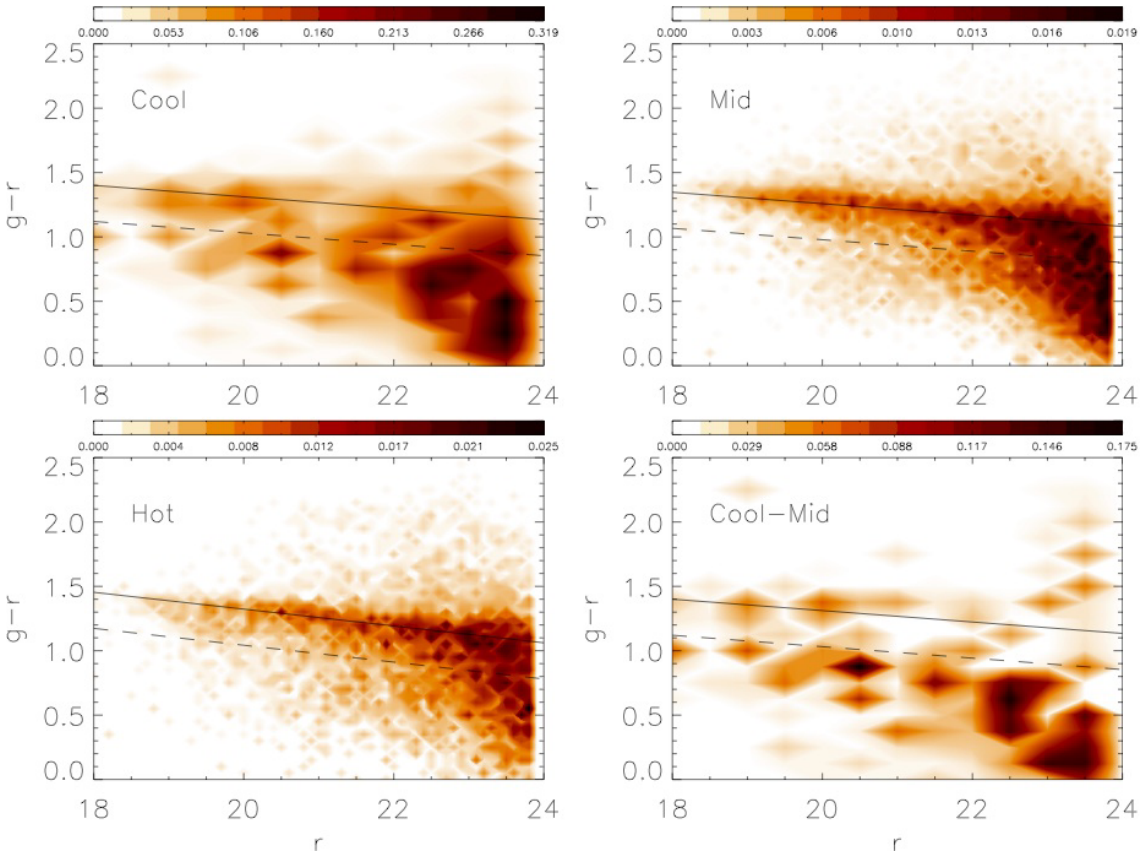

Figure 3.15: Stacked CMDs for the cool, mid, hot and (cool-mid) cluster samples (see text for details). All data are k-corrected to $z = 0.3$. In each panel the solid line marks the location of the red sequence and the dashed line marks the location of the corresponding Butcher-Oemler blue cut.

nature of such peaks and the low number of galxies involved (in the cool systems).

3.5 Conclusions

We have presented an analysis of the fraction of blue galaxies in a large sample of X-ray clusters spanning a wide range of X-ray temperature with uniform optical photometry. We have noted that the computed blue fraction values display a trend to decrease with both decreasing redshift and increasing temperature.

The trend of decreasing cluster blue fraction versus redshift has been observed previously and has been interpreted as a global effect driven by the decreasing rate of field galaxy infall onto the cluster environment (e.g. Ellingson et al. 2001). Coupled with the increasing cluster mass with decreasing redshift, the specific infall rate per unit cluster mass decreases at an even faster rate. Infall effects are further compounded with the sharply declining global star formation rate as a function of decreasing redshift (Hopkins and Beacom, 2006) which may be viewed as a decrease in the available gas supply of infalling galaxies. Looking beyond the redshift dependent component of the Butcher-Oemler effect, the decreasing blue fraction with increasing X-ray temperature identified in this paper is consistent with an environmental component to the Butcher-Oemler effect.

The trend of decreasing blue fraction versus temperature is most apparent when comparing across XMM-LSS and CCCP samples rather than within either sample. It remains possible that this difference is due in part to some subtle selection effect arising during the construction of the two samples rather than as a result of some physical process linked to the global environment. However, it is not clear what form such a bias would take. At this point we recall that the cool clusters may display a mild bias to higher gas densities or more centrally concentrated systems compared to the average population. One would naively expect such systems to be more effective at processing infalling field galaxies compared to the average (i.e. lower X-ray luminosity) cluster over the same temperature interval – effectively introducing a mild bias toward lower blue fractions in this temperature sub-sample. One could therefore argue that access to a more complete census of the low-temperature cluster population would only amplify the trend of blue fraction versus temperature. It has also been noted that optically selected clusters display different optical properties compared to X-ray selected samples (see Haines et al. 2009 for a discussion). However, X-ray samples of bright clusters are typically complete in terms of the optical properties they

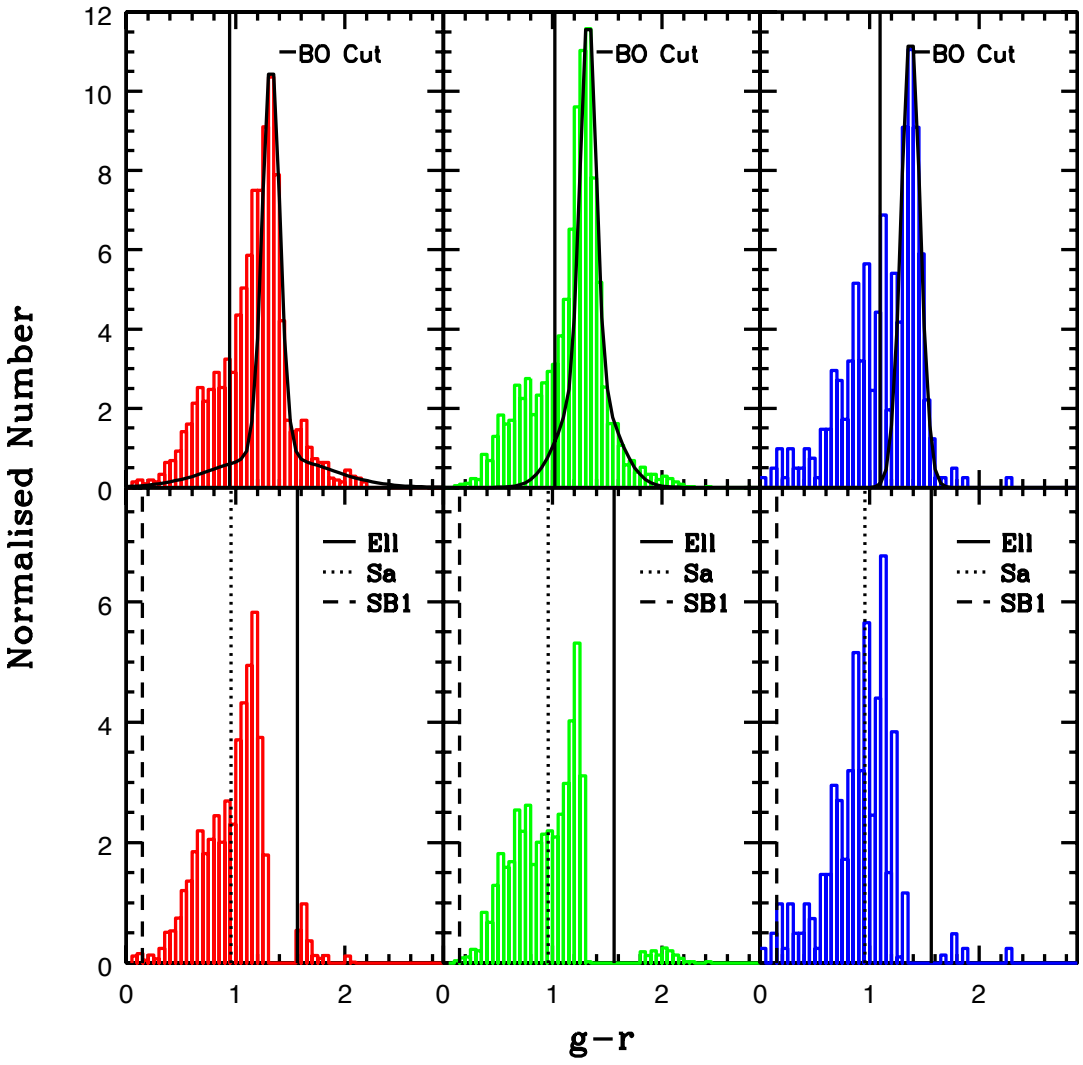

Figure 3.16: The top panels show stacked histograms for the cool, mid, and hot samples before red sequence subtraction. All cluster data are background subtracted and k-corrected to $z = 0.3$. The absolute numbers of galaxies in each bin have been re-scaled purely for visualisation purposes. The vertical line indicates the Butcher-Oemler blue cut location at $z = 0.3$. The bottom panels show the stacked histograms after red sequence subtraction (see text for details). The vertical lines incidate the observed frame colours of the Elliptical, Sa and Starburst 1 (SB1) models of Kinney et al. (1996).

sample (mainly because bright X-ray clusters are rare and thus it is possible to select complete samples). Moreover, clusters selected by single band optical observations (i.e. purely based upon the projected overdensity of bright galaxies) are more likely to be biased toward high blue fraction values due to the high mass-to-light ratios of blue star forming galaxies. We therefore note that any possible bias between the XMM-LSS and CCCP samples would naively be expected to generate the opposite trend to that observed in this paper and we remain confident that the trend of blue fraction versus temperature we have identified is not a result of sample selection effects.

A currently favoured explanation for the observed trend of blue fraction versus temperature is that infalling field galaxies are processed physically as they interact with the cluster environment. This interaction may take the form of ram pressure stripping whose effectiveness is a relatively simple function of the mass scale represented by the group or cluster into which the galaxies are falling. An alternative explanation is that infalling galaxies are processed via galaxy-galaxy interactions and therefore respond more readily to a combination of local rather than global velocity dispersion and galaxy density. Whatever the cause, it is clear that the process by which blue galaxies are processed to appear red is more complete in hotter (more massive) environments compared to cooler (less massive) environments.

Disentangling the above two effects is difficult as, to first order, the effects upon star formation in the infalling galaxy depend on environment in the same manner: ICM stripping and subsequent SF suppression are expected to be weakest (though not absent) in group environments – galaxy populations in these environments will display a larger fraction of blue galaxies relative to more massive clusters – while SF enhancements associated with galaxy-galaxy interactions will be greater on group scales. Each effect would naively generate the same observed trend of blue fraction versus temperature.

The blue fraction in each temperature sub-sample displays a very similar trend versus scaled radius and is consistent with an infalling field population albeit the cool sample is offset to higher blue fraction (Ellingson et al. 2001). However, the cool sample displays a marked increase in blue fraction with decreasing magnitude. The increase in the cool sample blue fraction with increasing magnitude results from both a moderate increase in the number of blue galaxies but also in a relative deficit in the numbers of red galaxies compared to those in the mid and hot samples. We will address the red sequence luminosity function of the cool, mid and hot samples in subsequent chapters. However, we note that the relative deficit of red galaxies in cool

clusters compared to the mid and hot samples is consistent with the scenario where the processing of blue galaxies to red galaxies during infall is relatively incomplete.

Our analysis has identified a clear environmental dependence in the blue fraction of galaxies. However, the cause of this environmental Butcher-Oemler effect – whether it be ram pressure stripping or galaxy-galaxy interactions – cannot be discerned unambiguously on the basis of the colour distribution of the blue galaxy population in each sample. Clearly further information is required, most notably the combination of colour information with morphological information. One would naively expect the above two environmental processes to affect galaxy morphology in markedly different ways, e.g. ram pressure effects should not disrupt galaxy disks whereas a strong disruptive effect is expected from galaxy-galaxy interactions. We will present this investigation in the next chapter.

Chapter 4

Probing the galaxy population mix as a function of environmental scale

This project focuses on the underlying physical processes which affect galaxy populations in different environments. These processes are broadly divided into two categories; "local" effects and "global" effects. Examples of the former include such mechanisms as galaxy-galaxy interactions, whereas examples of the latter could include ram pressure stripping (i.e. An interaction of a galaxy with the cluster environment itself).

4.1 Introduction

The population distribution of galaxies displays a clear relationship with the environment in which they reside. One manifestation of this relationship is that early-type galaxies (or more generally galaxies which are bulge dominated, relatively red, gas poor and display lower specific star formation rates) dominate the population mix of galaxies in dense environments (e.g. Dressler et al. 1980). The corresponding population mix of lower density or field regions of the universe appears to be dominated by later-type galaxies (or more generally those galaxies which are disk dominated, relatively bluer, more gas rich and display higher specific star formation rates). This change in the population mix as a function of environment coupled with the fact that dense structures such as galaxy clusters grow via the gravitational accretion of less

massive structures drawn from lower density regions of the universe indicates that some (or a number) of physical processes must be acting upon the accreted galaxy population with the result that their observed properties (e.g. colour, gas content, star formation rate) are transformed.

There has been a great deal of work undertaken to investigate what form these transformations take and to understand the root physical causes. Comparisons of galaxy populations drawn from low (the field) and high (rich galaxy clusters) density environments indicate that the population distribution does indeed vary as a function of changing environment. Balogh et al. (1999) confirmed this through the measurement of the spectral indices for 1823 galaxies selected from the Canadian Network for Observational Cosmology (CNOC1) sample. This study considered 15 X-Ray luminous clusters spanning the redshift range $0.18 < z < 0.55$ and found that, in the cluster environment, there is evidence for older stellar populations over those found in field galaxies. Furthermore the radial trends of the D4000 index (a measurement of the mean stellar age of a galaxy), and the rest frame equivalent widths $W_0(H\delta)$ and $W_0([OII])$ were all consistent with an age sequence in which the last episode of star formation occurred more recently in galaxies farther from the cluster centre (i.e. in the least dense regions of the clusters). This would suggest that the densest regions of these clusters were more efficient at quenching[1] star formation in galaxies than the less dense regions.

Poggianti et al. (2006) use the [OII] emission line as a signature of ongoing star formation to investigate how the proportion of star-forming galaxies evolves between $z = 0.8$ and $z = 0$ as a function of environment using galaxies from the ESO Distant Cluster Survey (EDisCS, a photometric and spectroscopic survey of galaxies in 20 fields containing galaxy clusters from $z = 0.4 - 1.0$) and a local comparison sample taken from the Sloan Digital Sky Survey (SDSS, $0.04 < z < 0.08$). The results indicated that at both high and low redshift, the fraction of star forming galaxies depends on the velocity dispersion of the cluster. At higher redshifts ($z = 0.4 - 0.8$), it was observed that more massive clusters (higher densities) displayed a lower fraction of star forming galaxies and that the strength of the star formation varies according to the cluster velocity dispersion.

Galaxy morphology also displays a clear relationship with environment as demonstrated by the morphology-density relation (e.g. Dressler et al. 1997, Treu et al. 2003), whereby bulge dominated or elliptical galaxies comprise the majority of the popula-

[1]Where quenching represents a physical process which suppresses current star formation.

tion mix in high density environments and with disk dominated or spiral galaxies preferentially located in lower density environments.

Other properties, such as the integrated colour of galaxies also vary as a function of changing environment. Blanton et al. (2005) studied the local environments of 114,994 galaxies as a function of their colours, luminosities, surface brightness and radial profile shapes selected from SDSS to have $14.5 < r < 17.7$ and $0.05 < z < 0.22$. The structural properties of the galaxies (i.e. Sersic index and surface brightness) appeared to be less related to environment than were measurements of the star formation history (e.g. integrated colour and luminosity).

Many studies have considered of the population mix as a function of environment as defined by the integrated galaxy colour (e.g. Baldry et al. 2004). Butcher and Oemler (1984) reported an increase in the fraction of blue galaxies in massive clusters out to z $\sim$ 0.5. This result has been subject to much discussion including the potential effects of the changing mass of the clusters (used as the environmental metric) with redshift and the potential effect of low mass, high mass-to-light ratio star-bursting galaxies biasing the resultant population mix (Holden et al. 2007). In Urquhart et al. (2010) and Chapter 3 we demonstrated that, employing a sample of 34 X-ray emitting clusters with measured X-ray temperatures and uniform optical photometry, the cluster blue fraction as defined by Butcher and Oemler (1984) responds to both redshift and the cluster X-ray temperature. The trend to observe higher blue fractions at higher redshift (at fixed cluster temperature) was confirmed in addition to demonstrating that at fixed redshift there exists a significant trend of blue fraction with X-ray temperature in that hotter (more massive) clusters display lower blue fractions.

The exact physical causes of this environmental dependence remain unclear. However, most mechanisms that result in the quenching of star formation act to deplete the gas content of a galaxy which in turn acts as the fuel for future star formation. They can be divided into two broad categories: gas depletion and gas consumption. Gas can be depleted from a galaxy if it is stripped as a result of the force experienced as the galaxy travels through the intracluster medium (ICM) of a galaxy cluster. Such ram pressure stripping (Gunn and Gott 1972) can potentially remove both the hot (Larson et al. 1980) and cold gas supply of a galaxy and thus suppress star formation activity. The rate at which a galaxy then evolves from blue to red will depend upon the gas stripping timescale, the cold gas consumption timescale (if only the hot component is stripped) and the rate of passive stellar evolution. The effectiveness of the

stripping depends upon the ICM gas density and the relative velocity of the galaxy to the cluster (both of which are greater for more massive clusters) in addition to the binding energy of the galactic gas. The existence of ram pressure stripping in galaxies include the observation of neutral Hydrogen tails associated with galaxies in nearby clusters (e.g. Scott et al. 2010) in addition to the observation of so-called "jellyfish" galaxies which display evidence of recent star formation in stripped gaseous regions (Cortese et al. 2007). Gas is rapidly consumed in a galaxy experiencing intense bursts of star formation resulting from interactions and mergers with other galaxies. Galaxy mergers and interactions are a two-body process and one expects the rate of merging to be proportional to the square of the local galaxy density (Makino and Hut 1997). Enhanced fractions of close pairs of galaxies and apparent merging events are observed in galaxy clusters to $z = 1$ (e.g. Kampczyk et al. 2013). However, one also expects that the internal disruption experienced by an interacting galaxy (which will be related to the star formation rate) to be stronger in interactions where the relative velocities of the galaxies are low (i.e. in less massive clusters).

We attempt to disentangle these physical effects and thus potentially learn about the principal/dominant quenching mechanism by comparing the cluster blue fraction to both a global (cluster X-ray temperature) and a local environmental metric (the local surface density of galaxies) while also accounting for possible redshift evolution in the sample. We employ a slightly expanded sample of galaxy clusters that is essentially similar in all properties to the 34 X-ray emitting clusters described in detail in Chapter 2. We therefore outline the salient aspects of the sample in the following sections before concentrating upon the new analyses.

4.2 Data Set

Although the sample of clusters analysed in Chapter 3 provides a good probe of the cluster blue fraction as a function of X-ray temperature – by design it does not sample a wide range of redshifts at fixed cluster temperature. In order to investigate the redshift evolution of the cluster blue fraction at fixed X-ray temperature we also employ a low redshift X-ray detected cluster comparison sample in Section 4.5. This sample contains clusters from the MultiEpoch Nearby Cluster Survey (MENeaCS; Sand et al. 2012) The MENeaCs sample displays X-ray temperatures $3.58 < \mathrm{T_X(keV)} < 8.24$ and redshifts $0.04 < z < 0.14$. It is therefore a low-z counterpart to the CCCP "mid" sample. Each cluster possesses CFHT $g'r'$ imaging similar to the XMM-LSS/CCCP

Table 4.1: Properties of the low redshift MENeaCS cluster sample.

Cluster	R.A. (deg.)	Dec. (deg.)	T_X (keV)	z
A2597	351.3244	-12.1264	3.58	0.085
A133	15.6607	-21.8984	3.71	0.057
A1068	160.1951	39.9511	3.87	0.138
A2670	358.5667	-10.4112	3.98	0.076
A2033	227.8594	6.3534	4.16	0.082
A2440	335.9525	-1.6408	4.31	0.091
A2065	230.6200	27.7103	5.35	0.073
A1795	207.2098	26.5995	5.49	0.062
A990	155.9185	49.1411	5.75	0.144
A85	10.4372	-9.3110	5.87	0.055
A1650	194.6708	-1.7572	5.89	0.084
A119	14.0785	-1.2446	5.93	0.044
A1651	194.8418	-4.1928	5.97	0.085
A478	63.3588	10.4670	7.07	0.088
A1413	178.8236	23.4073	7.09	0.143
A644	124.3492	-7.5156	7.31	0.070
A2029	227.7335	5.7472	7.38	0.077
A401	44.7437	13.5780	8.07	0.074
A2142	239.5895	15.9726	8.24	0.091

sample which is described in Table 2.2. Table 4.1 describes the X-ray properties and redshifts of these 19 MENeaCS clusters.

We incorporated these additional clusters into our original Butcher-Oemler analysis from Chapter 3, reproducing Figures 3.8 and 3.9 now including the MENeaCS sample. These are shown here in Figures 4.1 and 4.2.

Once again, we performed non-parametric technique to investigate any observed trends through a partial Spearman rank analysis. The partial correlation coefficient describing blue fraction and redshift while controlling temperature is now found to be $r(f_B, z, T)$=0.48 and the partial correlation coefficient describing blue fraction and temperature while controlling redshift is now $r(f_B, T, z)$=-0.46. This once again confirms the evolution in cluster blue fraction with both redshift and temperature, further highlighting the importance of minimising the redshift range over which we study environmental effects in the previous and following investigations.

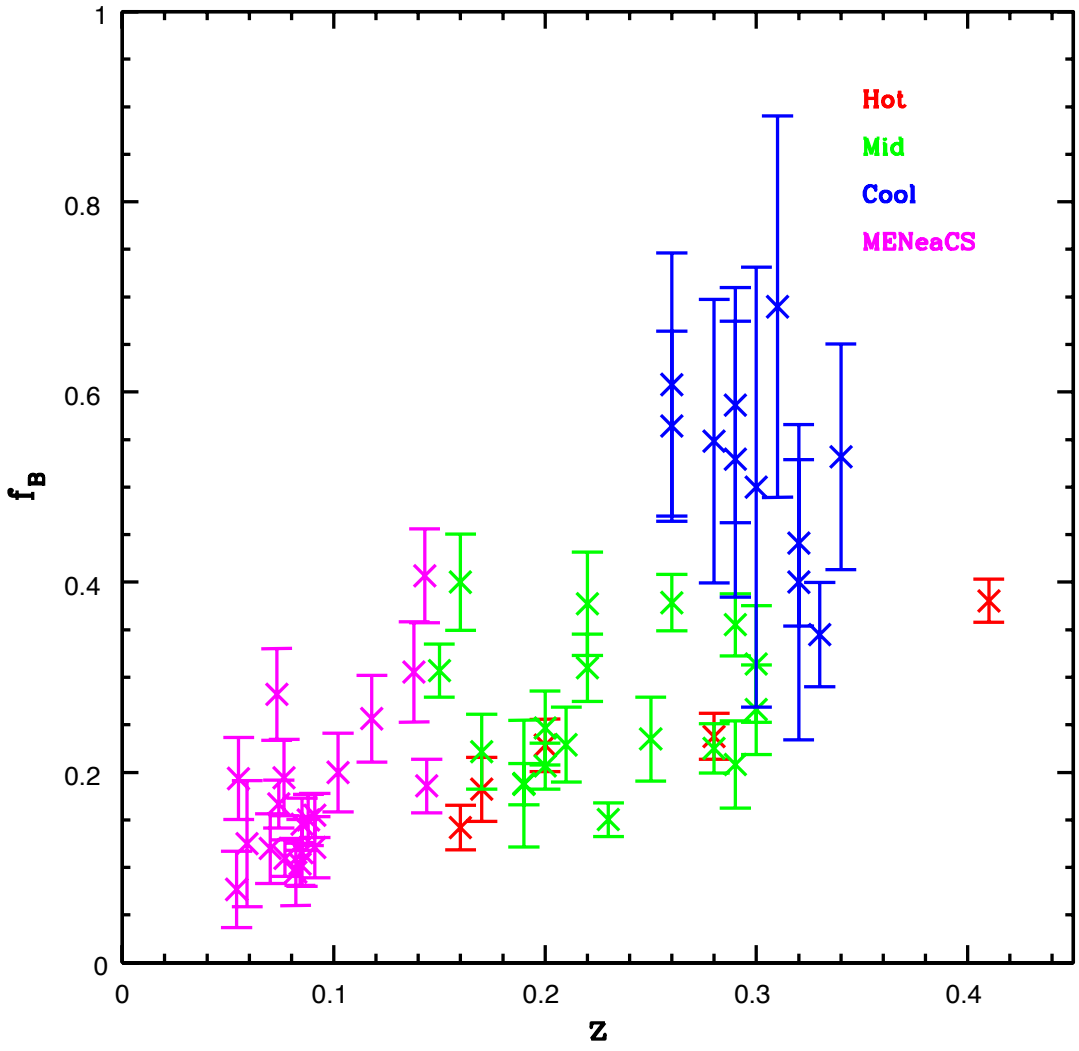

Figure 4.1: Cluster blue fraction as a function of redshift.

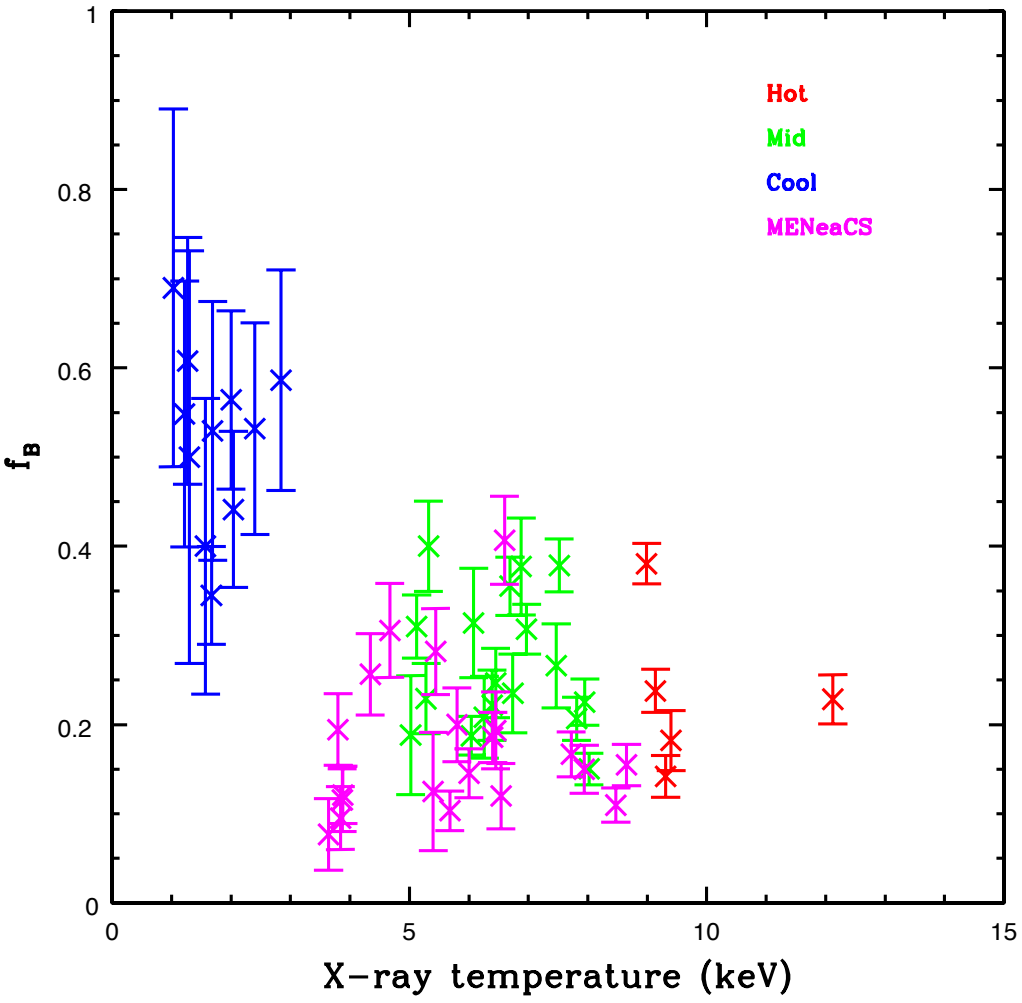

Figure 4.2: Cluster blue fraction as a function of X-Ray temperature.

4.3 Mass versus luminosity selection

There has been much discussion in the literature as to whether the Butcher-Oemler effect arises from changes in the galaxy population mix as a function of redshift or from observational biases. The original work of Butcher and Oemler (1984) employed a sample of galaxies selected via optical luminosity. This can introduce a possible bias arising from the inclusion of low-mass star forming galaxies whose low mass-to-light values can place them in the sample. This potential effect was investigated by Holden et al. (2007) who studied the morphology-density relation for galaxies selected using both luminosity and mass in five massive (having velocity dispersion $>850\text{kms}^{-1}$) X-ray clusters in the redshift range $0.23 < z < 0.83$ with colours and morphologies coming largely from *Hubble Space Telescope* imaging in the B and V bands. Luminosity selection generated a trend of cluster early-type fraction with redshift (see their Figures 3 & 4) such that lower early-type fractions were observed at higher redshift, consistent with the Butcher-Oemler effect. However, when using a mass selected sample, the observed early-type fraction trend with redshift appeared much shallower and was consistent with no evolution.

The importance of stellar mass versus luminosity selected samples in determining the cluster galaxy population mix was further investigated by Li et al. 2009. Mass selection effects were calculated for 16 clusters having $0.17 < z < 0.55$ taken from the Canadian Network for Observational Cosmology (CNOC1) sample. Following a similar analysis to that applied to their luminosity selected sample, they calculated the cluster red fraction f_{red} for galaxies lying within r_{200} of the cluster centre and found that for 3 different mass limited samples, all show a decrease in f_{red} with increasing cluster redshift. The lower mass selected sample showed the most pronounced $f_{red} - z$ trend and the highest mass selected sample showed the shallowest $f_{red} - z$ slope – a result consistent with the down sizing model of galaxy evolution (e.g. De Lucia et al. 2006, Kodama et al. 2004). The authors suggest that this may explain the weak evolution seen in the Holden et al. (2007) given the relatively high stellar mass limit used.

Given the above considerations, we also investigate the effect of mass versus luminosity selection on the computed cluster blue fraction. To convert from a luminosity threshold to one based on stellar mass, we employed the relation of Bell et al. (2003), i.e. $\log(M_*/L_r) = -0.306 + 1.097(g - r)$ (and noting the conversion from Sloan to

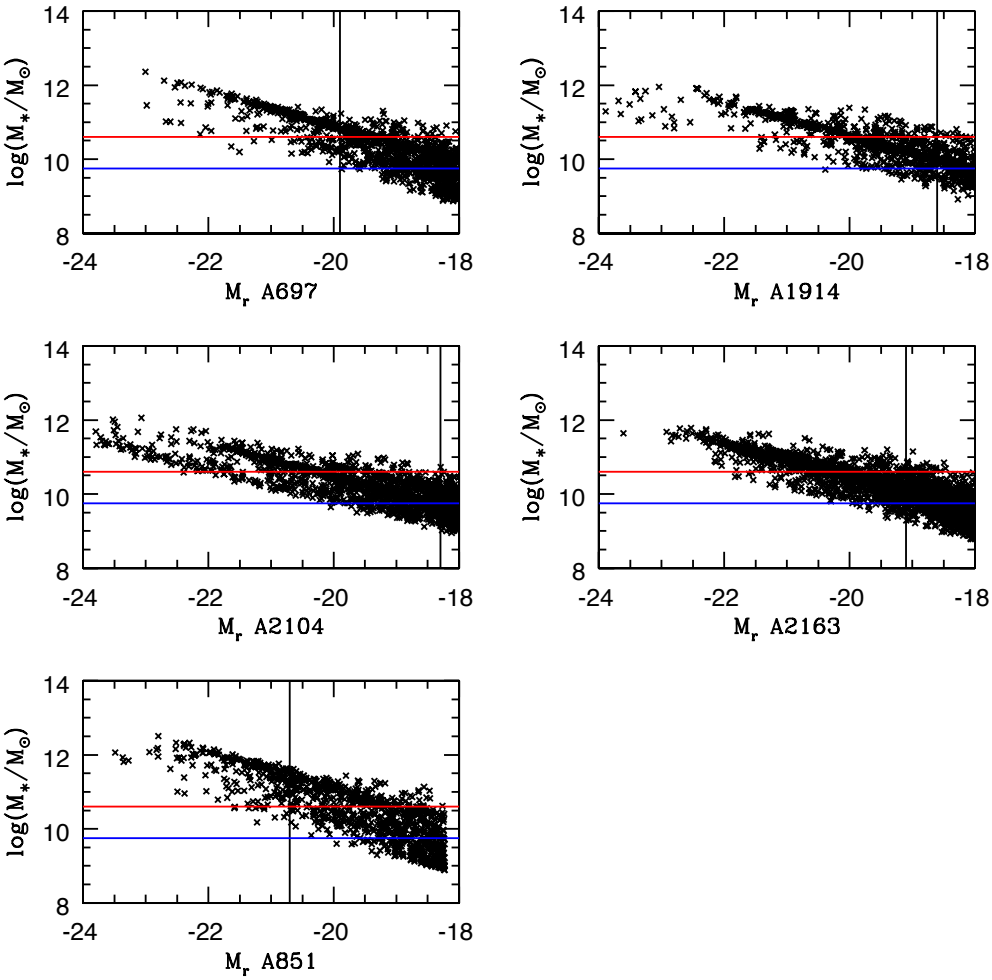

Figure 4.3: Hot sample clusters. All sources within r_{500} of the cluster centre are plotted. The blue line marks $\log(M_*/M_\odot)$=9.75 and the red line marks $\log(M_*/M_\odot)$=10.6 as described in the text. The vertical dashed line indicates the M_r magnitude corresponding to $M_V = -20$ at the cluster redshift.

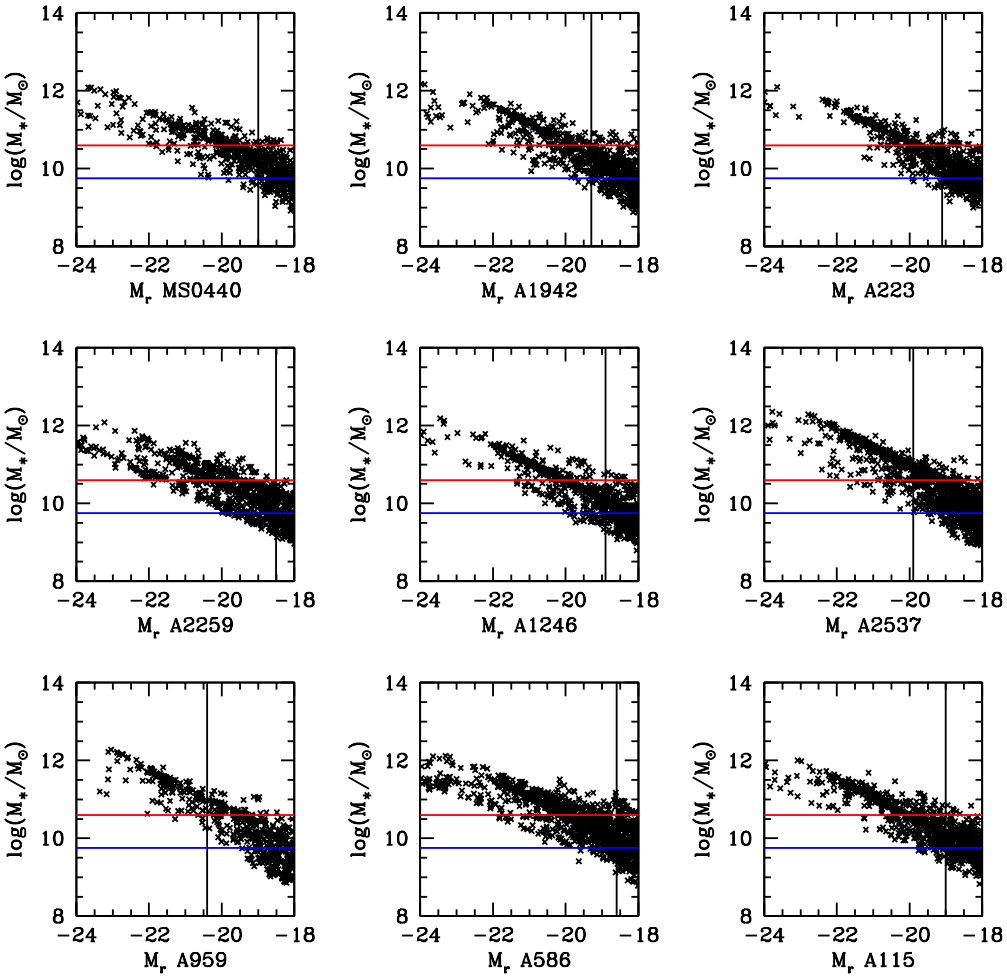

Figure 4.4: Mid sample clusters. All sources within r_{500} of the cluster centre are plotted. The blue line marks $\log(M_*/M_\odot)$=9.75 and the red line marks $\log(M_*/M_\odot)$=10.6 as described in the text. The vertical dashed line indicates the M_r magnitude corresponding to $M_V = -20$ at the cluster redshift.

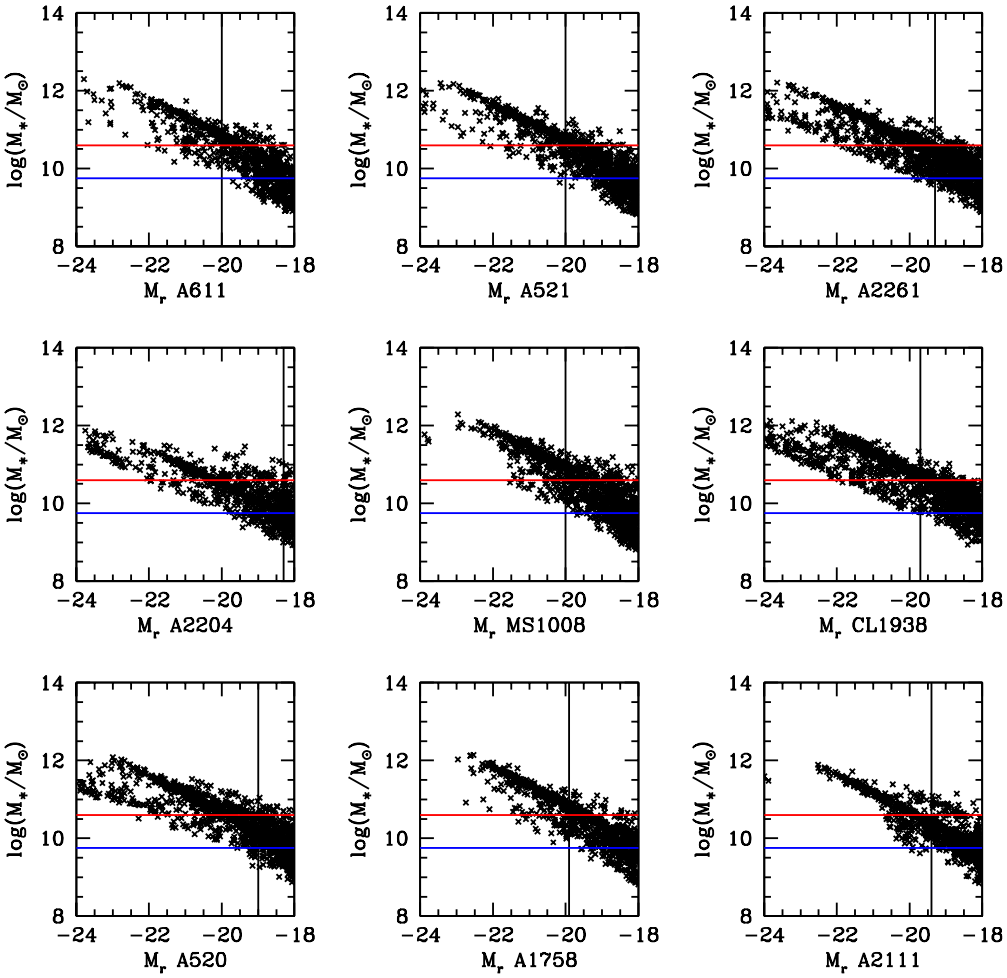

Figure 4.5: Mid sample clusters. All sources within r_{500} of the cluster centre are plotted. The blue line marks $\log(M_*/M_\odot)$=9.75 and the red line marks $\log(M_*/M_\odot)$=10.6 as described in the text. The vertical dashed line indicates the M_r magnitude corresponding to $M_V = -20$ at the cluster redshift.

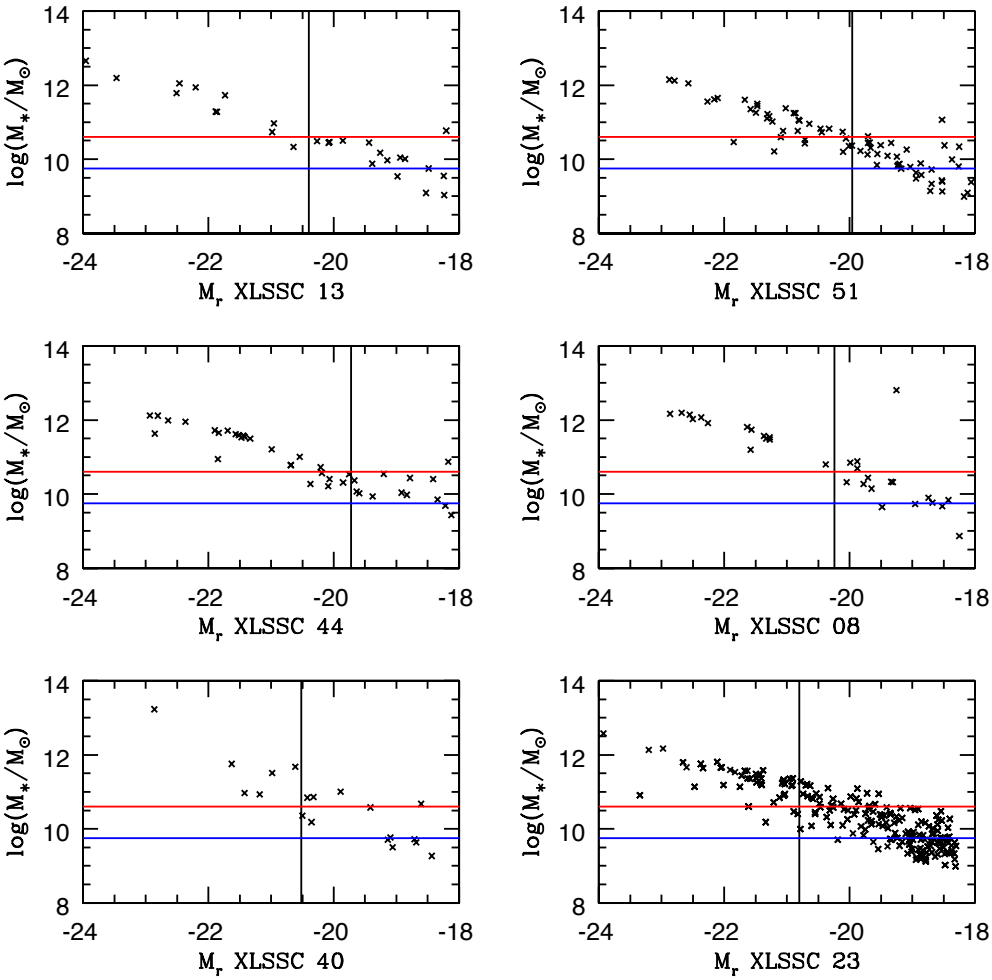

Figure 4.6: Cool sample clusters. All sources within r_{500} of the cluster centre are plotted. The blue line marks $\log(M_*/M_\odot)$=9.75 and the red line marks $\log(M_*/M_\odot)$=10.6 as described in the text. The vertical dashed line indicates the M_r magnitude corresponding to $M_V = -20$ at the cluster redshift.

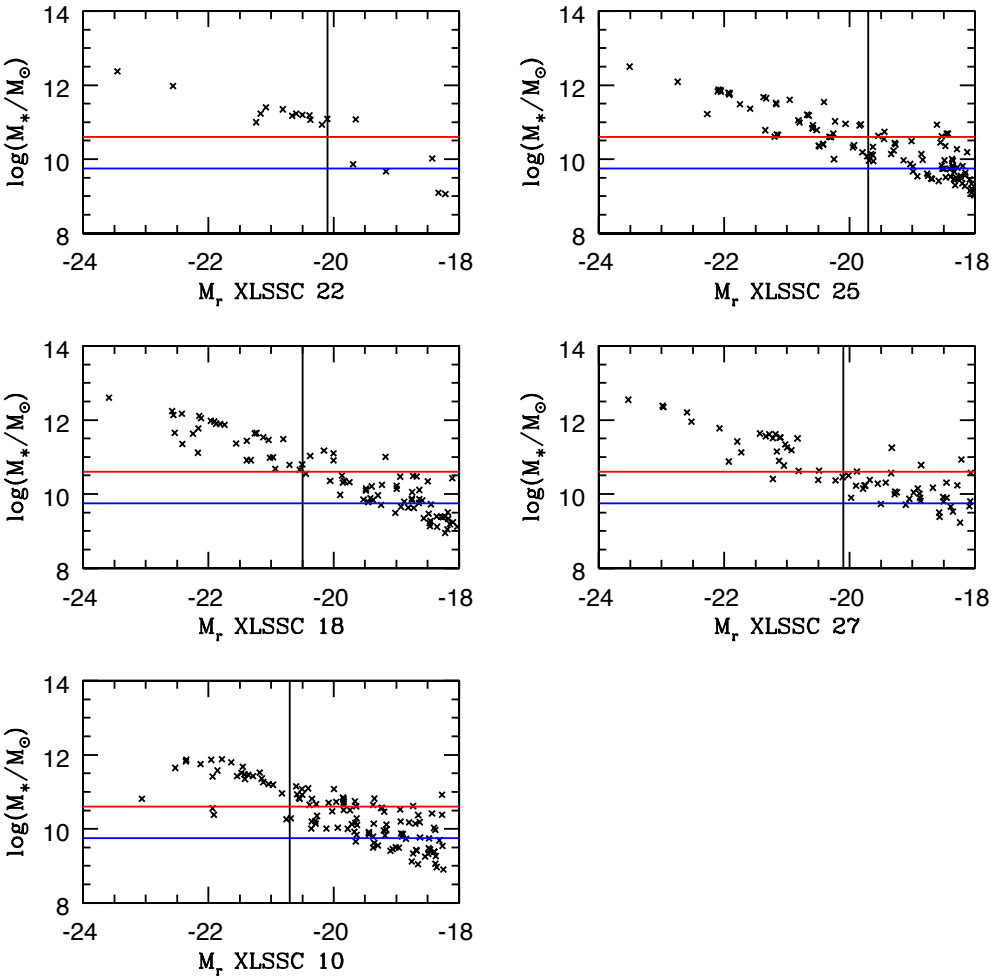

Figure 4.7: Cool sample clusters. All sources within r_{500} of the cluster centre are plotted. The blue line marks $\log(M_*/M_\odot)$=9.75 and the red line marks $\log(M_*/M_\odot)$=10.6 as described in the text. The vertical dashed line indicates the M_r magnitude corresponding to $M_V = -20$ at the cluster redshift.

CFHT Megacam photometry[2]). The mass-magnitude diagrams for the hot sample are shown as an example in figure 4.3. The horizontal blue and red lines correspond to $\log(M_*/M_\odot) = 9.75$ and $\log(M_*/M_\odot) = 10.6$ respectively. The mass cut of $\log(M_*/M_\odot) = 9.75$ was adopted for all subsequent analyses and corresponds roughly to the typical stellar mass of blue galaxies at the magnitude limit of the cluster.

Figure 4.8 compares f_B values for the luminosity and mass selected samples. In general, lower blue fractions result from using a mass selected sample, although the same overall trends are observed regardless of whether luminosity or mass selection is applied. The largest discrepancies between the two methods occur for cool clusters. If this was solely the result of the low number of members in such systems then we would expect the scatter to be symmetric. However, the scatter lies preferentially in the upper left of the figure, i.e. cool clusters display lower f_B values when computed using a mass selected sample. This result is consistent with low mass, low M/L ratio galaxies contributing to the f_B values of cool clusters when applying luminosity selection. The suggestion that the Butcher-Oemler effect is primarily driven by low stellar mass galaxies has also been commented upon by Pimbblet and Jensen (2012) and Tajiri and Kamaya (2001).

We further compute the differential cluster blue fraction as a function of the stellar mass. The results are shown in Figure 4.9 which considers sources within 4 r_{500}. Adopting a radial limit of 4 r_{500} generates a large enough galaxy sample to compute the differential blue fraction with relatively small errors and covers an interval of clustercentric radius where there is no rapid change in the blue fraction versus radius for any of the cluster sub-samples. We note that there seems to be a maximum difference between the cool and the mid and hot samples at a stellar mass of $\sim 10^9 \mathrm{M}_*$, however it is unclear as to the underlying physical reason(s) for this.

4.4 The effect of local environment: The local surface density of galaxies and the computed blue fraction.

The idea that the galaxy population mix within a cluster is influenced by both global and local physical effects was established in Section 4.1 motivated by the fact that

[2]http://www2.cadc-ccda.hia-iha.nrc-cnrc.gc.ca/megapipe/docs/filters.html

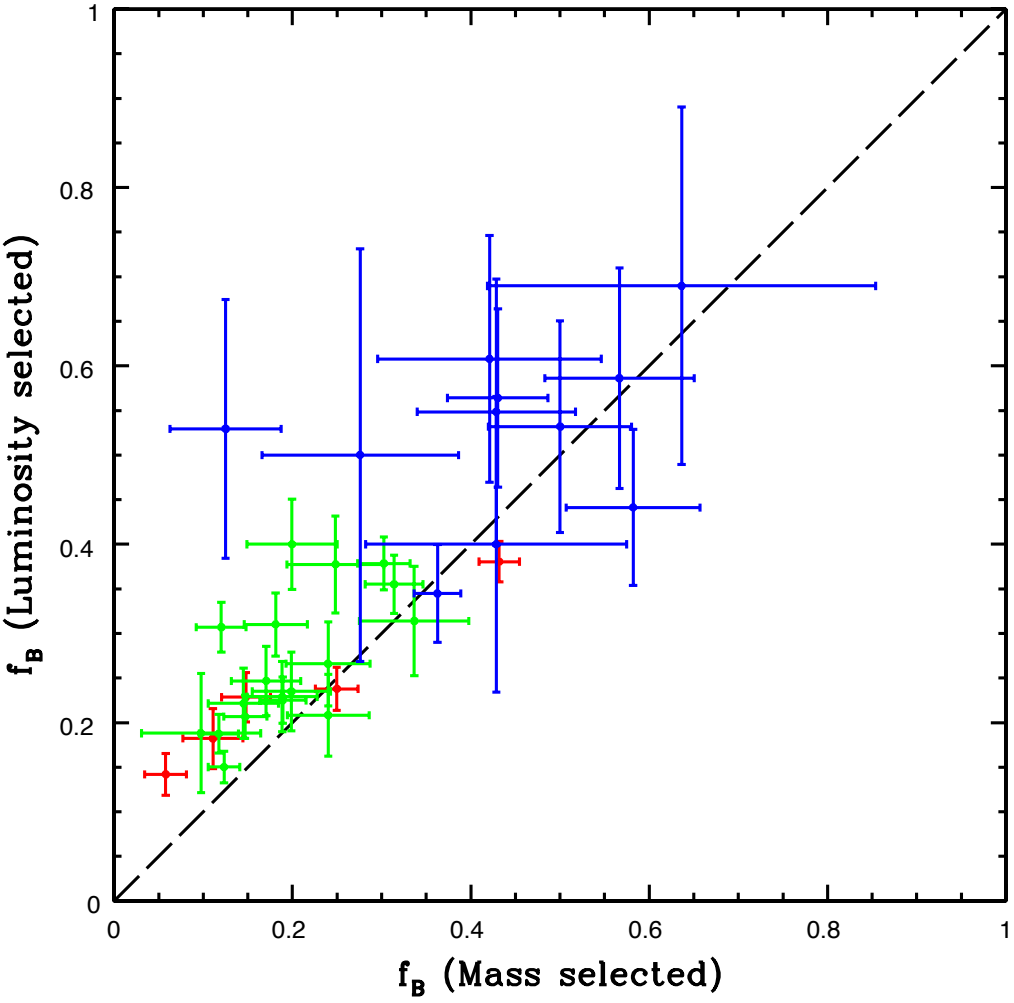

Figure 4.8: Comparison between f_B calculated for a luminosity selected sample and f_B calculated for a mass selected sample.

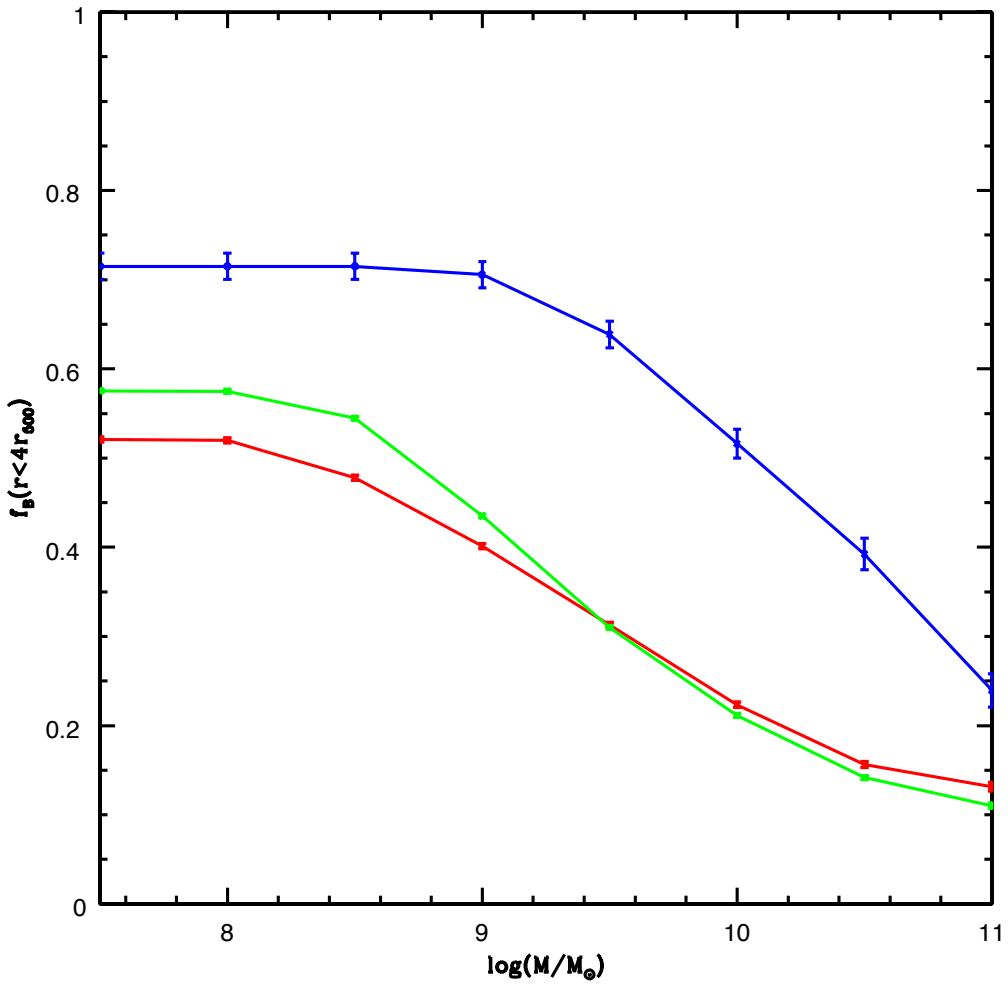

Figure 4.9: Differential f_B for the cool, mid and hot samples (blue, green and red respectively) for all sources within $4r_{500}$.

the main physical drivers of evolution occur on different scales. To investigate this idea further, we define the local environmental metric as the projected surface density based upon the distance to the 5th nearest neighbour, i.e.

$$\Sigma_5 = \frac{5}{\pi D_5^2}, \tag{4.1}$$

where D_5 is the distance to the 5th nearest neighbour in kiloparsecs. This is calculated for each of the 100 background subtraction realisations for each cluster within different radial bins. The mean values of Σ_5 were calculated in these radial bins, again per cluster and then combined for the cool, mid and hot samples. This is shown in Figure 4.10.

Cooper et al. (2007) demonstrate that the choice of $n = 5$ compared to, for example, $n = 3$ or $n = 10$ as the n-th nearest neighbour on which the surface density calculation is based does not result in a significant variation of the trends of measured galaxy population parameters versus surface density. We also confirmed this assertion by performing the subsequent analyses using Σ_3, Σ_5 and Σ_{10} as the local environmental metric and we present Σ_5 measures in the following results. Figure 4.11 displays the total distribution of Σ_5 values for all galaxies within $r < 4\ r_{500}$ for each temperature sub-sample of clusters.

The variation of Σ_5 with projected clustercentric distance is shown in Figure 4.10. The galaxy surface density data for each temperature sub-sample are compared to a model prediction based upon a best-fitting projected Plummer profile,

$$\rho(r) = \left(\frac{3M}{4\pi r_0^3}\right)\left[1 + \left(\frac{r}{r_0}\right)^2\right]^{-5/2} \tag{4.2}$$

where M is the cluster mass and r_0 is the Plummer radius which sets the size of the cluster core. Best-fitting profile parameters were determined using a non-linear least squares algorithm (MPFIT; Markwardt 2009) and provide a sensible match to the data (with the fitted values of the Plummer radius increasing with decreasing cluster mass). We note that the local surface density of galaxies is weakly correlated with scaled clustercentric distance. Average Σ_5 values reach a maximum at $r < r_{500}$ in the distribution of clusters stacked by temperature with any decline at $r > r_{500}$ small compared to the standard deviation about the mean Σ_5 value at any temperature. Given this weak trend we consider the variation of the computed blue fraction versus

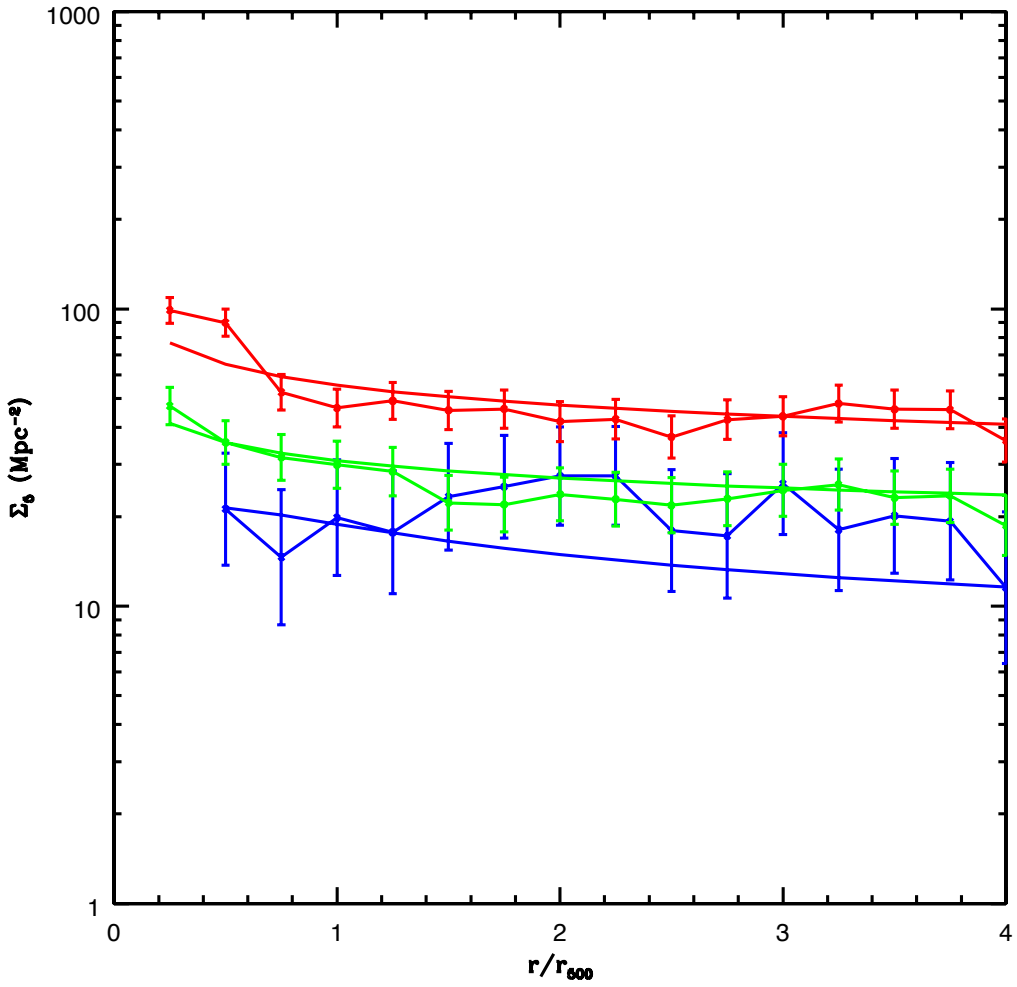

Figure 4.10: Variation of Σ_5 with scaled radius for the cool, mid and hot samples (blue, green and red respectively). Error estimates are Poissonian. The coloured curves displays the best fitting projected density based upon a Plummer model (see text for details).

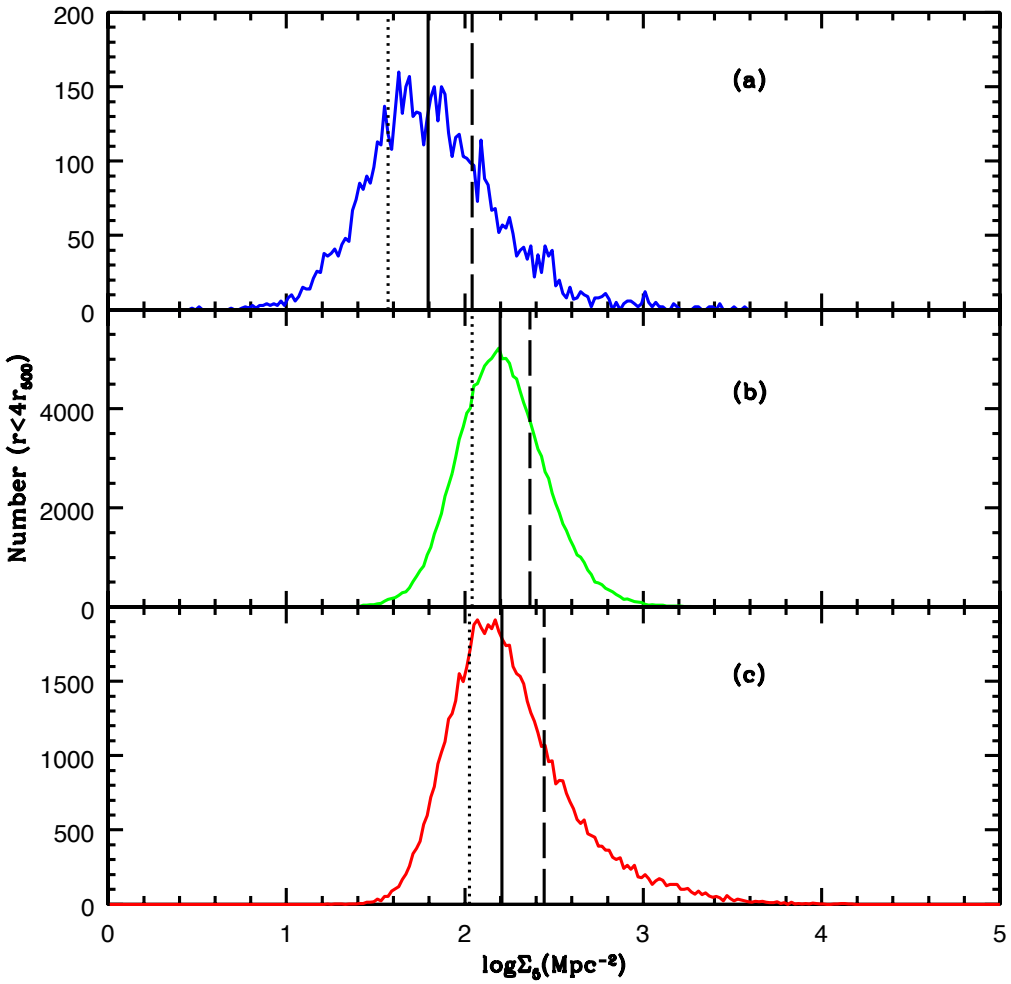

Figure 4.11: Projected surface density distributions, Σ_5 within 4 r_{500} for all three cluster samples; cool (blue), mid (green) and hot (red). The dotted, solid and dashed lines mark the location of the interquartile points of each distribution. Values of Σ_5 for each cluster are computed based upon 100 realisations of the background subtraction method described in Section 3.2.1. The plotted number distributions created by summing the contriubtions from all clusters in each temperature sub-sample are rescaled by this factor of 100.

Σ_5 for all galaxies displaying $r < 4\ r_{500}$ (though we have repeated the following analysis for samples based upon two further radial bins: $r < r_{500}$ and $r_{500} < r < 4\ r_{500}$ and note no significant differences in the results obtained).

For each cluster we compute the blue fraction for all galaxies above the stellar mass limit $\log M^*/M_\odot = 9.75$. Each cluster is further characterised by X-ray temperature, redshift and mean galaxy projected surface density for all galaxies within $4\ r_{500}$, ($\bar{\Sigma_5}$). In Urquhart et al. (2010) we employed a partial Spearman rank correlation test to investigate the relationship between the cluster blue fraction and both redshift and X-ray temperature. This approach is appropriate in situations where the relationship between the variables in question is unknown and a linear correlation test would be inappropriate. We repeat the approach here and compute the following correlation values (ρ): $\rho(f_B, T_X|z, \bar{\Sigma_5}) = -0.59$, $\rho(f_B, z|T_X, \bar{\Sigma_5}) = 0.58$ and $\rho(f_B, \bar{\Sigma_5}|T_X, z) = 0.24$. This analysis confirms the trend of f_B versus T_X and z described in Urquhart et al. (2010). However, the analysis indicates a weak relationship between f_B and $\bar{\Sigma_5}$ of low significance. This result is unsurprising as $\bar{\Sigma_5}$ is a local variable and fails to describe the range of projected surface density values within an individual cluster.

In an attempt to separate the dependence of the cluster blue fraction on local (Σ_5) and global (X-ray temperature) effects we therefore compute the blue fraction for galaxies residing in environments defined by X-ray temperature and Σ_5 values. Galaxies are considered to occupy clusters of either cool, mid or hot temperature as defined previously. In addition, galaxies within each cluster temperature sub-sample are considered in bins of surface density with the bin boundaries defined by the inter-quartile points of the distributions displayed in Figure 4.11 and the bin centre defined as the mid-point of each bin boundary. Galaxies displaying $r < 4\ r_{500}$ are included in the analysis. The tail of low Σ_5 values in the hot sample comes from the cluster A851, however this cluster is atypical in that it shows greater substructure and a larger population of disturbed galaxies (Oemler et al. 2009) and therefore is not expected to follow the same local density trends as the other hot sample clusters.

The distributions of Σ_5 were created for each of the 100 realisations of the background subtraction technique. These were then combined into one distribution and using the mean number of galaxies in a Σ_5 bin, this number was applied to the bins of the combined distribution to randomly select that number of galaxies. Shown in Figure 4.11 is the result of one realistion of the background subtracted Σ_5 distribution.

Figure 4.12 displays the cluster blue fraction versus Σ_5 split by cluster X-ray temperature. The figure indicates that f_B depends upon both the cluster X-ray tempera-

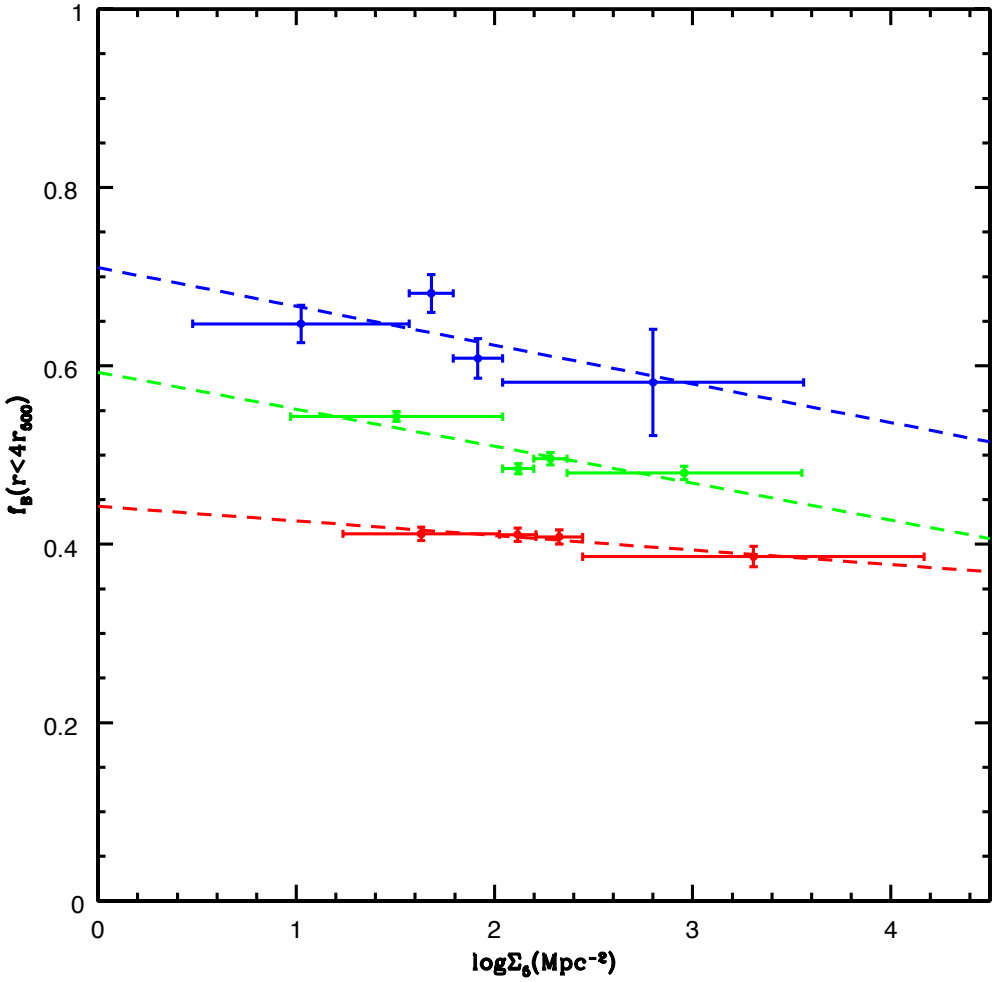

Figure 4.12: Blue fractions in bins of Σ_5. The dashed lines are the linear least squares lines of best fit

ture (as demonstrated in Urquhart et al. 2010) and the local projected surface density of galaxies. At fixed cluster temperature the value of f_B decreases with increasing local surface density. This trend in f_B is consistent with the colour-morphology-density relation (Vogt et al. 2004) whereby red or elliptical galaxies preferentially reside in areas of higher density (e.g. Cooper et al. 2007). The magnitude of the difference in blue fraction between the highest and lowest density bins are 0.065, 0.063 and 0.026 for the cool, mid and hot samples respectively. The differences between these values can be interpreted within the context of galaxy-galaxy interactions, where mergers between galaxies with relatively low pairwise velocities can occur (Coziol and Plauchu-Frayn 2007) with the potential result that blue star forming galaxies merge to form red passive galaxies. Therefore one might expect that the difference in f_B between the lowest and highest Σ_5 bins would be greatest for the cool sample (groups with lower velocity dispersion) and least for the hot sample (massive clusters with higher velocity dispersions) as is observed in Figure 4.12. This observation is also consistent with the results of Li et al. (2009) who found an increasing red fraction ($\sim 1 - f_B$) with increasing Σ_5 for all redshifts studied ($0.15 < z < 0.55$) within 3 r_{200}(~ 6 r_{500}).

In addition to the dependence of f_B with projected surface density, Figure 4.12 also displays a clear trend whereby a decreasing value of f_B is associated with increasing cluster X-ray temperature. This is essentially the result identified in Urquhart et al. (2010). However, it is now clear that the magnitude of the offset in f_B between clusters in each temperature sub-sample is typically twice that of the f_B difference between the highest and lowest surface density bins for all cluster temperature samples. The observed trend in f_B versus cluster temperature is consistent with the effects of ram pressure stripping, which is expected to be increasingly effective in higher mass (i.e. high X-ray temperature) clusters (e.g. Fujita 2001). This scenario is consitent with the findings of Bahcall (1977) who found a positive correlation between X-ray luminosity and the ratio of S0 to spiral galaxies in clusters and the aforementioned Urquhart et al. (2010) study. What is now clear from the magnitude of the f_B dependence on Σ_5 and T_X is that ram pressure stripping appears to be the stronger effect driving the cluster blue fraction – at least on the mass scale represented by the clusters in this study.

We apply a partial Spearman rank analysis to the above data to provide a non-parametric measure of the partial correlation of either projected surface density or cluster X-ray temperature to the computed blue fraction. The correlation coefficient for blue fraction versus X-ray temperature whilst controlling for projected surface

density was found to be $r(f_B, T|\Sigma_5) = -0.46$ and for blue fraction versus projected surface density whilst controlling for X-ray temperature was $r(f_B, \Sigma_5|T) = -0.18$. The negative values indicate that the blue fraction increases with both decreasing X-ray temperature and decreasing projected surface density as indicated in Figure 4.12.

The results of the linear fits shown in Figure 4.12 are, for the cool sample, a gradient of -0.043 and intercept of 0.71. For the mid, a gradient of -0.041 and intercept of 0.59 and for the hot, a gradient of -0.014 and intercept of 0.49. The offsets between the samples in a fixed bin of Σ_5 are of the order of 0.2 whereas the difference between the lowest and highest Σ_5 bins within a sample is approximately half this, suggesting that variations between rather than within the cluster samples may play a larger part.

The relative values of these correlation coefficients and differences in the linear fit values between samples, support the hypothesis that the global environment as described by the cluster X-ray temperature is playing a more important role in determining the value of cluster blue fraction than the local environment as described by the projected galaxy surface density.

In the above analysis, we neglected to include the effects of redshift evolution. To determine how much this influences our results, the partial Spearman rank analysis was repeated using a subset of clusters spanning $0.26 < z < 0.34$. The results of this were that the correlation coefficient for blue fraction versus temperature whilst controlling for Σ_5 was $r(f_B, T, \Sigma_5) = -0.61$ and whilst controlling temperature was $r(f_B, \Sigma_5, T) = -0.19$. Again, these coefficients support the idea that it is the global rather than the local environment which is dominating.

The cluster blue fraction responds to both the local and global environment measured within the sample of galaxy clusters. The effect of global environment traced by X-ray temperature (and which we associate with ram pressure stripping) appears to have a greater effect than that of local environment traced by the projected surface density of galaxies (which we assume is related to the rate of galaxy-galaxy interactions). We find, that at fixed Σ_5, f_B is a function of X-ray temperature, isolating the effect of local environment. In the remainder of this chapter we consider simple models describing these physical effects to investigate whether they provide a plausible description of the trends observed in the data.

4.5 Ram Pressure Modelling

First suggested by Gunn and Gott (1972), ram pressure stripping provides a plausible physical mechanism for the truncation of star formation in a galaxy falling into a cluster of galaxies. Gas within the infalling galaxy experiences a force resulting from collisional interactions with the ICM. Assuming that the galaxy is travellling face-on, the pressure exerted on the gas particles in the galaxy may be expressed as

$$P_{ram} = \rho_{ICM}\sigma_{gal}^2 \tag{4.3}$$

where ρ_{ICM} is the ICM density and σ_{gal} is the velocity of the galaxy relative to the ICM. In the case where the work done on the gas is larger than the binding energy per particle the gas will be unbound from the infalling galaxy, i.e. stripped.

Although originally expressed as a mechanism for the removal of the cold gas from an infalling galaxy, all gas particles experience the ram pressure force irrespective of their energy. Therefore, one could also view the removal of hot gas from an infalling galaxy (termed "strangulation" in the literaure e.g. Kawata and Mulchaey 2008) as a result of the same ram pressure interaction. The quantity $\rho_{ICM}(r)$ describes the three dimensional radial variation of the cluster ICM and may be represented employing a β profile as

$$\rho_{ICM}(r) = \rho_{ICM,0}\left[1 + \left(\frac{r}{r_c}\right)^2\right]^{\frac{-3\beta}{2}}, \tag{4.4}$$

where r_c is the core radius of the cluster, $\rho_{ICM,0}$ is the central ICM density and β is the ratio of the specific energies of dark matter to gas. The β-profile was introduced by Cavaliere and Fusco-Femiano (1976) to represent the spatial distribution of the ICM, using the distribution expected for an isothermal plasma in hydrostatic equilibrium having a virialised mass distribution. The values of β and r_c used for the XMM and CCCP clusters in this work are taken from respectively Alshino et al. (2010) and Fukazawa et al. (2004) who fitted PSF-convolved projected β profiles to the two dimensional X-ray images of each cluster.

The central ICM density ($\rho_{ICM,0}$) was calculated employing

$$\rho_{ICM,0} = \frac{1}{4\pi}\left[\frac{f_{gas}M_{500}}{\int_0^{r_{500}}\left[1 + \left(\frac{r}{r_c}\right)^2\right]^{\frac{-3\beta}{2}} r^2 dr}\right] \tag{4.5}$$

where f_{gas} represents the fraction of baryons contained within M_{500}. This was calculated on a cluster by cluster basis using the relation from Pratt et al. (2009). In this work, the authors examined the X-ray luminosity scaling relations of 31 nearby galaxy clusters from the Representative XMM-Newton Cluster Structure Survey (*REXCESS*). Using the total mass from the published hydrostatic estimates of a combined sample of cluster in the $10^{13} - 10^{15} M_{\odot}$ range, they determine that the gas fraction depends on the total mass through:

$$h(z)^{3/2} ln f_{gas,500} = (-2.37 \pm 0.03) + (0.21 \pm 0.03) \times ln(M/2 \times 10^{14} M_{\odot}) \tag{4.6}$$

For the cool sample, M_{500} and velocity dispersions are taken from Pacaud et al. 2007. For the mid and hot samples, the values of M_{500} were calculated using (e.g. Ettori 2000):

$$M_{500} = (1.11 \times 10^{14}) \beta r_c T \left(\frac{x_{500}^3}{1 + x_{500}^2} \right) \tag{4.7}$$

with $x_{500} = r_{500}/r_c$ yielding M_{500} in units of $M_{\odot}$. The velocities of the CCCP clusters were then calculated using

$$\sigma = \sqrt{\frac{kT}{\mu m_p}} \tag{4.8}$$

and the subsequent values of the ram pressure were converted to ergcm^{-3}.

The results of this modelling can be seen in Figure 4.13 where the radial variation of the ram-pressure stripping strength is shown in the left panel for each of the cool ($\bar{T}_X$=1.73keV), mid ($\bar{T}_X$=6.56keV) and hot ($\bar{T}_X$=9.81keV) samples along with the radial variation of ρ_{ICM} in the right panel. The clusters within each sample were averaged to highlight the trends in each temperature subset. As expected (e.g. Fujita 2001), the magnitude of the effect of ram pressure stripping appears to be higher in the mid and hot clusters (i.e. Clusters of higher mass). This difference in the magnitude of the ram pressure between clusters and groups becomes more pronounced as we travel out from the cluster (group) centre to distances of 10 r_{500}. This would suggest that, even at such large distances from the cluster (group) centres, there are differences in the environmental effects acting on the constituent galaxies. Such environmental effects have been observed by a number of different groups whereby a decrease in the

star formation rate has been found even beyond the cluster virial radius (e.g. Gómez et al. 2003, Bahé et al. 2013).

To further investigate this, we then define a quantity which will be referred to as the ram pressure work (RPW). This is obtained by integrating the ram pressure (Equation4.3) from 10 r_{500} to the radius of each galaxy for all galaxies lying within 4 r_{500} per cluster.

The distributions of the RPW, for the 3 temperature samples were created to allow a binning system based, once again, on the interquartile points, as shown in Figure 4.14.. Also included at this point was an analysis of the low redshift MENeaCS sample, performed in the same way. The most intriguing result from Figure 4.15 is that, at fixed values of RPW, f_B is still a function of T_X. This suggests that there is something missing in our explanation (e.g. Inaccuracy in the RPW calcuation). Modulo this potential missing information, the value of f_B does not depend strongly on the current state of the X-ray gas. There is a dependence of f_B on RPW at fixed T, but we are unable to explain the offset of our cool from our mid and hot samples using the RPW quantity alone.

4.6 Merging Model

Another proposed mechanism which could be occurring in galaxy clusters alongside ram pressure stripping is that of galaxy-galaxy interactions. These may be of particular importance in the "pre-processing" of galaxy clusters since interactions are believed to be more efficient in groups as opposed to massive galaxy clusters due to the lower internal velocity dispersions of the galaxies in group systems. A "local" rather than a "global" environmental effect.

In order to investigate the magnitude of these interactions, a simple merger model has been constructed, based upon Σ_5 as follows:

$$\Gamma = \frac{\Sigma_5}{(\sqrt{(}3\sigma^2)^3} \propto \frac{\Sigma_5}{T^{3/2}} \tag{4.9}$$

where Σ_5 remains the surface density of galaxies based on the distance to the 5^{th} nearest neighbour and σ is the velocity dispersion of the galaxy cluster. The problem with this measure of the merging rate, is that, as can be seen in Equation 4.9, it is no longer simply a measure of the local environment due to the dependence of the velocity dispersion upon the cluster X-ray temperature.

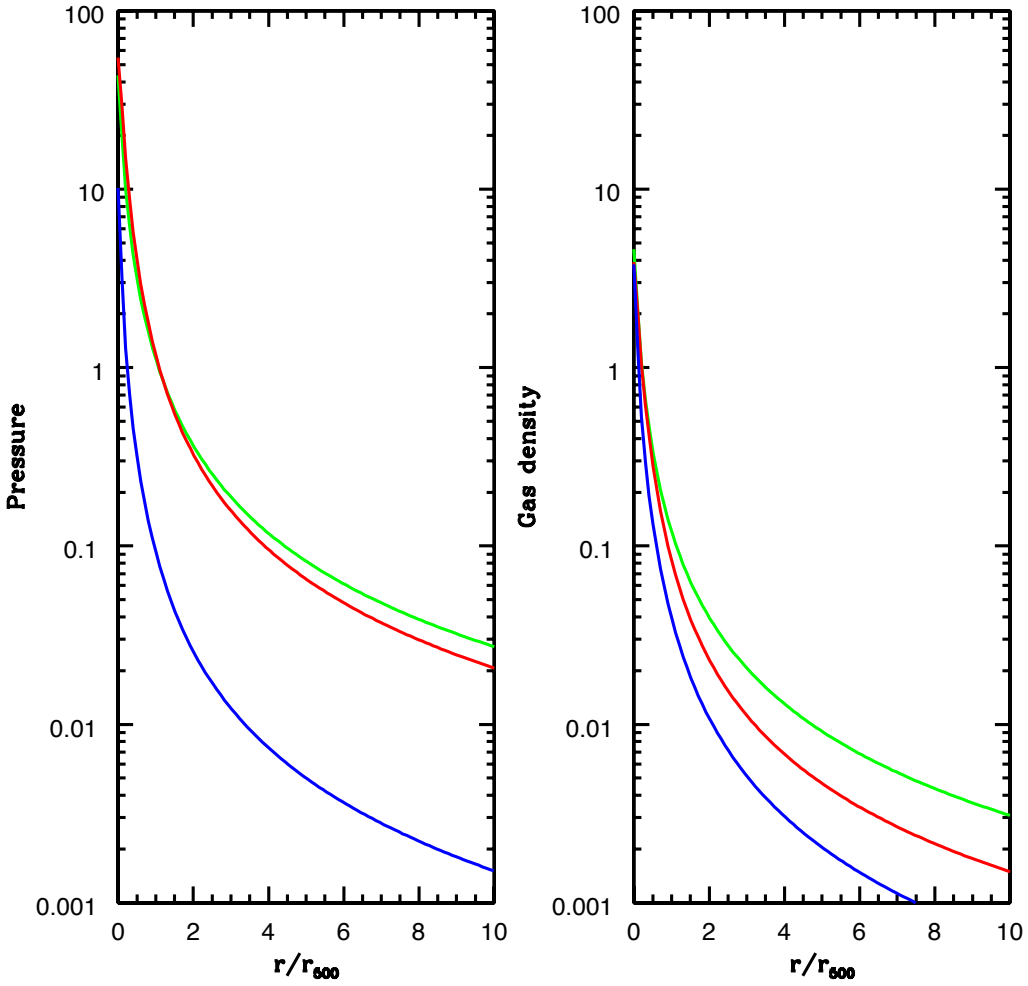

Figure 4.13: Radial variation of ram pressure stripping and radial variation of ρ_{ICM} for the "cool" (blue line), "mid" (green line) and "hot" (red line) samples.

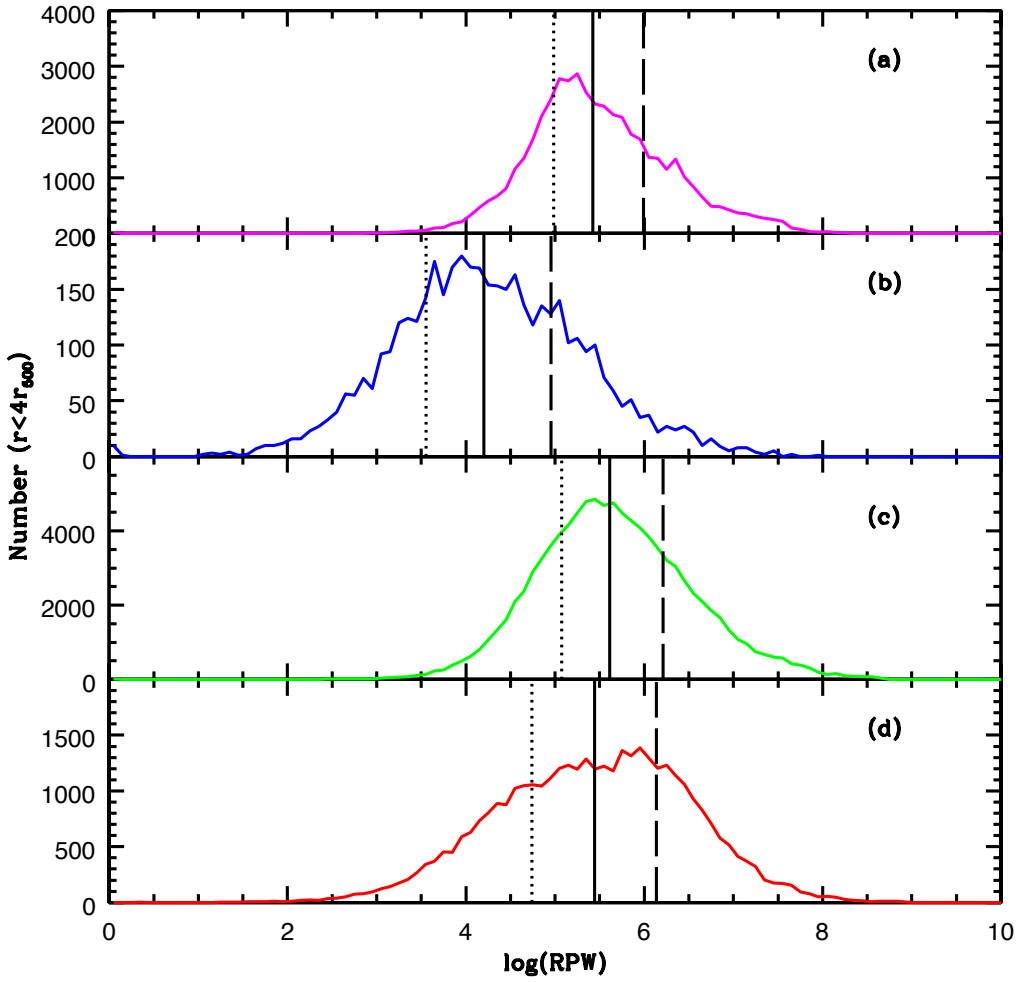

Figure 4.14: Distributions of the ram-pressure work for the MENeaCS (a), cool (b), mid (c) and hot (d) samples. The vertical lines mark the bins used the subsequent analysis.

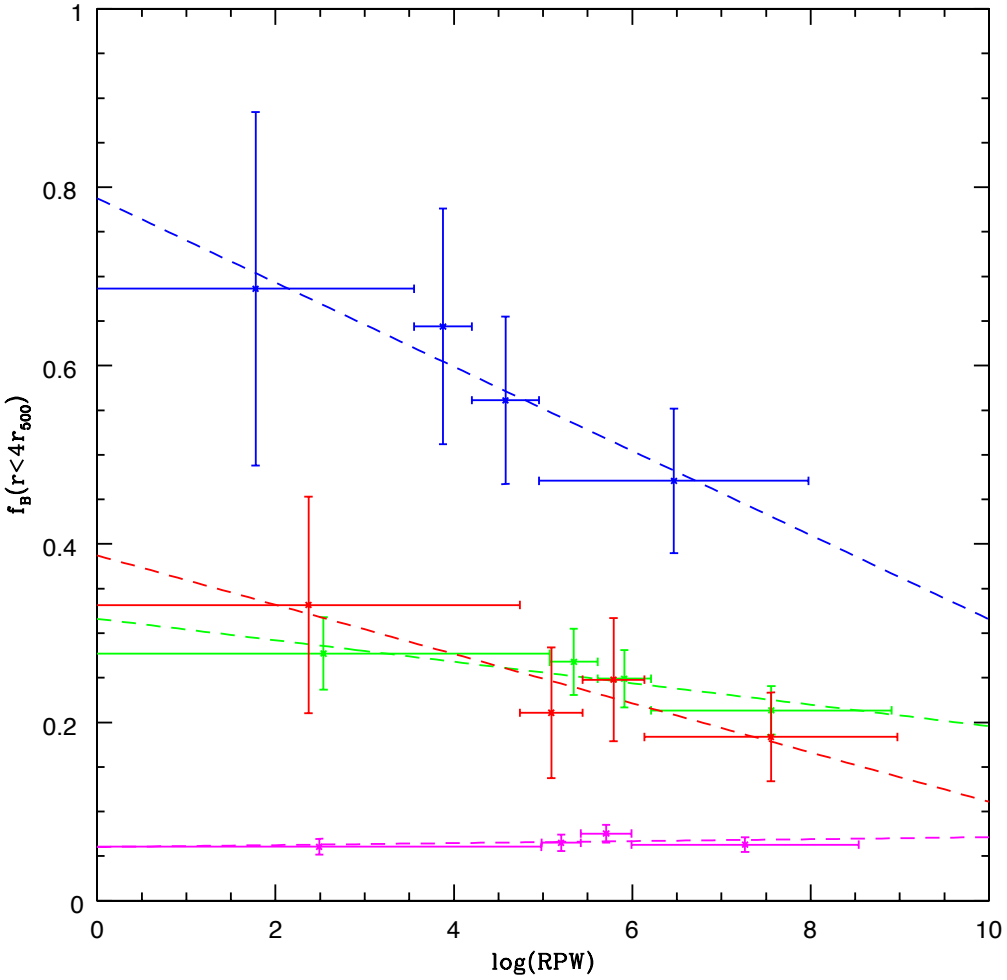

Figure 4.15: Blue fraction as a function of ram pressure work for the cool (blue), mid (green), hot (red) and low redshift MENeaCS (magenta) samples. See text for details

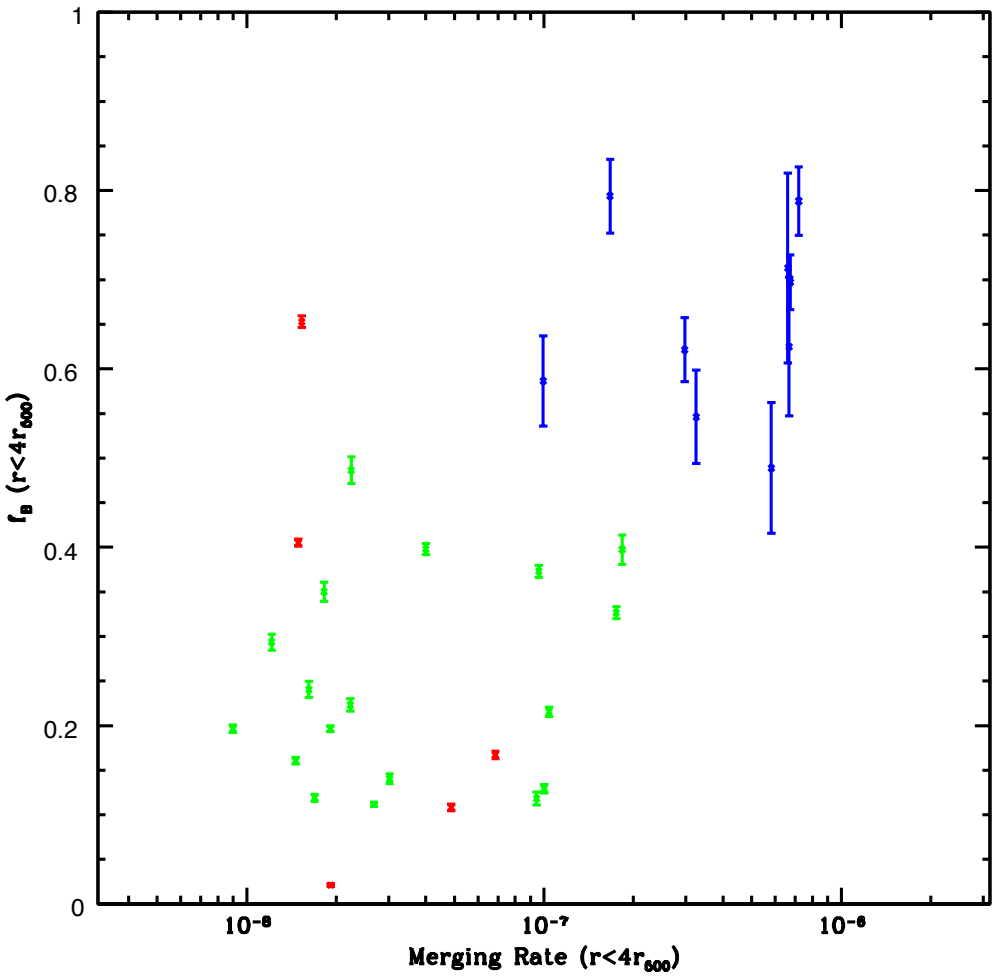

Figure 4.16: Variation of blue fraction within $4r_{500}$ with merging rate as defined in the text.

The results of this model can be seen in Figure 4.16. There is a general trend of a higher merging rate in the lower temperature clusters, consistent with lower velocity dispersions of the member galaxies.

However, the difficulty remains as to how to disentangle the dominance of ram pressure stripping versus galaxy-galaxy interactions. Therefore, as an alternative approach, and to create a more physically motivated division, instead of dividing the sample into cool, mid and hot, it was now decided to split the sample into low, mid and high ram pressure work before binning in terms of Γ, the merging rate.

This was done following an analogous method for that used to create Figure 4.12. The distribution of the ram pressure work for the cool, mid and hot samples was created as shown in Figure 4.17. Based upon this histogram, the new regimes of low, mid and high ram pressure work were defined as shown by the vertical lines in the Figure 4.14. Galaxy clusters were then assigned to the appropriate ram pressure work division, no longer being divided into cool, mid and hot but now into low, mid and high rpw samples. With these new definitions, the binning system for the merging rate was created based upon the distributions of Γ in Figure 4.18.

The combined results of this are presented in Figure 4.19 along with linear least squares fits to the data. Again, the results of this simple modelling reinforce the idea that global environmental effects are dominating over local given the larger offset between the galaxies experiencing "low" amounts of rpw and those experiencing higher amounts than within a sample itself.

As in Figure 4.12, the difference in f_B between samples is greater than that within an individual sample, especially between the sample defined as having low ram pressure work and those of mid and high ram pressure work. This further reinforces our earlier result that it is the global cluster environment (here taken to be the influence of ram pressure stripping) that is dominating galaxy evolution over the local (interactions) environment.

4.7 Modelling blue fractions

Following the work of McGee et al. (2009) where the authors used the semi-analytic model galaxy catalogue from Font et al. (2008). The model of Font et al. (2008) is based on merger trees derived from the dark matter Millennium Simulation (Springel et al. 2005) using a ΛCDM cosmologial box of sides $500h^{-1}$Mpc. The merger trees are complete down to haloes which host $\sim 10^8 h^{-1}\mathrm{M}_\odot$ galaxies, however McGee et al.

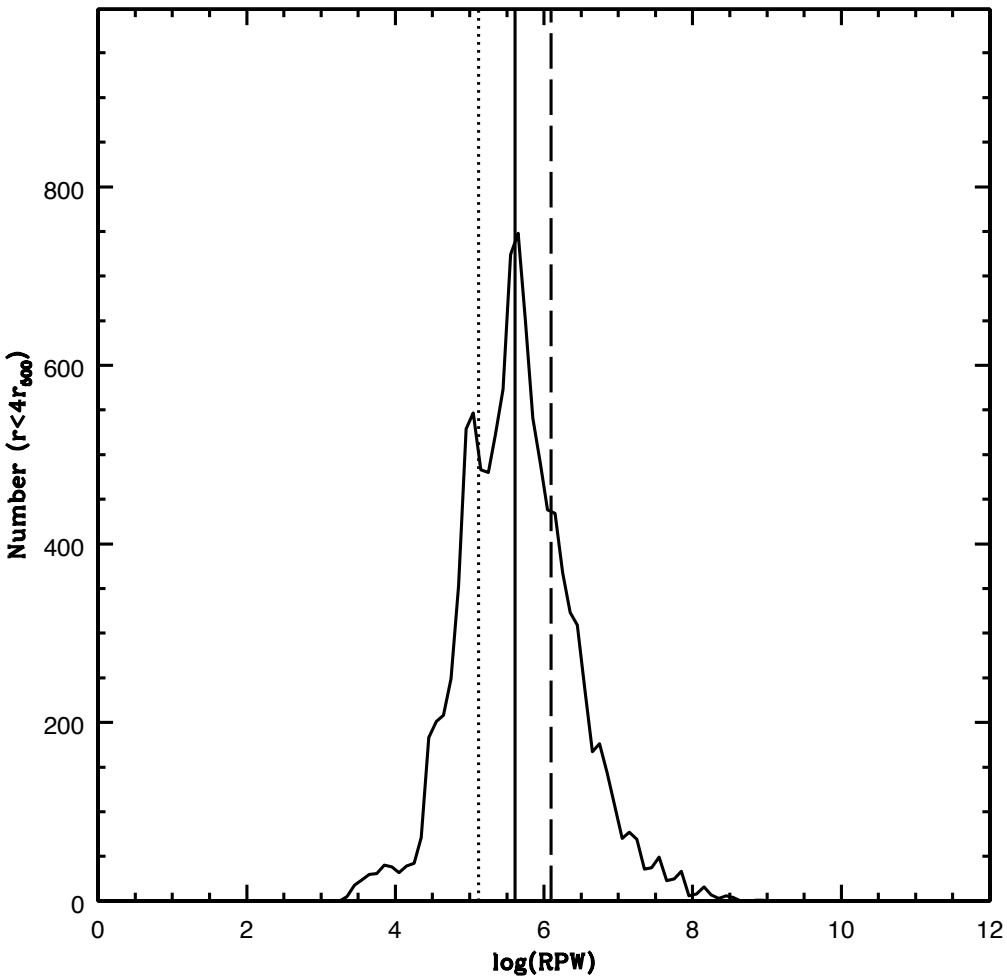

Figure 4.17: Number distributions within $4r_{500}$ for all three samples; cool, mid and hot. The dotted, solid and dashed lines mark the location of the interquartile points.

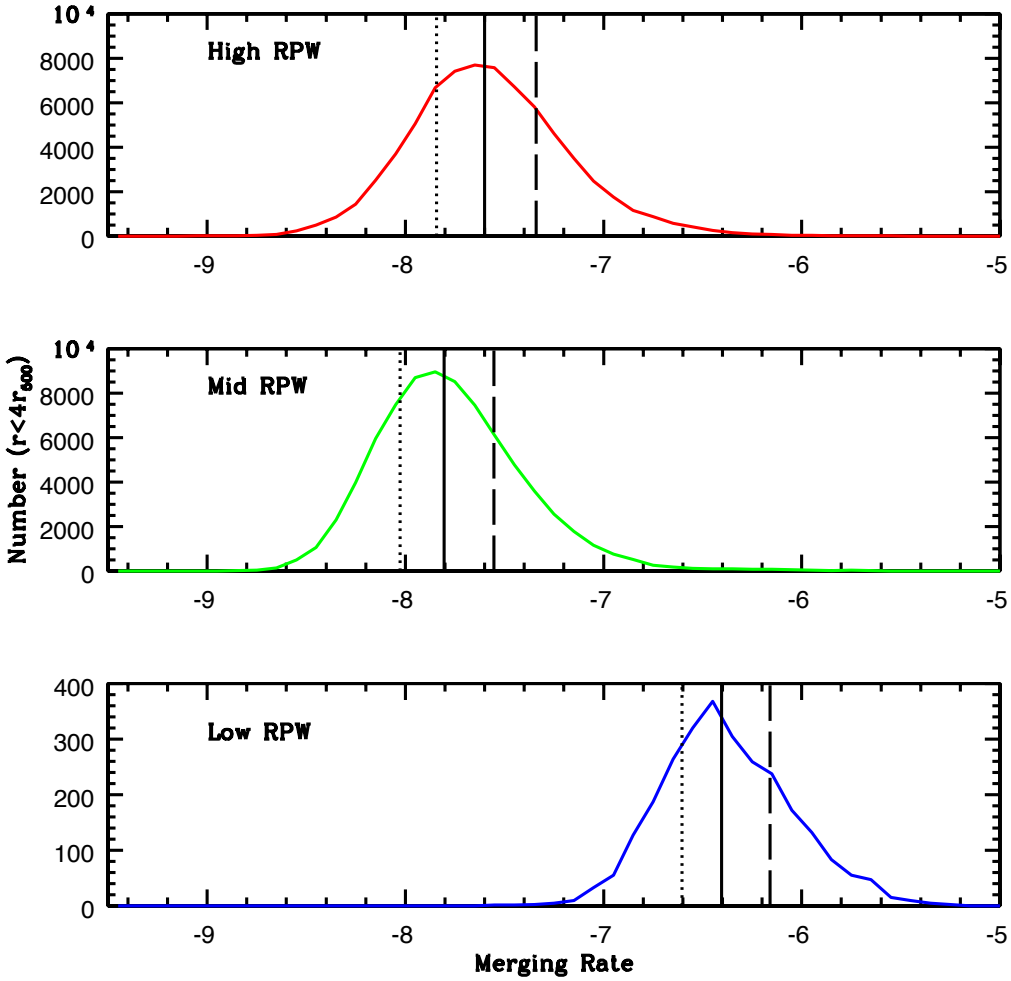

Figure 4.18: Number distributions within $4r_{500}$ for the three new samples, low (blue), mid (green) and high (red) RPW. The dotted, solid and dashed lines mark the location of the interquartile points.

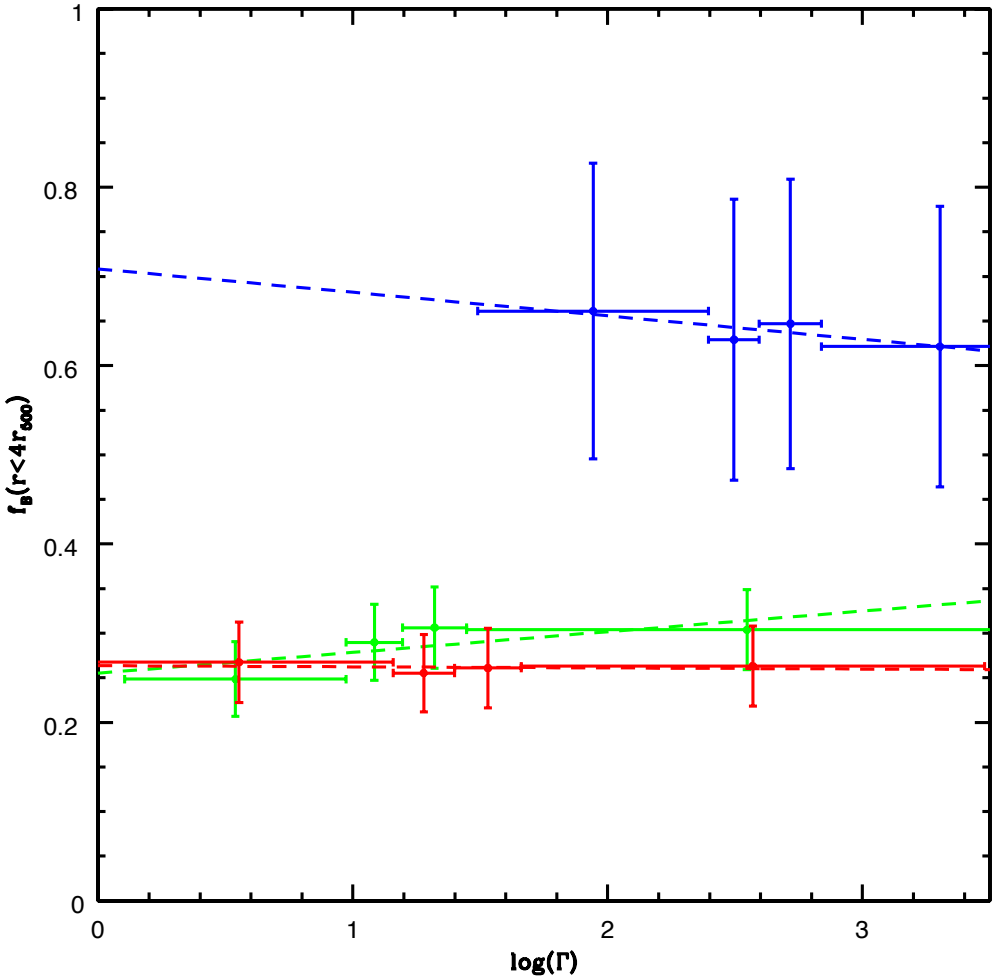

Figure 4.19: Blue fractions binned in Γ (where Γ has been rescaled for plotting purposes). Blue, green and red represent low, mid and high ram pressure work ranges with the dashed lines showing the linear least squares lines of best fit.

(2009) select only galaxies which are observationally accessible and as such specify a fixed stellar mass cut of M> $10^9 h^{-1}\mathrm{M}_\odot$ which is considerably higher than the completeness limit. Their analysis is performed on groups and clusters drawn from the Font et al. (2008) model with masses greater than M=$10^{12.9} h^{-1}\mathrm{M}_\odot$ at four redshift epochs (z=0,0.5,1,1.5).

To determine that the dominant environmental processes begin to occur in halos of 10^{12}-$10^{13} h^{-1}\mathrm{M}_\odot$ and act over timescales of > 2 Gyr, we create a simple blue fraction model and apply these results. The authors investigate the effect of varying T_{trunc} (the length of time it takes for a galaxy to experience an environmental effect) and M_{trunc} (a characteristic mass threshold above which environmental effects occur) on their results. They fix M_{trunc}, and vary T_{trunc} from 1-4 Gyr. They observe a Butcher-Oemler effect (clusters at higher redshift having fewer galaxies affected by environmental processes) for all values of T_{trunc}, however the size of the effect varies dramatically depending on the choice of timescale. When using only 1 Gyr, there is little evolution in the fraction of environmentally affected galaxies ($\sim$85% at z=0.5 to $\sim$95% today) whereas for T_{trunc}=4 Gyr there is a much stronger evolution (50% to 80% over z=0.5 to today). The authors compare this to the observed red fraction of cluster galaxies which show an evolution of $\sim$25% over a similar redshift range (Ellingson et al. 2001) and therefore argue that a relatively long timescale (> 2 Gyr) for the appearance of environmental effects is required to match the quick evolution and also that a similar timescale is needed to explain the radial gradient of passive galaxies in clusters (e.g. Balogh et al. 2000; Ellingson et al. 2001). The authors also state that there are observations of systems with masses of $10^{13} h^{-1}\mathrm{M}_\odot$ which have suffered from significant environmental affects (Wilman et al. 2005; Weinmann et al. 2006) and so we investigate our blue fractions using this mass limit and truncation timescales between 2 and 4 Gyr.

Using data from a private correspondence with Sean McGee, we modelled the evolutionary tracks for different mass haloes. Examples of some of the evolutionary tracks are shown in Figure 4.20. The upper dark shaded region marks the range of masses for the CCCP clusters as observed today and the lower, lighter shaded region marks the range of masses for the XMM clusters as observed today. Note that the halo masses are measured within r_{200}, converting from M_{500} (see Section 4.5) to M_{200}. We then apply a "truncation mass" limit of $10^{13} h^{-1}\mathrm{M}_\odot$ (the halo mass limit at which environmental effects begin), this is marked as the horizontal dot-dashed line in Figure 4.20.

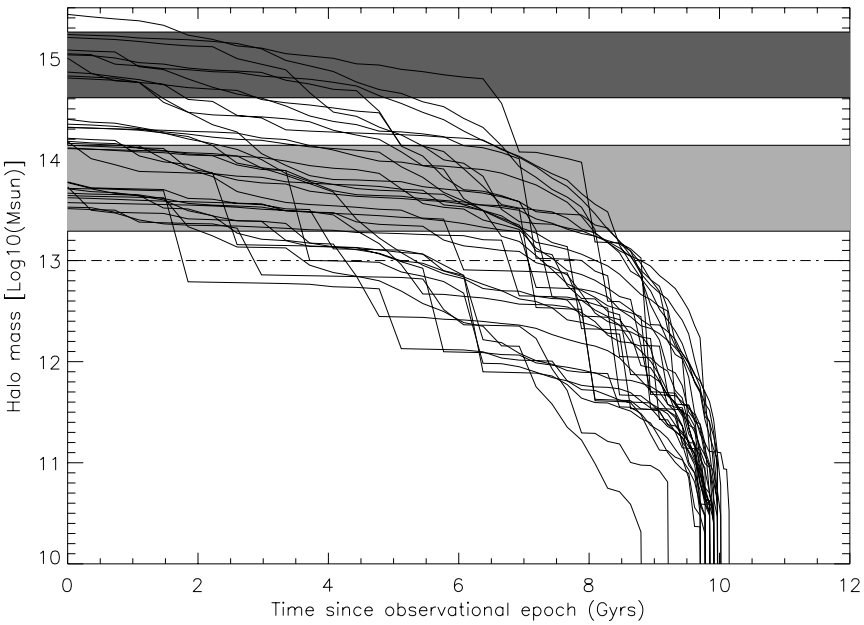

Figure 4.20: Halo evolution tracks from the models of Sean McGee. The upper, dark region marks the mass range of the CCCP clusters as observed today and the lower, lighter region marks the mass range of the XMM clusters as observed today. The dot-dashed line marks the truncation mass limit of $10^{13}h^{-1}\mathrm{M}_{\odot}$.

Our simple model for the blue fraction is then defined by

$$f_B \propto exp\left(-\frac{t}{\tau}\right) \tag{4.10}$$

where t is the time that the halo mass has exceeded the truncation mass and τ is the truncation timescale, taken in this case to be 2, 3 and 4 Gyr. The results of this modelling are shown in Figure 4.21. Our choice of model is based on the fact that, as we have shown in Chapters 3 & 4, the blue fraction will decrease with increasing environmental processing (regardless of the scale on which this is acting), and therefore f_B will decrease with increasing amount of time spent in a halo of mass greater than the truncation mass and incorporating an exponential decrease allows for the fact that there is no reason to expect that changes in f_B are constant in nature whilst still maintaining the "simple" nature of the model.

For clusters of masses similar to those of the mid and hot samples, the length of time that the halo mass has exceeded the truncation mass limit is greater than ~ 7.5 Gyr, considerably longer than the truncation timescale of 4 Gyr. For the cool sample, the time spent in a halo mass greater than the truncation mass spans a wide range from ~ 2 Gyr to ~ 7 Gyr. Figure 4.21 suggests then that for the mid and hot sample, f_B would take on a value on the order of 0.15 and less and for the cool sample, f_B would span the range of between approximately 0.18 to 0.55.

Since all of the mid and hot clusters have been, according to this model, in a halo of sufficient mass for a sufficient period of time, to experience environmental effects, we would expect lower values of f_B as star-formation has been quenched. For the cool sample, the observed scatter in the values of f_B is due to the scatter in their merger histories according to the McGee model. This variation is likely due in part to the varying density associated with peaks of the same total mass along with the effects of cosmic variance.

Our McGee model is able to explain $f_B(T|\Sigma_5, z)$, however it is harder to explain $f_B(\Sigma_5|T, z)$. Possible explanations for this latter trend include that Σ_5, as previously stated, is related to merging events. Alternatively, the Σ_5 peaks may be tracing the dense sub-halos within the parent halo. If these denser than average regions collapsed earlier than our McGee model predicts, then f_B should be lower.

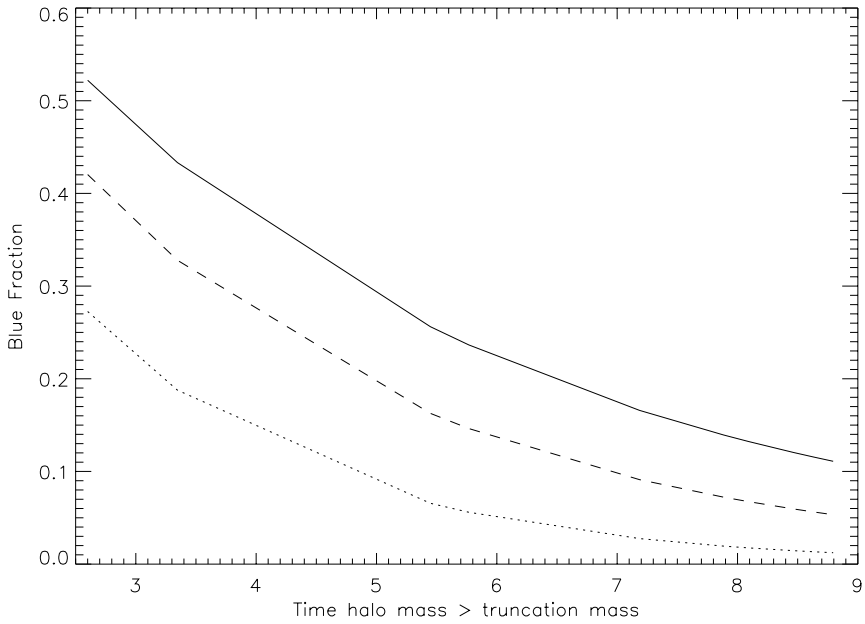

Figure 4.21: Modelled blue fractions as a function of how long the halo mass has exceeded the truncation mass. The dotted, dashed and solid lines are for truncation timescales of 2, 3, and 4 Gyr respectively.

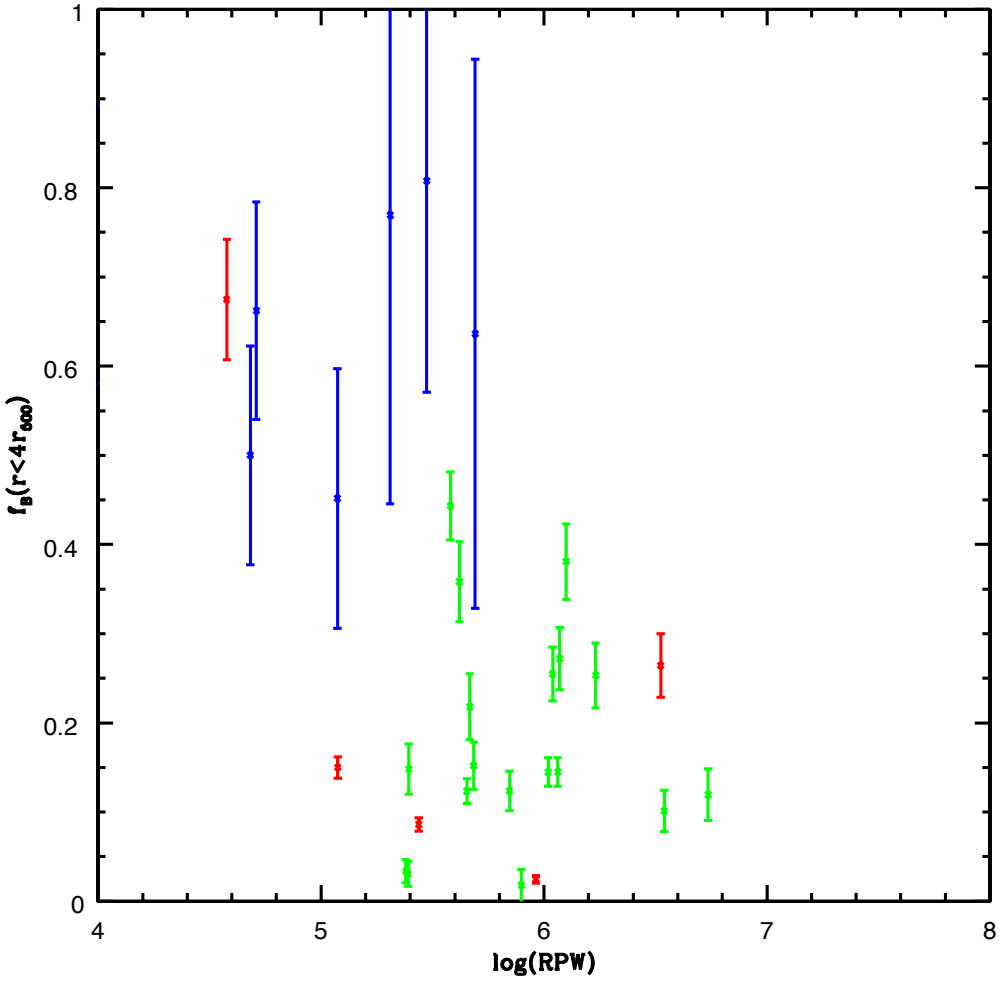

Figure 4.22: Variation of blue fraction within $4r_{500}$ with RPW.

4.8 Discussion and Conclusions

With a large sample of X-ray selected clusters having uniform photometry, it has been possible to study the effects of cluster environment on the fraction of star forming galaxies observed since a wide range in temperatures (and therefore masses) have been covered. As observed in Figure 4.12, there are trends in the blue fractions which are consistent with both "global" environmental processes and "local" environmental processes acting on the cluster members. Namely, a reduction in f_B with both increasing temperature and Σ_5.

One mechanism invoked to describe a global interaction is that of ram-pressure stripping which would be expected to be most efficient in the most massive cluster environments. Our results are broadly consistent with this theory, f_B does indeed reduce as one moves from the cool through the mid to the hot samples. Looking at galaxies of similar Σ_5 in Figure 4.12 (i.e. galaxies in the same local density bin), it can clearly be seen that there is a larger reduction in the star formation for the hot over the mid and for the mid over the cool samples.

However, at fixed values of the RPW (Figure 4.22), the blue fractions for each sample span a range of values. There are a number of possibilities for this. Our RPW calculation does not correctly represent the true extent of the RPW or it is based on a simple orbit argument which is not likely to be truly representative (Oman et al. 2013). What is clear is that the cluster blue fraction is not well described by our estimate of the current state of the X-ray gas, i.e. at the epoch of observation.

However, while the trend of decreasing f_b with increasing T_X appears to be dominant, one cannot say that this is the only parameter of interest since there is also a trend of decreasing f_B with increasing local density. If this process is more efficient in lower mass systems (groups rather than clusters), then one would expect a greater difference in the blue fraction between the lowest and highest density bins to occur in the lowest mass sample (our cool sample). This is observed, again, in Figure 4.12.

Trying to disentangle and quantify the magnitudes of these two different interactions is a difficult task. It appears that the effect of the global cluster environment is stronger than that of the local galaxy density. This is consistent with Li et al. (2009) who suggest that Σ_5 is not a fundamental parameter in galaxy evolution. Since local galaxy density is likely to be a tracer of merging events, we use the relation of Patton et al. (2002) who determine the galaxy merger rate using a sample of 4184 galaxies

having $0.12 \leq z \leq 0.55$ as being:

$$\Gamma = (1+z)^{2.3 \pm 0.7} \tag{4.11}$$

We then calculate that $\sim 2.27\%^{+1.0}_{-0.7}$ of cluster galaxies will have merged over the last 4 Gyr. This is clearly a small fraction of the overall cluster and is therefore unlikely to be the dominant environmental effect.

The McGee model provides a plausible model for the evolution in f_B versus temperature, explaining the observed trends in terms of the amount of time that has passed since the parent halo crossed a given mass threshold. This is shown in Figure 4.23 where overplotted on the observational results are boxes marking the expected range of values for f_B from our model clusters at the appropriate temperature and redshifts. The black points in each box mark the average values of f_B in that range (at the average T_X).

Although it remains challenging to conclusively say what the dominant physical processes acting are (e.g. ram-pressure stripping or galaxy-galaxy interactions) we can conclude from our McGee model that ram-pressure stripping is a plausible mechanism acting at the $10^{13} M_\odot$ scale along with some Σ_5 dependence due to the effects of merging or collapse bias. Future research into the disentangling of these effects may require the introduction of an additional technique, for example, multivariate statistics to simultaneously investigate more than one outcome variable.

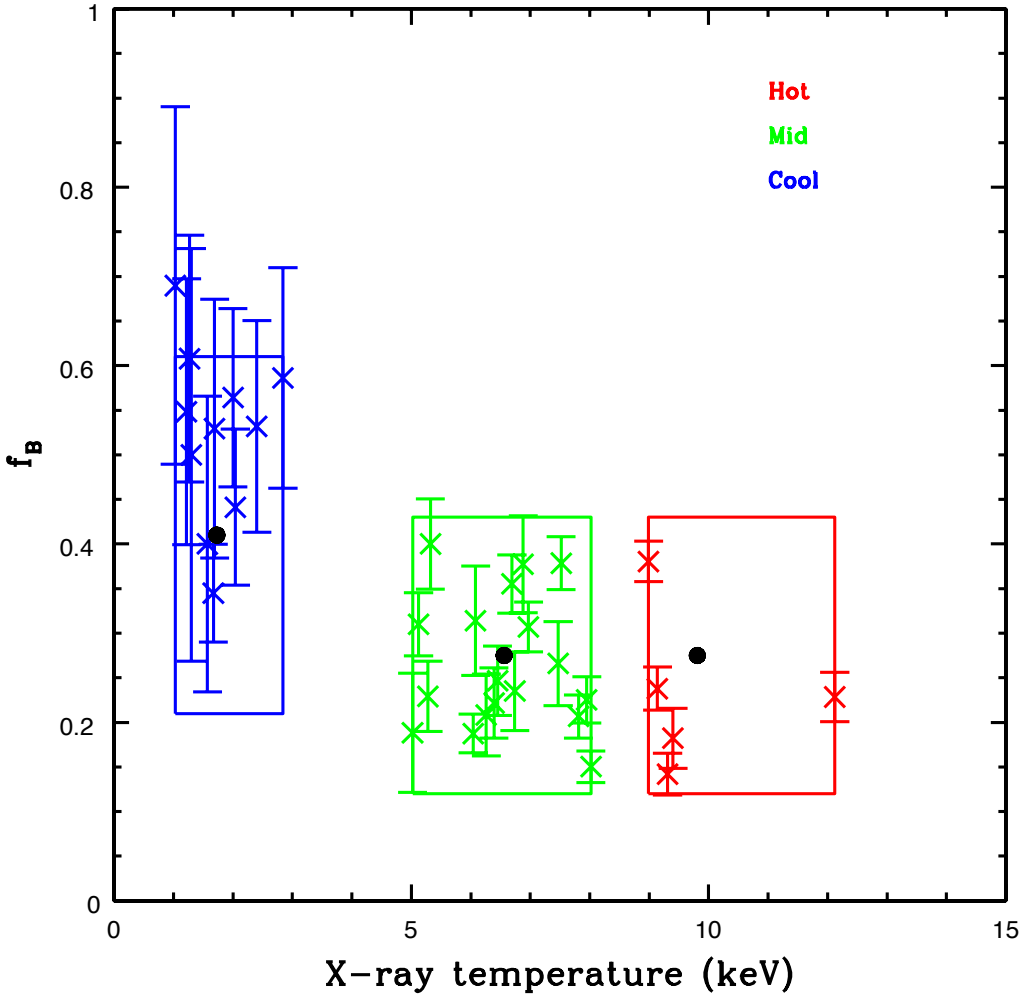

Figure 4.23: Variation of blue fraction with cluster X-Ray temperature for the cool, mid and hot samples (blue, green and red respectively) with the range of f_B values from our model marked as boxes.

Chapter 5

Galaxy processing along the red-sequence: Luminosity distributions and the dwarf-to-giant ratio

5.1 Introduction

Throughout this thesis, and like many past studies (e.g. Balogh et al. 2004) we have shown that the population of galaxies in clusters follow a bimodal distribution, whereby they can be divided into those galaxies which are red (more gas poor, lower specific star formation rates, preferentially found in denser environments) and those which are blue (actively forming stars). However, we have also shown that it is a difficult problem to disentangle the underlying physical processes governing these observations.

It is well established that this population of red galaxies form a tight locus in colour-magnitude space with very little scatter known as the "red-sequence" (Visvanathan and Sandage 1977) which has been observed out to $z \sim 1$ (Bell et al. 2004). This implies either an early formation epoch or a synchronisation of formation times (Bower et al. 1992). Understanding the origin and build up of this red sequence is an important and active area of research still with many unanswered questions.

One measurement that is often used in the study of these red-sequence galaxies is that of the galaxy luminosity function (LF). This is simply a measure of the number

of galaxies per unit volume having luminosity between L and $L + dL$. Despite the apparently basic nature of this measurement, it can yield crucial information. For example, the evolution of the red-sequence directly reflects the number of major galaxy mergers, so can be used to constrain formation models. Bell et al. (2004) found a mild evolution in luminosity density over the redshift range $0 < z \leq 1.1$ in their study of $\sim$ 25,000 galaxies, and over this time interval, ancient stellar populations would have faded by a factor of 2-3, an increase in stellar mass on the red-sequence of a minimum of a factor of 2. This is consistent with the predicted evolution from hierarchical structure formation through galaxy mergers in the ΛCMD model.

Other interesting features of the LF include an observed break at bright magnitudes. Following some simple scaling arguments, this seems to arise from a long cooling time of the gas in large haloes (e.g. Silk 1977, White and Rees 1978). Previous semi-analytic galaxy formation models using a cold dark matter cosmology supported this theory (e.g. Somerville and Primack 1999), however these were developed using a value of the mean baryon density in the universe of $\simeq 0.02$ which has since been deemed too low (e.g. Cuoco et al. 2004). Using a value of the mean baryon density almost twice this means that the gas cooling hypothesis is no longer sufficient to explain the observed break in the luminosity function. By adding in feedback due to active galactic nuclei (AGN), Bower et al. (2006) showed that this naturally creates a break in the local galaxy luminosity function at bright magnitudes, demonstrating that the hierarchical CDM model does indeed provide a good match to observations.

In this model, structures are built from the "bottom up" with smaller structures merging to form galaxies and clusters. However, evidence has been mounting for the evolution of star-formation in a "top down" manner, with the most massive galaxies actively forming stars in the past and moving to less massive galaxies with time. This is seemingly contradictory to the hierarchical formation model which would suggest that more massive early-type galaxies should be younger than less massive galaxies (e.g. Baugh et al. 1996). To overcome these apparent opposite arguments, it has been proposed that the most massive galaxies assembled mass later than lower mass galaxies but that the stellar mass has built through gas-poor mergers which cause no increase in star-formation, accounting for the earlier formation times of the stellar populations in these massive galaxies (Gilbank et al. 2008). Again however, the importance of mergers in the assembly and evolution of galaxies remains unknown.

Studying the faint-end of luminosity functions can prove to be particularly challenging since low-mass galaxies are difficult to observe, but since their evolution can

be different from that of more massive galaxies, being more susceptible to environmental effects including tidal disruptions and being better tracers of cluster structure than bright galaxies (since bright galaxies tend to subcluster around the very brightest galaxies; Biviano et al. 1996), they are an important consideration. Alongside this, the detected numbers of faint galaxies decreases with redshift (e.g. De Lucia et al. 2007, Stott et al. 2007) and conclusions can be dependent on both completeness corrections and depth issues. To accurately determine galaxy LFs requires the use of large, complete datasets with accurate photometry and redshifts. Liu et al. (2008) were able to study the faint-end of the rest frame V-band luminosity function for 80820, $z < 0.5$ galaxies using the Cosmic Evolution Survey (COSMOS) field. Using this data, the authors were able to ctreate LFs as a function of galaxy spectral type. The results were that, for all galaxy types, the slope of the faint end was shallower with increasing redshift, possibly due to a decrease in the number of faint, low mass galaxies at higher z. However, Andreon (2008) observed no differential evolution between bright and faint red galaxies out to a redshift of 1.3 in a sample of 28 clusters.

Evidence has also been found for a dependence of the red-sequence luminosity function upon cluster mass locally (Hansen et al. 2005; Hilton et al. 2005) as well as at intermediate redshifts (Koyama et al. 2007; Gilbank et al. 2008). Whereas others (e.g. Bildfell et al. 2012) have observed no such dependence on cluster mass. Clearly, there remains significant disagreement between studies which also extends to models of galaxy formation, for example Wolf et al. (2005) and Baldry et al. (2006) produce an excess of red galaxies in clusters and groups compared to observations, confirming the difficulties in fully understanding the effects of environment on star formation.

An alternative, but related way to investigate how different galaxy populations evolve in cluster and group environments is to calculate the dwarf-to-giant ratio (DGR) or the reciprocal giant-to-dwarf ratio (GDR). This non-parametric measurement is also a robust calculation of the fraction of faint-to-bright (or bright-to-faint) galaxies and has the advantage over the LF of not requiring a functional fit to the data yet still being a probe of galaxy evolution. The standard model of galaxy formation predicts that giants are more likely to form in high mass density regions than dwarfs (White et al. 1987), and environmental effects will likely take over as a galaxy evolves influencing the DGR measurement (Zabludoff and Mulchaey 2000). These include, for example, galaxy-galaxy mergers which are likely to be more dominant in low mass groups than rich clusters (see Chapter 4, Figure 4.16) and tidal fields (Zabludoff and Mulchaey 1998).

Lu et al. (2009) created r'-band red-sequence luminosity functions for 127 rich clusters in the redshift range $0.17 \leq z \leq 0.36$ along with calculations of the DGR. Their results showed that between z=0.2-0.4, there is no strong evolution in the faint-end of the luminosity function (or equivalently in the red-sequence DGR), but that from $z \sim 0.2$ to 0, the relative number of red-sequence dwarf galaxies has increased by a factor of 3, suggesting that it is over the last 2.5 Gyr that there has been a significant build up of the faint-end of galaxy cluster red-sequences. However, Bildfell et al. (2012), in their study of 97 galaxy clusters across $0.05 \leq z \leq 0.55$ find that their observations support an evolving GDR. For $z < 0.2$, the GDR evolution the authors observe is consistent with dry merging of massive giant galaxies (a roughly constant number of dwarfs concurrent with a decrease in the number of giants).

In this project, red-sequence LFs are created for the intermediate redshift clusters studied in previous chapters, spanning a relatively narrow redshift range ($0.15 < z < 0.41$) as well as comparing to samples from literature. The emphasis will be on comparing the red sequence LFs (and subsequent DGR/GDR calculations) for clusters (and groups) of different X-ray temperatures (spanning a range of $1 <$ kT(keV) < 12) to study the influence of global environment on the red sequence.

5.2 Dataset

The cluster sample used in this work is described in detail in Chapter 2 and is summarised in this section. As in previous chapters, the X-ray selected clusters are taken from two complementary samples and are defined and classified based on their X-ray temperatures. The first of these being drawn from the X-ray Multi-Mirror (XMM) Large Scale Structure (LSS) survey forming our "cool" cluster sample. Our "mid" and "hot" samples are taken from the Horner (2001) sample and form part of the Canadian Cluster Comparison Project (CCCP; Bildfell et al. 2008). The properties of the clusters are summarised in Table 5.1.

Table 5.1: Properties of the 3 cluster samples.

Sample	T range (keV)	z range	$\bar{T}$(keV)	$\bar{z}$
Cool	$1.03 < T < 2.40$	$0.25 < z < 0.35$	1.73	0.3
Mid	$5.02 < T < 8.02$	$0.15 < z < 0.30$	6.56	0.17
Hot	$8.99 < T < 12.12$	$0.16 < z < 0.41$	9.81	0.24

5.3 Luminosity Distributions

The initial analysis in this chapter involves the construction of luminosity distributions for the 3 stacked samples before determining the best fitting parameters to look for any environmental trends. Following this, the DGR (and GDR) are determined and investigated as a function of a number of cluster properties, with a similar anaylsis as applied in Chapters 3 & 4. For example, we look at the DGR as a function of both redshift and X-ray temperature as well as Σ_5 for the subsamples in an analagous fashion to Figure 4.12.

5.3.1 Background Subtraction

The first step in the construction of red-sequence luminosity functions (RSLF) was to create stacked colour-magnitude diagrams for the cool, mid and hot samples. The details of this are as given in Chapter 3.4 and are summarised as follows.

In order to calculate red-sequence luminosity functions (and the subsequent calculation of the dwarf-to-giant ratios), the location of the red-sequence must be determined as a reference, requiring the removal of foreground and background galaxy contamination. As in the previous work in this thesis, this was done following the statistical background subtraction method of Pimbblet et al. (2002). Field galaxies (all galaxies lying at a radii $> 8r_{500}$ from the X-ray cluster centre) were first represented on a colour-magnitude grid. For galaxies within r_{500}, we determined membership by assigning each a random number between 0 and 1 and comparing this to the calculated field probability. This process was repeated for all galaxies 100 times per cluster, with the red sequence location being calculated for each realisation to determine the mean and zero-point and applying adjustments if necessary through the use of a "red edge" diagram (see Section 3.2.1, Figure 3.6). Although successful for the mid and hot clusters, after subtraction of the background, there were typically insufficient members of the cool clusters to reliably determine the fit of the red-sequence, and so the relation found for the stacked mid clusters was also applied to the cool with suitable adjustments made again using the "red edge" diagram (Figure 3.6).

Since an accurate background subtraction is crucial in the calculation of the RSLF and DGR, an alternative method of determining cluster membership was tested. This was done by applying the same analysis (i.e. the same magnitude and colour cuts)

to the CFHTLS Deep fields and applying Equation 3 in Bildfell et al. (2012)

$$n_c = n_o - n_b \frac{A}{A_b} \tag{5.1}$$

where n_c is the number of cluster galaxies following background correction, n_o is the total observed number of galaxies, n_b is the number of galaxies in the background catalogue, A is the area of the cluster and A_b is the area of the background.

Red-sequence luminosity functions were created using both the method of Pimbblet et al. (2002) and this method from Bildfell et al. (2012) and are shown in Figure 5.1 for sources lying within $4r_{500}$ of the cluster centre. The solid lines and symbols show the results from the Pimbblet subtraction method and the dotted lines and symbols are from the method using the CFHTLS Deep fields. As in previous figures, red, green and blue colours represent the hot, mid and cool samples respectively. Across all samples, there is little change to the overall shape of the luminosity functions, with the cool sample suffering from low galaxy numbers in both methods. In order to maintain consistency between this project and previous projects, we decided to choose the method of Pimbblet et al. (2002) for the rest of this work.

5.3.2 Magnitude Cuts

The classification of a dwarf and giant galaxy used to compute the DGR were taken from De Lucia et al. (2007) and are based on the absolute magnitude of a galaxy. A galaxy is defined as a dwarf if it has $-20 < M_V < -18.2$ and as a giant if $M_V < -20$.

To convert the definitions of dwarf and giant galaxies from absolute V-magnitude to apparent r-magnitude requires the colour k-correction, K(V-r), which is computed assuming an appropriate early-type galaxy spectral energy distribution (SED;Kinney et al. (1996)). The best fitting SED describing the colour redshift evolution of the mid and hot cluster red sequences (see Figure 3.7) was determined to be a linear combination of 70% Elliptical and 30% Sab. This combined template provides the reference used to determine accurate k-corrections and colour thresholds.

The conversion from absolute magnitude cut to observed space is then given using the relation

$$m_{r'} = M_{r'} + 5\log(\mathrm{D_L}) + 25 - K \tag{5.2}$$

where K is the k-correction and D_L is the luminosity distance of the cluster given in Mpc. The evolution of r' cut with redshift is shown in Figure 5.2 with the blue and

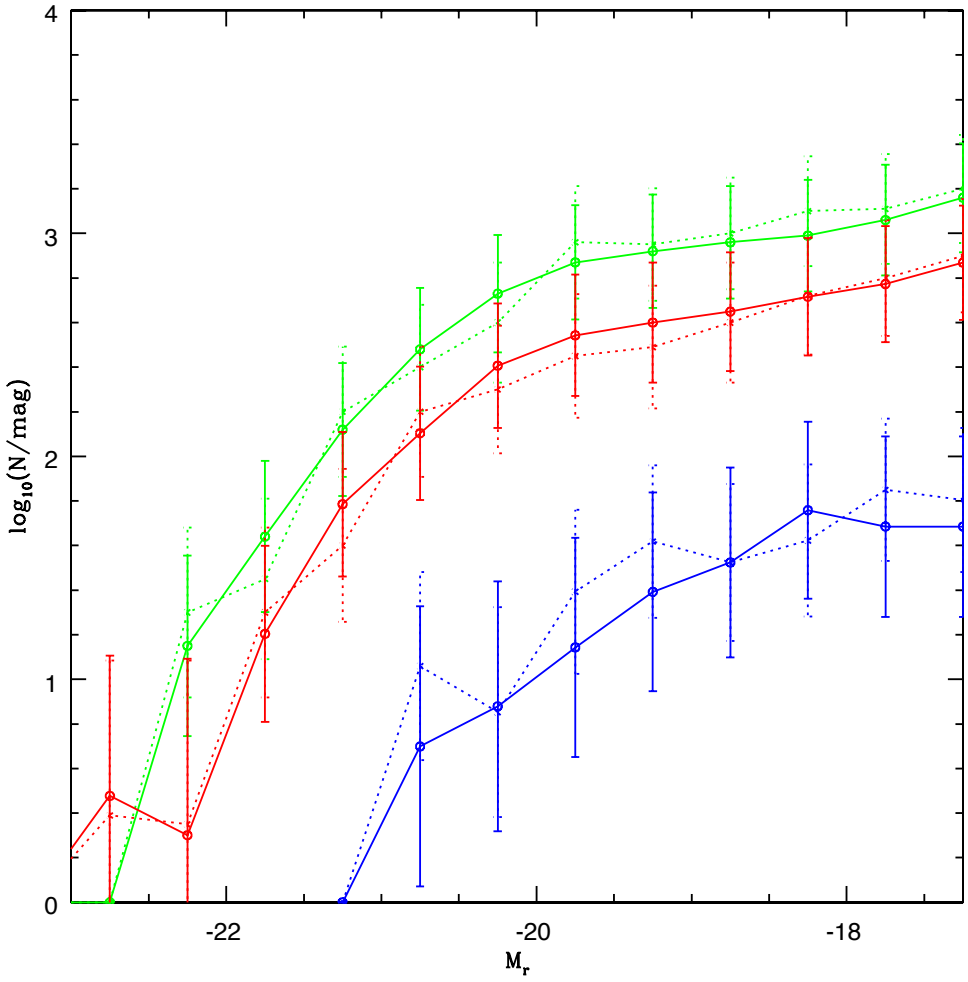

Figure 5.1: Luminosity functions for the cool, mid and hot (blue, green and red respectively) samples. Solid symbols are for the background subtraction method of Pimbblet et al. (2002) and the dotted symbols are for the background subtraction performed using the CFHT deep fields. See text for details.

red lines representing the dwarf and galaxy r'-magnitude cuts respectively.

An alternative approach would be to transform the data to absolute magnitudes, instead of transforming the absolute magnitude cuts to apparent magnitude cuts as was done here. We choose not to do this since it requires k-correcting all of the data and a k-correction based only on the g' and r' filters becomes degenerate beyond a redshift of 0.6 and would allow high-redshift background objects to contaminate both the dwarf and giant samples (Bildfell et al. 2012).

Individual CMDs could now be stacked on a colour-magnitude plane and transformed to a common redshift of z=0.3 accounting for the effects of distance dimming and k-corrections. An example of an individual CMD is shown in Figure 5.3 for the "hot" cluster A1914 (non-background subtracted). The red line marks the fitted location of the red-sequence and the blue lines mark the limits of the fixed box definition as defined in the following section. Shown in Figure 5.4 is the stacked (non-background subtracted) CMD for the "mid" sample, again, with the fitted location of the red sequence shown in red, the limits of the fixed box shown as the two blue lines and the vertical dotted and dot-dashed lines marking the giant and dwarf cuts respectively.

5.3.3 Red-sequence galaxy selection

Although the red-sequence as it appears on the galaxy CMD is a clearly identifiable feature, the specific methods employed to quantitatively select red sequence galaxies varies between authors working in this field. For example, Gilbank et al. (2008) overlaid model tracks for the expected red-sequence on their CMDs and rejected those galaxies which are bluer than 0.2 mag in $(R - z')$ than the expected colours. This isolated the red-sequence and allowed for a cleaner fit. Following this, the best-fit colour magnitude relation was subtracted, leaving a horizontal red-sequence in colour-magnitude space which is centred on zero colour and has no magnitude dependence. They then defined red-sequence galaxies to be those lying on the red side of the red-sequence ($R - z' > 0$). This eliminates contamination from bluer galaxies whose errors have scattered them onto the blue side of the red-sequence.

Barkhouse et al. (2009) take an alternative approach in creating their red sequence galaxy population. Following the fitting of the colour magnitude relation (CMR), galaxies are required to lie within ± 3.0 times the average dispersion of the Gaussian fit to the dispersion about the CMR or a galaxy must lie within 2.5 times the average

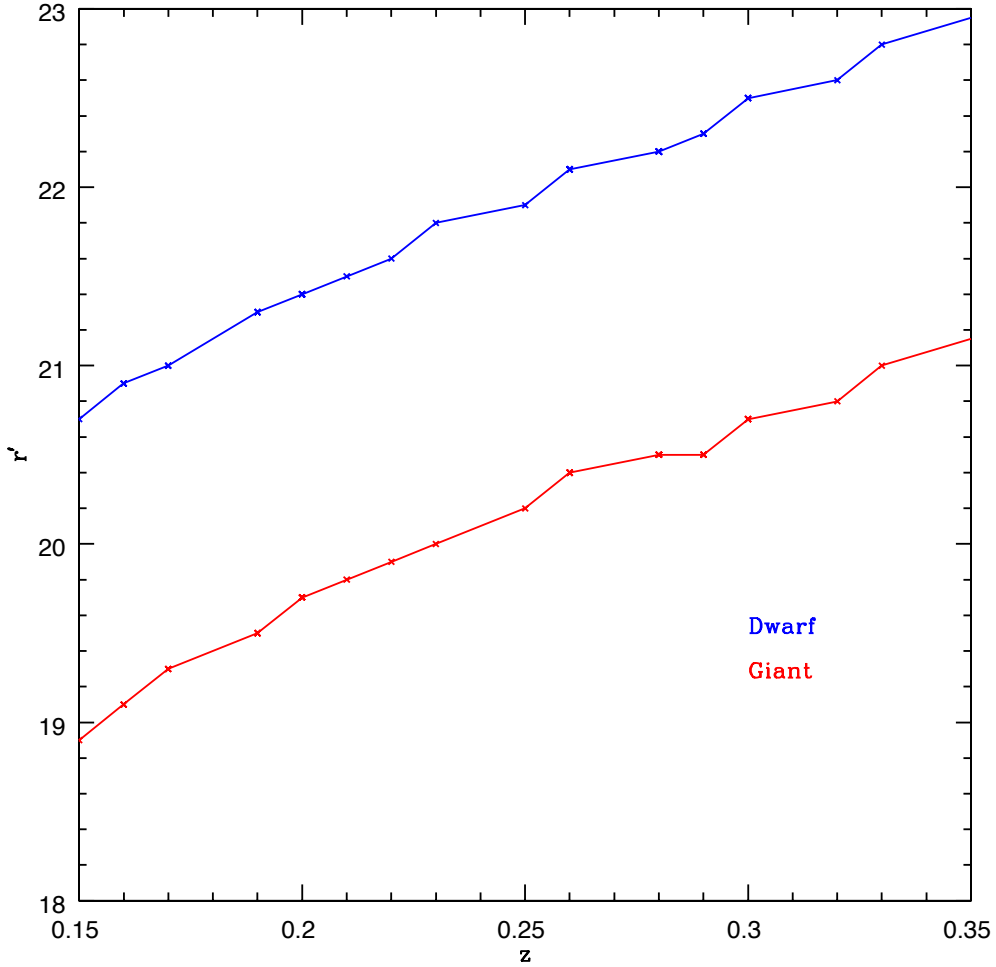

Figure 5.2: Evolution of the dwarf and giant galaxy r' cuts (blue and red lines respectively).

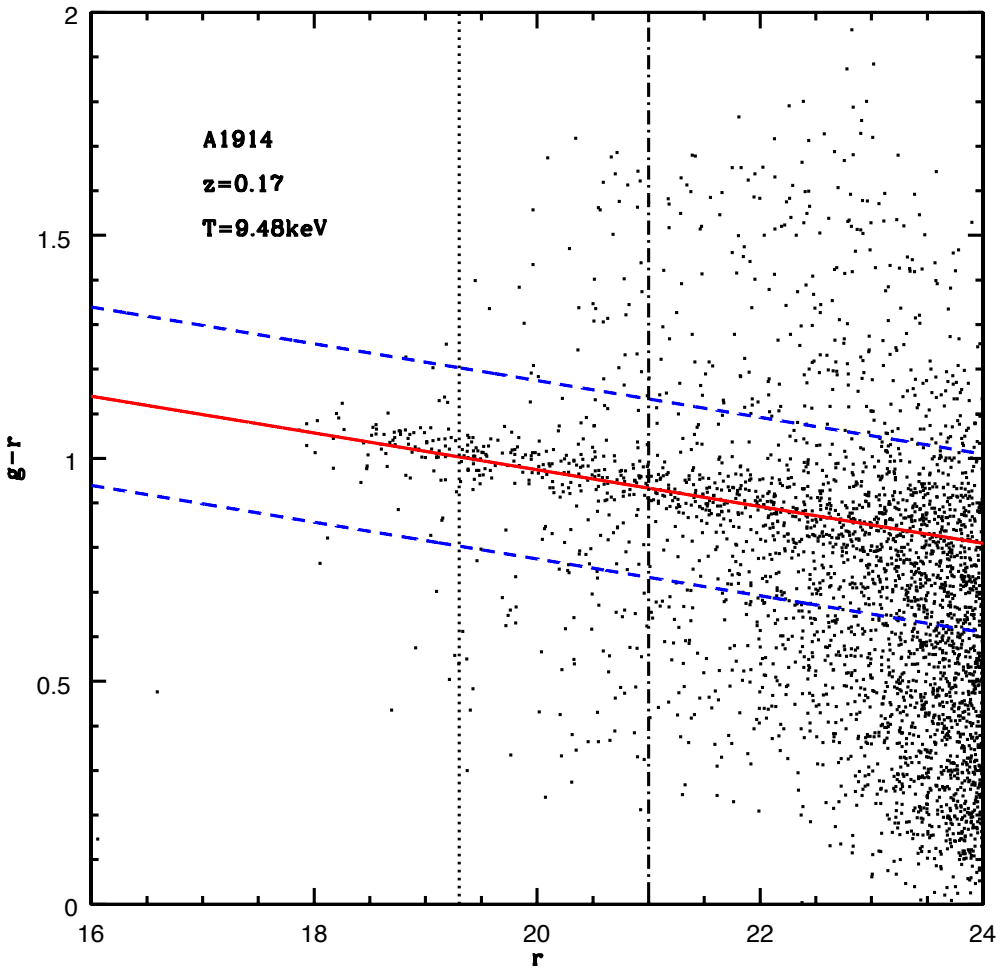

Figure 5.3: Non-background subtracted colour magnitude diagram for the "hot" cluster A1914. The red line marks the location of the red-sequence and the blue dashed lines mark the limits of the "fixed" box definition as defined in Section 5.3.3. The vertical dotted and dot-dashed lines mark the giant and dwarf cuts respectively.

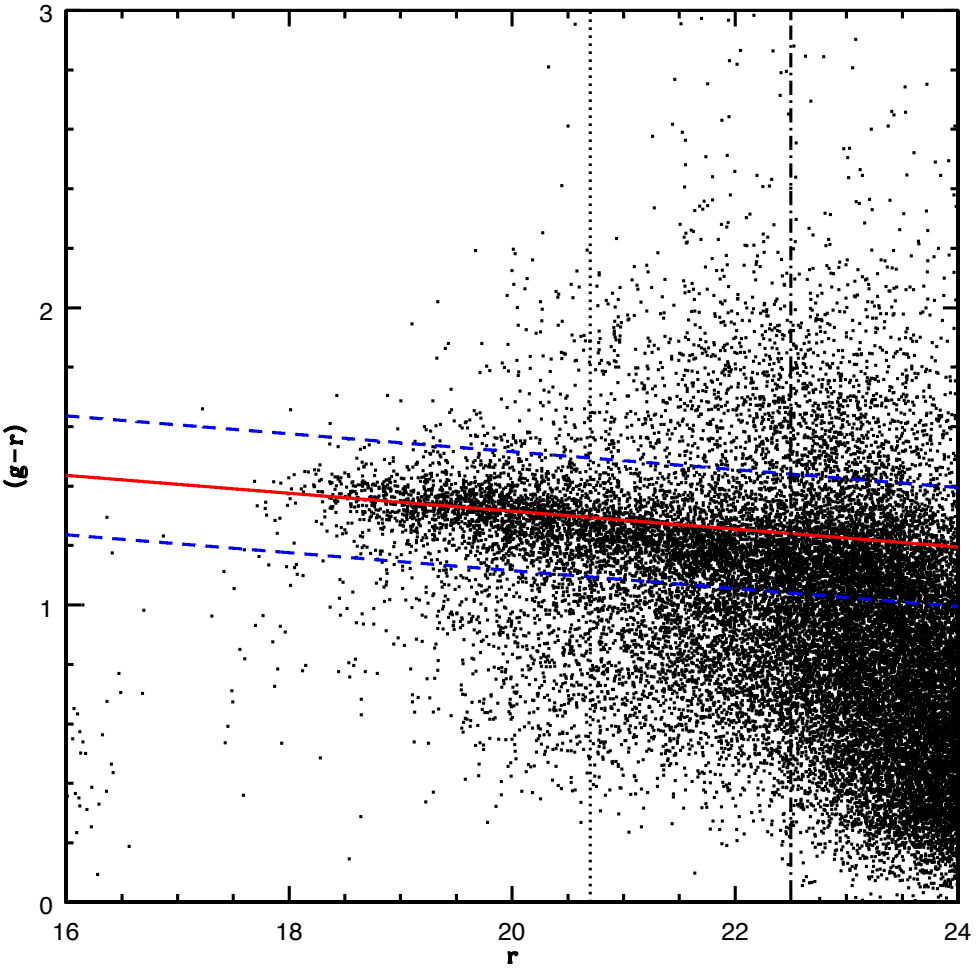

Figure 5.4: Non-background subtraced colour magnitude diagram for the stacked mid sample. The red line marks the location of the red-sequence and the blue dashed lines mark the limits of the "fixed" box definition as defined in Section 5.3.3. The vertical dotted and dot-dashed lines mark the giant and dwarf cuts respectively.

colour uncertainty redward of the CMR (depending on which of these is greater).

In a study of the evolution of the giant-to-dwarf ratio out to z$\sim$0.5, Bildfell et al. (2012) investigated how the applied colour selection criteria affected their results. The GDR was calculated based upon a fixed box size around the location of the red-sequence. This was done for box sizes $|\Delta(g' - r'| < 0.1$, 0.2 and 0.3 and found that the overall conclusions remained unaffected regardless of the choice of box size (though of course the detailed numbers changed).

Lu et al. 2009 checked and defined further selection criteria in the creation of luminosity functions for intermediate redshift clusters detected using the cluster-red-sequence (CRS; Gladders and Yee 2000) method applied to CFHTLS data. The authors split their data into a number of redshift bins and for each, created composite CMDs of galaxies lying within 0.5Mpc of the cluster centre to define the red-sequence. Following the fitting of the CMR, the authors subtract the best fitting CMR and plot the relative positions of each galaxy to this fitted CMR before creating histograms of these residual values. The width of the colour distribution around the fitted CMR (defined as σ) is calculated by mirroring galaxies redder than the fitted CMR (to avoid blue cloud contamination). Four methods of isolating red sequence galaxies are then defined. The first, Red_4σ, with red-sequence galaxies defined as being redder, but not more so than 4σ of the best fit CMR to the colour magnitude relation. The total is then twice this number. Red_ all based on the above criteria used by Gilbank et al. 2008. P10_2σ, where red sequence galaxies are those having greater than 10% probability of belonging to a colour slice $\pm 2\sigma$ from the CMR and finally NP_2σ, those that are contained within $\pm 2\sigma$ of the CMR. Testing these various methods, the authors found that the Red_4σ method was most successful in providing high enough net counts whilst keeping the background to a minimum.

In order to assess the potential impact of differing red-sequence selection methods on the resulting luminosity functions, we choose to compare our luminosity functions for three selection criteria, Red_4σ and Red_all as defined by Lu et al. (2009) and Gilbank et al. (2008) and finally, for a fixed box size ± 0.2 from the fitted CMR. Figure 5.5 shows luminosity functions created for our cool, mid and hot samples using these 3 different methods with associated Poisson errors. We use the fixed box method since it easily enables a comparison to literature in later sections. We also checked our results in the subserquent DGR analysis using the different selection methods and found no differences in the overal observed (and lack of observed) trends in the data.

In addition to variations in the colour selection, there are also variations in the projected radius used to define the extent of the galaxy cluster. Some authors choose to use a fixed projected radius to define the size of the clusters e.g. Lu et al. (2009) using 0.5Mpc, Bildfell et al. (2012) using 750kpc. However, in order to study clusters of differing masses (more massive clusters are physically larger than less massive clusters and groups), a scaled aperture size is required. This is done through the continuing use of r_{500} and its multiples in this project, thus attempting to remove radial sampling bias given the observed dependence of the shape of the LF on cluster-centric radius (e.g. Christlein and Zabludoff 2003). Further evidence of the importance of reducing the radial sampling bias was presented by Popesso et al. (2005), and Popesso et al. (2006) where the authors found correlations between DGR and a number of cluster properties (mass, velocity dispersion, X-ray and optical luminosity) when using a fixed aperture size, but that these correlations were significantly less significant when using a scaling aperture size (r_{200}).

5.3.4 Fitting the red-sequence luminosity distributions

The luminosity functions were fitted using a single Schechter (1976)) function. This takes the form (when expressed per unit magnitude) of

$$\phi(M)dM = 0.4\ln 10\phi^* 10^{0.4(M^*-M)(\alpha+1)}\exp\left\{-10^{0.4(M^*-M)}\right\}dM \tag{5.3}$$

where ϕ^* represents the characteristic number density of galaxies per unit volume per unit magnitude (a normalisation coefficient), M^* represents the characteristic magnitude where the growth of the luminosity function changes from exponential in nature to a power law and α is the slope of the power law describing the faint end of the luminosity function.

The parameters of the Schechter function are determined using the maximum likelihood method of Sandage et al. (1979). We consider a galaxy (i) which is observed at a redshift z_i in our sample for which there are apparent magnitude limits of m_{min} and m_{max}. $\phi(M)$ is the differential luminosity function of the sample, where M is the absolute magnitude. Therefore, the probability of a galaxy at z_i being in the sample is given by:

$$p_i = p(M_i|z_i) = \phi(M_i)/\int_{M_{Min}(z_i)}^{M_{Max}(z_i)} \phi(M)dM \tag{5.4}$$

Note that information on ϕ^* is lost at this stage. We can then define the likelihood

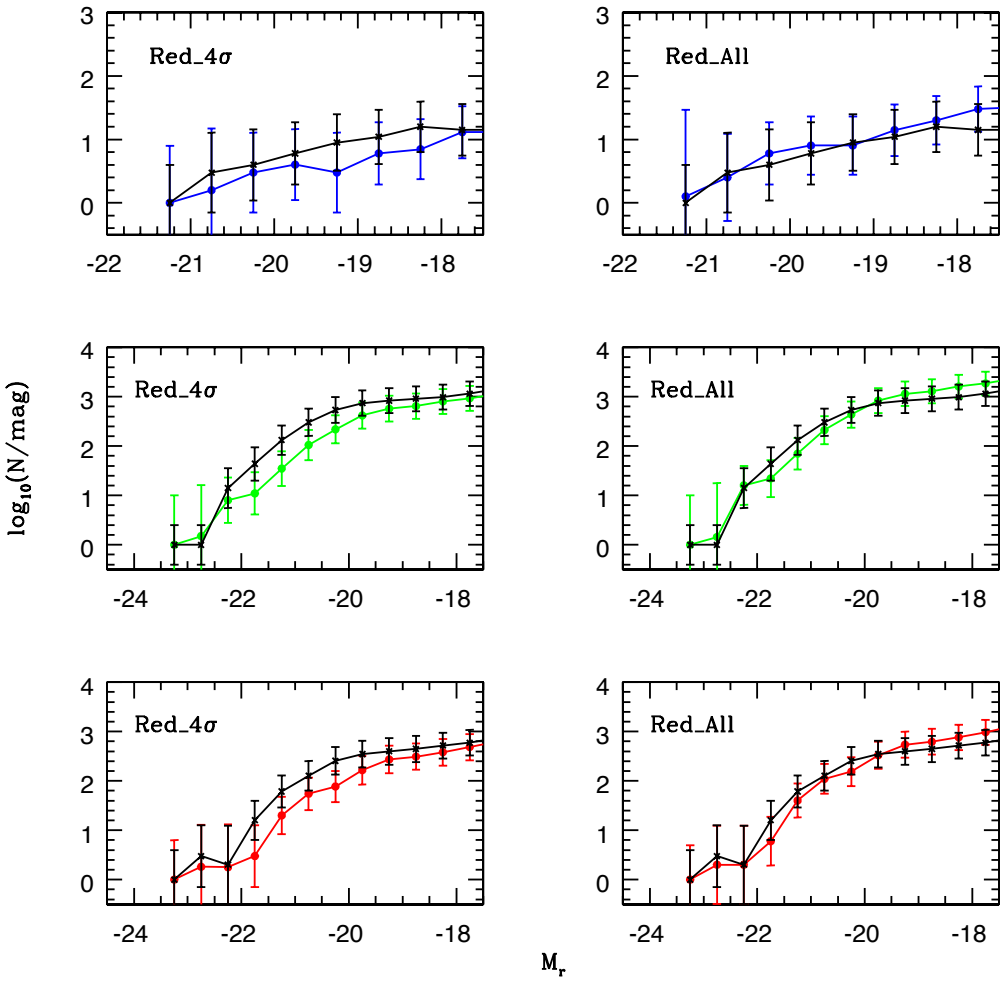

Figure 5.5: Red-sequence luminosity functions for the hot, mid and cool (red, green and blue respectively) samples for the Red_4σ and Red_All selection criteria as defined in the text. Plotted as black lines are the luminosity functions for the "fixed box" method. This is for galaxies having $r < r_{500}$. Also shown are the associated Poisson errors.

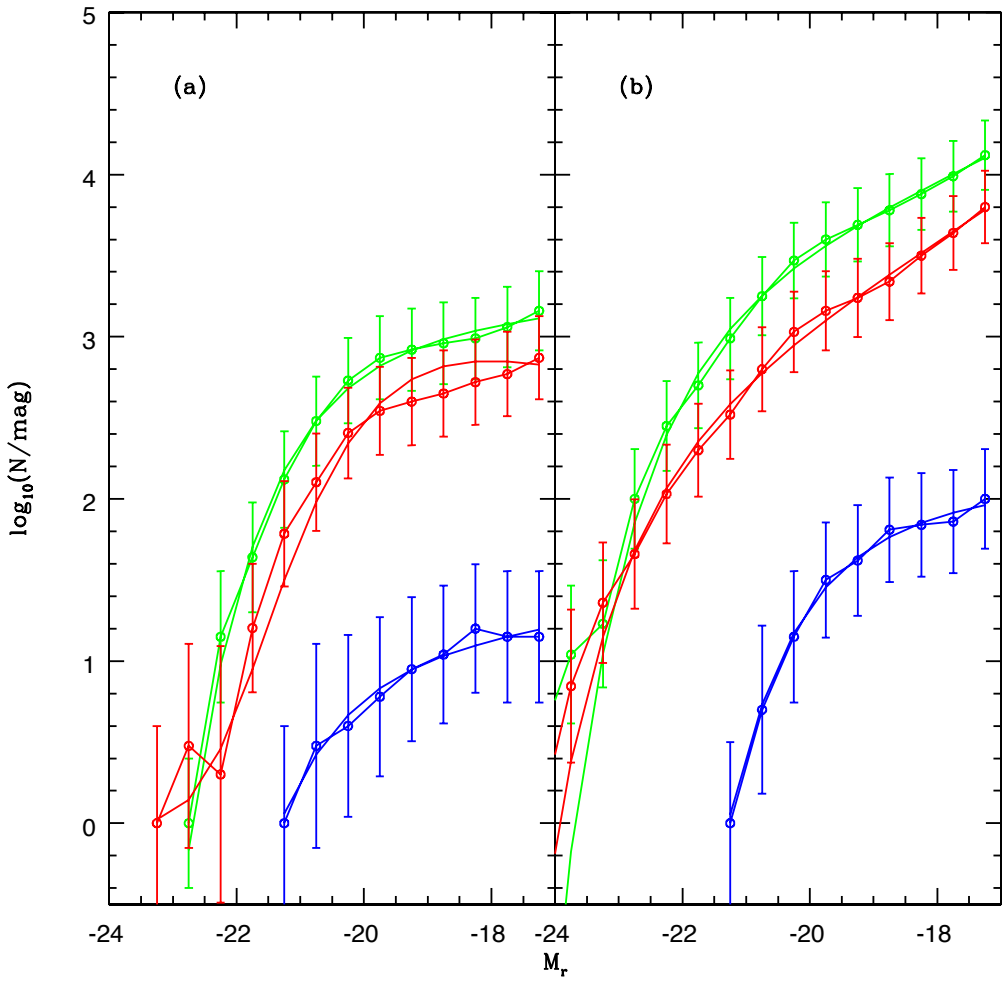

Figure 5.6: Panel (a): Red-sequence luminosity functions for the hot, mid and cool (red, green and blue respectively) samples within r_{500}. Panel (b): Red sequence luminosity functions for the hot, mid and cool (red, green and blue respectively) samples within $4r_{500}$.

Table 5.2: Best fitting Schechter parameters for fits to the red-sequence luminosity functions (within r_{500}).

Sample	$\bar{T}$(keV)	$\bar{z}$	M_r^*	α
Cool	1.73	0.3	-20.9±0.7	-1.04±0.12
Mid	6.56	0.17	-22.7±0.2	-0.99±0.05
Hot	9.81	0.24	-21.8±0.4	-1.00±0.1

Table 5.3: Best fitting Schechter parameters for fits to the red-sequence luminosity functions (within $4r_{500}$).

Sample	$\bar{T}$(keV)	$\bar{z}$	M_r^*	α
Cool	1.73	0.3	-20.55±0.2	-0.96±0.04
Mid	6.56	0.17	-22.5±0.12	-1.04±0.02
Hot	9.81	0.24	-21.6±0.12	-1.08±0.02

function, $\mathcal{L}$, as

$$\mathcal{L} = \prod_{i=1}^{N} p_i \tag{5.5}$$

This is the likelihood function for having a sample of N galaxies with absolute magnitudes M_i. This depends on the free parameters α and M_* and so the best estimates of these parameters come from maximising $\mathcal{L}$. It is generally more convenient to use the natural logarithm of $\mathcal{L}$,

$$\ln\mathcal{L} = \sum_{i=1}^{N} \left(\ln\phi(M_i) - \ln \int_{M_{Min}(z_i)}^{M_{Max}(z_i)} \phi(M) dM \right) \tag{5.6}$$

Appealing to the fact that the maximum likelihood estimate is asymptotically normal, error estimates are determined using

$$\ln\mathcal{L} = \ln\mathcal{L}_{Max} - \frac{1}{2}\chi^2_\beta(k) \tag{5.7}$$

where $\chi^2_\beta(k)$ is the confidence level of the χ^2 distribution with k degrees of freedom.

This method was used to determine the values of M_* and α. The density normalisation of the luminosity function, ϕ^* was then fit separately through the use of number counts (requiring the luminosity function to reproduce the total number of galaxies in the sample).

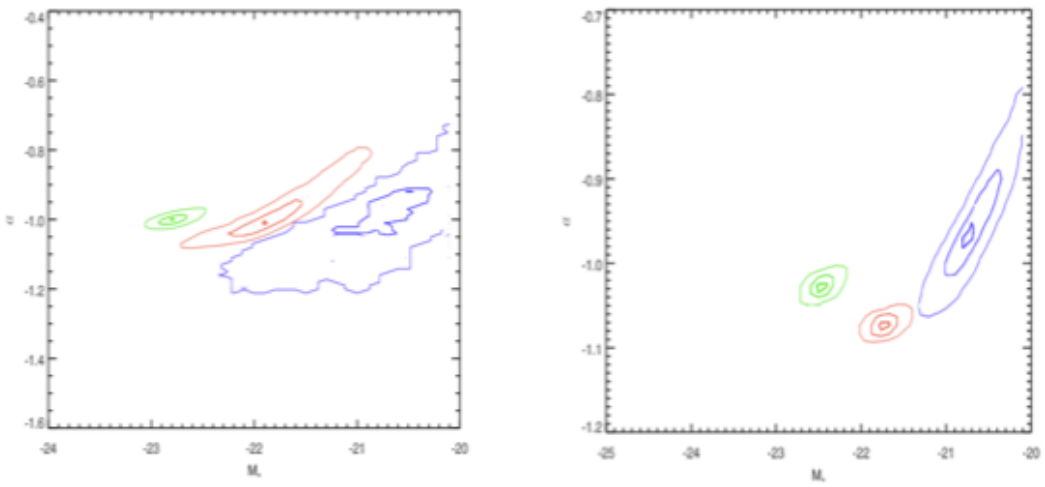

Figure 5.7: *Left*: LF 1σ and 2σ contour plots for the cool, mid and hot samples (blue, green and red respectively) for galaxies within r_{500}. *Right*: LF contour plots for the cool, mid and hot samples (blue, green and red respectively) for galaxies within 4 r_{500}.

5.3.5 Luminosity distributions as a function of temperature

The luminosity functions for the stacked hot, mid and cool samples, along with the best fitting Schechter functions are shown in Panel (a) of Figure 5.6. This is for galaxies lying within r_{500} of the cluster centre and for red galaxies determined using the fixed box method. Alshino et al. (2010) note that the effect of the choice of radial cut on the fitted Schechter function parameters was small, with α only changing within the 1σ errors between r_{500} and $1.8r_{500}$. The properties of the Schechter functions are given in Table 5.2. We also show the results when considering galaxies within 4 r_{500} in Panel (b) on Figure 5.6 and the associated fitting parameters in Table 5.3. The corresponding LF contour plots are shown in Figure 5.7.

Alshino et al. (2010) conducted a study of the galaxy luminosity functions of X-ray selected clusters from the XMM-LSS, a number of which overlap with those of this work. They performed a temperature stacked analysis in the r'-band, fitting a Schechter function to the data to determine α and M*. For their temperature bin which most closely matches that of this work, they found values of $\alpha = -1.26 \pm 0.05$ and M$^* = -21.71 \pm 0.18$. Given that we stack different clusters, we expect there to be some discrepancies between our results. They also conclude that they have seen no convincing correlation of the Schechter parameters with mean cluster temperature.

This is also consistent with our results when considering the mid and hot samples as well.

All three samples show steeper values of the faint-end slope when compared to the field which typically takes a value between $\alpha \sim -0.7$ to $\alpha \sim -1$ (e.g. Lin et al. 1996, Loveday et al. 1995). This translates to all of these environments having larger numbers of dwarf galaxies when compared to the field population.

In their study, Lu et al. (2009), using the Red_4σ classification of red-sequence galaxies found values of α of -1.15 for their sample of clusters around a redshift of 0.3 and for galaxies selected within a projected radius of 0.5Mpc.

Robotham et al. (2010) studied the variation of galaxy luminosity functions with group properties using the total group luminosity as an indicator of group mass, dividing their sample into red and blue galaxies before then stacking. Unlike our results, they find that there is a steepening of the faint end slope for their red galaxy samples as a function of group mass for a sample spanning the mass range $10^{12} \leq M_{200} \leq 10^{16}\mathrm{M}_{\odot}$.

5.4 Dwarf-to-giant Ratio (DGR)

To remove the uncertainties associated with requiring a fit to the LFs and to compare to other work in the field, we next calculate the dwarf-to-giant (and reciprocal giant-to-dwarf) ratios using the absolute magnitude cuts of De Lucia et al. (2007). This was done on both a cluster by cluster basis and for the stacked samples.

5.4.1 Redshift and Temperature Dependence

The results of the DGR calculations as a function of redshift are shown in Figure 5.8 along with the associated Poisson errors. The left-hand panel is for a fixed box around the fitted red sequence of ± 0.2 and for sources lying within r_{500} and the right-hand panel is for a fixed box around the fitted red-sequence of ± 0.2 and for sources lying within 4 r_{500}

We see an overall weak trend of decreasing DGR with increasing redshift within $r < r_{500}$ and results consistent with no trend for sources within 4 r_{500}. A partial Spearman rank analysis to determine any correlation between DGR and z yields, for sources within r_{500}, a partial correlation coefficient when controlling for T_X of $r(DGR, z|T)$= -0.51. This value suggests a weakly evolving DGR, decreasing with

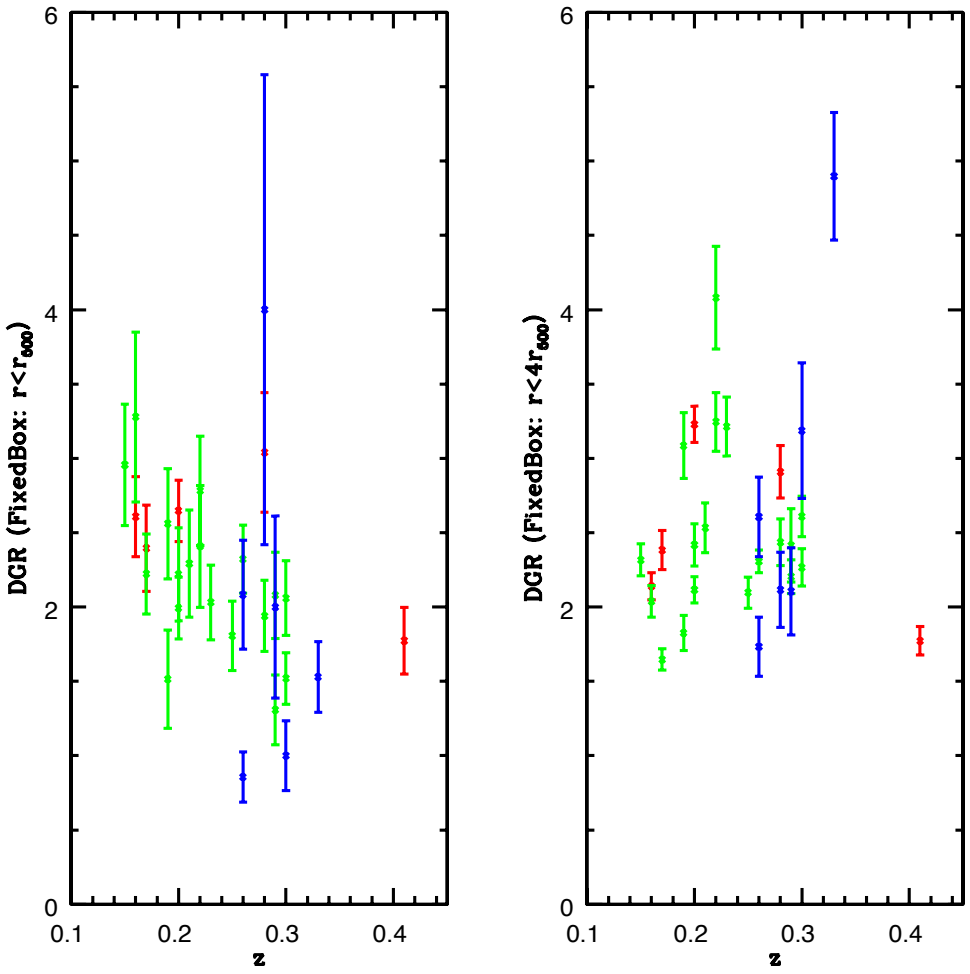

Figure 5.8: *Left*: DGR as a function of redshift for red-sequence galaxies selected using the fixed box method and lying within r_{500}. Blue, green and red represent cool, mid and hot clusters respectively. *Right*: DGR as a function of redshift for red-sequence galaxies selected using the fixed box method and lying within 4 r_{500}. Blue, green and red represent cool, mid and hot clusters respectively.

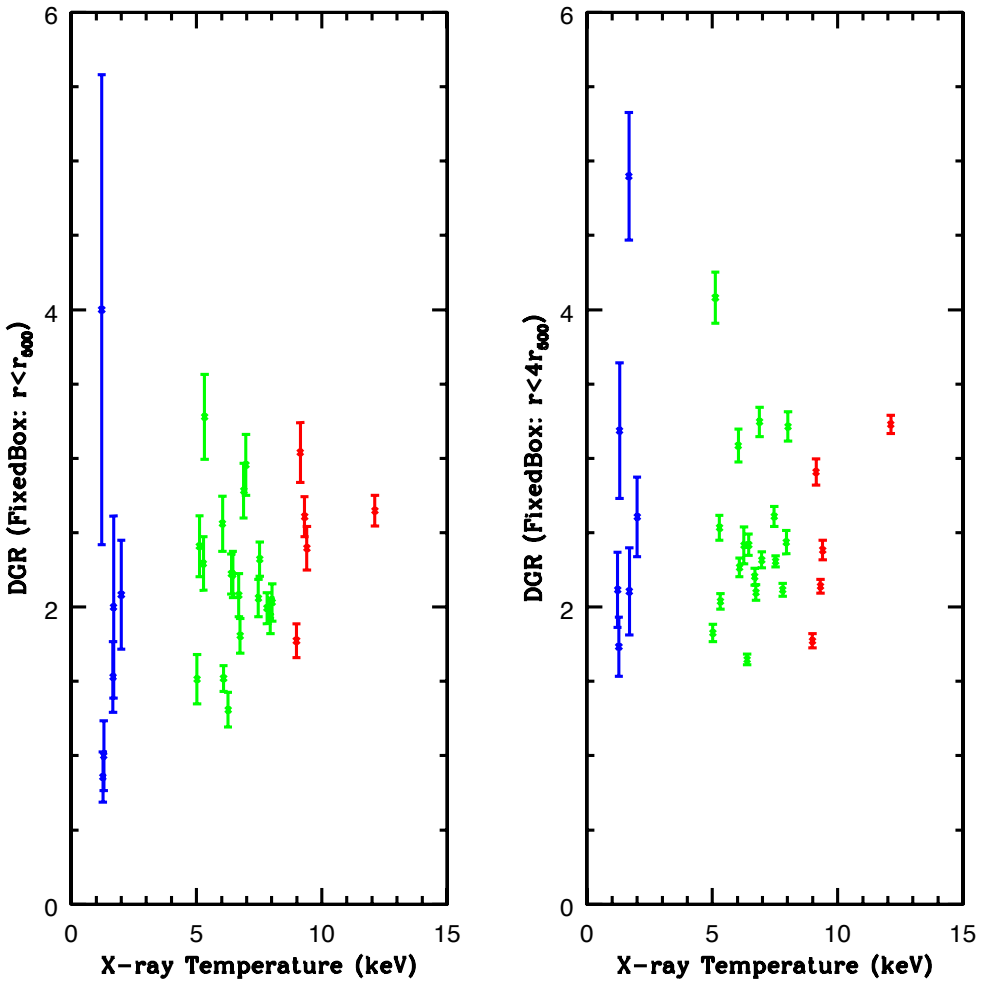

Figure 5.9: *Left*: DGR as a function of X-ray temperature for red-sequence galaxies selected using the fixed box method and lying within r_{500}. Blue, green and red represent cool, mid and hot clusters respectively. *Right*: DGR as a function of X-ray temperature for red-sequence galaxies selected using the fixed box method and lying within 4 r_{500}. Blue, green and red represent cool, mid and hot clusters respectively.

increasing redshift. If, as has been previously suggested (e.g. Scarlata et al. 2007), there is little evolution in the bright region of the LFs, then the observed evolution in DGR must be primarily driven by changes to the faint red-sequence galaxy populations. The lack of any trend at $r < 4\ r_{500}$ suggest a strong radial or density dependence of the DGR which we address explicitly in Section 5.4.2.

The overall observed trend is consistent with the results of De Lucia et al. (2007) who observed an increasing luminous-to-faint (i.e. Decreasing dwarf-to-giant) ratio from z=0 to z =0.8 as well as with Kodama et al. (2004) who observed a deficit of faint red galaxies in high density regions at $z \sim 1$. Our results are also in support of downsizing (Cowie et al. 1996) whereby star formation is halted first in the most massive galaxies before proceeding to less massive galaxies as the universe ages. Star formation stops first in giants before proceeding to dwarfs turning them red.

Shown in Figure 5.9 are our results for the DGR as a function of temperature. As in Figure 5.8, the left-hand panel is for a fixed box around the red-sequence of $\pm$0.2 and sources within r_{500}. The right-hand panel is also for a fixed box around the red-sequence of $\pm$0.2 but for sources within 4 r_{500}.

Our results of the correlation between DGR and X-ray temperature are consistent with there being no significant trend. Once again, we performed a Spearman rank analysis, this time controlling for z and find a correlation coefficient of $r(DGR, T|z)$=0.2 (for $r < r_{500}$), also suggesting very little trend between these quantities and that it is a less significant correlation than that between DGR and redshift. In this analysis, we are using the X-ray temperature as a proxy for the cluster environment, however another commonly used proxy is that of cluster richness. Barkhouse et al. (2009) calculated the DGR as a function of the richness parameter B_{gc} (a measure of the cluster centre-galaxy correlation amplitude). They observe no significant trend between DGR and this richness parameter with a Kendell's τ statistic indicating a 67% probability of a correlation between B_{gc} and DGR for the red-sequence galaxies in their sample. Richness however is not the best proxy for cluster mass due to a large scatter in the mass-richness relation which can be as large as $\pm$150% (Rozo et al. 2009). Bildfell et al. (2012) argue that an improved proxy is the X-ray temperature (as used in this work) which has significantly less scatter in the $M - T_X$ relation (36% in mass at fixed T within r_{500}).

An analagous analysis to that which created Figure 4.12 in Section 4.4 was applied using DGR instead of f_B. To remain consistent, the DGR was first calculated within $4r_{500}$ in bins of Σ_5 for the three stacked samples, the results of which are presented

in Figure 5.10. We see, at fixed values of Σ_5, an offset in the DGR between the 3 temperature subsamples. Alongside this, for the cool sample, there is a strong decrease in DGR with increasing local galaxy density which is much less in the mid and hot samples. This would suggest that once we exceed the group scale, merging becomes a far less significant process.

We also recreate Figure 5.10 for only sources within r_{500} as shown in Figure 5.11. Again, we see a decrease in the DGR with increasing local density, however this seems to be a stronger effect across all samples in these core regions, especially for the mid sample.

5.4.2 Radial Dependence of DGR

Given the likely dependence of DGR on environment (e.g. Barkhouse et al. 2009, Sánchez-Janssen et al. 2008), the variation of DGR with cluster-centric radius was calculated. This was done for the previously defined red-sequence galaxies. The results of this are shown in Figure 5.12. There is a trend, in all temperature samples, of increasing DGR with increasing cluster-centric radius, consistent with multiple past studies (e.g. de Filippis et al. 2011, Barkhouse et al. 2009). This has also been seen by Andreon (2001) who found the same trend in the K-band study of the $z = 0.3$ cluster AC118 and by Dahlén et al. (2002) where the authors studied the cluster CL11601+42 and found a steeper faint-end slope in outer parts of the cluster, equivalent to an increase in the DGR. This is due to dynamical friction drawing bright, massive galaxies to the cluster core faster than dwarfs and an increased Σ_5 and as such an increased merging rate at fixed values of the velocity dispersion causing the destruction of dwarfs.

5.4.3 Comparison to Bildfell et al. (2012)

A number of the clusters comprising our mid and hot samples are common to both this work and the work of Bildfell et al. (2012). The authors perform their analysis based on the reciprocal of the DGR, the giant-to-dwarf ratio and so to compare our results, we now recompute the GDR for all clusters studied here.

We no longer consider galaxies within r_{500} or it's multiples since Bildfell et al. (2012) calculate their GDR within a fixed radius, however this can introduce a number of problems. Popesso et al. (2006) found that when using a fixed aperture rather than one which samples the same fraction of the virialised region of each cluster, that there

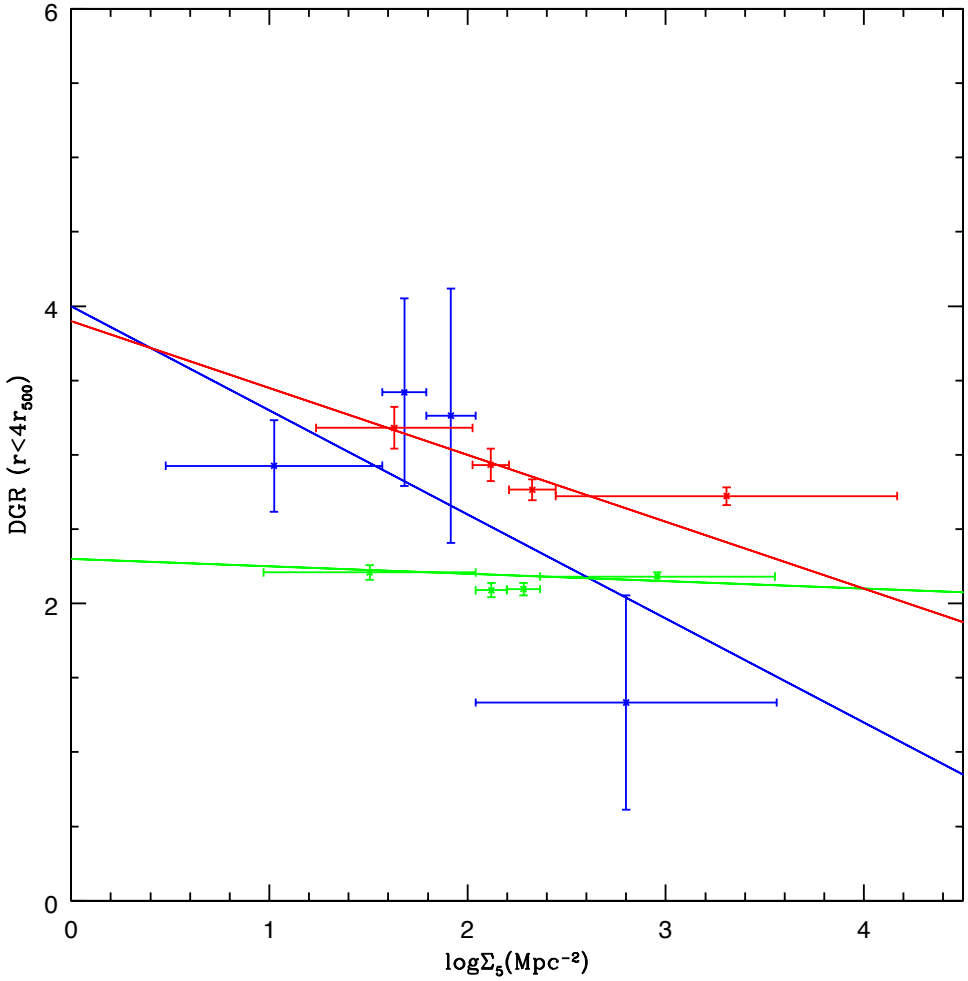

Figure 5.10: DGR as a function of temperature binned in Σ_5. Blue, green and red represent cool, mid and hot respectively. See text for details.

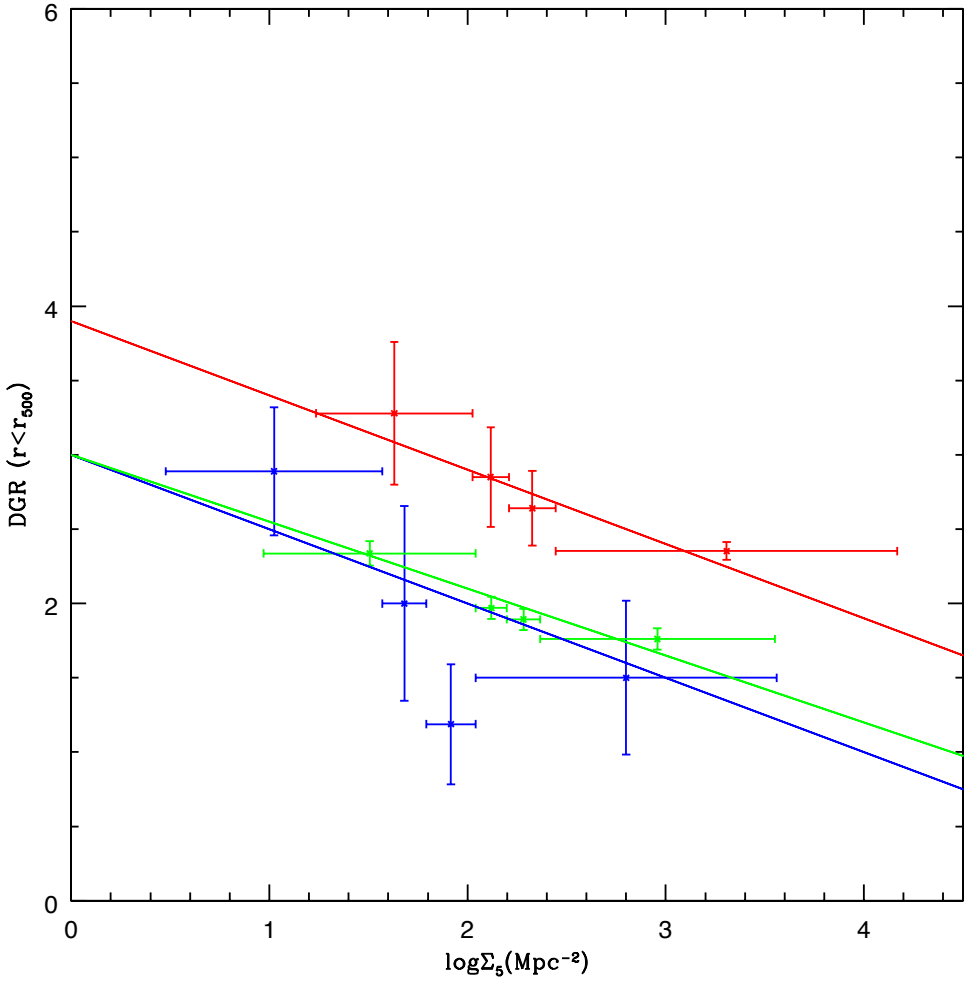

Figure 5.11: DGR as a function of temperature binned in Σ_5 for galaxies within r_{500}. Blue, green and red represent cool, mid and hot respectively. See text for details.

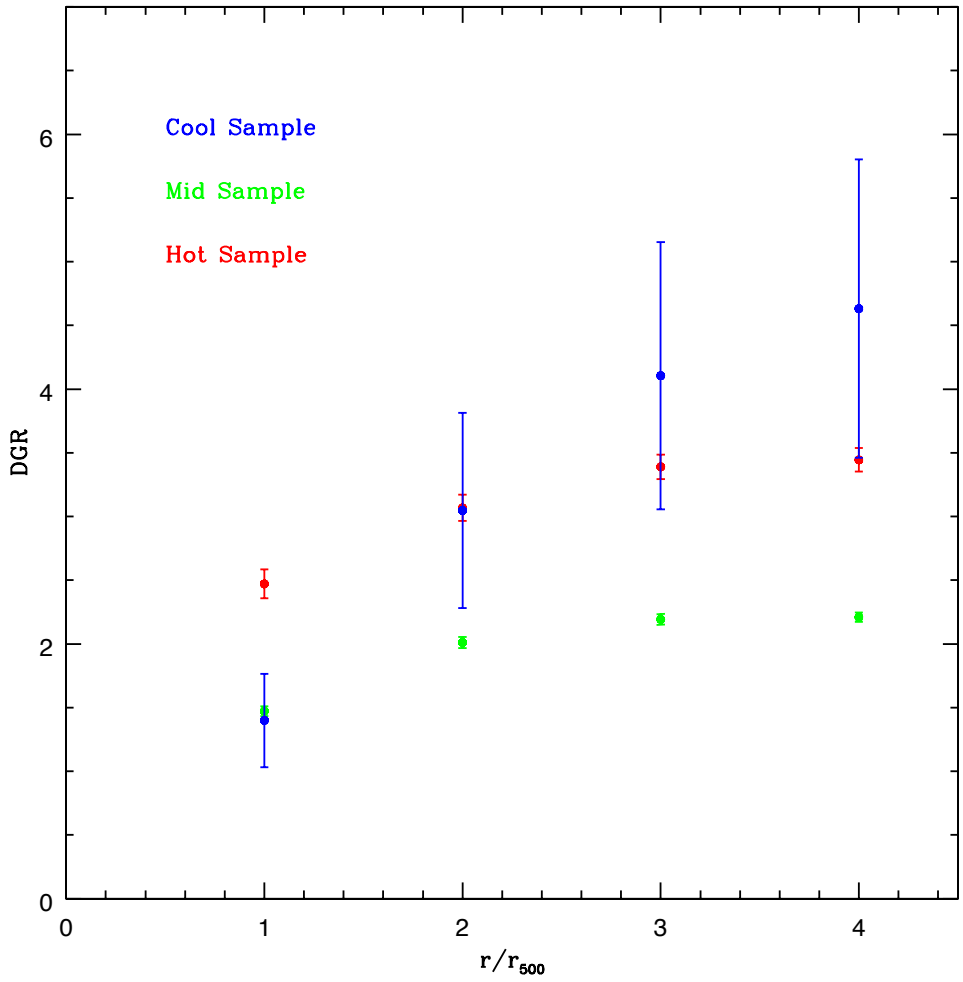

Figure 5.12: Differential DGR as a function of clustercentric distance for red sequence galaxies selected using the "fixed box" method.

existed an anti-correlation between the DGR and both the cluster velocity dispersion and mass. However, when they recalculated these values using either r_{200} or r_{500}, these trends disappeared and were no longer significant. Despite this however, to maintain a fair comparison, we recalculate our GDR in a fixed radius of 750kpc.

The results of this comparison can be seen in Figure 5.13. Clearly, there is a slight offset between the values in this work and those of Bildfell et al. (2012), with the latter being generally higher. Although we try to match their analysis as closely as possible, we still expect discrepancies arising from, for example, differing calculations of the k-correction as well as the statistical nature of the background subtraction technique.

Overall however, they observe no trend between GDR and cluster mass, consistent with the lack of trend we see between DGR and X-ray temperature (Figure 5.9). The authors argue, based upon their Figure 7, that there is evidence of an evolving GDR over their redshift range of $0.05 \leq z \leq 0.55$. The galaxies they select are within a fixed radial cut of 750kpc, less than r_{500} for all of the mid and hot clusters here. The weak trend they observe in GDR with redshift is also seen here in the left-hand panel of Figure 5.8, covering the cluster core.

5.5 Discussion and Conclusions

We have performed an analysis of our cool, mid and hot cluster samples to study the environmental influence on red-sequence luminosity distributions and the dwarf-to-giant ratio and once again, a picture is emerging where both the effects of galaxy-galaxy interactions and galaxy-cluster interactions are acting.

After selecting galaxies as members of the red-sequence, we created luminosity functions which were then fit using a Schechter function. The faint-end slope, α, for all three samples were the same within the 1σ errors for galaxies within r_{500}. When considering galaxies within $4r_{500}$, for the mid and hot samples, there was a steepening of α. This would suggest an increase in the number of dwarf galaxies at increasing cluster-centric distances. This is consistent with previous studies, for example that by Dahlén et al. (2004) who performed a study on 4 clusters of galaxies spanning $0.31< z <0.55$ and found an anti-correlation between DGR and surface density, suggesting that the high densities of the cluster cores are hostile to dwarf galaxies.

To remove the added uncertainty associated with a functional fit, we then went on to calculate the DGR for the clusters. The partial coefficients from a Spearman rank

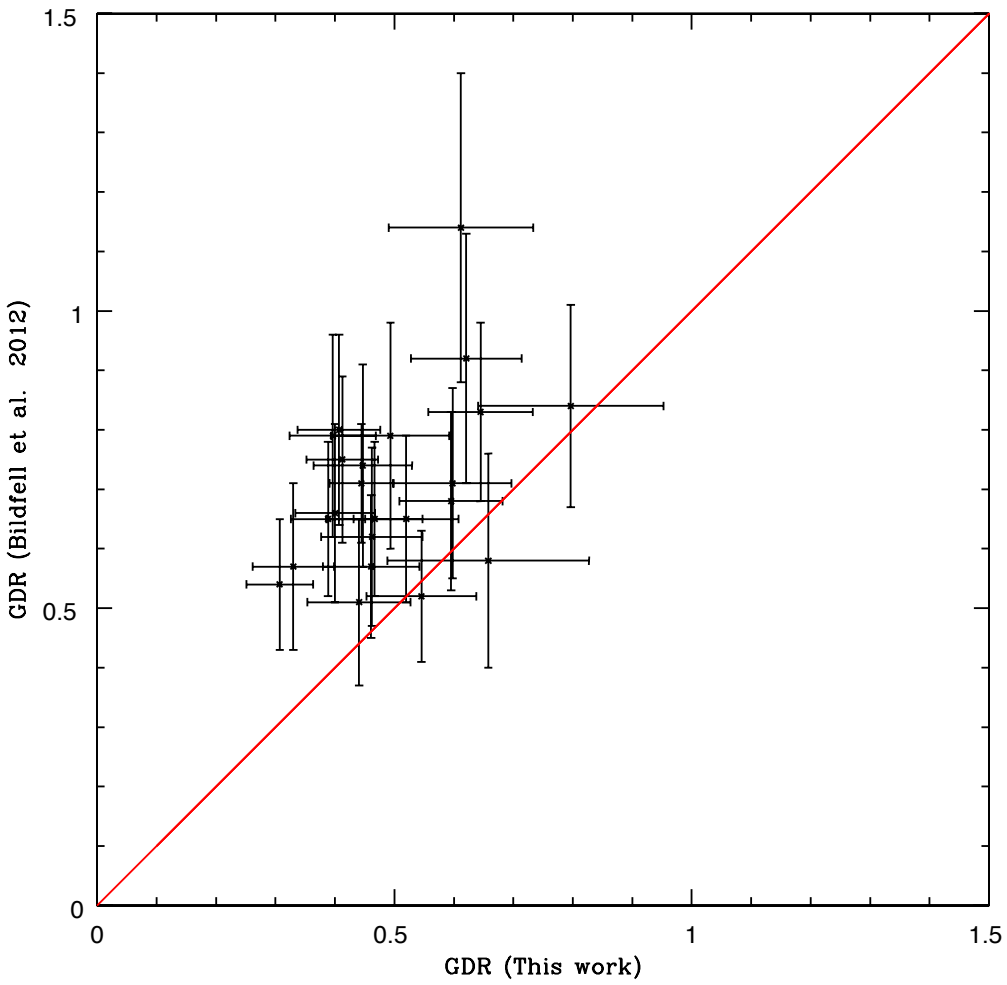

Figure 5.13: GDR for red-sequence galaxies selected using the "fixed box" method and lying within a fixed radial cut of 750kpc versus the GDR from the work of Bildfell et al. (2012).

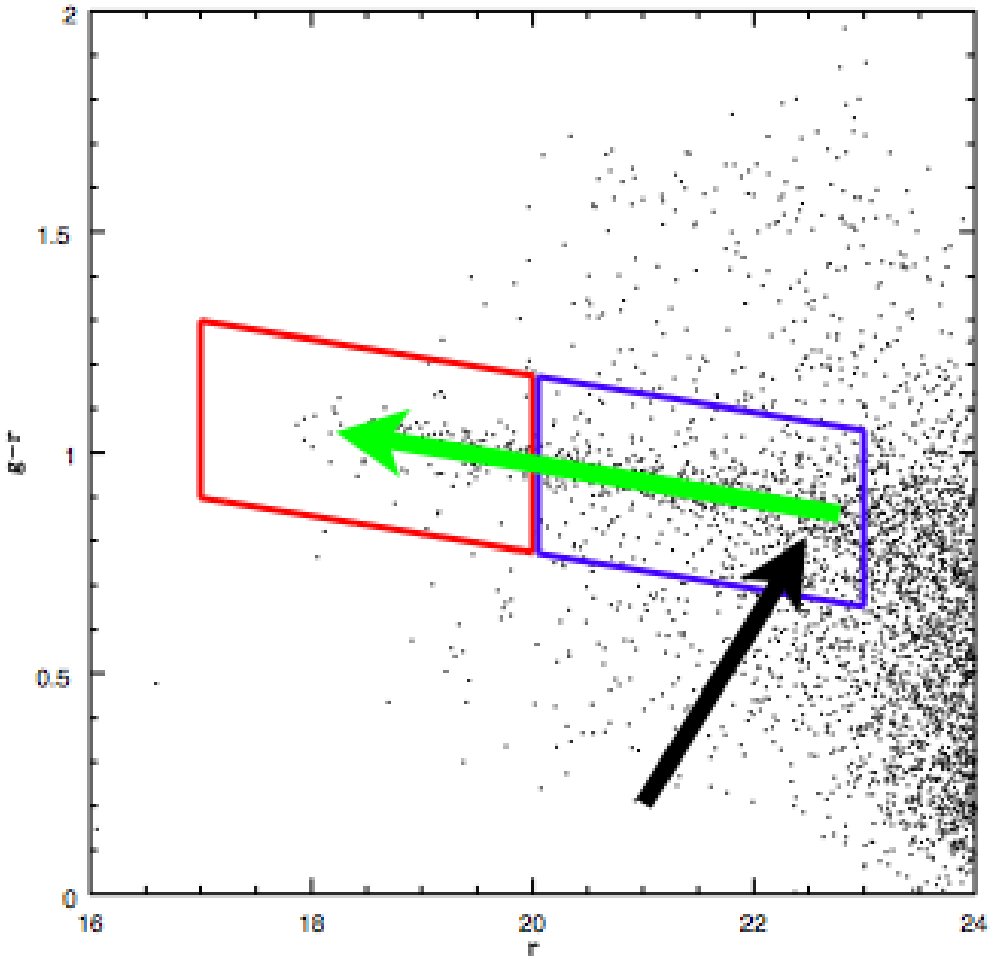

Figure 5.14: Schematic diagram showing the evolution of galaxies from the blue cloud to red-sequence dwarf, before evolution from dwarf to giant along the red sequence.

analysis were, when controlling for z, $r(DGR, T|z)$=0.2 and when controlling for T, $r(DGR, z|T)$= -0.51, suggesting that the correlation between DGR and z is a stronger effect, than DGR with T, but both are relatively weak. This is for galaxies within r<r_{500}, i.e. galaxies in the central regions of each cluster, where the environmental effects appear to be strongest.

The existence of these trends in DGR (and GDR) are still not agreed upon in the literature. Ferguson and Sandage (1991) argued that differences seen between the DGRs of groups and clusters arise largely due to an increase in the red-sequence DGR with richness, a result which was subsequently reinforced by Bromley et al. (1998) who observed an increase in the DGR with local surface density. Zabludoff and Mulchaey (2000) also observed a similar trend, that the DGR increases when going from the field to groups and to clusters. They argue that this can be explained by a combination of 2 effects. The first of these is the underlying morphology density relation (Dressler 1980), the second is that the observed surface density of dwarfs projected within $250h^{-1}$kpc of giant ellipticals is 3 times that around giant spirals, both of which would cause an increase in the DGR with environmental density.

More recently, but also using richness as a measurement of environmental influence, Gilbank et al. (2008) also found higher DGR values for richer systems (defined as having richness parameter B_{gc} >800, a detailed explanation of this is given in Yee and López-Cruz 1999). However, the De Lucia et al. (2007) work found no such trend when classifying clusters based upon their velocity dispersions. Our results would seem to agree with an observed relationship between environment and DGR (GDR).

De Propris et al. 2003 performed an analysis on 60 clusters from the 2dF Galaxy Redshift Survey having $z < 0.11$. They found no evidence for a variation in the LF for a range of cluster properties, being similar for high and low velocity dispersion clusters as well as for both rich and poor clusters.

Calculating the DGR for the three stacked samples from the LF fits gives 2.32±0.4, 1.58±0.4 and 1.74±0.3 for the cool, mid and hot samples respectively. The average redshifts of each of these samples are 0.3, 0.23 and 0.24 and the average temperatures are again for the cool, mid and hot samples respectively are 1.73keV, 6.56keV and 9.81 keV. Once again, we are seeing a weak trend of decreasing DGR with increasing cluster X-ray temperature.

In a similar analysis to Chapter 4, Section 4.4, we binned the cluster samples in Σ_5, our "local" environment parameter and calculated the DGR in each bin, for each sample. As before, at fixed local density, there is an offset in the DGR between our

cool, mid and hot samples. This offset is greatest in the highest density bin (cluster cores) where the global cluster environment is seemingly having the greatest effect on the relative populations of dwarfs and giants. Again, there is a consistent result with Section 4.4 that it is the cool sample that shows the greatest variation in the measured parameter across the different density bins, reinforcing the idea that the lower velocity dispersion group environment is more susceptible to the influence of the local environment (e.g. merging events) than the higher velocity clusters, explaining why the DGR in the cool systems is overall lower than in the mid and hot.

Figure 5.14 shows a schematic representation of how we expect galaxies to evolve in the colour-magnitude plane as a result of different environmental processes. The black arrow shows the track a galaxy will follow as it is undergoes ram-pressure stripping, transforming the galaxy into a red dwarf. Following this step, we then expect that the galaxy will move up the red-sequence, changing from a dwarf to a giant (green arrow) through merging events. We therefore expect that the DGR will anti-correlate with our local environment measure, Σ_5. There is some evidence of this in Figure 5.10 however it is not conclusive, particularly for the mid sample.

The focus of this chapter has been on the removal of red-sequence dwarfs via merging. The dwarfs are produced via ram-pressure stripping and passive reddening (with a strong dependence on the cluster X-ray temperature, which is actually telling us about the time since $\log(M/M_{\odot}) > 10^{13}$). These dwarfs are subsequently converted into giants through merging which is proportional to both Σ_5 and(or) r/r_{500} (see Figures 5.11 and 5.12). The trend in T_X is perhaps best understood from Figure 5.12. At large radius, the cool systems have the greatest number of dwarf galaxies since these are still being produced through ram-pressure stripping. However, these cool systems also have the steepest DGR as a function of radius which suggests strong merging in the core compared to the mid and hot samples.

We now go on in the final scientific analysis to determine how the cluster and group environments affect the morphologies of the constituent galaxy populations and how a morphological study can help us distinguish between the physical processes acting.

Chapter 6

Galaxy Morphologies

6.1 Introduction

We have so far divided and studied galaxy populations based on their colours, with blue galaxies considered to be forming stars and red galaxies being quiescent (colour bimodality, e.g. Baldry et al. 2004). However, given the imaging data we have available we are also able to study their physical morphology, dividing individual galaxies into, broadly speaking, two components: a bulge and a disk. These components are also related to the colour of a galaxy whereby bulge dominated galaxies are most often red and disk dominated galaxies are most often blue (Blanton et al. 2003). Clearly, there is a relation between galaxy colours and galaxy morphologies as shown in work by Driver et al. (2006). Here, the authors found a bimodality in both colour and in the distribution of the Sérsic index (n), with this bimodality becoming more pronounced when using the core rather than the global galaxy colour and is very well separated in the colour-log(n) plane. They suggest that the two components comprising this bimodality (old, red bulges and young blue discs) requires two formation mechanisms, early bulge formation through initial collapse along with ongoing disk formation through infall and merging/accretion.

It has also been shown that there has been a decline in cosmic star-formation since a peak at $z \sim 1 - 1.5$ (Lilly et al. 1996, Hopkins 2004) whilst at the same time there has been an increase in the fraction of red galaxies (e.g. Faber et al. 2007). Combining this with the correlations between galaxy colour and morphology and these observations suggest that whatever physical mechanism(s) are changing a galaxy from blue to red are also transforming a galaxy from disk to bulge dominated

(Bell et al. 2007).

As we have shown in previous chapters, the environment in which a galaxy resides has a strong influence on the colour properties. For example, there is a higher fraction of blue galaxies in our lower temperature (mass) sample and therefore we expect that environment also plays a role in the morphology of a galaxy.

This manifests in the long established *morphology-density relation* (Dressler 1980). The fraction of early-type galaxies increases with an increase in local galaxy surface density whilst the fraction of late-types decreases. Since there is also a relation between local galaxy density and clustercentric radius (see Figure 4.10), these observations are often expressed in the form of the *morphology-radius relation* (e.g. Whitmore et al. 1993) whereby cluster cores are dominated by elliptical and S0 galaxies with the outer regions of clusters containing higher fractions of spiral type galaxies approaching the field value.

The approach taken here is to study how the fractions of bulge-dominated (and at the same time, disk-dominated) galaxies varies as a function of local galaxy density (i.e. Local environment) as well as how the global cluster environment (i.e. X-ray temperature) influences galaxy morphology.

6.2 Morphological Measurements

6.2.1 GIM2D

GIM2D (Galaxy IMage 2D; Marleau and Simard 1998, Simard et al. 2002) is an *IRAF* [1] package designed to perform such bulge/disk decompositions, specifically for low signal-to-noise ratio distant galaxies. GIM2D uses a Metropolis (1953) algorithm to search a 12 dimensional parameter space. This algorithm takes an initial set of user supplied parameters and calculates the likelihood that these are the best fitting parameters. Random perturbations about these initial values are then generated and new probabilites are calculated. If the new probability is higher than the previous one, then this is accepted. Once the most likely parameters are found, a model image, residual image and log file are produced for each galaxy.

The bulge component is fit using a Sersic (1968) profile which has the form

$$I_b(R) = I_e exp{-b_n}[(R/R_e)^{1/n} - 1] \tag{6.1}$$

[1] Image Reduction and Analysis Facility.

where I_e is the intensity at the bulge effective radius, R_e. n is the Sérsic index and b is chosen to ensure that R_e is the projected radius containing half the light in the bulge component and is set to 1.9992n-0.3271 (Capaccioli 1989). A profile with $n = 4$, the de Vaucouleurs profile, is used for the bulge fitting model since bright ellipticals and the bulges of early-type spirals are generally well fit using this value.

The disk component is fit using an exponential profile of the form

$$I_d(R) = I_0 exp(-R/r_d) \tag{6.2}$$

where I_0 is the central intensity and r_d is the disk scale length. This is equivalent to a Sérsic profile having $n = 1$.

The 12 parameters fit in the `GIM2D` model are then the total luminosity L, bulge fraction B/T, bulge effective radius R_e, bulge ellipticity e, bulge position angle ϕ_e, Sérsic index n, disk scale length, r_d, disk inclination i, disk position angle ϕ_d, centroiding offsets dx and dy and the residual sky background level db.

6.2.2 Sextractor

The first step required to run GIM2D was to perform source extraction and photometry using `SExtractor v2.5.0` (Bertin and Arnouts 1996) in two-image mode with source detection being performed on the r-band images. Five quantities were required for each object. These were the X and Y coordinates, local sky background, local sky sigma and the isophotal area (`X_IMAGE, Y_IMAGE, BACKGROUND, BKGSIG and ISOAREA_IMAGE`). The file generated through this process is then used in the subsequent `GIM2D` tasks. SExtractor was also configured to create a segmentation image for each of the original images consisting of a pixel map with background pixels declared to have a value of 0 and source pixels equal to 1.

6.2.3 Cluster Membership

Before proceeding with morphological fitting, background galaxy subtraction was again performed using the statistical method of Pimbblet et al. (2002) as described in Chapter 3 to determine cluster membership. However, due to computation limitations, it was not feasible to run perform background subtraction followed by `GIM2D` fitting for 100 iterations. Therefore, an alternative approach was taken.

Background galaxy subtraction was performed 100 times per cluster and if a galaxy

was labelled as a cluster member in more than 80 of the realisations, it was kept as a cluster member. This then determined the sample per cluster upon which the C2GIMFIT2D routine was subsequently run. An example of the background subtraction is shown in Figure 6.1. This map shows the cluster members in blue and the field galaxies in black. The inner dotted line marks r_{500} and the outer dashed line marks $4r_{500}$. Different cuts were tested for a cool, mid and hot cluster to determine the influence of the cut off. A value of 80 was chosen since it gave sufficient cluster members across all samples, although the results did not vary dramatically with varying cut.

6.3 GIM2D Setup

6.3.1 Point Spread Function (PSF)

In order to account for image distortions arising from both the properties of the telescope and instruments and blurring due to the atmosphere, the point spread function (PSF) must be modelled. When performing the fitting, GIM2D then convolves the morphological model with the model PSF.

The creation of a model PSF was done by initially selecting objects classified as stars. As in Chapter 2 (Figure 2.7), we selected stars based on their half light radius and r-band magnitudes where a clear stellar locus can be seen. As a further check, the CLASS_STAR parameter from SExtractor for these stellar locus objects was also determined and found to be >0.8 in all cases (SExtractor defines a CLASS_STAR value of 1 to be a star).

To then determine the PSF across each image, the DAOPHOT (Stetson 1987) package with IRAF was used. Using the selection of stars as described above, the PSF routine was used to model the PSF across each image, with typically 50 point sources used to generate each model. To ensure sufficient spatial coverage, we ensured that stars were selected across the entire image since, as was shown in Chapter 2, there is a chip to chip variation across the MEGACAM CCD.

Given the importance of the PSF, we visually inspected the results. This was done using the ALLSTAR routine which convolves point sources with the model PSF and subsequently subtracts these point sources from the original image. If the model is successful, then following subtraction, all that should remain is sky noise. Where there was residual structure left (for example for very bright, saturated stars) on a

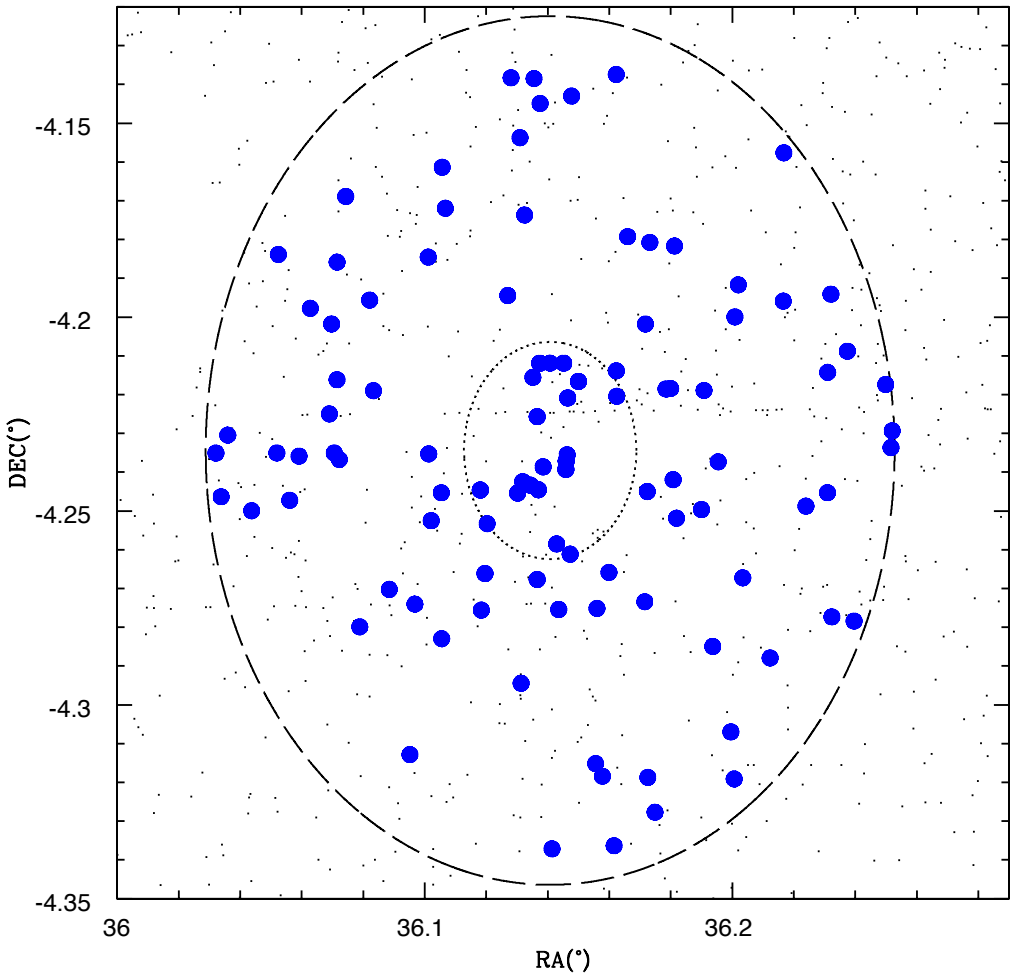

Figure 6.1: Map of XLSSC 44 showing cluster members in blue and field galaxies in black. The inner dotted circle marks r_{500} and the outer dashed circle marks $4r_{500}$.

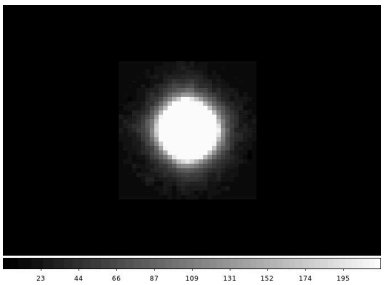

Figure 6.2: Example PSF at the location of on of the modelled galaxies.

few occasions, the PSF was remodelled using a modified list of stars. Using these models, an artificial star was created at the same location of the galaxies to be fitted.

6.3.2 Morphological Fitting

The first task to be run was `GSCRIPTER` which produces an `IRAF` cl script to allow for the subsequent running of the fitting routine in batch mode. In addition to this, it creates a file to allow the `XGAL` task to extract postage size images from the science and segmentation images produced by `SExtractor`.

To perform bakground sky subtraction, `GIM2D` uses all of those pixels which are flagged as background in the `SExtractor` segmentation image (having a flag value=0). This is further refined as any pixels deemed background but lying within five pixels from an object are excluded so that the background estimate is not biased by object pixels having isophots below the detection threshold (1.5-σ_{bkg}).

It was then possible to run the 2D bulge/disk galaxy decomposition. There are three fitting options in `GIM2D`. The first is two-bandpass separate fitting, the second is a two-bandpass simultaneous fit and the third is a single-bandpass multiple image fit. For this work, the first and second options were used. Fits were first performed separately in the g and r bands using the `GIMFIT2D` routine and then performed simultaneously using the `C2GIMFIT2D` task since, as was noted in Simard et al. (2002), performing fits is two bandpasses separately does not make maximum use of all the available information.

Shown in Figure 6.3 are examples of the r'-band postage stamp images and their corresponding `GIM2D` model output. From top to bottom, this is for galaxies having B/T values of 0.11, 0.64 and 0.82 respectively (i.e. from largely disk-dominated to increasing bulge-domination).

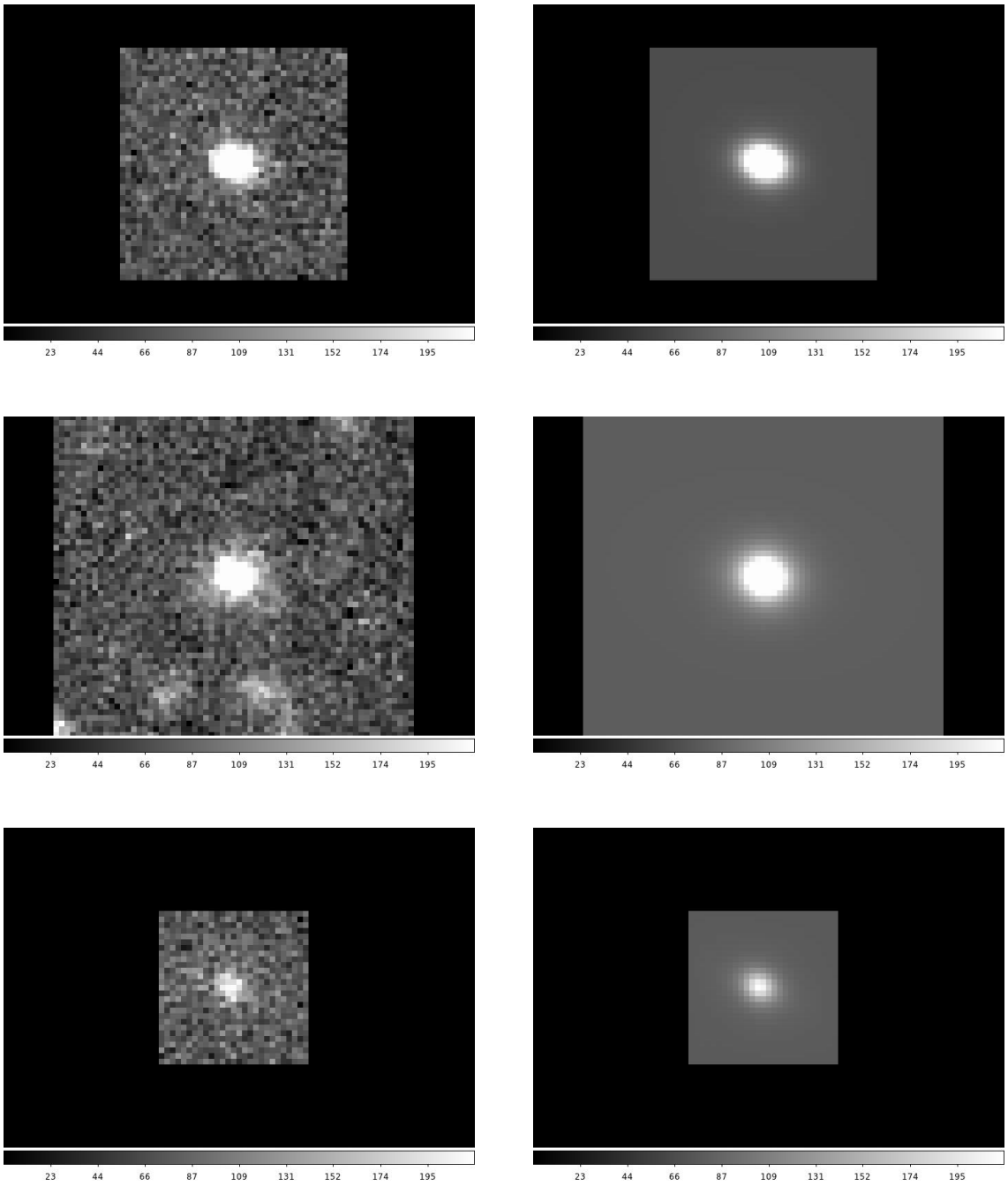

Figure 6.3: *Left-hand column*: Sample r'-band postage stamp images. *Right-hand column*: Corresponding output models from `GIM2D` *Top row*: Galaxy with B/T= 0.11. *Middle row*: Galaxy with B/T= 0.64. *Bottom row*: Galaxy with B/T=0.82.

6.3.3 Simulated Clusters

Häussler et al. (2007) performed extensive testing and analysis of GIM2D through a comparison of simulated data with the Galaxy Evolution from Morphology and SEDs (GEMS; Rix et al. 2004) survey. Galaxies were simulated for two different light profiles, purely exponential (n=1) to represent the galactic disk and Sérsic profiles with an n=4 de Vaucouleurs profile to represent the bulge. The authors developed an IDL routine to compute Sérsic galaxy models (simulate_galaxy) which allows for the creation of a simulated sample of galaxies with user specified parameters. These parameters are the location, luminosity, size, orientation and axis ratio b/a.

To test GIM2D as used in this work, we used this routine in conjunction with the results from the fitting to the real data to determine the range of parameters to input. Following the method described in Häussler et al. (2007), the simulated galaxy profiles were placed in an empty image. We also added Poisson noise using the IDL routine POIDEV to the simulations before convolving the generated image with a real point-spread function used in the fitting procedure.

These simulated galaxies were then processed through SExtractor and GIM2D in the same way as the real data. A comparison between the inputted B/T values for the simulated galaxies and those returned from GIM2D is shown in Figure 6.4 along with a comparison between the inputted disk scale length values and those returned from GIM2D shown in Figure 6.5 for example simulated images. There is quite a wide dispersion at B/T values <0.5, however, we use wide cuts for our definitions of bulge and disk dominated galaxies, a sensible approach given the limitations of the fitting procedure. For galaxies with B/T<0.3 (which we later define as our disk-dominated population), the fraction we miss which should fall into this category is only ∼0.1 and we see very little dispersion for galaxies with B/T>0.7 (which we later define as being bulge-dominated). There is even less dispersion shown for the input versus output disk scale lengths, with the typical error on these values being ∼0.1.

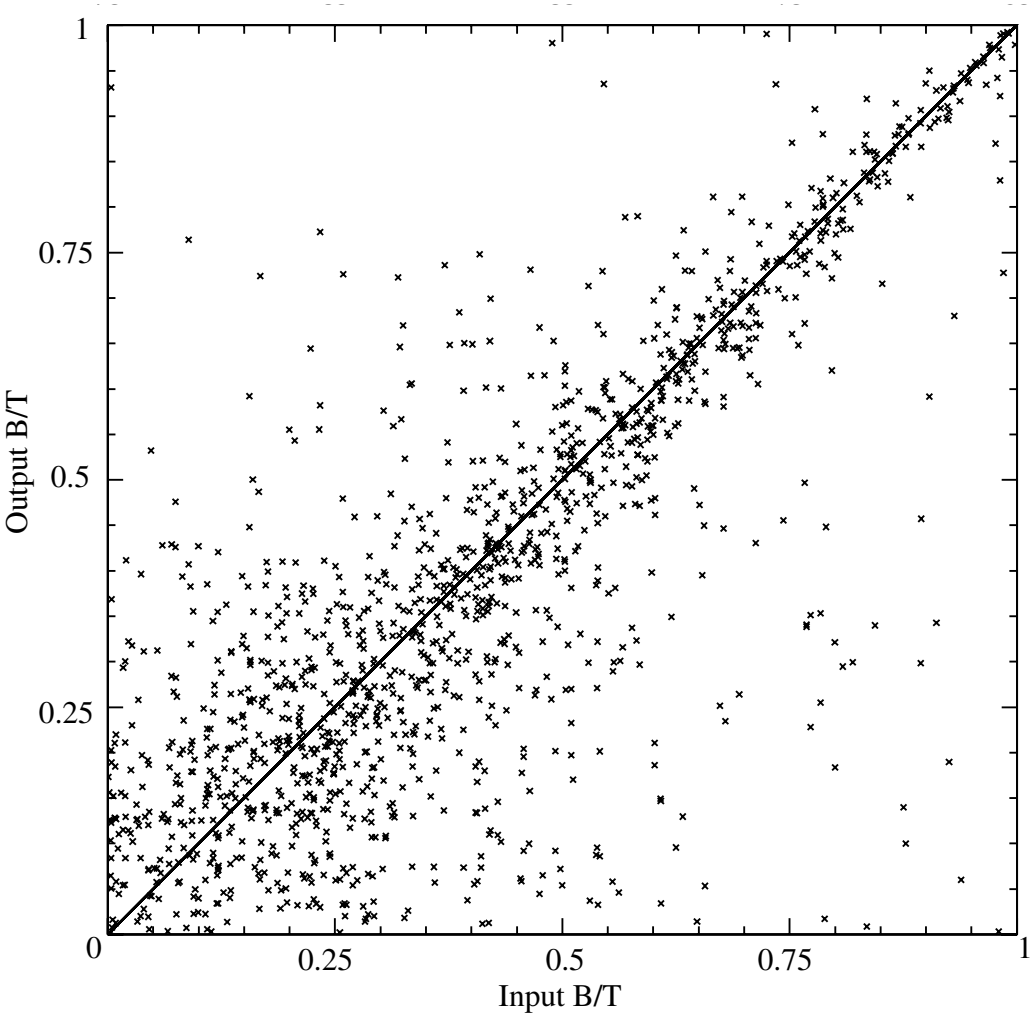

Figure 6.4: Example comparison between the inputted B/T values and the output GIM2D B/T values.

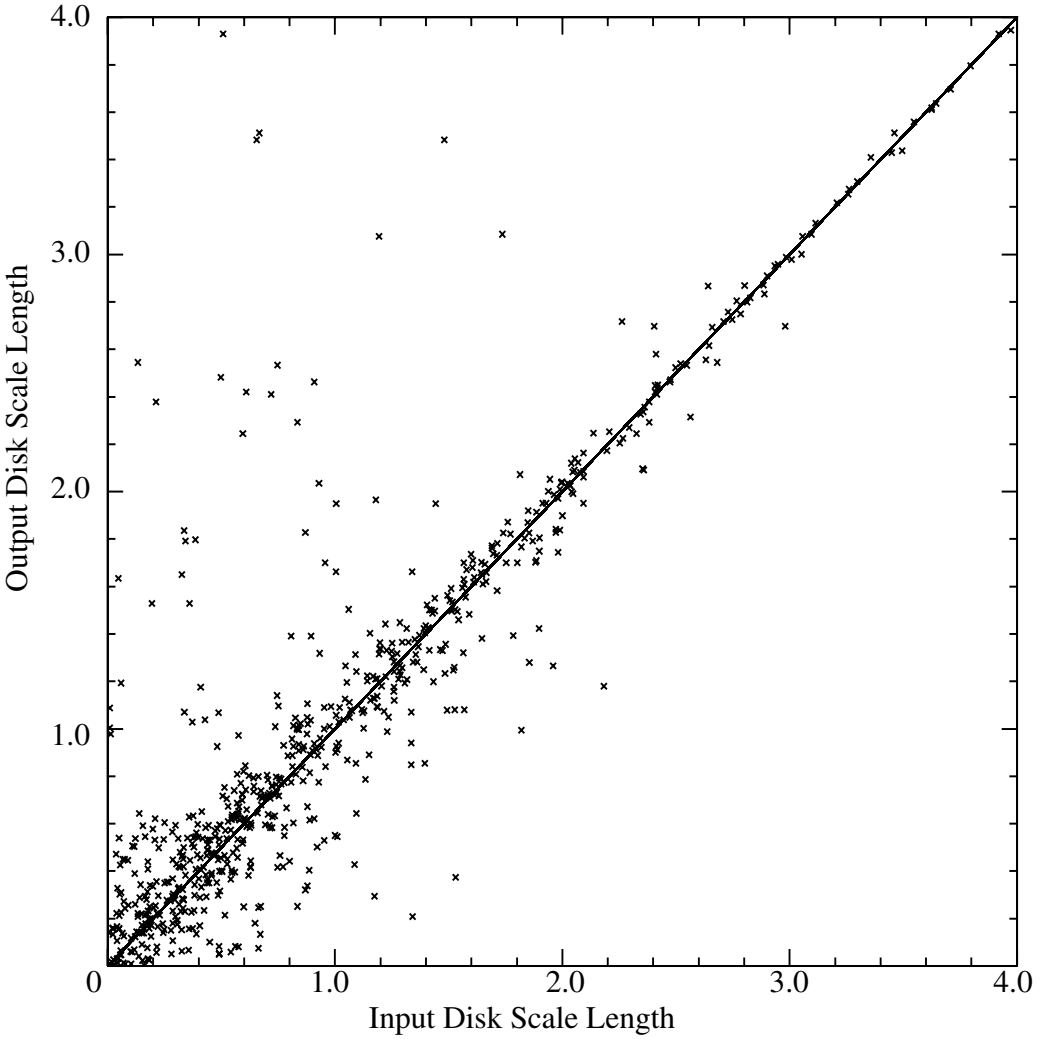

Figure 6.5: Example comparison between the inputted disk scale length values and the output `GIM2D` disk scale length values.

6.4 Results and Discussion

6.4.1 Environmental Impact on the bulge and disk components

We concentrate here on the GIM2D output parameters of bulge fraction (B/T) and disk scale length (r_d). We would expect that enivronmental processing will affect these parameters in different ways. For example, given the fragile nature of the disk component, through tidal and/or galaxy-galaxy interactions, we would expect to see a truncated or fully disrupted disk. On the other hand, we would expect to see bulge dominated galaxies being built up through a series of merging events.

In an analogous fashion to the previous chapters, the fraction of bulge dominated galaxies were split into temperature subsamples and then binned in Σ_5. Bulge-dominated galaxies are defined here as having a bulge-to-total ratio of 0.7 or greater to ensure that we are truly selecting bulge-dominated systems. The results of this are shown in Figure 6.6. Shown in Figure 6.7 is the variation of disk fraction for the different temperature samples as a function of local galaxy density for those systems having B/T<0.3 to select disk-dominated systems. Both Figures 6.6 and 6.7 are consistent with the expected morphology-density relation whereby we see an increase in bulge-dominated galaxies with increasing local galaxy density alongside a decrease in disk-dominated galaxies. However, the morphology-density relations shown in Figure 6.7 is much weaker than those of, for example, Treu et al. (2003). A possible explanation for this can be seen in Figure 6.4 where it appears that there is a potential bias towards low B/T galaxies being characterised by GIM2D, introducing a large scatter which could lessen the slope of the morphology-density relation for these disk-dominated galaxies. Figure 6.4 shows a tighter relation for higher values of B/T and so for bulge-dominated galaxies, this bias would be less of an effect, thus maintaining the stronger morphology-density relation we observe in Figure 6.6. Additionally, Figure 6.6 is consistent with Figure 10 from the study of Capak et al. (2007) who observe an increase in elliptical fraction of galaxies drawn from the COSMOS survey and the literature with increasing local galaxy density for various redshift ranges, including $z < 0.4$ which is most closely comparable to the redshift range presented here

However, unlike Figure 4.12, the differences across the temperature subsamples are of the order of the differences between the highest and lowest density bins at fixed temperature. This would suggest that the morphological mix responds less strongly

to variations in global environment (cluster X-ray temperature) than does the colour mix, consistent with the view that colours respond to ram-pressure stripping (i.e. T_X) and luminosity functions and morphology respond to merging (i.e. Σ_5).

We also looked at the distributions of the B/T ratios for red-sequence galaxies and blue cloud galaxies as shown in Figures 6.8 and 6.9. Figure 6.8 shows similar distributions for the mid and hot samples, however the main difference is the peak in the cool clusters at B/T $\sim$ 0.2. These are the passively reddening disks prior to disruption via merging. They come exactly from the B/T $\sim$ 0.2 systems in the blue cloud. Although the cool systems may well have the strongest merging, this process is incomplete (as shown in Chapter 5). Merging does proceed in the mid and hot clusters but destroys the signature. There are disks on the mid and hot red-sequences, consistent with a red, passive spiral population (e.g. Wolf et al. 2009) as well as the work by Poggianti et al. (1999) and Wilman et al. (2008) who both propose that the large fractions of passive spirals observed at intermediate redshifts suggests that star-formation is truncated before any morphological transformation occurs, however this is not the main underlying story. We also observe, in Figure 6.9, an increase in the fraction of disk dominated galaxies for all three samples which is what we expect given that this distribution is created for the blue, star-forming population.

Once again, we wish to study which underlying mechanism is the most dominant in the varying environments. Figure 6.10 supports the idea that, whilst ram-pressure stripping of gas is inevitable in the rich cluster environment, it does not alter the disk morphology (Abadi et al. 1999). Moore et al. (1999) further comment that the morphological transformation of the dwarf galaxy population ($M_b > -16$) in clusters since z=0.4 can be explained through rapid gravitational encounters between galaxies and accreting substructure (galaxy harassment), the heating from interactions causing a transformation from disks to spheroidals.

Even if ram-pressure stripping is the most effective process at work removing gas, the stars are not removed, leaving a population of red disks with no truncation, as we observe in Figure 6.8. Since it is possible to have galaxy-galaxy tidal interactions along with galaxy-cluster tidal interactions, then, as observed in Figure 6.10, the distribution of disk scale lengths should be similar across all environments.

Our lack of environmental dependence on disk scale length was also seen in the study of Maltby et al. (2012). In their analysis of V-band spiral galaxies from *HST*/ACS imaging and the Space Telescope A901/2 Galaxy Evolution Survey (STAGES)

from field and cluster environments, they find no evidence of a dependence of outer disk scale length upon environment, suggesting that the stellar distribution in the outer disk of spiral galaxies is environmentally independent.

In a study of intermediate redshift clusters and the field also using the *HST*/ACS by Homeier et al. (2006), the authors found no significant differences between the disk scale lengths of the cluster versus the field galaxies. In other words, there appears to be no environmental dependence of the global cluster properties on the physical size of the cluster disk galaxies.

The key observation from Figures 6.8 and 6.9 is that we see results which imply that the destruction of disks in the mid and hot samples is rapid (i.e. we do not see it happening) with the distribution of the disk scale lengths being the same between all three sub-samples.

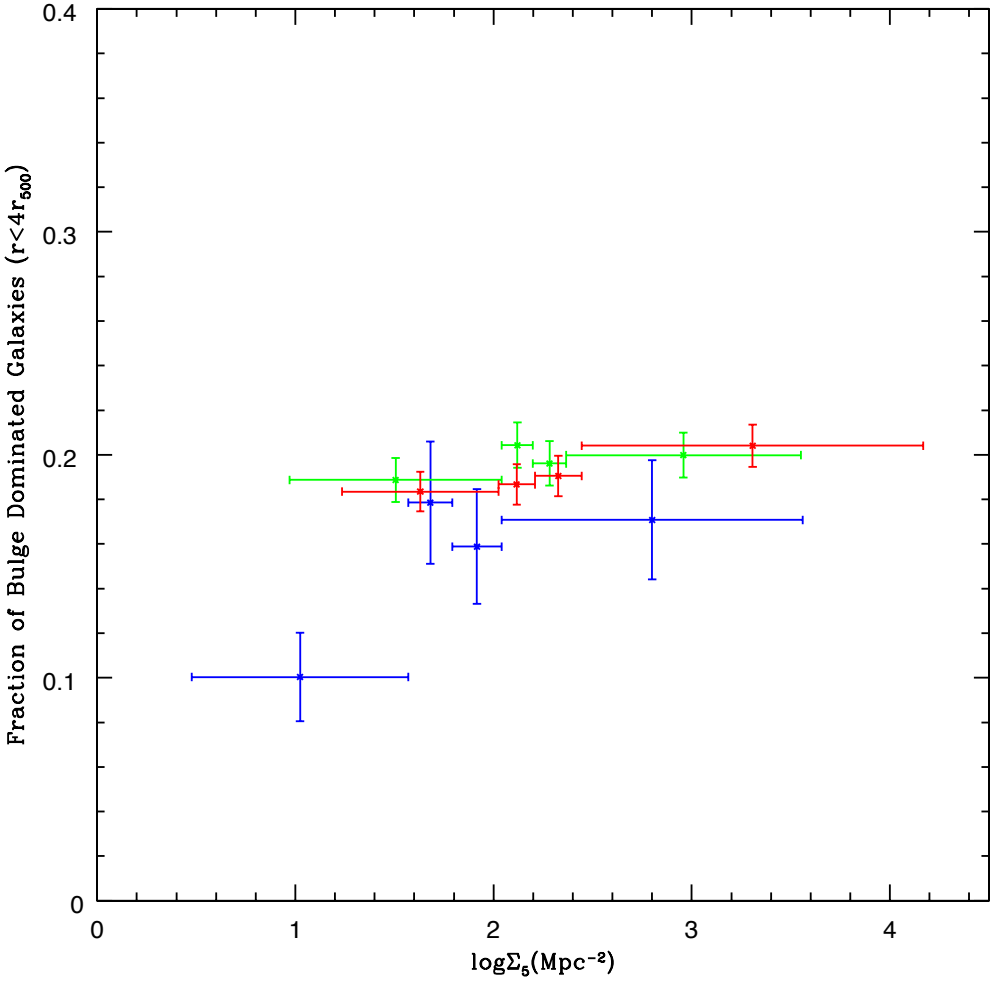

Figure 6.6: Variation of the fraction of bulge dominated galaxies binned in Σ_5 and split by temperature. Blue, green and red lines represent cool, mid and hot respectively.

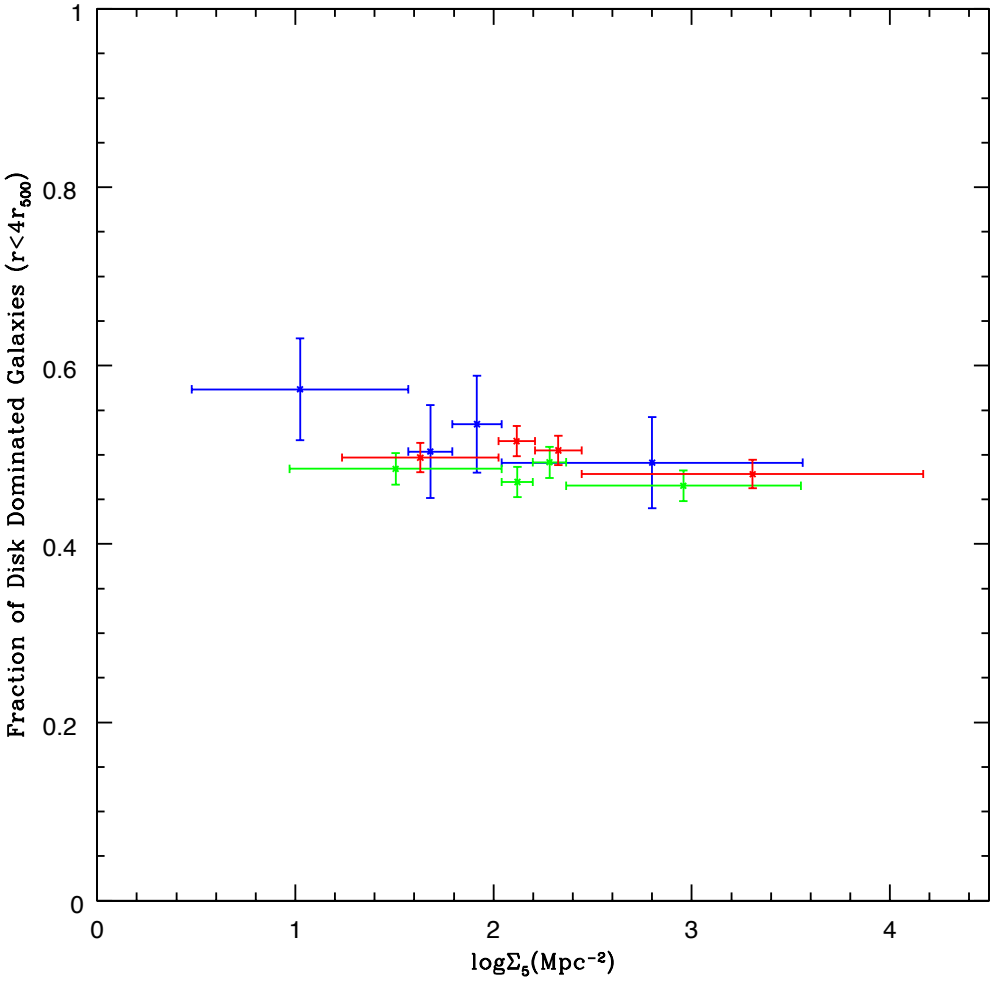

Figure 6.7: Variation of the fraction of disk dominated galaxies binned in Σ_5 and split by temperature. Blue, green and red lines represent cool, mid and hot respectively.

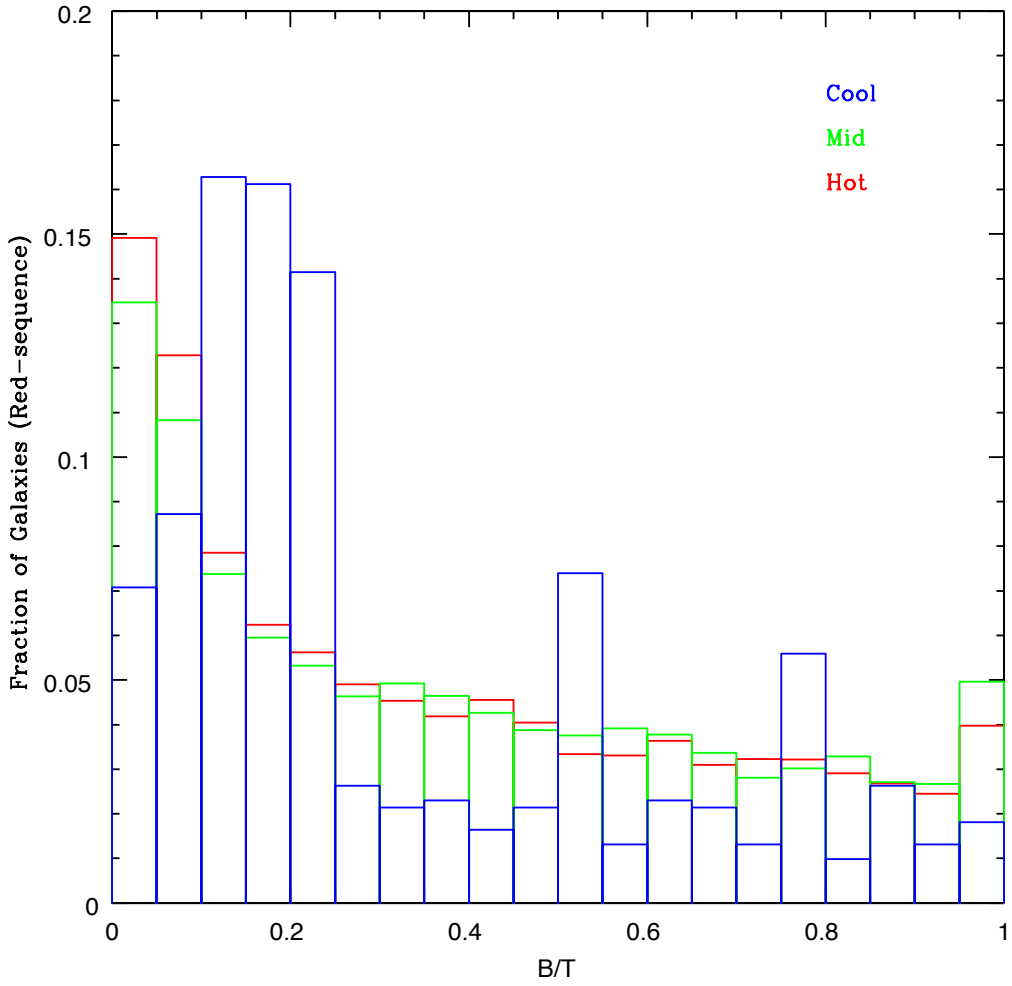

Figure 6.8: Distribution of B/T for galaxies lying on the red-sequence.

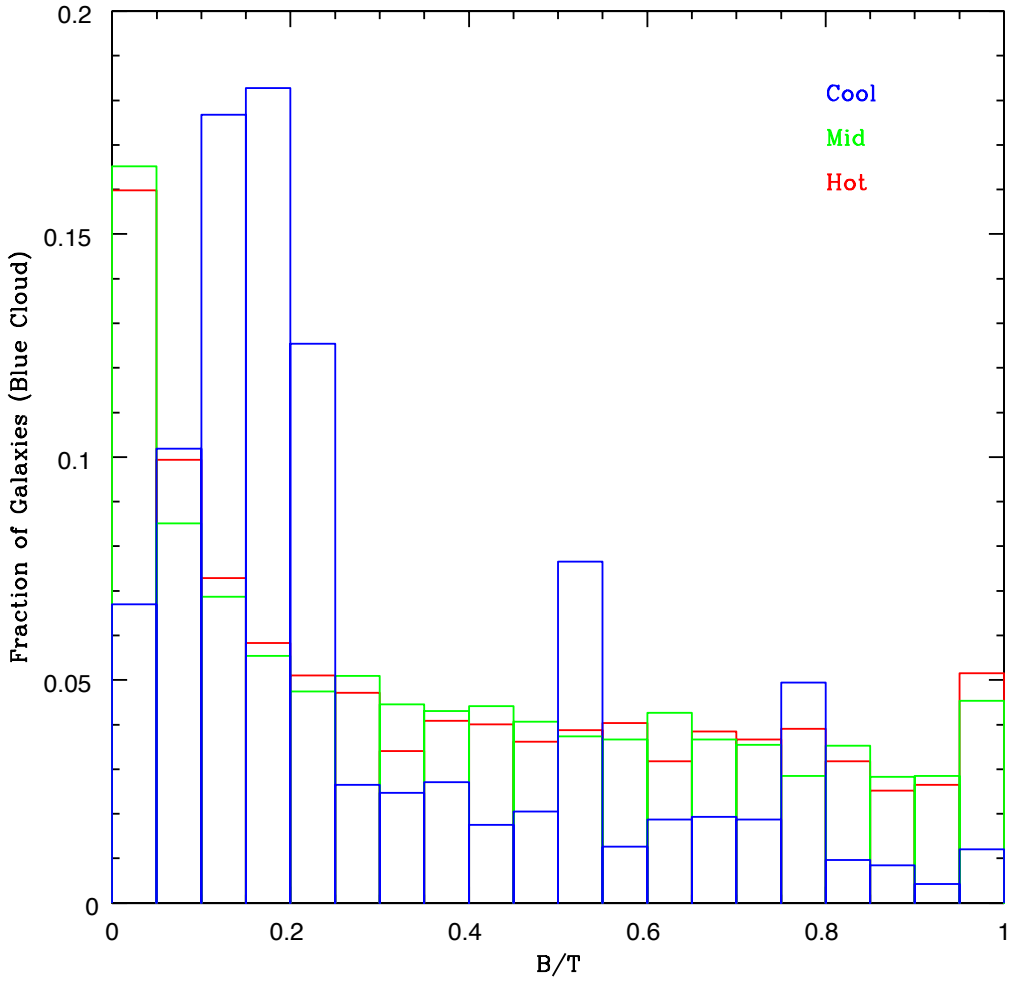

Figure 6.9: Distribution of B/T for galaxies belonging to the blue cloud.

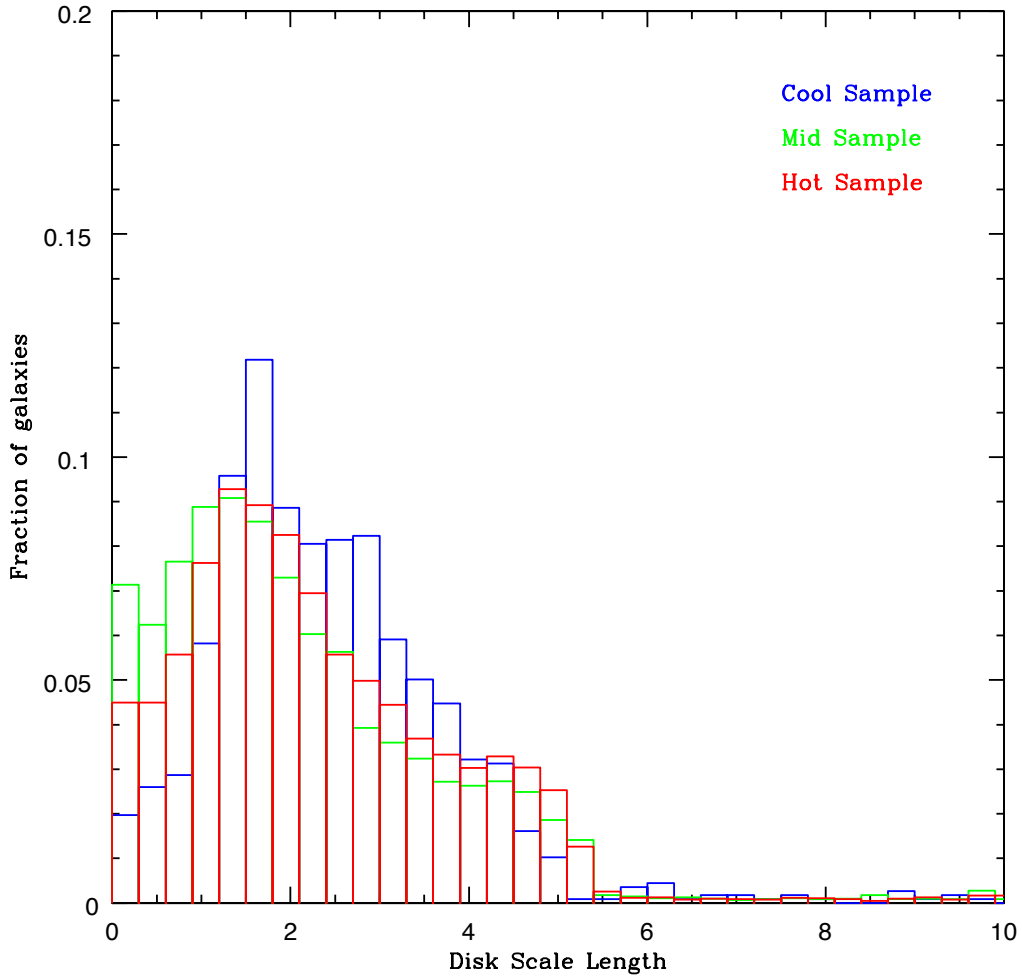

Figure 6.10: Distribution of disk scale lengths for all galaxies.

Chapter 7

Conclusions and Future Work

7.1 Conclusions

Throughout this thesis, evidence has mounted for a clear environmental influence upon galaxy evolution, manifesting in two broad categories; galaxy-galaxy interactions and galaxy-cluster interactions. Shown in Figure 7.1 is a schematic representation of our conclusions.

Chapters 3 & 4 showed that galaxies residing in the blue cloud region migrate onto the red-sequence due to ram-pressure stripping, an effect which is proportional to the cluster X-ray temperature (and therefore proportional to the cluster mass). Chapter 3 showed a clear anti-correlation between galaxy cluster blue fractions and X-ray temperature, there are higher values of f_B in the lower T_X clusters. This result alone would suggest that there is a strong "global" environmental influence on the members of a cluster, with those in a more massive environment likely to have suffered greater effects from ram-pressure stripping. Chapter 4 considered the timescales over which we expect environmental effects to occur. Through the creation of a simple model and using the results of numerical simulations, we determined that our mid and hot sample clusters have all been of a sufficient mass to have undergone the effects of ram-pressure stripping, but not all of the cool sample met this criteria. This would manifest itself in lower mid and hot values of f_B compared to a range of values for the cool clusters, as we saw in our observations in Chapter 3. We find that the value of f_B does not depend strongly on the current state of the X-ray gas.

Following this, as an alternative to calculating f_B, we then created red-sequence luminosity functions and calculated the dwarf-to-giant ratios in Chapter 5, demon-

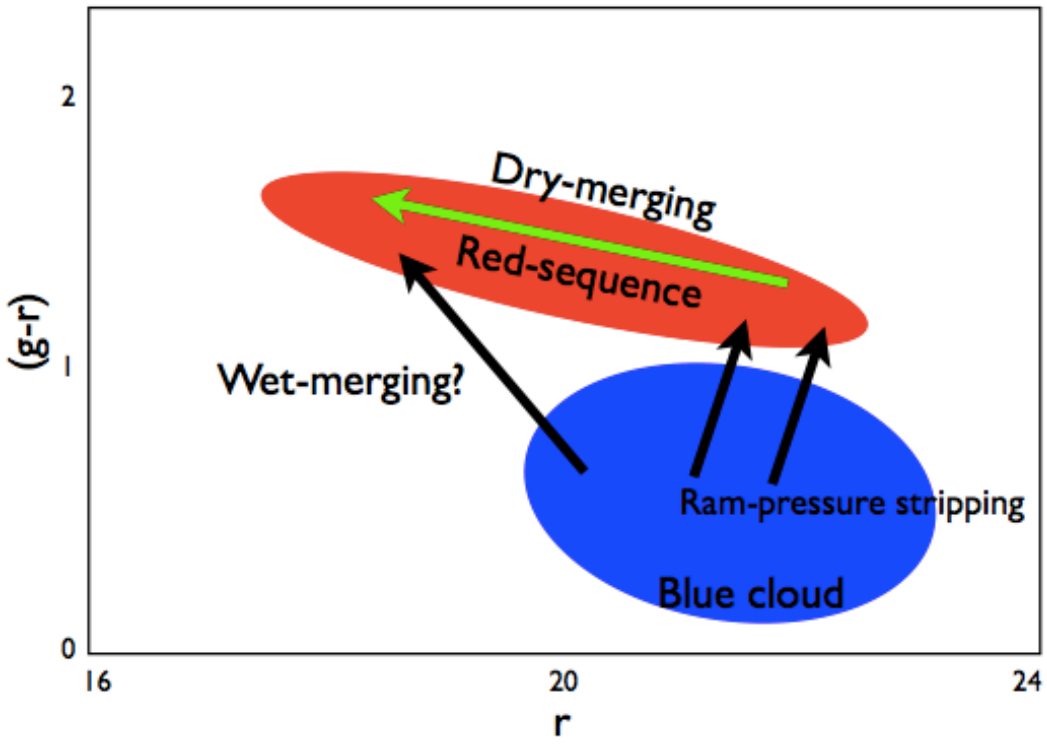

Figure 7.1: Schematic representation of the effects of environment upon galaxy evolution

strating the effects of merging. These cause a galaxy to migrate along the red-sequence from the faint to the bright end (green arrow). Our DGR measurement is proportional to the cluster redshift (more time for merging to take place), it is also inversely proportional to Σ_5 (higher DGR in lower density regions) and proportional to r/r_{500} (we cannot unambiguously disentangle r and Σ_5). Our results showed that the global environment dominates in rich cluster cores and galaxy-galaxy interactions have most effect on our low mass cool sample.

Our morphological analysis in Chapter 6 then showed that B/T is proportional to Σ_5, with disk morphologies being initially preserved. The distributions of B/T (Figures 6.8 and 6.9) imply that disks are destroyed and that this destruction must occur rapidly in the mid and hot samples since we do not see it, we do not see any intermediate cases in the distribution of disk scale lengths (Figure 6.10).

An effect that we have not investigated in this thesis is that of "wet-merging". These are gas-rich merging events (shown in Figure 7.1) which were not accessible with our data set since it ideally requires the use of spectroscopic data to detect, for example, starburst events and is one proposal for my future work which is now described in the final Section.

7.2 Future Work

The key focus of this thesis work was the study of the effects of environment on the properties of the constituent galaxy populations. Whilst this has been studied extensively in the past, our unique approach was to divide our large, uniform sample into temperature subsamples to investigate "global" effects and to divide these based upon "local" measurements (the local galaxy density). We also purposely minimised the redshift range that was studied to try to reduce the effects of evolution on our results.

In future work, there are a number of different ways in which I wish to extend this analysis. The first is to now include higher redshift clusters to study and quantify the effects of evolution. I would like to combine my current results (around $z \sim 0.3$) with a sample extending to $z \sim 1.5 - 2$, the so-called epoch of galaxy assembly.

This is becoming possible with publicly available surveys such as the Cosmic Assembly Near-IR Deep Extragalactic Legacy Survey (CANDELS; Grogin et al. (2011), Koekemoer et al. (2011)). This survey is designed to look at galactic evolution from z=8 to z=1.5 using deep imaging of over 250,000 galaxies with WFC3/IR and ACS of

the GOODS fields (over ∼0.04sq. degrees). The large field of view of the images from this survey mean the cluster and field populations are examined in a single, uniform data set allowing environmental trends to be investigated. I would like to look for overdensities in these CANDELS fields as a means of identifying different clusters and groups.

In addition to this, to fill in the "gap" between my current work (to z=0.41) and the CANDELS data at z=1.5 and above, I would like to make use of the (also publicly available) PRIsm MUlti-object (PRISM) survey. This is a spectroscopic survey to z=1 consisting of ∼120,000 galaxy redshifts and is complimented by Spitzer, optical, GALEX and X-ray data. Magellan/IMACS was used to obtain low resolution spectroscopy allowing redshifts to be measured to <0.5%. With spectroscopic redshifts, the uncertainty in using photometric redshifts to determine cluster membership is greatly reduced. Alongside the multiwavelength coverage, this would allow a number of different properties of constituent cluster galaxies to be measured over a large redshift interval.

As well as extending my analysis in redshift, I feel that another vital component in any study of this sort is the obtaining of spectroscopic data. Whilst it is possible to utilise broad band photometry to obtain galaxy redshifts for potential cluster members by comparing this photometry to galaxy spectral energy distributions (SEDs) for a number of different galaxy types, there are large uncertainties associated with this (e.g. from template choice). This is particularly important when studying the outskirts of clusters where there is a high background density of galaxies and therefore a statistical background subtraction becomes a much less successful technique.

As well as providing redshifts and measurements of velocity dispersions, spectroscopy also provides detailed information on the stellar populations of a galaxy and star formation rates. Obtaining Near InfraRed (NIR) spectra of galaxies will allow me to measure the optical star formation diagnostic lines which have been shifted into the NIR at high redshifts. These include the OII line (indicative of ongoing star formation), the OIII line and the Balmer absorption lines. It is possible to achieve this by observing a selection of galaxies in clusters of varying properties using, for example, the KMOS instrument on the VLT. This is a near-infrared multi-object spectrograph using 24 deployable integral field units (IFUs) allowing spatially resolved spectra for up to 24 target objects to be obtained.

With accurate star formation measurements, it will be possible to look for *direct* signatures of merging and stripping events. For example, peaks in the star formation

at the virial radius of the cluster (likely to represent a merger event) and the calculation of rotation curves and velocity dispersions to search for disturbances and scatter in the fundamental plane (FP). If, for example, a large scatter is observed in the FP residuals of the early-type population, this is indicative of a turbulent assembly history. Essentially, observed "abnormalities" in the cluster/group relations compared to the field suggest that some physical process has occurred.

Another measurement that I think will be interesting to pursue is that of the cold gas component of the galaxies. With the new ALMA telescope, the future for this type of work is promising. Using ALMA, it will be possible to overcome the problems of dust obscured star formation by taking sensitive measurements of higher redshift clusters. It will also enable the measurement of the cold gas content of galaxies through the detection of the CO molecular line with subsequent mapping, a sensitive probe of the mechanisms affecting galaxy evolution; critical if we are to understand how gas is accreted and processed in galaxies.

Since ALMA will observe on a galaxy by galaxy basis, I would select a subset of galaxies in different clusters which show signatures of the effects of ram-pressure stripping and interactions, identified through a combination of morphological, photometric and spectroscopic results. This would make maximum use of the ALMA facility, providing a direct measure of the disruption to a galaxy and will also provide constraints on what can be learned from, for example, modelling galaxy structures.

As outlined above, it will be possible to further investigate the underlying physical processes dominating galaxy evolution (i.e. gas stripping, merging events) through the use of spectra and morphological modelling for different environments and for different regions within the clusters themselves (e.g. results from the core where mergers are suppressed compared to the less dense cluster outskirts where mergers are more likely to occur).

Combining a range of environments with a range in redshifts will also allow me to further address timescale issues such as whether a cluster has been around long enough to achieve sufficient mass for the effects of, for example, ram pressure stripping to become significant and how the morphology and star-formation density relations have evolved with time to become what is observed today.

Clearly, with such a wealth of data currently available and the prospects of obtaining high quality spectra with the latest technology, it will be possible to provide further constraints on the many outstanding questions relating to the formation and evolution of galaxies.

Appendix A

SExtractor Parameter and Configuration Files

Presented below are the parameter and configuration files used for source extraction and photometry using SExtractor v2.5.0 (Bertin and Arnouts 1996).

Detection Parameter File

```
ALPHA_J2000
DELTA_J2000
XWIN_IMAGE
YWIN_IMAGE
ELONGATION
ELLIPTICITY
FLUX_RADIUS
CLASS_STAR
MAG_AUTO
MAGERR_AUTO
MAG_APER(1)
MAGERR_APER(1)
MAG_APER(2)
MAGERR_APER(2)
MAG_APER(3)
MAGERR_APER(3)
FLAGS
```

	Catalogues	
CATALOG_NAME	*.cat	Name of the output catalog
CATALOG_TYPE	ASCII	None, ASCII, ASCII_HEAD, ASCII_SKYCAT
PARAMETERS_NAME	*.param	Name of the file containing catalog contents
	Extraction	
DETECT_TYPE	CCD	CCD (linear) or PHOTO (with gamma correction)
DETECT_MINAREA	3	Minimum number of pixels above threshold
DETECT_THRESH	1.0	<sigmas> or <threshold>, <ZP> mag.arcsec^{-2}
THRESH_TYPE	RELATIVE	Use number of background sigmas
ANALYSIS_THRESH	1.0	<sigmas> or <threshold>, <ZP> mag.arcsec^{-2}
FILTER	Y	Apply filter for detection (Y or N)?
FILTER_NAME	*.conv	Name of the file containing the filter
DEBLEND_NTHRESH	32	Number of deblending sub-thresholds
DEBLEND_MINCONT	0.005	Minimum contrast parameter for deblending
CLEAN	Y	Clean spurious detections? (Y or N)?
CLEAN_PARAM	1.0	Clening efficiency
MASK_TYPE	CORRECT	Type of detection : can be one of NONE, BLANK or CORRECT
WEIGHT_IMAGE	*.weight.fits	
WEIGHT_TYPE	MAP_WEIGHT	
	Photometry	
PHOT_APERTURES	11,16,22	MAG_APER aperture diameter(s) in pixels
PHOT_AUTOPARAMS	2.5, 3.5	MAG_AUTO parameters: <Kron_fact>, <min_radius>
PHOT_FLUXFRAC	0.5	Fraction of $\widehat{\text{F}}$LUX_AUTO def FLUX_RADIUS <for Half light rad, HLR>
SATUR_LEVEL	60000.0	Level (in ADUs) at which arises saturation
MAG_ZEROPOINT	30.0	Magnitude zero-point
MAG_GAMMA	4.0	Gamma of emulsion (for photographic scans)
GAIN	7	Detector gain in e-/ADU
PIXEL_SCALE	0.186	Size of pixel in arcsec (0=use FITS WCS info)

Star/Galaxy Separation		
SEEING_FWHM	0.75	Stellar FWHM in arcsec
STARNNW_NAME	*.nnw	Neural-Network_Weight table filename
Background		
BACK_SIZE	512	Background mesh: <size> or <width>, <height>
BACK_FILTERSIZE	9	Background filter: <size> or <width>, <height>
BACKPHOTO_TYPE	LOCAL	Can be GLOBAL or LOCAL
BACKPHOTO_THICK	30	Thickness of the background LOCAL annulus
Check Image		
CHECKIMAGE_TYPE	NONE	Can be NONE, BACKGROUND, BACKGROUND_RMS, MINIBACKGROUND, MINIBACK_RMS, -BACKGROUND, FILTERED, OBJECTS, -OBJECTS, SEGMENTATION, or APERTURES
CHECKIMAGE_NAME	*.fits	Filename for the check-image
Memory		
MEMORY_OBJSTACK	2000	Number of objects in stack
MEMORY_PIXSTACK	5000000	Number of pixels in stack
MEMORY_BUFSIZE	512	Number of lines in buffer
Miscellaneous		
VERBOSE_TYPE	NORMAL	Can be QUIET, NORMAL or FULL

Appendix B

Background Subtraction

The following Figure is a representative example of our background subtraction technique for the mid sample cluster Abell 115. Shown as small points are those galaxies identified as belonging to the field with the heavy circles showing the cluster galaxies as determined after 100 realisations of the subtraction method.

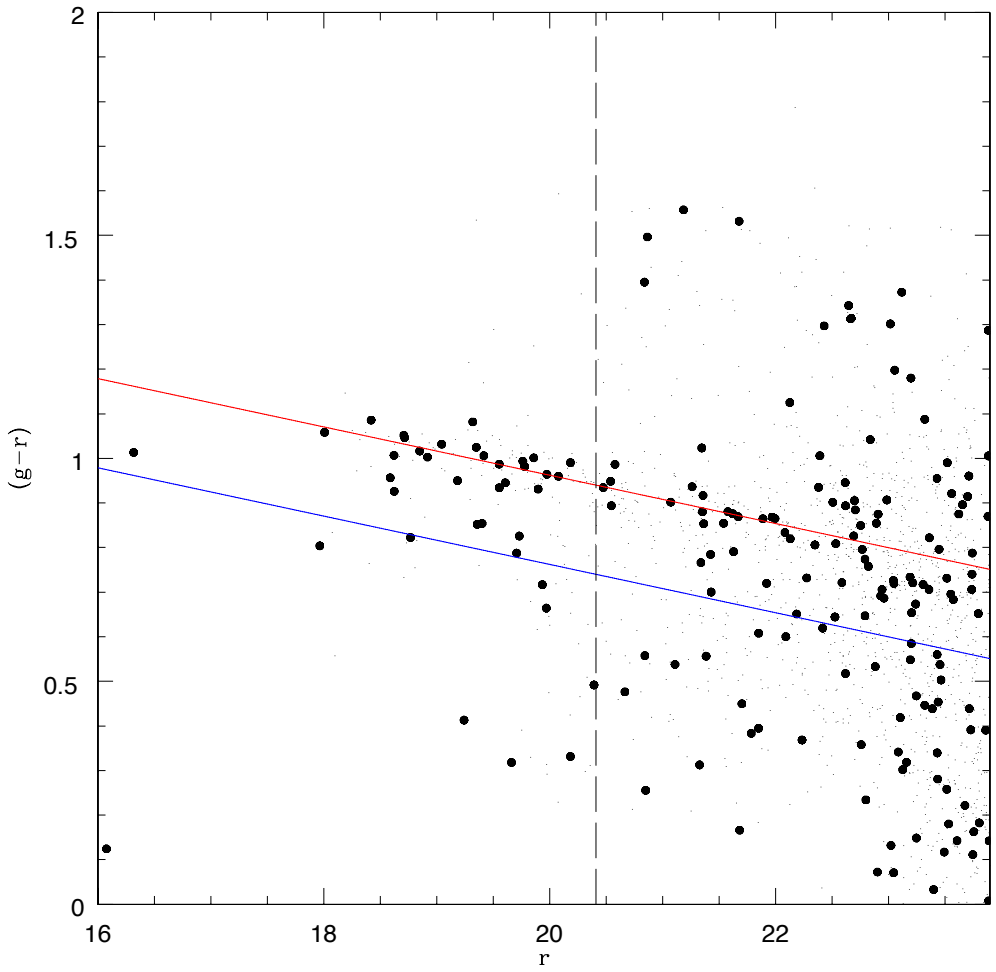

Figure B.1: Example of the background subtraction technique for Abell 115. Galaxies identified as cluster members within r_{500} following 100 realisations are plotted as heavy circles, galaxies rejected as field galaxies are shown as small points. The vertical line marks the r magnitude corresponding to M_V=-20, the red line marks the location of the red sequence and the blue line marks the Butcher and Oemler 1984 cut.

Bibliography

M. G. Abadi, B. Moore, and R. G. Bower. Ram pressure stripping of spiral galaxies in clusters. , 308:947–954, October 1999. doi: 10.1046/j.1365-8711.1999.02715.x.

G. O. Abell. The Distribution of Rich Clusters of Galaxies. , 3:211, May 1958. doi: 10.1086/190036.

R. G. Abraham and S. van den Bergh. The Morphological Evolution of Galaxies. *Science*, 293:1273–1278, August 2001. doi: 10.1126/science.1060855.

C. Adami, F. Durret, A. Mazure, R. Pelló, J. P. Picat, M. West, and B. Meneux. Spatial variations of the optical galaxy luminosity functions and red sequences in the Coma cluster: clues to its assembly history. , 462:411–427, February 2007. doi: 10.1051/0004-6361:20065848.

A. Alshino, T. Ponman, F. Pacaud, and M. Pierre. Evolution of the X-ray profiles of poor clusters from the XMM-LSS survey. , 407:2543–2556, October 2010. doi: 10.1111/j.1365-2966.2010.17088.x.

S. Andreon. Deep Near-Infrared Luminosity Function of a Cluster of Galaxies at Z=0.3. , 547:623–634, February 2001. doi: 10.1086/318381.

S. Andreon. Galaxy luminosity evolution: How much is due to model choice? , 416: 865–873, March 2004. doi: 10.1051/0004-6361:20031748.

S Andreon. The fabulous density of galaxies: Bridging past and present, 2005.

S. Andreon. The history of mass assembly of faint red galaxies in 28 galaxy clusters since z = 1.3. , 386:1045–1052, May 2008. doi: 10.1111/j.1365-2966.2008.13100.x.

S. Andreon and S. Ettori. Is the Butcher-Oemler Effect a Function of the Cluster Redshift? , 516:647–659, May 1999. doi: 10.1086/307129.

S. Andreon, C. Lobo, and A. Iovino. Extending the Butcher-Oemler effect up to z˜ 0.7. , 349:889–898, April 2004. doi: 10.1111/j.1365-2966.2004.07554.x.

E. Bañados, L.-W. Hung, R. De Propris, and M. J. West. The Faint End of the Galaxy Luminosity Function in A1689: A Steep Red Faint End Upturn at z = 0.18. , 721:L14–L18, September 2010. doi: 10.1088/2041-8205/721/1/L14.

N. A. Bahcall. X-ray clusters of galaxies - Correlations with optical morphology and galaxy density. , 217:L77–L82, October 1977. doi: 10.1086/182543.

Y. M. Bahé, I. G. McCarthy, M. L. Balogh, and A. S. Font. Why does the environmental influence on group and cluster galaxies extend beyond the virial radius? , 430:3017–3031, April 2013. doi: 10.1093/mnras/stt109.

I. K. Baldry, K. Glazebrook, J. Brinkmann, Ž. Ivezić, R. H. Lupton, R. C. Nichol, and A. S. Szalay. Quantifying the Bimodal Color-Magnitude Distribution of Galaxies. , 600:681–694, January 2004. doi: 10.1086/380092.

I. K. Baldry, M. L. Balogh, R. G. Bower, K. Glazebrook, R. C. Nichol, S. P. Bamford, and T. Budavari. Galaxy bimodality versus stellar mass and environment. , 373: 469–483, December 2006. doi: 10.1111/j.1365-2966.2006.11081.x.

M. L. Balogh, S. L. Morris, H. K. C. Yee, R. G. Carlberg, and E. Ellingson. Differential Galaxy Evolution in Cluster and Field Galaxies at z˜0.3. , 527:54–79, December 1999. doi: 10.1086/308056.

M. L. Balogh, J. F. Navarro, and S. L. Morris. The Origin of Star Formation Gradients in Rich Galaxy Clusters. , 540:113–121, September 2000. doi: 10.1086/309323.

M. L. Balogh, I. K. Baldry, R. Nichol, C. Miller, R. Bower, and K. Glazebrook. The Bimodal Galaxy Color Distribution: Dependence on Luminosity and Environment. , 615:L101–L104, November 2004. doi: 10.1086/426079.

W. A. Barkhouse, H. K. C. Yee, and O. López-Cruz. The Galaxy Population of Low-redshift Abell Clusters. , 703:2024–2032, October 2009. doi: 10.1088/0004-637X/703/2/2024.

J. E. Barnes and L. Hernquist. Formation of dwarf galaxies in tidal tails. , 360: 715–717, December 1992. doi: 10.1038/360715a0.

C. M. Baugh, S. Cole, and C. S. Frenk. Evolution of the Hubble sequence in hierarchical models for galaxy formation. , 283:1361–1378, December 1996.

L. P. Bautz and W. W. Morgan. On the Classification of the Forms of Clusters of Galaxies. , 162:L149, December 1970. doi: 10.1086/180643.

E. F. Bell, D. H. McIntosh, N. Katz, and M. D. Weinberg. The Optical and Near-Infrared Properties of Galaxies. I. Luminosity and Stellar Mass Functions. , 149: 289–312, December 2003. doi: 10.1086/378847.

E. F. Bell, C. Wolf, K. Meisenheimer, H.-W. Rix, A. Borch, S. Dye, M. Kleinheinrich, L. Wisotzki, and D. H. McIntosh. Nearly 5000 Distant Early-Type Galaxies in COMBO-17: A Red Sequence and Its Evolution since z˜1. , 608:752–767, June 2004. doi: 10.1086/420778.

E. F. Bell, X. Z. Zheng, C. Papovich, A. Borch, C. Wolf, and K. Meisenheimer. Star Formation and the Growth of Stellar Mass. , 663:834–843, July 2007. doi: 10.1086/518594.

J. C. Berrier, K. R. Stewart, J. S. Bullock, C. W. Purcell, E. J. Barton, and R. H. Wechsler. The Assembly of Galaxy Clusters. , 690:1292–1302, January 2009. doi: 10.1088/0004-637X/690/2/1292.

E. Bertin and S. Arnouts. SExtractor: Software for source extraction. , 117:393–404, June 1996.

C. Bildfell, H. Hoekstra, A. Babul, and A. Mahdavi. Resurrecting the red from the dead: optical properties of BCGs in X-ray luminous clusters. , 389:1637–1654, October 2008. doi: 10.1111/j.1365-2966.2008.13699.x.

C. Bildfell, H. Hoekstra, A. Babul, D. Sand, M. Graham, J. Willis, S. Urquhart, A. Mahdavi, C. Pritchet, D. Zaritsky, J. Franse, and P. Langelaan. Evolution of the red sequence giant to dwarf ratio in galaxy clusters out to z
0.5. , 425:204–221, September 2012. doi: 10.1111/j.1365-2966.2012.21426.x.

B. Binggeli, A. Sandage, and G. A. Tammann. The luminosity function of galaxies. , 26:509–560, 1988. doi: 10.1146/annurev.aa.26.090188.002453.

A. Biviano, F. Durret, D. Gerbal, O. Le Fevre, C. Lobo, A. Mazure, and E. Slezak. Unveiling hidden structures in the Coma cluster. , 311:95–112, July 1996.

M. R. Blanton, D. W. Hogg, N. A. Bahcall, I. K. Baldry, J. Brinkmann, I. Csabai, D. Eisenstein, M. Fukugita, J. E. Gunn, Ž. Ivezić, D. Q. Lamb, R. H. Lupton, J. Loveday, J. A. Munn, R. C. Nichol, S. Okamura, D. J. Schlegel, K. Shimasaku, M. A. Strauss, M. S. Vogeley, and D. H. Weinberg. The Broadband Optical Properties of Galaxies with Redshifts 0.02z0.22. , 594:186–207, September 2003. doi: 10.1086/375528.

M. R. Blanton, D. Eisenstein, D. W. Hogg, D. J. Schlegel, and J. Brinkmann. Relationship between Environment and the Broadband Optical Properties of Galaxies in the Sloan Digital Sky Survey. , 629:143–157, August 2005. doi: 10.1086/422897.

A. Boselli and G. Gavazzi. Environmental Effects on Late-Type Galaxies in Nearby Clusters. , 118:517–559, April 2006. doi: 10.1086/500691.

R. G. Bower, J. R. Lucey, and R. S. Ellis. Precision Photometry of Early Type Galaxies in the Coma and Virgo Clusters - a Test of the Universality of the Colour / Magnitude Relation - Part Two - Analysis. , 254:601, February 1992.

R. G. Bower, A. J. Benson, R. Malbon, J. C. Helly, C. S. Frenk, C. M. Baugh, S. Cole, and C. G. Lacey. Breaking the hierarchy of galaxy formation. , 370: 645–655, August 2006. doi: 10.1111/j.1365-2966.2006.10519.x.

B. C. Bromley, W. H. Press, H. Lin, and R. P. Kirshner. Spectral Classification and Luminosity Function of Galaxies in the Las Campanas Redshift Survey. , 505: 25–36, September 1998. doi: 10.1086/306144.

H. Butcher and A. Oemler, Jr. The evolution of galaxies in clusters. I - ISIT photometry of C1 0024+1654 and 3C 295. , 219:18–30, January 1978. doi: 10.1086/155751.

H. Butcher and A. Oemler, Jr. The evolution of galaxies in clusters. V - A study of populations since Z approximately equal to 0.5. , 285:426–438, October 1984. doi: 10.1086/162519.

E. T. Byram, T. A. Chubb, and H. Friedman. Cosmic X-ray Sources, Galactic and Extragalactic. *Science*, 152:66–71, April 1966. doi: 10.1126/science.152.3718.66.

M. Capaccioli. Photometry of early-type galaxies and the R exp 1/4 law. In H. G. Corwin, Jr. and L. Bottinelli, editors, *World of Galaxies (Le Monde des Galaxies)*, pages 208–227, 1989.

P. Capak, R. G. Abraham, R. S. Ellis, B. Mobasher, N. Scoville, K. Sheth, and A. Koekemoer. The Effects of Environment on Morphological Evolution at 0z1.2 in the COSMOS Survey. , 172:284–294, September 2007. doi: 10.1086/518424.

J. E. Carlstrom, G. P. Holder, and E. D. Reese. Cosmology with the Sunyaev-Zel'dovich Effect. , 40:643–680, 2002. doi: 10.1146/annurev.astro.40.060401.093803.

A. Cavaliere and R. Fusco-Femiano. X-rays from hot plasma in clusters of galaxies. , 49:137–144, May 1976.

A. G. Cavaliere, H. Gursky, and W. H. Tucker. Extragalactic X-ray Sources and Associations of Galaxies. , 231:437–438, June 1971. doi: 10.1038/231437a0.

L. Chiappetti, N. Clerc, F. Pacaud, M. Pierre, A. Gueguen, L. Paioro, M. Polletta, O. Melnyk, A. Elyiv, J. Surdej, and L. Faccioli. The XMM-LSS catalogue: X-ray sources and associated multiwavelength data. Version II. *ArXiv e-prints*, November 2012.

D. Christlein and A. I. Zabludoff. Galaxy Luminosity Functions from Deep Spectroscopic Samples of Rich Clusters. , 591:764–783, July 2003. doi: 10.1086/375529.

A. Chung, J. H. van Gorkom, J. D. P. Kenney, and B. Vollmer. Virgo Galaxies with Long One-sided H I Tails. , 659:L115–L119, April 2007. doi: 10.1086/518034.

M. Colless, G. Dalton, S. Maddox, W. Sutherland, P. Norberg, S. Cole, J. Bland-Hawthorn, T. Bridges, R. Cannon, C. Collins, W. Couch, N. Cross, K. Deeley, R. De Propris, S. P. Driver, G. Efstathiou, R. S. Ellis, C. S. Frenk, K. Glazebrook, C. Jackson, O. Lahav, I. Lewis, S. Lumsden, D. Madgwick, J. A. Peacock, B. A. Peterson, I. Price, M. Seaborne, and K. Taylor. The 2dF Galaxy Redshift Survey: spectra and redshifts. , 328:1039–1063, December 2001. doi: 10.1046/j.1365-8711.2001.04902.x.

M. C. Cooper, J. A. Newman, A. L. Coil, D. J. Croton, B. F. Gerke, R. Yan, M. Davis, S. M. Faber, P. Guhathakurta, D. C. Koo, B. J. Weiner, and C. N. A. Willmer. The DEEP2 galaxy redshift survey: evolution of the colour-density relation at 0.4 z 1.35. , 376:1445–1459, April 2007. doi: 10.1111/j.1365-2966.2007.11534.x.

L. Cortese, G. Gavazzi, A. Boselli, P. Franzetti, R. C. Kennicutt, K. O'Neil, and S. Sakai. Witnessing galaxy preprocessing in the local Universe: the case of a star-bursting group falling into Abell 1367. , 453:847–861, July 2006. doi: 10.1051/0004-6361:20064873.

L. Cortese, D. Marcillac, J. Richard, H. Bravo-Alfaro, J.-P. Kneib, G. Rieke, G. Covone, E. Egami, J. Rigby, O. Czoske, and J. Davies. The strong transformation of spiral galaxies infalling into massive clusters at z ˜ 0.2. , 376:157–172, March 2007. doi: 10.1111/j.1365-2966.2006.11369.x.

L. L. Cowie and A. Songaila. Thermal evaporation of gas within galaxies by a hot intergalactic medium. , 266:501–503, April 1977. doi: 10.1038/266501a0.

L. L. Cowie, A. Songaila, E. M. Hu, and J. G. Cohen. New Insight on Galaxy Formation and Evolution From Keck Spectroscopy of the Hawaii Deep Fields. , 112:839, September 1996. doi: 10.1086/118058.

T. J. Cox, P. Jonsson, R. S. Somerville, J. R. Primack, and A. Dekel. The effect of galaxy mass ratio on merger-driven starbursts. , 384:386–409, February 2008. doi: 10.1111/j.1365-2966.2007.12730.x.

R. Coziol and I. Plauchu-Frayn. Evidence for Tidal Interactions and Mergers as the Origin of Galaxy Morphology Evolution in Compact Groups. , 133:2630–2642, June 2007. doi: 10.1086/513514.

A. Cuoco, F. Iocco, G. Mangano, G. Miele, O. Pisanti, and P. D. Serpico. Present Status of Primordial Nucleosynthesis after Wmap:. *International Journal of Modern Physics A*, 19:4431–4453, 2004. doi: 10.1142/S0217751X04019548.

T. Dahlén, C. Fransson, and M. Näslund. The galaxy population of Cl1601+42 at. , 330:167–183, February 2002. doi: 10.1046/j.1365-8711.2002.05054.x.

T. Dahlén, C. Fransson, G. Östlin, and M. Näslund. The galaxy population of intermediate-redshift clusters. , 350:253–266, May 2004. doi: 10.1111/j.1365-2966.2004.07638.x.

E. de Filippis, M. Paolillo, G. Longo, F. La Barbera, R. R. de Carvalho, and R. Gal. The luminosity function of the NoSOCS galaxy cluster sample. , 414:2771–2784, July 2011. doi: 10.1111/j.1365-2966.2011.18596.x.

G. De Lucia, V. Springel, S. D. M. White, D. Croton, and G. Kauffmann. The formation history of elliptical galaxies. , 366:499–509, February 2006. doi: 10.1111/j.1365-2966.2005.09879.x.

G. De Lucia, B. M. Poggianti, A. Aragón-Salamanca, S. D. M. White, D. Zaritsky, D. Clowe, C. Halliday, P. Jablonka, A. von der Linden, B. Milvang-Jensen, R. Pelló, G. Rudnick, R. P. Saglia, and L. Simard. The build-up of the colour-magnitude relation in galaxy clusters since z ˜ 0.8. , 374:809–822, January 2007. doi: 10.1111/j.1365-2966.2006.11199.x.

R. De Propris, M. Colless, S. P. Driver, W. Couch, J. A. Peacock, I. K. Baldry, C. M. Baugh, J. Bland-Hawthorn, T. Bridges, R. Cannon, S. Cole, C. Collins, N. Cross, G. B. Dalton, G. Efstathiou, R. S. Ellis, C. S. Frenk, K. Glazebrook, E. Hawkins, C. Jackson, O. Lahav, I. Lewis, S. Lumsden, S. Maddox, D. S. Madgwick, P. Norberg, W. Percival, B. Peterson, W. Sutherland, and K. Taylor. The 2dF Galaxy Redshift Survey: the luminosity function of cluster galaxies. , 342:725–737, July 2003. doi: 10.1046/j.1365-8711.2003.06510.x.

V. Desai, J. J. Dalcanton, A. Aragón-Salamanca, P. Jablonka, B. Poggianti, S. M. Gogarten, L. Simard, B. Milvang-Jensen, G. Rudnick, D. Zaritsky, D. Clowe, C. Halliday, R. Pelló, R. Saglia, and S. White. The Morphological Content of 10 EDisCS Clusters at 0.5 z 0.8. , 660:1151–1164, May 2007. doi: 10.1086/513310.

P. Di Matteo, F. Combes, A.-L. Melchior, and B. Semelin. Star formation efficiency in galaxy interactions and mergers: a statistical study. , 468:61–81, June 2007. doi: 10.1051/0004-6361:20066959.

A. Dressler. A catalog of morphological types in 55 rich clusters of galaxies. , 42: 565–609, April 1980. doi: 10.1086/190663.

A. Dressler, A. Oemler, Jr., W. B. Sparks, and R. A. Lucas. New images of the distant, rich cluster CL 0939+4713 with WFPC2. , 435:L23–L26, November 1994. doi: 10.1086/187585.

A. Dressler, A. Oemler, Jr., W. J. Couch, I. Smail, R. S. Ellis, A. Barger, H. Butcher, B. M. Poggianti, and R. M. Sharples. Evolution since Z = 0.5 of the Morphology-Density Relation for Clusters of Galaxies. , 490:577, December 1997. doi: 10.1086/304890.

S. P. Driver, W. J. Couch, and S. Phillipps. Luminosity distributions within rich clusters - III. A comparative study of seven Abell/ACO clusters. , 301:369–381, December 1998. doi: 10.1046/j.1365-8711.1998.01995.x.

S. P. Driver, P. D. Allen, A. W. Graham, E. Cameron, J. Liske, S. C. Ellis, N. J. G. Cross, R. De Propris, S. Phillipps, and W. J. Couch. The Millennium Galaxy Catalogue: morphological classification and bimodality in the colour-concentration plane. , 368:414–434, May 2006. doi: 10.1111/j.1365-2966.2006.10126.x.

J. Dubinski and R. G. Carlberg. The structure of cold dark matter halos. , 378: 496–503, September 1991. doi: 10.1086/170451.

P.-A. Duc, B. M. Poggianti, D. Fadda, D. Elbaz, H. Flores, P. Chanial, A. Franceschini, A. Moorwood, and C. Cesarsky. Hidden star-formation in the cluster of galaxies Abell 1689. , 382:60–83, January 2002. doi: 10.1051/0004-6361:20011754.

O. J. Eggen, D. Lynden-Bell, and A. R. Sandage. Evidence from the motions of old stars that the Galaxy collapsed. , 136:748, November 1962. doi: 10.1086/147433.

E. Ellingson, H. Lin, H. K. C. Yee, and R. G. Carlberg. The Evolution of Population Gradients in Galaxy Clusters: The Butcher-Oemler Effect and Cluster Infall. , 547: 609–622, February 2001. doi: 10.1086/318423.

S. Ettori. Note on a polytropic β-model to fit the X-ray surface brightness of clusters of galaxies. , 311:313–316, January 2000. doi: 10.1046/j.1365-8711.2000.03037.x.

S. M. Faber, C. N. A. Willmer, C. Wolf, D. C. Koo, B. J. Weiner, J. A. Newman, M. Im, A. L. Coil, C. Conroy, M. C. Cooper, M. Davis, D. P. Finkbeiner, B. F. Gerke, K. Gebhardt, E. J. Groth, P. Guhathakurta, J. Harker, N. Kaiser, S. Kassin, M. Kleinheinrich, N. P. Konidaris, R. G. Kron, L. Lin, G. Luppino, D. S. Madgwick, K. Meisenheimer, K. G. Noeske, A. C. Phillips, V. L. Sarajedini, R. P. Schiavon, L. Simard, A. S. Szalay, N. P. Vogt, and R. Yan. Galaxy Luminosity Functions to z˜1 from DEEP2 and COMBO-17: Implications for Red Galaxy Formation. , 665: 265–294, August 2007. doi: 10.1086/519294.

B. W. Fairley, L. R. Jones, D. A. Wake, C. A. Collins, D. J. Burke, R. C. Nichol, and A. K. Romer. Galaxy colours in high-redshift, X-ray-selected clusters - I. Blue galaxy fractions in eight clusters. , 330:755–767, March 2002. doi: 10.1046/j.1365-8711.2002.05121.x.

S. Farrens, F. B. Abdalla, E. S. Cypriano, C. Sabiu, and C. Blake. Friends-of-friends groups and clusters in the 2SLAQ catalogue. , 417:1402–1416, October 2011. doi: 10.1111/j.1365-2966.2011.19356.x.

C. Fedeli and M. Bartelmann. Selection effects on X-ray and strong-lensing clusters in various cosmologies. , 474:355–364, November 2007. doi: 10.1051/0004-6361:20077572.

J. E. Felten, R. J. Gould, W. A. Stein, and N. J. Woolf. X-Rays from the Coma Cluster of Galaxies. , 146:955–958, December 1966. doi: 10.1086/148972.

H. C. Ferguson and A. Sandage. Population studies in groups and clusters of galaxies. IV - Comparison of the luminosity functions and morphological-type distributions in seven nearby groups. , 101:765–782, March 1991. doi: 10.1086/115721.

A. Finoguenov, T. H. Reiprich, and H. Böhringer. Details of the mass-temperature relation for clusters of galaxies. , 368:749–759, March 2001. doi: 10.1051/0004-6361:20010080.

A. S. Font, R. G. Bower, I. G. McCarthy, A. J. Benson, C. S. Frenk, J. C. Helly, C. G. Lacey, C. M. Baugh, and S. Cole. The colours of satellite galaxies in groups and clusters. , 389:1619–1629, October 2008. doi: 10.1111/j.1365-2966.2008.13698.x.

Y. Fujita. Ram-Pressure Stripping of Galaxies in High-Redshift Clusters and the Influence of Intracluster Medium Heating. , 550:612–621, April 2001. doi: 10.1086/319811.

Y. Fujita. Pre-Processing of Galaxies before Entering a Cluster. , 56:29–43, February 2004.

Y. Fukazawa, K. Makishima, and T. Ohashi. ASCA Compilation of X-Ray Properties of Hot Gas in Elliptical Galaxies and Galaxy Clusters: Two Breaks in the Temperature Dependences. , 56:965–1009, December 2004.

J. E. Geach, I. Smail, S. M. Moran, T. Treu, and R. S. Ellis. The Nature of Dusty Starburst Galaxies in a Rich Cluster at z = 0.4: The Progenitors of Lenticulars? , 691:783–793, January 2009. doi: 10.1088/0004-637X/691/1/783.

R. Giacconi, S. Murray, H. Gursky, E. Kellogg, E. Schreier, and H. Tananbaum. The Uhuru catalog of X-ray sources. , 178:281–308, December 1972. doi: 10.1086/151790.

D. G. Gilbank, H. K. C. Yee, E. Ellingson, M. D. Gladders, Y.-S. Loh, L. F. Barrientos, and W. A. Barkhouse. The Red-Sequence Luminosity Function in Galaxy Clusters since z ˜ 1. , 673:742–751, February 2008. doi: 10.1086/524398.

M. D. Gladders and H. K. C. Yee. A New Method For Galaxy Cluster Detection. I. The Algorithm. , 120:2148–2162, October 2000. doi: 10.1086/301557.

P. L. Gómez, R. C. Nichol, C. J. Miller, M. L. Balogh, T. Goto, A. I. Zabludoff, A. K. Romer, M. Bernardi, R. Sheth, A. M. Hopkins, F. J. Castander, A. J. Connolly, D. P. Schneider, J. Brinkmann, D. Q. Lamb, M. SubbaRao, and D. G. York. Galaxy Star Formation as a Function of Environment in the Early Data Release of the Sloan Digital Sky Survey. , 584:210–227, February 2003. doi: 10.1086/345593.

T. Goto, M. Sekiguchi, R. C. Nichol, N. A. Bahcall, R. S. J. Kim, J. Annis, Ž. Ivezić, J. Brinkmann, G. S. Hennessy, G. P. Szokoly, and D. L. Tucker. The Cut-and-Enhance Method: Selecting Clusters of Galaxies from the Sloan Digital Sky Survey Commissioning Data. , 123:1807–1825, April 2002. doi: 10.1086/339303.

T. Goto, M. Postman, N. J. G. Cross, G. D. Illingworth, K. Tran, D. Magee, M. Franx, N. Benítez, R. J. Bouwens, R. Demarco, H. C. Ford, N. L. Homeier, A. R. Martel, F. Menanteau, M. Clampin, G. F. Hartig, D. R. Ardila, F. Bartko, J. P. Blakeslee, L. D. Bradley, T. J. Broadhurst, R. A. Brown, C. J. Burrows, E. S. Cheng, P. D. Feldman, D. A. Golimowski, C. Gronwall, B. Holden, L. Infante, M. J. Jee, J. E. Krist, M. P. Lesser, S. Mei, G. R. Meurer, G. K. Miley, V. Motta, R. Overzier, M. Sirianni, W. B. Sparks, H. D. Tran, Z. I. Tsvetanov, R. L. White, W. Zheng, and A. Zirm. Luminosity Functions of the Galaxy Cluster MS 1054-0321 at z=0.83 based on ACS Photometry. , 621:188–200, March 2005. doi: 10.1086/427492.

N. A. Grogin, D. D. Kocevski, S. M. Faber, H. C. Ferguson, A. M. Koekemoer, A. G. Riess, V. Acquaviva, D. M. Alexander, O. Almaini, M. L. N. Ashby, M. Barden, E. F. Bell, F. Bournaud, T. M. Brown, K. I. Caputi, S. Casertano, P. Cassata, M. Castellano, P. Challis, R.-R. Chary, E. Cheung, M. Cirasuolo, C. J. Conselice, A. Roshan Cooray, D. J. Croton, E. Daddi, T. Dahlen, R. Davé, D. F. de Mello,

A. Dekel, M. Dickinson, T. Dolch, J. L. Donley, J. S. Dunlop, A. A. Dutton, D. Elbaz, G. G. Fazio, A. V. Filippenko, S. L. Finkelstein, A. Fontana, J. P. Gardner, P. M. Garnavich, E. Gawiser, M. Giavalisco, A. Grazian, Y. Guo, N. P. Hathi, B. Häussler, P. F. Hopkins, J.-S. Huang, K.-H. Huang, S. W. Jha, J. S. Kartaltepe, R. P. Kirshner, D. C. Koo, K. Lai, K.-S. Lee, W. Li, J. M. Lotz, R. A. Lucas, P. Madau, P. J. McCarthy, E. J. McGrath, D. H. McIntosh, R. J. McLure, B. Mobasher, L. A. Moustakas, M. Mozena, K. Nandra, J. A. Newman, S.-M. Niemi, K. G. Noeske, C. J. Papovich, L. Pentericci, A. Pope, J. R. Primack, A. Rajan, S. Ravindranath, N. A. Reddy, A. Renzini, H.-W. Rix, A. R. Robaina, S. A. Rodney, D. J. Rosario, P. Rosati, S. Salimbeni, C. Scarlata, B. Siana, L. Simard, J. Smidt, R. S. Somerville, H. Spinrad, A. N. Straughn, L.-G. Strolger, O. Telford, H. I. Teplitz, J. R. Trump, A. van der Wel, C. Villforth, R. H. Wechsler, B. J. Weiner, T. Wiklind, V. Wild, G. Wilson, S. Wuyts, H.-J. Yan, and M. S. Yun. CANDELS: The Cosmic Assembly Near-infrared Deep Extragalactic Legacy Survey. , 197:35, December 2011. doi: 10.1088/0067-0049/197/2/35.

J. E. Gunn and J. R. Gott, III. On the Infall of Matter Into Clusters of Galaxies and Some Effects on Their Evolution. , 176:1, August 1972. doi: 10.1086/151605.

S. M. Hansen, T. A. McKay, R. H. Wechsler, J. Annis, E. S. Sheldon, and A. Kimball. Measurement of Galaxy Cluster Sizes, Radial Profiles, and Luminosity Functions from SDSS Photometric Data. , 633:122–137, November 2005. doi: 10.1086/444554.

S. M. Hansen, E. S. Sheldon, R. H. Wechsler, and B. P. Koester. The Galaxy Content of SDSS Clusters and Groups. , 699:1333–1353, July 2009. doi: 10.1088/0004-637X/699/2/1333.

B. Häussler, D. H. McIntosh, M. Barden, E. F. Bell, H.-W. Rix, A. Borch, S. V. W. Beckwith, J. A. R. Caldwell, C. Heymans, K. Jahnke, S. Jogee, S. E. Koposov, K. Meisenheimer, S. F. Sánchez, R. S. Somerville, L. Wisotzki, and C. Wolf. GEMS: Galaxy Fitting Catalogs and Testing Parametric Galaxy Fitting Codes: GALFIT and GIM2D. , 172:615–633, October 2007. doi: 10.1086/518836.

J. D. Hernández-Fernández, J. M. Vílchez, and J. Iglesias-Páramo. Disentangling the Role of Environmental Processes in Galaxy Clusters. , 751:54, May 2012. doi: 10.1088/0004-637X/751/1/54.

M. Hilton, C. Collins, R. De Propris, I. K. Baldry, C. M. Baugh, J. Bland-Hawthorn, T. Bridges, R. Cannon, S. Cole, M. Colless, W. J. Couch, G. B. Dalton, S. P. Driver, G. Efstathiou, R. S. Ellis, C. S. Frenk, K. Glazebrook, C. A. Jackson, O. Lahav, I. Lewis, S. Lumsden, S. J. Maddox, D. Madgwick, P. Norberg, J. A. Peacock, B. A. Peterson, W. Sutherland, and K. Taylor. The 2dF Galaxy Redshift Survey: correlation with the ROSAT-ESO flux-limited X-ray galaxy cluster survey. , 363: 661–674, October 2005. doi: 10.1111/j.1365-2966.2005.09470.x.

B. P. Holden, G. D. Illingworth, M. Franx, J. P. Blakeslee, M. Postman, D. D. Kelson, A. van der Wel, R. Demarco, D. K. Magee, K.-V. Tran, A. Zirm, H. Ford, P. Rosati, and N. Homeier. Mass Selection and the Evolution of the Morphology-Density Relation from z = 0.8 to 0. , 670:190–205, November 2007. doi: 10.1086/521777.

G. P. Holder, J. J. Mohr, J. E. Carlstrom, A. E. Evrard, and E. M. Leitch. Expectations for an Interferometric Sunyaev-Zeldovich Effect Survey for Galaxy Clusters. , 544:629–635, December 2000. doi: 10.1086/317227.

N. L. Homeier, M. Postman, F. Menanteau, J. P. Blakeslee, S. Mei, R. Demarco, H. C. Ford, G. D. Illingworth, and A. Zirm. Imprints of Environment on Cluster and Field Late-Type Galaxies at z˜1. , 131:143–157, January 2006. doi: 10.1086/498675.

A. M. Hopkins. On the Evolution of Star-forming Galaxies. , 615:209–221, November 2004. doi: 10.1086/424032.

A. M. Hopkins and J. F. Beacom. On the Normalization of the Cosmic Star Formation History. , 651:142–154, November 2006. doi: 10.1086/506610.

D. J. Horner. *X-ray scaling laws for galaxy clusters and groups*. PhD thesis, University of Maryland College Park, 2001.

J. P. Huchra and M. J. Geller. Groups of galaxies. I - Nearby groups. , 257:423–437, June 1982. doi: 10.1086/160000.

R. A. Ibata, G. Gilmore, and M. J. Irwin. A dwarf satellite galaxy in Sagittarius. , 370:194–196, July 1994. doi: 10.1038/370194a0.

N. Kaiser. Evolution and clustering of rich clusters. , 222:323–345, September 1986.

P. Kampczyk, S. J. Lilly, L. de Ravel, O. Le Fèvre, M. Bolzonella, C. M. Carollo, C. Diener, C. Knobel, K. Kovač, C. Maier, A. Renzini, M. T. Sargent, D. Vergani,

U. Abbas, S. Bardelli, A. Bongiorno, R. Bordoloi, K. Caputi, T. Contini, G. Coppa, O. Cucciati, S. de la Torre, P. Franzetti, B. Garilli, A. Iovino, J.-P. Kneib, A. M. Koekemoer, F. Lamareille, J.-F. Le Borgne, V. Le Brun, A. Leauthaud, V. Mainieri, M. Mignoli, R. Pello, Y. Peng, E. Perez Montero, E. Ricciardelli, M. Scodeggio, J. D. Silverman, M. Tanaka, L. Tasca, L. Tresse, G. Zamorani, E. Zucca, D. Bottini, A. Cappi, P. Cassata, A. Cimatti, M. Fumana, L. Guzzo, J. Kartaltepe, C. Marinoni, H. J. McCracken, P. Memeo, B. Meneux, P. Oesch, C. Porciani, L. Pozzetti, and R. Scaramella. Environmental Effects in the Interaction and Merging of Galaxies in zCOSMOS. , 762:43, January 2013. doi: 10.1088/0004-637X/762/1/43.

D. Kawata and J. S. Mulchaey. Strangulation in Galaxy Groups. , 672:L103–L106, January 2008. doi: 10.1086/526544.

E. Kellogg, H. Gursky, H. Tananbaum, R. Giacconi, and K. Pounds. The Extended X-Ray Source at M87. , 174:L65, June 1972. doi: 10.1086/180950.

S. Khochfar, J. Silk, R. A. Windhorst, and R. E. Ryan, Jr. The Evolving Faint End of the Luminosity Function. , 668:L115–L118, October 2007. doi: 10.1086/522790.

A. L. Kinney, D. Calzetti, R. C. Bohlin, K. McQuade, T. Storchi-Bergmann, and H. R. Schmitt. Template Ultraviolet to Near-Infrared Spectra of Star-forming Galaxies and Their Application to K-Corrections. , 467:38, August 1996. doi: 10.1086/177583.

T. Kodama and R. G. Bower. Reconstructing the history of star formation in rich cluster cores. , 321:18–36, February 2001. doi: 10.1046/j.1365-8711.2001.03981.x.

T. Kodama, T. Yamada, M. Akiyama, K. Aoki, M. Doi, H. Furusawa, T. Fuse, M. Imanishi, C. Ishida, M. Iye, M. Kajisawa, H. Karoji, N. Kobayashi, Y. Komiyama, G. Kosugi, Y. Maeda, S. Miyazaki, Y. Mizumoto, T. Morokuma, F. Nakata, J. Noumaru, R. Ogasawara, M. Ouchi, T. Sasaki, K. Sekiguchi, K. Shimasaku, C. Simpson, T. Takata, I. Tanaka, Y. Ueda, N. Yasuda, and M. Yoshida. Down-sizing in galaxy formation at z˜ 1 in the Subaru/XMM-Newton Deep Survey (SXDS). , 350:1005–1014, May 2004. doi: 10.1111/j.1365-2966.2004.07711.x.

A. M. Koekemoer, S. M. Faber, H. C. Ferguson, N. A. Grogin, D. D. Kocevski, D. C. Koo, K. Lai, J. M. Lotz, R. A. Lucas, E. J. McGrath, S. Ogaz, A. Rajan, A. G.

Riess, S. A. Rodney, L. Strolger, S. Casertano, M. Castellano, T. Dahlen, M. Dickinson, T. Dolch, A. Fontana, M. Giavalisco, A. Grazian, Y. Guo, N. P. Hathi, K.-H. Huang, A. van der Wel, H.-J. Yan, V. Acquaviva, D. M. Alexander, O. Almaini, M. L. N. Ashby, M. Barden, E. F. Bell, F. Bournaud, T. M. Brown, K. I. Caputi, P. Cassata, P. J. Challis, R.-R. Chary, E. Cheung, M. Cirasuolo, C. J. Conselice, A. Roshan Cooray, D. J. Croton, E. Daddi, R. Davé, D. F. de Mello, L. de Ravel, A. Dekel, J. L. Donley, J. S. Dunlop, A. A. Dutton, D. Elbaz, G. G. Fazio, A. V. Filippenko, S. L. Finkelstein, C. Frazer, J. P. Gardner, P. M. Garnavich, E. Gawiser, R. Gruetzbauch, W. G. Hartley, B. Häussler, J. Herrington, P. F. Hopkins, J.-S. Huang, S. W. Jha, A. Johnson, J. S. Kartaltepe, A. A. Khostovan, R. P. Kirshner, C. Lani, K.-S. Lee, W. Li, P. Madau, P. J. McCarthy, D. H. McIntosh, R. J. McLure, C. McPartland, B. Mobasher, H. Moreira, A. Mortlock, L. A. Moustakas, M. Mozena, K. Nandra, J. A. Newman, J. L. Nielsen, S. Niemi, K. G. Noeske, C. J. Papovich, L. Pentericci, A. Pope, J. R. Primack, S. Ravindranath, N. A. Reddy, A. Renzini, H.-W. Rix, A. R. Robaina, D. J. Rosario, P. Rosati, S. Salimbeni, C. Scarlata, B. Siana, L. Simard, J. Smidt, D. Snyder, R. S. Somerville, H. Spinrad, A. N. Straughn, O. Telford, H. I. Teplitz, J. R. Trump, C. Vargas, C. Villforth, C. R. Wagner, P. Wandro, R. H. Wechsler, B. J. Weiner, T. Wiklind, V. Wild, G. Wilson, S. Wuyts, and M. S. Yun. CANDELS: The Cosmic Assembly Near-infrared Deep Extragalactic Legacy SurveyThe Hubble Space Telescope Observations, Imaging Data Products, and Mosaics. , 197:36, December 2011. doi: 10.1088/0067-0049/197/2/36.

Y. Koyama, T. Kodama, M. Tanaka, K. Shimasaku, and S. Okamura. Dependence of the build-up of the colour-magnitude relation on cluster richness at z ˜ 0.8. , 382: 1719–1728, December 2007. doi: 10.1111/j.1365-2966.2007.12445.x.

R. B. Larson, B. M. Tinsley, and C. N. Caldwell. The evolution of disk galaxies and the origin of S0 galaxies. , 237:692–707, May 1980. doi: 10.1086/157917.

I. Lewis, M. Balogh, R. De Propris, W. Couch, R. Bower, A. Offer, J. Bland-Hawthorn, I. K. Baldry, C. Baugh, T. Bridges, R. Cannon, S. Cole, M. Colless, C. Collins, N. Cross, G. Dalton, S. P. Driver, G. Efstathiou, R. S. Ellis, C. S. Frenk, K. Glazebrook, E. Hawkins, C. Jackson, O. Lahav, S. Lumsden, S. Maddox, D. Madgwick, P. Norberg, J. A. Peacock, W. Percival, B. A. Peterson, W. Sutherland, and K. Taylor. The 2dF Galaxy Redshift Survey: the environmental depen-

dence of galaxy star formation rates near clusters. , 334:673–683, August 2002. doi: 10.1046/j.1365-8711.2002.05558.x.

I. H. Li, H. K. C. Yee, and E. Ellingson. Individual and Group Galaxies in CNOC1 Clusters. , 698:83–98, June 2009. doi: 10.1088/0004-637X/698/1/83.

S. J. Lilly, O. Le Fevre, F. Hammer, and D. Crampton. The Canada-France Redshift Survey: The Luminosity Density and Star Formation History of the Universe to Z approximately 1. , 460:L1, March 1996. doi: 10.1086/309975.

H. Lin, R. P. Kirshner, S. A. Shectman, S. D. Landy, A. Oemler, D. L. Tucker, and P. L. Schechter. The Luminosity Function of Galaxies in the Las Campanas Redshift Survey. , 464:60, June 1996. doi: 10.1086/177300.

C. T. Liu, P. Capak, B. Mobasher, T. A. D. Paglione, R. M. Rich, N. Z. Scoville, S. M. Tribiano, and N. D. Tyson. The Faint-End Slopes of Galaxy Luminosity Functions in the COSMOS Field. , 672:198–206, January 2008. doi: 10.1086/522361.

Y.-S. Loh, E. Ellingson, H. K. C. Yee, D. G. Gilbank, M. D. Gladders, and L. F. Barrientos. The Color Bimodality in Galaxy Clusters since z ˜ 0.9. , 680:214–223, June 2008. doi: 10.1086/587830.

J. Loveday, S. J. Maddox, G. Efstathiou, and B. A. Peterson. The Stromlo-APM redshift survey. 2: Variation of galaxy clustering with morphology and luminosity. , 442:457–468, April 1995. doi: 10.1086/175453.

T. Lu, D. G. Gilbank, M. L. Balogh, and A. Bognat. Recent arrival of faint cluster galaxies on the red sequence: luminosity functions from 119deg^2 of CFHTLS. , 399:1858–1876, November 2009. doi: 10.1111/j.1365-2966.2009.15418.x.

A. Mahdavi, H. Hoekstra, A. Babul, C. Bildfell, T. Jeltema, and J. P. Henry. Joint Analysis of Cluster Observations. II. Chandra/XMM-Newton X-Ray and Weak Lensing Scaling Relations for a Sample of 50 Rich Clusters of Galaxies. , 767:116, April 2013. doi: 10.1088/0004-637X/767/2/116.

J. Makino and P. Hut. Merger Rate of Equal-Mass Spherical Galaxies. , 481:83, May 1997. doi: 10.1086/304013.

D. T. Maltby, M. E. Gray, A. Aragón-Salamanca, C. Wolf, E. F. Bell, S. Jogee, B. Häußler, F. D. Barazza, A. Böhm, and K. Jahnke. The environmental dependence of the structure of outer galactic discs in STAGES spiral galaxies. , 419: 669–686, January 2012. doi: 10.1111/j.1365-2966.2011.19727.x.

G. A. Mamon. Are cluster ellipticals the products of mergers? , 401:L3–L6, December 1992. doi: 10.1086/186656.

V. E. Margoniner, R. R. de Carvalho, R. R. Gal, and S. G. Djorgovski. The Butcher-Oemler Effect in 295 Clusters: Strong Redshift Evolution and Cluster Richness Dependence. , 548:L143–L146, February 2001. doi: 10.1086/319099.

C. B. Markwardt. Non-linear Least-squares Fitting in IDL with MPFIT. In D. A. Bohlender, D. Durand, and P. Dowler, editors, *Astronomical Data Analysis Software and Systems XVIII*, volume 411 of *Astronomical Society of the Pacific Conference Series*, page 251, September 2009.

F. R. Marleau and L. Simard. Quantitative Morphology of Galaxies in the Hubble Deep Field. , 507:585–600, November 1998. doi: 10.1086/306356.

T. A. Matthews, W. W. Morgan, and M. Schmidt. A Discussion of Galaxies Indentified with Radio Sources. , 140:35, July 1964. doi: 10.1086/147890.

I. G. McCarthy, C. S. Frenk, A. S. Font, C. G. Lacey, R. G. Bower, N. L. Mitchell, M. L. Balogh, and T. Theuns. Ram pressure stripping the hot gaseous haloes of galaxies in groups and clusters. , 383:593–605, January 2008. doi: 10.1111/j.1365-2966.2007.12577.x.

S. L. McGee, M. L. Balogh, R. G. Bower, A. S. Font, and I. G. McCarthy. The accretion of galaxies into groups and clusters. , 400:937–950, December 2009. doi: 10.1111/j.1365-2966.2009.15507.x.

J. F. Meekins, G. Fritz, T. A. Chubb, and H. Friedman. Physical Sciences: X-rays from the Coma Cluster of Galaxies. , 231:107–108, May 1971. doi: 10.1038/231107a0.

J.-B. Melin, J. G. Bartlett, and J. Delabrouille. The selection function of SZ cluster surveys. , 429:417–426, January 2005. doi: 10.1051/0004-6361:20048093.

J. C. Mihos and L. Hernquist. Gasdynamics and Starbursts in Major Mergers. , 464: 641, June 1996. doi: 10.1086/177353.

B. Moore, N. Katz, G. Lake, A. Dressler, and A. Oemler. Galaxy harassment and the evolution of clusters of galaxies. , 379:613–616, February 1996. doi: 10.1038/379613a0.

B. Moore, G. Lake, T. Quinn, and J. Stadel. On the survival and destruction of spiral galaxies in clusters. , 304:465–474, April 1999. doi: 10.1046/j.1365-8711.1999.02345.x.

J. S. Mulchaey, D. S. Davis, R. F. Mushotzky, and D. Burstein. An X-Ray Atlas of Groups of Galaxies. , 145:39–64, March 2003. doi: 10.1086/345736.

R. F. Mushotzky and C. A. Scharf. The Luminosity-Temperature Relation at z=0.4 for Clusters of Galaxies. , 482:L13, June 1997. doi: 10.1086/310676.

P. E. J. Nulsen. Transport processes and the stripping of cluster galaxies. , 198: 1007–1016, March 1982.

A. Oemler, Jr., A. Dressler, D. Kelson, J. Rigby, B. M. Poggianti, J. Fritz, G. Morrison, and I. Smail. Abell 851 and the Role of Starbursts in Cluster Galaxy Evolution. , 693:152, March 2009. doi: 10.1088/0004-637X/693/1/152.

K. A. Oman, M. J. Hudson, and P. S. Behroozi. Disentangling satellite galaxy populations using orbit tracking in simulations. , 431:2307–2316, May 2013. doi: 10.1093/mnras/stt328.

F. Pacaud, M. Pierre, C. Adami, B. Altieri, S. Andreon, L. Chiappetti, A. Detal, P.-A. Duc, G. Galaz, A. Gueguen, J.-P. Le Fèvre, G. Hertling, C. Libbrecht, J.-B. Melin, T. J. Ponman, H. Quintana, A. Refregier, P.-G. Sprimont, J. Surdej, I. Valtchanov, J. P. Willis, D. Alloin, M. Birkinshaw, M. N. Bremer, O. Garcet, C. Jean, L. R. Jones, O. Le Fèvre, D. Maccagni, A. Mazure, D. Proust, H. J. A. Röttgering, and G. Trinchieri. The XMM-LSS survey: the Class 1 cluster sample over the initial 5 deg^2 and its cosmological modelling. , 382:1289–1308, December 2007. doi: 10.1111/j.1365-2966.2007.12468.x.

M. Paolillo, S. Andreon, G. Longo, E. Puddu, R. R. Gal, R. Scaramella, S. G. Djorgovski, and R. de Carvalho. Luminosity function of clusters of galaxies. , 367: 59–71, February 2001. doi: 10.1051/0004-6361:20000442.

D. R. Patton, C. J. Pritchet, R. G. Carlberg, R. O. Marzke, H. K. C. Yee, P. B. Hall, H. Lin, S. L. Morris, M. Sawicki, C. W. Shepherd, and G. D. Wirth. Dynamically Close Galaxy Pairs and Merger Rate Evolution in the CNOC2 Redshift Survey. , 565:208–222, January 2002. doi: 10.1086/324543.

M. Pierre, I. Valtchanov, B. Altieri, S. Andreon, M. Bolzonella, M. Bremer, L. Disseau, S. Dos Santos, P. Gandhi, C. Jean, F. Pacaud, A. Read, A. Refregier, J. Willis, C. Adami, D. Alloin, M. Birkinshaw, L. Chiappetti, A. Cohen, A. Detal, P.-A. Duc, E. Gosset, J. Hjorth, L. Jones, O. Le Fèvre, C. Lonsdale, D. Maccagni, A. Mazure, B. McBreen, H. McCracken, Y. Mellier, T. Ponman, H. Quintana, H. Rottgering, A. Smette, J. Surdej, J.-L. Starck, L. Vigroux, and S. White. The XMM-LSS survey. Survey design and first results. , 9:011, September 2004. doi: 10.1088/1475-7516/2004/09/011.

K. A. Pimbblet and P. C. Jensen. The role of stellar mass and environment for cluster blue fraction, AGN fraction and star formation indicators from a targeted analysis of Abell 1691. , 426:1632–1646, October 2012. doi: 10.1111/j.1365-2966.2012.21855.x.

K. A. Pimbblet, I. Smail, T. Kodama, W. J. Couch, A. C. Edge, A. I. Zabludoff, and E. O'Hely. The Las Campanas/AAT Rich Cluster Survey - II. The environmental dependence of galaxy colours in clusters at z˜0.1. , 331:333–350, March 2002. doi: 10.1046/j.1365-8711.2002.05186.x.

B. M. Poggianti, I. Smail, A. Dressler, W. J. Couch, A. J. Barger, H. Butcher, R. S. Ellis, and A. Oemler, Jr. The Star Formation Histories of Galaxies in Distant Clusters. , 518:576–593, June 1999. doi: 10.1086/307322.

B. M. Poggianti, A. von der Linden, G. De Lucia, V. Desai, L. Simard, C. Halliday, A. Aragón-Salamanca, R. Bower, J. Varela, P. Best, D. I. Clowe, J. Dalcanton, P. Jablonka, B. Milvang-Jensen, R. Pello, G. Rudnick, R. Saglia, S. D. M. White, and D. Zaritsky. The Evolution of the Star Formation Activity in Galaxies and Its Dependence on Environment. , 642:188–215, May 2006. doi: 10.1086/500666.

T. J. Ponman and D. Bertram. Hot gas and dark matter in a compact galaxy group. , 363:51–54, May 1993. doi: 10.1038/363051a0.

P. Popesso, H. Böhringer, M. Romaniello, and W. Voges. RASS-SDSS galaxy cluster survey. II. A unified picture of the cluster luminosity function. , 433:415–429, April 2005. doi: 10.1051/0004-6361:20041870.

P. Popesso, A. Biviano, H. Böhringer, and M. Romaniello. RASS-SDSS Galaxy cluster survey. IV. A ubiquitous dwarf galaxy population in clusters. , 445:29–42, January 2006. doi: 10.1051/0004-6361:20052954.

M. Postman, M. Franx, N. J. G. Cross, B. Holden, H. C. Ford, G. D. Illingworth, T. Goto, R. Demarco, P. Rosati, J. P. Blakeslee, K.-V. Tran, N. Benítez, M. Clampin, G. F. Hartig, N. Homeier, D. R. Ardila, F. Bartko, R. J. Bouwens, L. D. Bradley, T. J. Broadhurst, R. A. Brown, C. J. Burrows, E. S. Cheng, P. D. Feldman, D. A. Golimowski, C. Gronwall, L. Infante, R. A. Kimble, J. E. Krist, M. P. Lesser, A. R. Martel, S. Mei, F. Menanteau, G. R. Meurer, G. K. Miley, V. Motta, M. Sirianni, W. B. Sparks, H. D. Tran, Z. I. Tsvetanov, R. L. White, and W. Zheng. The Morphology-Density Relation in z ˜ 1 Clusters. , 623:721–741, April 2005. doi: 10.1086/428881.

G. W. Pratt, J. H. Croston, M. Arnaud, and H. Böhringer. Galaxy cluster X-ray luminosity scaling relations from a representative local sample (REXCESS). , 498: 361–378, May 2009. doi: 10.1051/0004-6361/200810994.

H.-W. Rix, M. Barden, S. V. W. Beckwith, E. F. Bell, A. Borch, J. A. R. Caldwell, B. Häussler, K. Jahnke, S. Jogee, D. H. McIntosh, K. Meisenheimer, C. Y. Peng, S. F. Sanchez, R. S. Somerville, L. Wisotzki, and C. Wolf. GEMS: Galaxy Evolution from Morphologies and SEDs. , 152:163–173, June 2004. doi: 10.1086/420885.

A. Robotham, S. Phillipps, and R. de Propris. The variation of the galaxy luminosity function with group properties. , 403:1812–1828, April 2010. doi: 10.1111/j.1365-2966.2010.16252.x.

E. Rozo, E. S. Rykoff, A. Evrard, M. Becker, T. McKay, R. H. Wechsler, B. P. Koester, J. Hao, S. Hansen, E. Sheldon, D. Johnston, J. Annis, and J. Frieman. Constraining the Scatter in the Mass-richness Relation of maxBCG Clusters with Weak Lensing and X-ray Data. , 699:768–781, July 2009. doi: 10.1088/0004-637X/699/1/768.

A. Saintonge, K.-V. H. Tran, and B. P. Holden. Spitzer/MIPS 24 μm Observations of Galaxy Clusters: An Increasing Fraction of Obscured Star-forming Members from z = 0.02 to z = 0.83. , 685:L113–L116, October 2008. doi: 10.1086/592730.

R. Sánchez-Janssen, J. A. L. Aguerri, and C. Muñoz-Tuñón. Properties of the Dwarf Galaxy Population in Galaxy Clusters. , 679:L77–L80, June 2008. doi: 10.1086/589617.

D. J. Sand, M. L. Graham, C. Bildfell, D. Zaritsky, C. Pritchet, H. Hoekstra, D. W. Just, S. Herbert-Fort, S. Sivanandam, R. J. Foley, and A. Mahdavi. The Multi-Epoch nearby Cluster Survey: Type Ia Supernova Rate Measurement in z ˜ 0.1 Clusters and the Late-time Delay Time Distribution. , 746:163, February 2012. doi: 10.1088/0004-637X/746/2/163.

A. Sandage, G. A. Tammann, and A. Yahil. The velocity field of bright nearby galaxies. I - The variation of mean absolute magnitude with redshift for galaxies in a magnitude-limited sample. , 232:352–364, September 1979. doi: 10.1086/157295.

C. L. Sarazin. *X-ray emission from clusters of galaxies*. 1988.

C. Scarlata, C. M. Carollo, S. J. Lilly, R. Feldmann, P. Kampczyk, A. Renzini, A. Cimatti, C. Halliday, E. Daddi, M. T. Sargent, A. Koekemoer, N. Scoville, J.-P. Kneib, A. Leauthaud, R. Massey, J. Rhodes, L. Tasca, P. Capak, H. J. McCracken, B. Mobasher, Y. Taniguchi, D. Thompson, M. Ajiki, H. Aussel, T. Murayama, D. B. Sanders, S. Sasaki, Y. Shioya, and M. Takahashi. The Redshift Evolution of Early-Type Galaxies in COSMOS: Do Massive Early-Type Galaxies Form by Dry Mergers? , 172:494–510, September 2007. doi: 10.1086/517972.

P. Schechter. An analytic expression for the luminosity function for galaxies. , 203: 297–306, January 1976. doi: 10.1086/154079.

T. C. Scott, H. Bravo-Alfaro, E. Brinks, C. A. Caretta, L. Cortese, A. Boselli, M. J. Hardcastle, J. H. Croston, and I. Plauchu. Probing evolutionary mechanisms in galaxy clusters: neutral atomic hydrogen in Abell1367. , 403:1175–1192, April 2010. doi: 10.1111/j.1365-2966.2009.16204.x.

L. Searle and R. Zinn. Compositions of halo clusters and the formation of the galactic halo. , 225:357–379, October 1978. doi: 10.1086/156499.

J. L. Sersic. *Atlas de galaxias australes*. 1968.

L. D. Shaw, G. P. Holder, and P. Bode. The Impact of Halo Properties, Energy Feedback, and Projection Effects on the Mass-SZ Flux Relation. , 686:206–218, October 2008. doi: 10.1086/589849.

J. Silk. On the fragmentation of cosmic gas clouds. I - The formation of galaxies and the first generation of stars. , 211:638–648, February 1977. doi: 10.1086/154972.

L. Simard, C. N. A. Willmer, N. P. Vogt, V. L. Sarajedini, A. C. Phillips, B. J. Weiner, D. C. Koo, M. Im, G. D. Illingworth, and S. M. Faber. The DEEP Groth Strip Survey. II. Hubble Space Telescope Structural Parameters of Galaxies in the Groth Strip. , 142:1–33, September 2002. doi: 10.1086/341399.

G. P. Smith, T. Treu, R. S. Ellis, S. M. Moran, and A. Dressler. Evolution since z = 1 of the Morphology-Density Relation for Galaxies. , 620:78–87, February 2005. doi: 10.1086/426930.

R. J. Smith, J. R. Lucey, D. Hammer, A. E. Hornschemeier, D. Carter, M. J. Hudson, R. O. Marzke, M. Mouhcine, S. Eftekharzadeh, P. James, H. Khosroshahi, E. Kourkchi, and A. Karick. Ultraviolet tails and trails in cluster galaxies: a sample of candidate gaseous stripping events in Coma. , 408:1417–1432, November 2010. doi: 10.1111/j.1365-2966.2010.17253.x.

R. S. Somerville and J. R. Primack. Semi-analytic modelling of galaxy formation: the local Universe. , 310:1087–1110, December 1999. doi: 10.1046/j.1365-8711.1999.03032.x.

V. Springel, S. D. M. White, A. Jenkins, C. S. Frenk, N. Yoshida, L. Gao, J. Navarro, R. Thacker, D. Croton, J. Helly, J. A. Peacock, S. Cole, P. Thomas, H. Couchman, A. Evrard, J. Colberg, and F. Pearce. Simulations of the formation, evolution and clustering of galaxies and quasars. , 435:629–636, June 2005. doi: 10.1038/nature03597.

V. Springel, C. S. Frenk, and S. D. M. White. The large-scale structure of the Universe. , 440:1137–1144, April 2006. doi: 10.1038/nature04805.

P. B. Stetson. DAOPHOT - A computer program for crowded-field stellar photometry. , 99:191–222, March 1987. doi: 10.1086/131977.

J. P. Stott, I. Smail, A. C. Edge, H. Ebeling, G. P. Smith, J.-P. Kneib, and K. A. Pimbblet. An Increase in the Faint Red Galaxy Population in Massive Clusters since z ˜ 0.5. , 661:95–101, May 2007. doi: 10.1086/514329.

R. A. Sunyaev and Y. B. Zeldovich. The Spectrum of Primordial Radiation, its Distortions and their Significance. *Comments on Astrophysics and Space Physics*, 2:66, March 1970.

R. A. Sunyaev and Y. B. Zeldovich. The Observations of Relic Radiation as a Test of the Nature of X-Ray Radiation from the Clusters of Galaxies. *Comments on Astrophysics and Space Physics*, 4:173, November 1972.

Y. Y. Tajiri and H. Kamaya. Anomalous Star Formation Activity of Less-Luminous Galaxies in a Cluster Environment. , 562:L125–L128, December 2001. doi: 10.1086/338251.

M. Tanaka, T. Kodama, N. Arimoto, S. Okamura, K. Umetsu, K. Shimasaku, I. Tanaka, and T. Yamada. The build-up of the colour-magnitude relation as a function of environment. , 362:268–288, September 2005. doi: 10.1111/j.1365-2966.2005.09300.x.

A. Toomre. Mergers and Some Consequences. In B. M. Tinsley and R. B. G. Larson, D. Campbell, editors, *Evolution of Galaxies and Stellar Populations*, page 401, 1977.

A. Toomre and J. Toomre. Galactic Bridges and Tails. , 178:623–666, December 1972. doi: 10.1086/151823.

T. Treu, R. S. Ellis, J.-P. Kneib, A. Dressler, I. Smail, O. Czoske, A. Oemler, and P. Natarajan. A Wide-Field Hubble Space Telescope Study of the Cluster Cl 0024+16 at z = 0.4. I. Morphological Distributions to 5 Mpc Radius. , 591:53–78, July 2003. doi: 10.1086/375314.

Y. Ueda, M. G. Watson, I. M. Stewart, M. Akiyama, A. D. Schwope, G. Lamer, J. Ebrero, F. J. Carrera, K. Sekiguchi, T. Yamada, C. Simpson, G. Hasinger, and S. Mateos. The Subaru/XMM-Newton Deep Survey (SXDS). III. X-Ray Data. , 179:124–141, November 2008. doi: 10.1086/591083.

S. A. Urquhart, J. P. Willis, H. Hoekstra, and M. Pierre. An environmental Butcher-Oemler effect in intermediate-redshift X-ray clusters. , 406:368–381, July 2010. doi: 10.1111/j.1365-2966.2010.16766.x.

P. G. van Dokkum, M. Franx, D. Fabricant, D. D. Kelson, and G. D. Illingworth. A High Merger Fraction in the Rich Cluster MS 1054-03 at Z = 0.83: Direct Evidence for Hierarchical Formation of Massive Galaxies. , 520:L95–L98, August 1999. doi: 10.1086/312154.

N. Visvanathan and A. Sandage. The color-absolute magnitude relation for E and S0 galaxies. I - Calibration and tests for universality using Virgo and eight other nearby clusters. , 216:214–226, August 1977. doi: 10.1086/155464.

N. P. Vogt, M. P. Haynes, R. Giovanelli, and T. Herter. M/L, Hα Rotation Curves, and H I Gas Measurements for 329 Nearby Cluster and Field Spirals. II. Evidence for Galaxy Infall. , 127:3300–3324, June 2004. doi: 10.1086/420702.

D. A. Wake, C. A. Collins, R. C. Nichol, L. R. Jones, and D. J. Burke. The Environmental Dependence of Galaxy Colors in Intermediate-Redshift X-Ray-selected Clusters. , 627:186–202, July 2005. doi: 10.1086/430117.

S. M. Weinmann, F. C. van den Bosch, X. Yang, and H. J. Mo. Properties of galaxy groups in the Sloan Digital Sky Survey - I. The dependence of colour, star formation and morphology on halo mass. , 366:2–28, February 2006. doi: 10.1111/j.1365-2966.2005.09865.x.

S. D. M. White and M. J. Rees. Core condensation in heavy halos - A two-stage theory for galaxy formation and clustering. , 183:341–358, May 1978.

S. D. M. White, M. Davis, G. Efstathiou, and C. S. Frenk. Galaxy distribution in a cold dark matter universe. , 330:451–453, December 1987. doi: 10.1038/330451a0.

S. D. M. White, J. F. Navarro, A. E. Evrard, and C. S. Frenk. The baryon content of galaxy clusters: a challenge to cosmological orthodoxy. , 366:429–433, December 1993. doi: 10.1038/366429a0.

B. C. Whitmore, D. M. Gilmore, and C. Jones. What determines the morphological fractions in clusters of galaxies? , 407:489–509, April 1993. doi: 10.1086/172531.

J. P. Willis, F. Pacaud, I. Valtchanov, M. Pierre, T. Ponman, A. Read, S. Andreon, B. Altieri, H. Quintana, S. Dos Santos, M. Birkinshaw, M. Bremer, P.-A. Duc, G. Galaz, E. Gosset, L. Jones, and J. Surdej. The XMM Large-Scale Structure survey: an initial sample of galaxy groups and clusters to a redshift z 0.6*. , 363: 675–691, October 2005. doi: 10.1111/j.1365-2966.2005.09473.x.

D. J. Wilman, M. L. Balogh, R. G. Bower, J. S. Mulchaey, A. Oemler, R. G. Carlberg, V. R. Eke, I. Lewis, S. L. Morris, and R. J. Whitaker. Galaxy groups at 0.3 =z= 0.55 - II. Evolution to z˜ 0. , 358:88–100, March 2005. doi: 10.1111/j.1365-2966.2005.08745.x.

D. J. Wilman, D. Pierini, K. Tyler, S. L. McGee, A. Oemler, Jr., S. L. Morris, M. L. Balogh, R. G. Bower, and J. S. Mulchaey. Unveiling the Important Role of Groups in the Evolution of Massive Galaxies: Insights from an Infrared Passive Sequence at Intermediate Redshift. , 680:1009–1021, June 2008. doi: 10.1086/587478.

C. Wolf, M. E. Gray, and K. Meisenheimer. Red-sequence galaxies with young stars and dust: the cluster Abell 901/902 seen with COMBO-17. , 443:435–449, November 2005. doi: 10.1051/0004-6361:20053585.

C. Wolf, A. Aragón-Salamanca, M. Balogh, M. Barden, E. F. Bell, M. E. Gray, C. Y. Peng, D. Bacon, F. D. Barazza, A. Böhm, J. A. R. Caldwell, A. Gallazzi, B. Häußler, C. Heymans, K. Jahnke, S. Jogee, E. van Kampen, K. Lane, D. H. McIntosh, K. Meisenheimer, C. Papovich, S. F. Sánchez, A. Taylor, L. Wisotzki, and X. Zheng. The STAGES view of red spirals and dusty red galaxies: mass-dependent quenching of star formation in cluster infall. , 393:1302–1323, March 2009. doi: 10.1111/j.1365-2966.2008.14204.x.

M. Yagi, N. Kashikawa, M. Sekiguchi, M. Doi, N. Yasuda, K. Shimasaku, and S. Okamura. Luminosity Functions of 10 Nearby Clusters of Galaxies. II. Analysis of the Luminosity Function. , 123:87–99, January 2002. doi: 10.1086/324732.

H. K. C. Yee and O. López-Cruz. A Quantitative Measure of the Richness of Galaxy Clusters. , 117:1985–1994, May 1999. doi: 10.1086/300837.

H. K. C. Yee, S. L. Morris, H. Lin, R. G. Carlberg, P. B. Hall, M. Sawicki, D. R. Patton, G. D. Wirth, E. Ellingson, and C. W. Shepherd. The CNOC2 Field Galaxy Redshift Survey. I. The Survey and the Catalog for the Patch CNOC 0223+00. , 129:475–492, August 2000. doi: 10.1086/313426.

D. G. York, J. Adelman, J. E. Anderson, Jr., S. F. Anderson, J. Annis, N. A. Bahcall, J. A. Bakken, R. Barkhouser, S. Bastian, E. Berman, W. N. Boroski, S. Bracker, C. Briegel, J. W. Briggs, J. Brinkmann, R. Brunner, S. Burles, L. Carey, M. A. Carr, F. J. Castander, B. Chen, P. L. Colestock, A. J. Connolly, J. H. Crocker,

I. Csabai, P. C. Czarapata, J. E. Davis, M. Doi, T. Dombeck, D. Eisenstein, N. Ellman, B. R. Elms, M. L. Evans, X. Fan, G. R. Federwitz, L. Fiscelli, S. Friedman, J. A. Frieman, M. Fukugita, B. Gillespie, J. E. Gunn, V. K. Gurbani, E. de Haas, M. Haldeman, F. H. Harris, J. Hayes, T. M. Heckman, G. S. Hennessy, R. B. Hindsley, S. Holm, D. J. Holmgren, C.-h. Huang, C. Hull, D. Husby, S.-I. Ichikawa, T. Ichikawa, Ž. Ivezić, S. Kent, R. S. J. Kim, E. Kinney, M. Klaene, A. N. Kleinman, S. Kleinman, G. R. Knapp, J. Korienek, R. G. Kron, P. Z. Kunszt, D. Q. Lamb, B. Lee, R. F. Leger, S. Limmongkol, C. Lindenmeyer, D. C. Long, C. Loomis, J. Loveday, R. Lucinio, R. H. Lupton, B. MacKinnon, E. J. Mannery, P. M. Mantsch, B. Margon, P. McGehee, T. A. McKay, A. Meiksin, A. Merelli, D. G. Monet, J. A. Munn, V. K. Narayanan, T. Nash, E. Neilsen, R. Neswold, H. J. Newberg, R. C. Nichol, T. Nicinski, M. Nonino, N. Okada, S. Okamura, J. P. Ostriker, R. Owen, A. G. Pauls, J. Peoples, R. L. Peterson, D. Petravick, J. R. Pier, A. Pope, R. Pordes, A. Prosapio, R. Rechenmacher, T. R. Quinn, G. T. Richards, M. W. Richmond, C. H. Rivetta, C. M. Rockosi, K. Ruthmansdorfer, D. Sandford, D. J. Schlegel, D. P. Schneider, M. Sekiguchi, G. Sergey, K. Shimasaku, W. A. Siegmund, S. Smee, J. A. Smith, S. Snedden, R. Stone, C. Stoughton, M. A. Strauss, C. Stubbs, M. SubbaRao, A. S. Szalay, I. Szapudi, G. P. Szokoly, A. R. Thakar, C. Tremonti, D. L. Tucker, A. Uomoto, D. Vanden Berk, M. S. Vogeley, P. Waddell, S.-i. Wang, M. Watanabe, D. H. Weinberg, B. Yanny, N. Yasuda, and SDSS Collaboration. The Sloan Digital Sky Survey: Technical Summary. , 120:1579–1587, September 2000. doi: 10.1086/301513.

A. I. Zabludoff and J. S. Mulchaey. The Properties of Poor Groups of Galaxies. I. Spectroscopic Survey and Results. , 496:39, March 1998. doi: 10.1086/305355.

A. I. Zabludoff and J. S. Mulchaey. The Properties of Poor Groups of Galaxies. III. The Galaxy Luminosity Function. , 539:136–148, August 2000. doi: 10.1086/309191.